

# New MRI techniques for staging malignant lymphoma

**Thomas Christian Kwee**

## **New MRI techniques for staging malignant lymphoma**

The copyright of the articles that have been published or accepted for publication has been transferred to the respective journals.

© T.C. Kwee, Utrecht, 2011

ISBN:	978-90-393-5521-3
Layout:	Roy Sanders
Coverdesign:	Prof. dr. Taro Takahara
Printing:	Gildeprint Drukkerijen B.V., Enschede

# New MRI techniques for staging malignant lymphoma

Nieuwe MRI technieken voor het stageren van maligne lymfomen

(met een samenvatting in het Nederlands)

## **Proefschrift**

ter verkrijging van de graad van doctor  
aan de Universiteit Utrecht op gezag  
van de rector magnificus, prof. dr. G.J. van der Zwaan,  
ingevolge het besluit van het college  
van promoties in het openbaar te verdedigen op  
donderdag 14 april 2011 des morgens te 10.30 uur

door

**Thomas Christian Kwee**

Geboren op 23 maart 1981 te Nijmegen

**Promotor:** Prof. dr. W.P.Th.M. Mali

**Co-promotor:** Dr. R.A.J. Nievelstein

This project was financially supported by:

-ZonMw Program for Health Care Efficiency Research (grant number 80-82310-98-08012)

-ZonMW AGIKO stipend (grant number 92003497)

Additional financial support was generously provided by Philips Healthcare, the Rontgen Stichting Utrecht, Bayer Healthcare, Guerbet Nederland B.V., Roche, Pfizer, and Schering-Plough

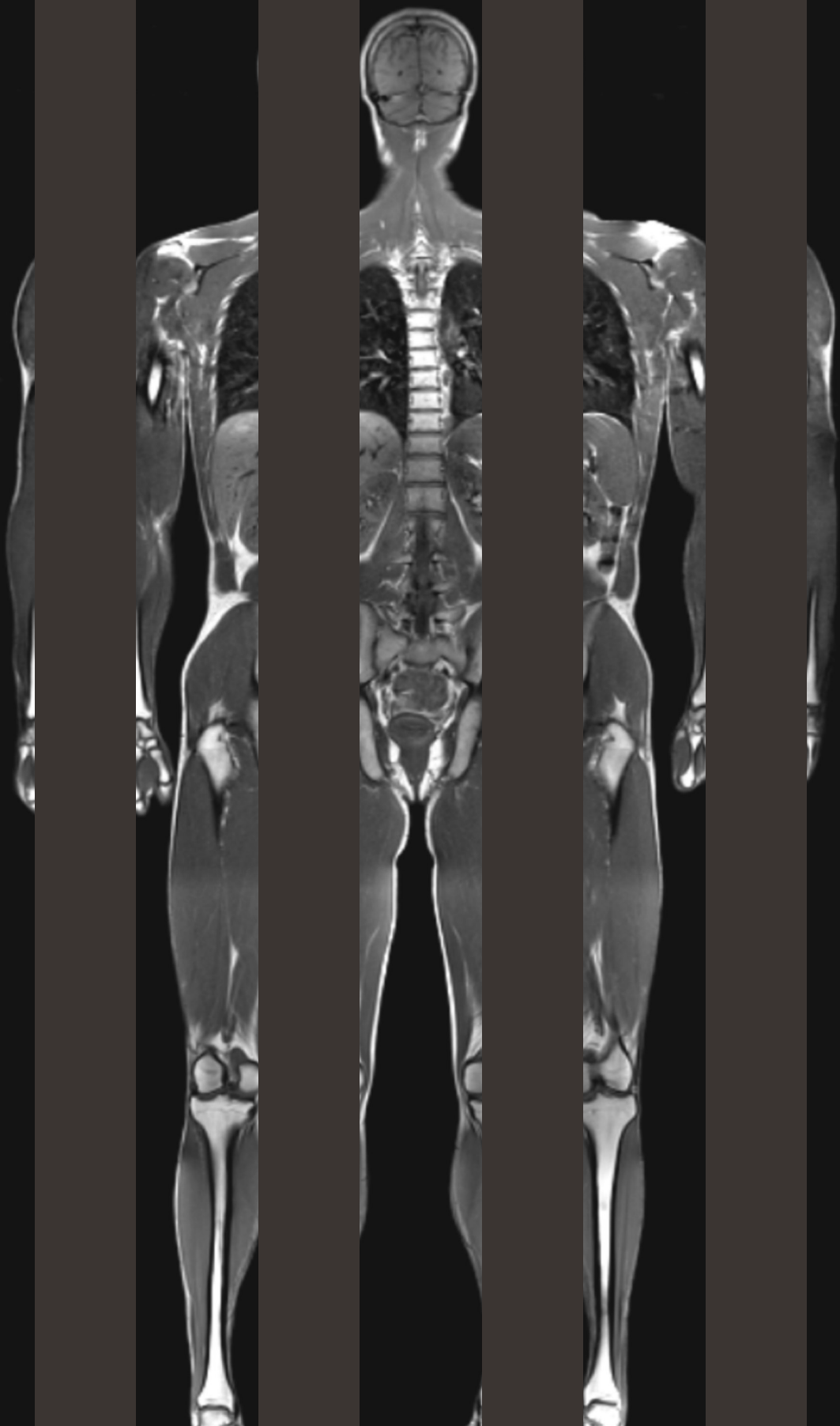




## Contents

Chapter 1	General introduction	9
Chapter 2	Imaging in staging of malignant lymphoma: a systematic review	17
Chapter 3	Radiation exposure and mortality risk from CT and PET imaging of patients with malignant lymphoma	49
Chapter 4.1	Diffusion-weighted whole-body imaging with background body signal suppression (DWIBS): features and potential applications in oncology	67
Chapter 4.2	Whole-body diffusion-weighted magnetic resonance imaging	93
Chapter 4.3	Whole-body diffusion-weighted imaging for staging malignant lymphoma in children	113
Chapter 5	Whole-body MRI using a sliding table and repositioning surface coil approach	135
Chapter 6.1	ADC measurements of lymph nodes: inter- and intra-observer reproducibility study and an overview of the literature	151
Chapter 6.2	ADC measurements in the evaluation of lymph nodes in patients with non-Hodgkin lymphoma: feasibility study	165
Chapter 7.1	MRI for the detection of bone marrow involvement in malignant lymphoma	183
Chapter 7.2	Whole-body magnetic resonance imaging, including diffusion-weighted imaging, for diagnosing bone marrow involvement in malignant lymphoma	201
Chapter 8.1	Whole-body MRI, including diffusion-weighted imaging, for the initial staging of malignant lymphoma: comparison to computed tomography	217

Chapter 8.2	Whole-body MRI, including diffusion-weighted imaging, for staging newly diagnosed lymphoma: comparison to computed tomography in 101 patients	239
Chapter 8.3	Newly diagnosed lymphoma: initial results with whole-body T1-weighted, STIR, and diffusion-weighted MRI compared with <sup>18</sup> F-FDG PET-CT	261
Chapter 9	MRI for staging lymphoma: whole-body or less?	281
Chapter 10	General discussion	299
Chapter 11	Summary	315
	Nederlandse samenvatting	321
Chapter 12	Dankwoord	327
	Curriculum Vitae	333
	List of publications	337



# Chapter 1

General introduction  
and thesis outline

## Introduction

### Staging malignant lymphoma

The malignant lymphomas, Hodgkin lymphoma and non-Hodgkin lymphoma, comprise approximately 5.0% of all cancers and account for approximately 3.7% of all cancer deaths in the Western world [1]. Once the diagnosis malignant lymphoma has been established by excision biopsy of a particular site, determination of disease extent (staging) is important for appropriate treatment planning and determining prognosis [2-4]. The currently most frequently used staging system for malignant lymphomas is the Ann Arbor staging system. The Ann Arbor staging system divides patients into four stages based on localized disease, multiple sites of disease on one or the other side of the diaphragm, lymphatic disease on both sides of the diaphragm, and disseminated extranodal disease [2-4].

### Development of staging procedures for malignant lymphoma

In the 1970s, it was common practice to subject patients with malignant lymphoma to a battery of radiologic studies, including chest radiography, intravenous pyelography, lymphangiography, skeletal surveys, and isotope scans. On top of this, most patients with Hodgkin lymphoma underwent staging laparotomy with its attendant risks [5]. The disadvantages of these burdensome staging procedures have been overcome by the introduction of imaging modalities that are able to noninvasively provide cross-sectional images of the entire body, including computed tomography (CT) [6], positron emission tomography (PET) [7], and magnetic resonance (MR) imaging [8, 9]. CT is currently the most commonly used means for staging patients with malignant lymphoma [2-4], thanks to its widespread availability and scan speed. PET, using the radiotracer  $^{18}\text{F}$ -fluoro-2-deoxyglucose (FDG), has an important role in the assessment of response to therapy and in the detection of persistent or recurrent disease [10]. Of note, most FDG-PET studies are currently performed as part of a combined FDG-PET/CT combination.

### Radiation exposure from CT and FDG-PET

Disadvantages of CT and FDG-PET are exposure of the patient to ionizing radiation, which may induce the development of second neoplasms in later life [11-13]. Especially in the present era, in which treatment strategies are aimed at maximizing chance of cure while minimizing late toxicity [2-4], prevention of second neoplasms due to ionizing radiation from medical imaging has become an important issue. This issue is of particular interest in children, because rapidly dividing cells are more sensitive to radiation induced effects, and children will have more years ahead in which cancerous changes might occur [11-13].

*Whole-body MR imaging*

MR imaging is a radiation-free imaging method, with a good spatial resolution and excellent soft-tissue contrast, making it an ideal tool for the detection of parenchymal and bone marrow abnormalities. Therefore, it may be an attractive alternative to CT and FDG-PET. Previously, long scan times and hardware limitations made it impossible to routinely acquire whole-body MR images. Technological advances, including the development of high-performance magnetic field gradients, parallel imaging, and the sliding table platform, have eventually made whole-body MR imaging clinically feasible [14]. In 2003, 2004, and 2005, the first reports were published on the potential utility of whole-body MR imaging for staging malignant lymphoma [15-17].

*Whole-body diffusion-weighted MR imaging*

Commonly applied sequences for whole-body MR imaging include (contrast-enhanced) T1-weighted and (fat-suppressed) T2-weighted sequences. A disadvantage of these conventional MR sequences, however, is the large amount of data that have to be evaluated, including data from a lot of normal structures such as fat, muscles, and vascular structures. Consequently, image interpretation can be time-consuming and subtle lesions can be overlooked. Diffusion-weighted imaging (DWI) may overcome this disadvantage of conventional whole-body MR imaging. DWI is able to highlight lesions, including (malignant) tumors, while suppressing signals of surrounding normal structures [18]. In addition, DWI provides functional information because it allows quantifying diffusion by means of apparent diffusion coefficient (ADC) measurements [18]. ADC measurements may aid in the characterization of lesions and lymph nodes. Previously, however, DWI could only be applied in the brain for the diagnosis of acute ischemic stroke [19]. Extracranial DWI was still impossible because the use of a long echo-planar imaging train would lead to severe image degradation in the heterogeneous tissue of the trunk with its many air-tissue and air-bone boundaries. This limitation has been overcome by the development of high-performance magnetic field gradients and, most importantly, the introduction of parallel imaging. At present, DWI is feasible in any part of the body [20]. Another major breakthrough was the discovery of the feasibility of DWI under free breathing, which is also known as the concept of Diffusion-weighted Whole-body Imaging with Background body signal Suppression (DWIBS) [21]. The fact that DWI can be acquired under free breathing is somehow counterintuitive at a first sight, because respiratory motion takes place on the order of centimeters and diffusion takes place on the order of micrometers. Nevertheless, unlike breathhold or respiratory triggered acquisitions, it allows for whole-body DWI. Another feature of DWI, and DWIBS in particular, is its ability to highlight lymph nodes, because diffusion in these structures is relatively low [21]. As such, it may be of particular value for the staging of malignant lymphoma.

*Current role of MR imaging in staging malignant lymphoma*

Studies investigating the value of whole-body MR imaging for staging malignant lymphoma are still scarce and only included a relatively low number of patients [15-17]. In addition, the feasibility of the routine use of whole-body DWI and its application in the staging of malignant lymphoma have not been explored yet. Therefore, implementation of whole-body MR imaging in clinical practice has not been achieved yet. At present, CT and FDG-PET(/CT) are still the mainstays in staging of malignant lymphoma in routine clinical practice, while the role of MR imaging is still very limited.

## Aim of this thesis

The aim of this thesis is to introduce and assess the value of whole-body MR imaging, including whole-body DWI, for the staging of malignant lymphoma.

## Outline of this thesis

**Chapter 2** will give a short introduction to the technical aspects and procedures of CT, FDG-PET, FDG-PET/CT fusion, and whole-body MR imaging. The same chapter will also provide a systematic review of the published literature on the diagnostic performance of CT, FDG-PET, combined FDG-PET/CT, and whole-body MR imaging for staging malignant lymphoma. Furthermore, advantages, drawbacks, and limitations of each imaging modality will be outlined.

It is generally accepted that CT and FDG-PET may cause radiation-induced fatal cancer. However, quantitative measures of this risk in patients with malignant lymphoma are still lacking. **Chapter 3** aims to provide more insight into the mortality that is associated with ionizing radiation from CT and FDG-PET(/CT) in patients with malignant lymphoma.

**Chapters 4.1** and **4.2** will focus on whole-body DWI: the concept of DWIBS will be explained, and potential oncological and non-oncological applications of this concept will be discussed and richly illustrated. **Chapter 4.3** is an extension of the previous two chapters, and will review and discuss whole-body MR techniques for staging malignant lymphoma in children, and whole-body DWI in particular.

**Chapter 5** will present and assess a novel approach for acquiring whole-body MR images, including diffusion-weighted images, using a single surface coil.

ADC measurements have been proposed as a potentially useful quantitative method for the diagnosis of metastatic lymph nodes. However, there is no consensus yet on its exact value. **Chapter 6.1** will assess the inter- and intra-observer reproducibility of ADC measurements of lymph nodes, and will provide an overview of the literature regarding this subject. In addition, **chapter 6.2** will report our own results regarding the value of ADC measurements in the evaluation of lymph nodes in patients with non-Hodgkin lymphoma.



MR imaging is a potentially sensitive method for the detection of bone marrow involvement in patients with malignant lymphoma, which, if present, by definition, represents the highest stage (stage IV) according to the Ann Arbor staging system. **Chapter 7.1** will provide a review on the published literature regarding the value of MR imaging for the detection of bone marrow involvement, and **chapter 7.2** will report on the performance of whole-body MR imaging, including DWI, for the diagnosis of bone marrow involvement based on our own series of patients.

**Chapters 8.1, 8.2, and 8.3** represent the core of this thesis, in that they compare the staging performance of whole-body MR imaging, including DWI, to CT and FDG-PET/CT.

Whole-body MR imaging refers to MR imaging of the area from the cranial vertex to the toes. However, it is unknown whether a whole-body MR imaging protocol is necessary, or whether an MR imaging protocol that only includes the head/neck and trunk (similar to the usual CT coverage) is comparable while less time-consuming: **chapter 9** will answer this question.

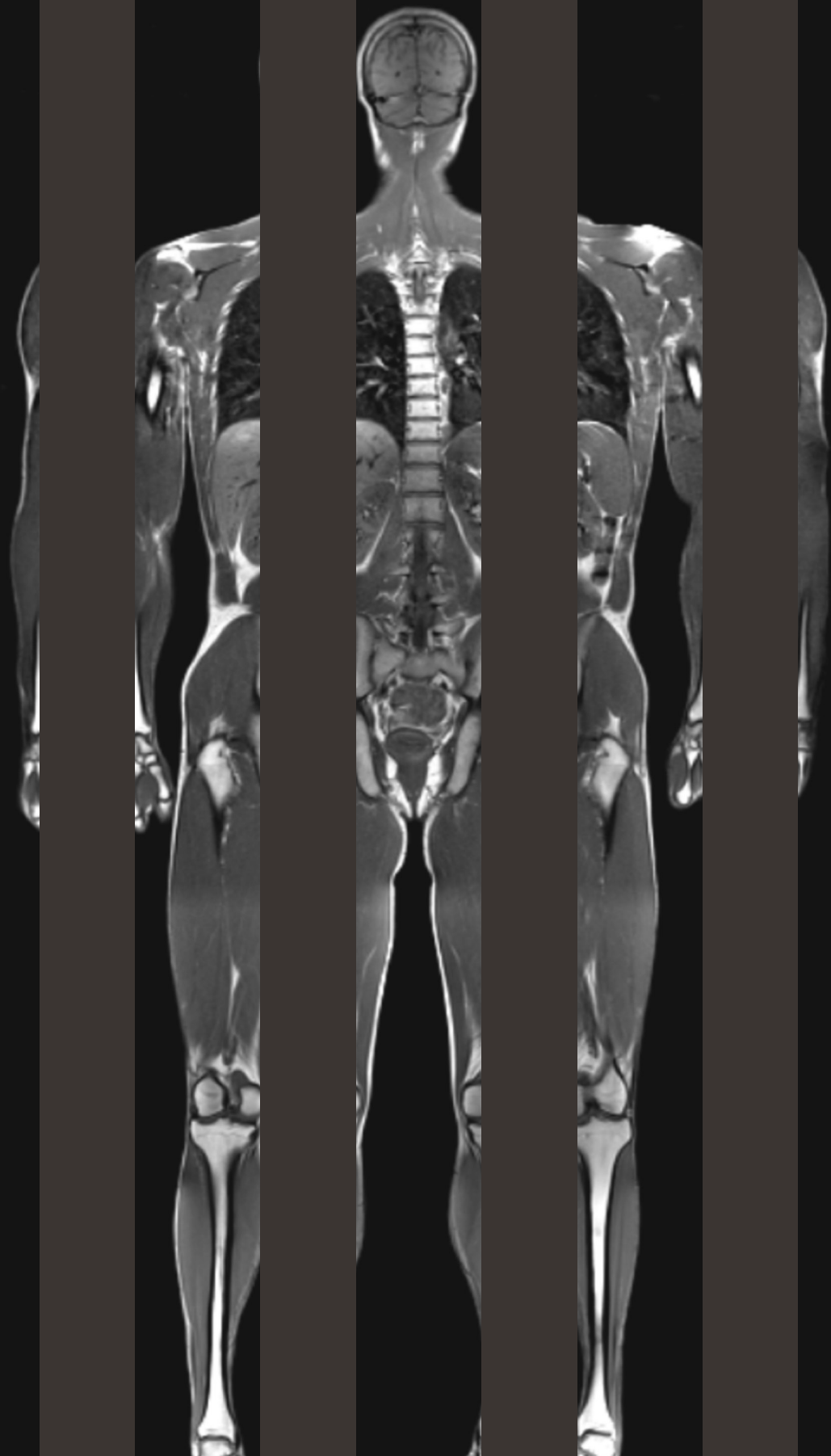
In **chapter 10**, results of the studies that have been performed in this thesis and future research directions will be discussed.

A summary of the results of this thesis will be provided in **chapter 11**.

## References

1. Jemal A, Siegel R, Xu J, Ward E. Cancer statistics, 2010. *CA Cancer J Clin* 2010;60:277-300
2. Connors JM. State-of-the-art therapeutics: Hodgkin's lymphoma. *J Clin Oncol* 2005;23:6400-6408
3. Armitage JO. Staging non-Hodgkin lymphoma. *CA Cancer J Clin* 2005;55:368-376
4. Ansell SM, Armitage J. Non-Hodgkin lymphoma: diagnosis and treatment. *Mayo Clin Proc* 2005;80:1087-1097
5. Rosenberg SA, Boiron M, DeVita VT Jr, et al. Report of the Committee on Hodgkin's Disease Staging Procedures. *Cancer Res* 1971;31:1862-1863
6. The EMI-scanner: computerised transverse axial tomography--a new technique. *Radiography* 1973;39:18-20
7. Phelps ME, Eichling JO. Application of annihilation coincidence detection to transaxial reconstruction tomography. *J Nucl Med* 1974;15:814-817
8. Damadian R. Tumor detection by nuclear magnetic resonance. *Science* 1971;171:1151-1153
9. Lauterbur PC. Image Formation by Induced Local Interactions: Examples Employing Nuclear Magnetic Resonance. *Nature* 1973;242:190-191
10. Juweid ME, Stroobants S, Hoekstra OS, et al; Imaging Subcommittee of International Harmonization Project in Lymphoma. Use of positron emission tomography for response assessment of lymphoma: consensus of the Imaging Subcommittee of International Harmonization Project in Lymphoma. *J Clin Oncol* 2007;25:571-578
11. Barentsz J, Takahashi S, Oyen W, et al. Commonly used imaging techniques for diagnosis and staging. *J Clin Oncol* 2006;24:3234-3244
12. Brenner DJ, Hall EJ. Computed tomography--an increasing source of radiation exposure. *N Engl J Med* 2007;357:2277-2284
13. Huang B, Law MW, Khong PL. Whole-body PET/CT scanning: estimation of radiation dose and cancer risk. *Radiology* 2009;251:166-174
14. Lauenstein TC, Semelka RC. Emerging techniques: whole-body screening and staging with MRI. *J Magn Reson Imaging* 2006;24:489-498
15. Amano Y, Tajika K, Uchiyama N, Takahama K, Dan K, Kumazaki T. Staging of malignant lymphoma with three-station black-blood fast short-inversion time inversion recovery (STIR). *Magn Reson Med Sci* 2003;2:9-15
16. Kellenberger CJ, Miller SF, Khan M, Gilday DL, Weitzman S, Babyn PS. Initial experience with FSE STIR whole-body MR imaging for staging lymphoma in children. *Eur Radiol* 2004;14:1829-1841
17. Brennan DD, Gleeson T, Coate LE, Cronin C, Carney D, Eustace SJ. A comparison of whole-body MRI and CT for the staging of lymphoma. *AJR Am J Roentgenol* 2005;185:711-716
18. Le Bihan D, Breton E, Lallemand D, Grenier P, Cabanis E, Laval-Jeantet M. MR imaging of intravoxel incoherent motions: application to diffusion and perfusion in neurologic disorders. *Radiology* 1986;161:401-407
19. Schaefer PW, Grant PE, Gonzalez RG. Diffusion-weighted MR imaging of the brain. *Radiology* 2000;217:331-345
20. Koh DM, Collins DJ. Diffusion-weighted MRI in the body: applications and challenges in oncology. *AJR Am J Roentgenol* 2007;188:1622-1635

21. Takahara T, Imai Y, Yamashita T, Yasuda S, Nasu S, Van Cauteren M. Diffusion weighted whole body imaging with background body signal suppression (DWIBS): technical improvement using free breathing, STIR and high resolution 3D display. *Radiat Med* 2004;22:275-282



# Chapter 2

## Imaging in staging of malignant lymphoma: a systematic review

Kwee TC, Kwee RM, Niewelstein RA

*Blood* 2008;111:504-516

## Abstract

Computed tomography (CT) is currently the most commonly used means for staging malignant lymphoma. <sup>18</sup>F-fluoro-2-deoxyglucose positron emission tomography (FDG-PET), FDG-PET/CT fusion, and whole-body magnetic resonance imaging (WB-MRI) are potential alternatives. The purpose of this study was to systematically review published data on the diagnostic performance of CT, FDG-PET, FDG-PET/CT fusion, and WB-MRI in staging of malignant lymphoma. In addition, technical aspects, procedures, advantages, and drawbacks of each imaging modality are outlined. Nineteen studies were included in this systematic review: 3 CT studies, 17 FDG-PET studies, and 4 FDG-PET/CT fusion studies. The studies were of moderate methodological quality and used different scoring systems to stage malignant lymphoma. CT remains the standard imaging modality for initial staging of malignant lymphoma, while FDG-PET has an essential role in restaging after treatment. Early results suggest that FDG-PET/CT fusion outperforms both CT alone and FDG-PET alone. Data on the diagnostic performance of WB-MRI are lacking. Future well-designed studies, expressing their results according to the Ann Arbor staging system, are needed to determine which imaging modality is most accurate and cost-effective in staging malignant lymphoma.

## Introduction

The malignant lymphomas, Hodgkin's disease (HD) and non-Hodgkin's lymphoma (NHL), comprise approximately 5-6% of all malignancies, and are the fifth most frequently occurring type of cancer in the United States. In 2007, an estimated 9,260 new cases of HD and 81,850 new cases of NHL will be diagnosed in the United States [1]. Once the diagnosis HD or NHL has been established by biopsy of a particular site, determination of disease extent (staging) is important for appropriate treatment planning and determining prognosis. In addition, knowing the sites of involvement at time of diagnosis makes it possible to accurately restage at the end of therapy and document a complete remission [2, 3]. Staging of HD and NHL is based on the Ann Arbor classification with the addition of a definition of bulky disease often referred to as the Cotswold modification (**Table 1**). This staging system encompasses the number of sites of disease involved, the type of involvement (nodal or extranodal), and the distribution of disease [4].

**Table 1.** Cotswold-modified Ann Arbor classification.

Stage	Involvement
I	Single lymph node region (I) or one extralymphatic site (IE)
II	Two or more lymph node regions, same side of the diaphragm (II) or local extralymphatic extension plus one or more lymph node regions same side of the diaphragm (IIE).
III	Lymph node regions on both sides of the diaphragm (III), which may be accompanied by local extralymphatic extension (IIIE)
IV	Diffuse involvement of one or more extralymphatic organs or sites

Suffix	Features
A	No B symptoms
B	Presence of at least one of these: unexplained weight loss >10% baseline during 6 months prior to staging; recurrent unexplained fever >38°C; recurrent night sweats
X	Bulky tumor is defined as either a single mass of tumor tissue exceeding 10 cm in largest diameter or a mediastinal mass exceeding one third of the maximum transverse transthoracic diameter measured on a standard posterior-anterior chest radiograph.

Computed tomography (CT) is currently the most commonly used means for staging patients with malignant lymphoma [2, 3]. However, CT lacks functional information, which impedes identification of disease in normal-sized organs. <sup>18</sup>F-fluoro-2-deoxyglucose positron emission tomography (FDG-PET) may be an alternative to CT [5, 6]. Other promising alternatives to CT are FDG-PET/CT fusion [7, 8] and whole-body magnetic resonance imaging (WB-MRI) [9, 10]. The purpose of this study is to provide an up-to-date overview of the diagnostic performance of CT, FDG-PET, FDG-PET/CT fusion, and WB-MRI in staging of malignant lymphoma.

In the first part of this article, technical aspects and procedures of each imaging modality are summarized. Subsequently, we describe our literature search strategy, study selection methods, and study analysis. Next, literature search results and results of analyzed articles are demonstrated. Finally, results are discussed, and advantages, drawbacks, and limitations of each imaging technique are outlined.

## Technical aspects and procedures

### CT

Before the CT era, patients with a diagnosis of malignant lymphoma were subjected to a battery of radiologic studies that included chest radiography, intravenous pyelography, lymphangiography, skeletal surveys, and isotope scans. On top of this, most patients with HD underwent staging laparotomy with its attendant risks [11]. The introduction of CT in the early 1970s was a tremendous breakthrough in non-invasive imaging and its potential for staging malignant lymphoma was soon recognized and investigated [12]. Since then, CT has gradually become the imaging modality of choice for staging malignant lymphoma. CT technology has continuously been developed and refined; major milestones include the introduction of spiral CT in the early 1990s and the advent of multidetector-row CT in 1998. The concept of multidetector-row CT deserves special attention; multidetector-row CT scanners have multiple (X) data acquisition systems connected to multidetector arrays to provide a multiple (X) -section scan, increasing the speed of data collection by a factor X over single detector-row CT scanners. In addition, current multidetector-row CT scanners have a faster gantry rotation. These two properties enable acquisition of thinner slices in a shorter time, compared with single detector-row CT scanners, which minimizes or eliminates breathing artifacts [13, 14]. As a result, lymph nodes of 5 mm or less in diameter can be detected throughout the whole body. In combination with powered injectors for rapid bolus administration of intravenous contrast medium, focal extranodal lesions on the order of a few millimetres can be identified [15, 16].

State-of-the-art CT for staging malignant lymphoma is currently performed on  $\geq 4$ -section multidetector-row CT scanners. Patients receive an intravenous injection of iodinated contrast medium and generally are given oral contrast agent prior to scanning.

Determination of nodal involvement is based on size criteria. Lymph nodes with a short-axis diameter greater than 10 mm are generally considered positive. Furthermore, clustering of normal-sized but prominent lymph nodes in the anterior mediastinum and the mesentery is suspicious for disease. The use of intravenous contrast medium is not helpful in differentiating normal from malignant lymph nodes. General criteria for extranodal involvement are organomegaly, abnormal mass or structural changes in a normal-sized organ, and abnormal contrast enhancement (Figures 1A, 1B, and 1C) [16].



## FDG-PET

Positron emission tomography (PET) was developed in the early 1970s soon after CT [17]. PET is based on the utilisation of positron-emitting radiopharmaceuticals and the detection in coincidence of the two nearly collinear 511-keV photons emitted following positron annihilation with an electron. The increased glycolytic rate of malignant cells is the rationale behind the common use of <sup>18</sup>F-fluoro-2-deoxyglucose (FDG) as a radiotracer in oncological PET studies [6]. Imaging of malignant lymphoma with FDG was first described in 1987 [18] and the first reports on FDG-PET as a whole-body staging method in malignant lymphoma appeared in the 1990s [19-22]. PET technology has improved dramatically since its development. Initial patient imaging units had a system resolution greater than 15 mm, whereas current units have a 4-5 mm resolution [6].

FDG-PET examinations for staging malignant lymphoma should be performed on dedicated (full ring) PET scanners, because dual-head gamma cameras in coincidence mode are unreliable in detecting lesions <15-20 mm in diameter [23-26]. Raw data should be reconstructed by means of iterative expectation maximization algorithms, which provide superior signal-to-noise ratio compared to filtered back-projection images [6]. Attenuation effects (scatter or absorption of emitted photons in the body) produce regional nonuniformities, distortions of intense structures, and edge effects. To improve anatomic delineation, additional transmission scanning for attenuation correction using an external radiation source is required. Attenuation correction also allows for semi-quantitative evaluation, which offers a more objective way to assess FDG uptake. Non-attenuation corrected images should, however, also be evaluated, because the attenuation correction itself may also introduce image artifacts [6, 27]. Patients are required to fast for at least 4-6 hours prior to scanning, which starts approximately 60 minutes after the injection of a typical FDG dose of 370 MBq. Serum glucose levels of less than 150 mg/dL are desirable. Patients are also instructed to avoid any kind of strenuous activity prior to the examination and following injection of the radioisotope to avoid physiologic muscle uptake of FDG.

Any focus of visually elevated FDG uptake relative to the background, not located in areas of physiologically increased uptake or where the clinical data do not suggest the presence of a non-malignant hypermetabolic lesion, is regarded as positive for malignant lymphoma. In organs with physiologic FDG uptake (eg, spleen and liver), focal or inhomogeneous uptake patterns are considered to be indicative of malignant lymphoma (Figures 1D, 1E, and 1F). Cut-off values for semi-quantitative evaluation (measurement of standardized uptake values) of suspected foci have not been reported yet in the literature, to our knowledge.

Although beyond the scope of this review, FDG-PET also has high potential as a biomarker of response to chemotherapy in malignant lymphoma [28, 29]. Early interim FDG-PET has already proven to overshadow the prognostic value of the International

Prognostic Score and appears to be the single most important tool for planning risk-adapted treatment in advanced HD [30].

#### FDG-PET/CT fusion

FDG-PET and CT provide functional and anatomic information, respectively. Integration of both modalities may outperform both FDG-PET alone and CT alone in staging of malignant lymphoma. In traditional visual image fusion, FDG-PET and CT images are viewed and compared next to each other, with the fusion taking place in the interpreter's mind. Integration of separate FDG-PET and CT image sets into a single study can be achieved with software fusion. However, differences in scanner bed profiles, external patient positioning, and internal organ movement present a challenge to the software approaches (**Figure 1I**). These challenges have recently been addressed by the introduction of the combined PET/CT scanner, a hardware-oriented approach to image fusion. With this type of scanner, accurately registered anatomic and functional images can be acquired in a single examination, which has been shown to increase both the accuracy of the interpretation and the confidence level of the readers. Several manufacturers are now offering integrated FDG-PET/CT

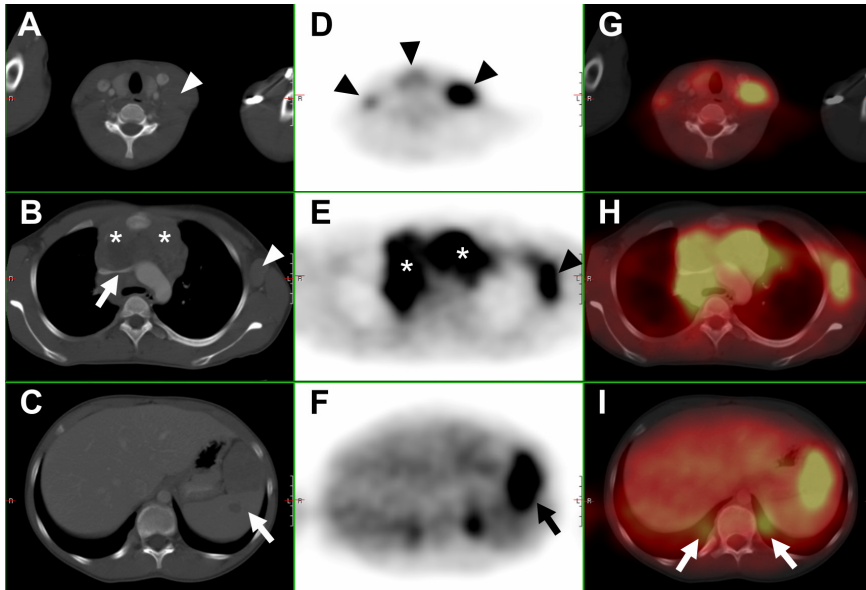


**Figure 1.** CT, FDG-PET, and FDG-PET/CT fusion in a 13-year-old female with Hodgkin's disease. (**A, B, C**) Axial CT images show (**A**) a cervical lymph node mass (arrowhead), (**B**) a large mediastinal mass (asterisks) compressing the left brachiocephalic vein (arrow) and an enlarged axillary lymph node (arrowhead), and (**C**) an enlarged inhomogeneous spleen (arrow). (**D, E, F**) Axial PET images show pathologic FDG uptake in (**D**) cervical lymph nodes (arrowheads), (**E**) in the mediastinum (asterisks) and in a left axillary lymph node mass (arrowhead), and (**F**) in the spleen (arrow). (**G, H, I**) Fused PET/CT images. (**I**) Note the misregistration of normal renal FDG excretion (arrows).

systems combining different models of dedicated PET scanners and multidetector-row CT scanners in line with a common imaging bed [7, 8].

Patient preparation is similar to that of FDG-PET alone. It is important to apply an appropriate respiration protocol to minimize the mismatch between CT and FDG-PET. On completion of the CT portion of the examination, the patient couch is advanced into the PET field-of-view, and a multibed PET study is acquired over the same range as the CT scan. CT images are used for attenuation correction of the FDG-PET emission data. Again, both images with and without attenuation correction should be evaluated. There is no consensus yet whether intravenous and oral contrast materials are needed for a combined FDG-PET/CT examination [7, 8].

Fused FDG-PET/CT images are interpreted using a combination of the criteria as described for CT and FDG-PET alone (Figures 1G, 1H, and 1I).

#### WB-MRI

The concept that MRI might become the ultimate whole-body imaging tool was initially proposed by the MRI pioneers Damadian and Lauterbur in 1980 [31, 32]. The high spatial resolution and excellent soft-tissue contrast make MRI an ideal tool for the detection of parenchymal and osseous lesions. However, because of long imaging time, limited availability, and extensive costs, MRI was previously only used as a tool to image limited anatomical areas of the body. Recent improvements in MRI technology have resulted in the availability of sufficiently fast and diagnostic sequences for WB-MRI. Additionally, the introduction of a rolling bed patient platform, enabling data acquisition of different anatomical regions in rapid succession, has overcome the time-consuming problem of stepwise manual repositioning of the patient. As a result, WB-MRI has become feasible for staging malignancies, including malignant lymphoma [9, 10].

MRI systems operating at 1.5 T are widely available and provide high image quality of all body regions in reasonable measuring times. WB-MRI at higher field strength (3.0 T) has high potential, but has not yet proven to be equal or superior to WB-MRI at 1.5 T [33, 34]. The use of a phased-array surface coil is preferred because it provides an increased signal-to-noise ratio and spatial resolution compared to an integrated body coil. There is no standard WB-MRI protocol for staging malignant lymphoma yet; data regarding preferred sequence and imaging plane are lacking. A commonly recommended approach for tumor staging in general is the application of fat-suppressed, T1-weighted gradient echo sequences, before and after the administration of intravenous gadolinium. The fluid-sensitive, fat-suppressed, T2-weighted short-tau-inversion-recovery sequence is useful for the assessment of the bone marrow (Ann Arbor stage IV) and the pelvis [9, 10].

Although MRI inherently provides superior soft-tissue contrast to CT and has the potential to characterize lesions on the basis of signal characteristics, assessment of nodal involvement is still based on size criteria, where lymph nodes with a short-axis

diameter greater than 10 mm are generally considered positive (similar to CT). General criteria for extranodal involvement are any signal abnormalities or mass lesions involving soft tissues, bones, parenchymal organs and serosal cavities (**Figure 2**).

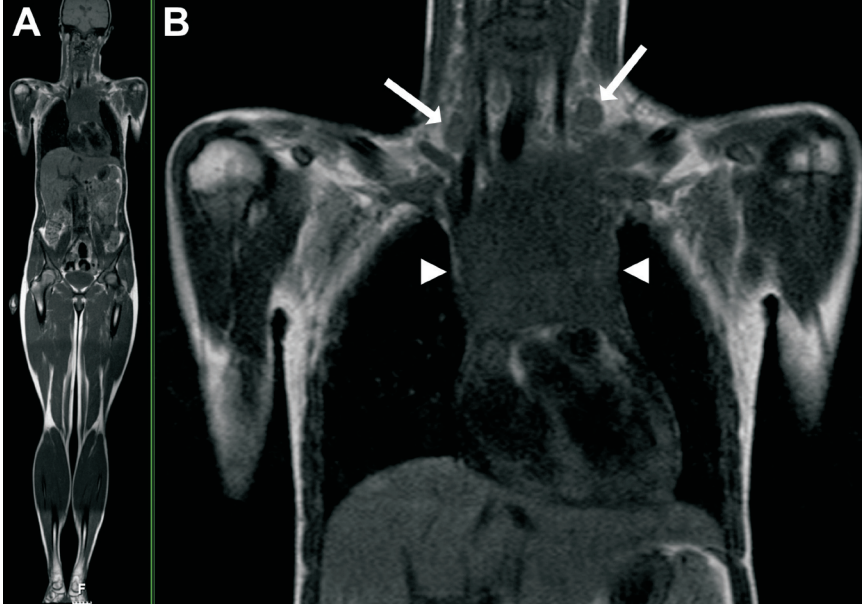


**Figure 2.** WB-MRI in a 16-year-old female with Hodgkin's disease. **A)** Coronal T1-weighted WB-MRI. **B)** Close-up image shows bilateral enlarged cervical lymph nodes (arrows) and a large mediastinal mass (arrowheads) consistent with confluent lymphadenopathy.

## Methods

### Data sources

A computer-aided search of the PubMed/MEDLINE and Embase databases was conducted to find relevant publications on the diagnostic performance of CT, FDG-PET, FDG-PET/CT fusion, and WB-MRI in the staging of malignant lymphoma. The search strategy is presented in **Table 2**. No beginning date limit was used. The search was updated until 25 July 2007. Only English-, German-, or French-language studies were considered because the investigators were familiar with these languages. To expand our search, bibliographies of articles which finally remained after the selection process were screened for potentially suitable references.

### Study selection

At the first stage, two researchers (T.C.K., R.M.K.) independently reviewed the titles and abstracts of the retrieved articles. Studies investigating the diagnostic performance of

**Table 2.** Search strategy and results as on 25 July 2007.

#	Search string	PubMed/Medline	Embase
1	Computed tomography OR Computerized tomography OR Computed tomographic OR CT OR CAT	414,143	258,730
2	Fluorodeoxyglucose OR 2-fluoro-2-deoxy-D-glucose OR FDG OR Positron emission tomography OR Positron-emission tomography OR PET	36,616	41,132
3	Magnetic resonance OR MR imaging OR MRI OR Magnetic resonance tomography OR Nuclear magnetic resonance OR NMR	349,864	342,766
4	Hodgkin OR Lymphoma	170,373	114,531
5	Staging OR Stage OR Follow-up OR Remission OR Relapse OR Recurrence OR Progression OR Progressive	1,323,267	1,002,278
6	(#1 OR #2 OR #3) AND #4 AND #5	4,003	2,937

CT, FDG-PET, FDG-PET/CT fusion, or WB-MRI in staging or restaging of patients with histologically proven malignant lymphoma were included. Only studies, in which at least the area from the neck to the pelvis was imaged, were included. In oncology, histological proof of presence or absence of viable tumor is the most accurate reference test. However, in an often diffuse disease such as malignant lymphoma, surgical exploration of all possibly involved sites and subsequent histological examination is not possible for practical and ethical reasons. As there is no other gold standard, follow-up is required to validate or invalidate index test findings which could not be histologically verified. Therefore, we included only those studies which applied a clinico-radiological follow-up period of at least 6 months as the standard of reference in all patients. Studies performed in animals, review articles, meta-analyses, abstracts, editorials or letters, case reports, studies investigating 10 or fewer patients, tutorials, and guidelines for management were excluded. Studies which did not make a separate analysis for either initial staging or restaging of malignant lymphoma, and studies only dealing with the detection of bone marrow metastases in patients with malignant lymphoma were excluded. Studies investigating older generations of CT scanners (incremental, single-section, or dual-section CT), studies which examined FDG with a gamma camera in coincidence mode, and studies using low field scanners (<1.0 T) for WB-MRI were also excluded. Articles were rejected if they were clearly ineligible. At the second stage, the same researchers (T.C.K., R.M.K.) independently evaluated the full text version of all articles that were found to be potentially eligible for inclusion, using the same inclusion and exclusion criteria as mentioned above. If it was unclear from the information provided in a study as to whether all inclusion criteria were fulfilled and all exclusion criteria were absent, the study was excluded. Studies were only included if absolute numbers could be extracted to calculate confidence intervals for the reported estimates of diagnostic performance. When data or subsets of data

were presented in more than one article, the article with the most details or the most recent article was chosen.

At both stages, disagreements between the two researchers (T.C.K., R.M.K.) were discussed and resolved in a consensus meeting.

#### Study analysis

The methodological quality of the included studies was assessed in terms of the potential for bias (internal validity) and lack of generalizability (external validity). For this purpose, a checklist adapted from Kelly et al. [35] and Whiting et al. [36, 37] was used. The complete criteria list is presented in **Table 3**. Internal validity criteria and external validity scores were scored as positive (adequate methods) or negative (inadequate methods, potential bias). If insufficient information was provided on a specific item, a negative score was given. Two reviewers (T.C.K., R.M.K.) independently assigned the scores. Disagreements were discussed and resolved by consensus. Subtotals were calculated for internal (maximum seven) and external (maximum five) validity separately. Total quality scores were expressed as a percentage of the maximum score.

**Table 3.** Criteria list used to assess the methodological quality of the studies.

Criteria of validity	Positive score
<b>Internal validity</b>	
1. Prospective study	Mentioned in publication
2. Avoidance of incorporation bias	The index test did not form part of the reference test
3. Avoidance of diagnostic review bias	Blind interpretation of index test without knowledge of reference test
4. Avoidance of test review bias	Blind interpretation of reference test without knowledge of index test
5. Avoidance of comparator review bias	Blinding index test to the other imaging modality, if more than one imaging modality was applied
6. Minimum of withdrawal bias	< 10% of patients withdrew after the index test
7. Avoidance of study examination bias	< 10% of indeterminate or uninterpretable results
<b>External validity</b>	
1. Avoidance of patient filtering bias	Selection criteria described, age and sex of patients reported
2. Avoidance of spectrum bias	All stages of disease
3. Avoidance of selection bias	Consecutive series of patients
4. Standard execution of index test	Application of the same hardware and imaging protocol in all patients
5. Avoidance of observer variability bias	Interpreter(s) of index test described

Separate analyses were made for studies or subsets in studies investigating patients for initial staging (i.e. staging prior to any treatment) and studies or subsets in studies investigating patients for restaging (i.e. staging after treatment). Separate analyses

were also made for HD and NHL, where possible. Reported estimates of diagnostic performance, with corresponding 95% CIs, were calculated from the original numbers given in the included studies. Statistical analyses were executed using Statistical Package for the Social Sciences version 12.0 software (SPSS Inc, Chicago, IL).

## Results

### Literature search

The computer-aided search revealed 4,003 articles from PubMed/Medline and 2,973 articles from Embase (**Table 2**). Reviewing titles and abstracts from PubMed/Medline revealed 99 articles potentially eligible for inclusion. Reviewing titles and abstracts from Embase revealed 89 articles potentially eligible for inclusion, of which 88 were already identified by the PubMed/MEDLINE search. Thus, 100 studies remained for possible inclusion and were retrieved in full text version. After reviewing the full article, 81 articles were excluded, the majority (54%) because of the lack of an adequate standard of reference (**Table 4**). Eventually, 19 studies [38-56] met all inclusion and exclusion criteria, and they were included in this review. Screening references of these articles did not result in other potentially relevant articles. Of the 18 included studies,

**Table 4.** Reasons for exclusion of fulltext articles.

Reason of exclusion	No. of studies
Not all patients received an adequate reference test (clinico-radiological follow-up period of at least 6 months), or this was unclear	44
Only discrepant findings between the index test and conventional imaging procedure(s) were verified using a standard of reference	11
Absolute numbers to calculate confidence intervals for the reported estimates of diagnostic performance could not be extracted	7
The area from the neck to the pelvis was not imaged in all patients or it was unclear whether this was done	5
The prognostic value of interim FDG-PET in predicting treatment outcome was investigated	4
Ten or less patients with malignant lymphoma were included	3
Patients were not examined using a quad-section (or higher) multidetector-row CT scanner, or it was unclear whether this was done	3
Only patients with negative FDG-PET scans were included	1
Patients were examined using a dual-head gamma cameras in coincidence mode for FDG imaging	1
Prior FDG-PET studies were included in the interpretation of findings	1
No separate analysis was made of patients undergoing initial staging and patients undergoing restaging	1
<b>Total</b>	<b>81</b>

**Abbreviations:** CT: computed tomography; FDG: <sup>18</sup>F-fluoro-2-deoxyglucose; FDG-PET: <sup>18</sup>F-fluoro-2-deoxyglucose positron emission tomography



3 studies investigated CT, 17 studies investigated FDG-PET, and 3 studies investigated FDG-PET/CT fusion for staging malignant lymphoma. No eligible studies on WB-MRI were identified for inclusion. The characteristics of the included CT, FDG-PET, and FDG-PET/CT fusion studies are presented in **Tables 5 through 7**.

#### Methodological quality assessment

Methodological quality was assessed by 12 items. The scores for internal and external validity are presented in **Tables 8** (CT), **9** (FDG-PET), and **10** (FDG-PET/CT fusion). For the CT studies, the FDG-PET studies, and the FDG-PET/CT fusion studies, the total scores for combined internal and external validity, expressed as a fraction of the maximum score, ranged from 50% to 58% (median, 50%), from 42% to 58% (median, 50%), and from 50% to 67% (median, 54%), respectively.

#### Diagnostic performance

##### CT

Results of the 3 studies investigating CT [38-40] are displayed in **Table 11**. Only one study (separately) investigated patients with HD, with sensitivity and specificity of 87.5% and 85.6% (region-based) for initial staging, and sensitivity and specificity of 85.7% and 75.6% (region-based) for restaging, respectively [39].

The other two studies were performed in a mixture of patients with HD and NHL, with sensitivities of 25% and 100% (patient-based), and specificities of 41.7% and 58.8% (patient-based) for restaging, respectively [38, 40].

##### FDG-PET

Results of the 17 studies investigating FDG-PET [38-54] are displayed in **Table 12**. Nine studies (separately or exclusively) investigated patients with HD [38, 41-45, 50, 51, 54]. Only one study investigated FDG-PET for initial staging of HD, with sensitivity and specificity of 87.5% and 100% (lesion-based), respectively [54]. Sensitivities and specificities for restaging HD ranged between 85.0% (lesion-based) [54] and 100% (patient-based) [38, 41, 44, 50, 51], and between 57.1% (patient-based) [41] and 100% (patient-based) [43], respectively.

Five studies (separately or exclusively) investigated patients with NHL [46, 47, 50, 51, 54]. One study did not describe the histologic subtype(s) of NHL investigated [50], two studies investigated patients with both high-grade and low-grade NHL [46, 54], and two studies investigated patients with aggressive NHL [47, 51] (**Table 12**). Only one study investigated FDG-PET for initial staging of NHL (high-grade and low-grade), with sensitivity and specificity of 83.3% and 100% (lesion-based), respectively [54]. Sensitivities and specificities for restaging NHL ranged between 60.0% (patient-based) [47] and 100% (lesion-based) [54], and between 80.0% (patient-based) [50] and 100% (patient-based and lesion-based) [47, 51, 54], respectively.

The remaining six studies were performed in a mixture of patients with HD and



NHL. Sensitivity and specificity for initial staging approached 100% in the study of La Fougere et al. [39]. Sensitivities and specificities for restaging ranged between 71.4% (patient-based) [48, 52] and 100% (patient-based) [40], and between 86.2% (patient-based) [52] and 100% (patient-based) [49], respectively.

*FDG-PET/CT fusion*

Results of the 4 studies investigating FDG-PET/CT fusion [39, 49, 55, 56] are displayed in **Table 13**. Only one study (exclusively) investigated patients with HD, with sensitivity and specificity of 100% and 90.7% (patient-based) for restaging [55].

The other three studies were performed in a mixture of patients with HD and NHL. Sensitivity and specificity for initial staging approached 100% in the study of La Fougere et al. [39]. Sensitivities and specificities for restaging exceeded 90% (region-based and patient-based) [39, 49, 56].

Table 5. Characteristics of the 3 included studies investigating CT.

HD/NHL	Study and year	No. of patients/ scans	Mean or median age in years (range)	Sex (M/F)	Criteria for positivity	Interpreter(s)
<b>HD</b>	Rigacci et al. [38], 2005	28/28	30.6 (16-73)	14/14	Any mass above the limit of 1.5 cm in the longest diameter or any abnormalities that were not consistent with previous therapy	NR
<b>Mixed</b>	La Fougere et al. [39], 2006	50/50	NR (19-70)	24/26	-Anatomical abnormalities -Abnormal contrast enhancement patterns of solid organs -Lymph nodes with a short-axis diameter > 1.0 cm in the transverse plane, combined with abnormal contrast uptake or absence of hilar fatty degeneration	Two board-certified radiologists and nuclear medicine specialists with more than 10 years of experience in CT and PET
	Hernandez-Pampaloni et al. [40], 2006	16/21	NR	NR	-Suspected tumorous lesion -Lymph nodes with a short-axis diameter in the axial direction >15 mm in the axillary and iliac/inguinal regions and > 10 mm for the rest of the regions	An experienced pediatric radiologist

**Abbreviations:** CT: computed tomography; HD: Hodgkin's disease; NHL: non-Hodgkin's lymphoma; NR: not reported; PET: positron emission tomography

**Table 6.** Characteristics of the 17 included studies investigating FDG-PET.

HD/NHL	Study and year	No. of patients/ scans	Mean or median age in years (range)	Sex (M/F)	Criteria for positivity	Interpreter(s)
<b>HD</b>	Meany et al. [41], 2007	23/23	14.2 (5-19)	10/13	NR	NR
	Bjurberg et al. [42], 2006	26/34	NR (8-70)	NR	Any focus of elevated FDG metabolism not located in areas of normal FDG uptake or where the clinical data did not suggest the presence of non-malignant hypermetabolic lesions.	Two experienced investigators
	Zinzani et al. [43], 2006	40/40	32 (14-48)	19/21	Areas of focal uptake, unless they were at the sites of known accumulation, including the kidney and bladder, gastrointestinal tract, skeletal areas showing symmetric uptake (especially in the shoulder) were considered as due to arthritis	Three experienced readers
<b>NHL</b>	Rigacci et al. [38], 2005	28/28	30.6 (16-73)	14/14	Foci of hyperactivity outside areas of known physiologic uptake, in comparison with liver and mediastinum	NR
	Filmont et al. [44], 2004	32/32	30 (6-65)	15/17	NR	An experienced reader
	Dittmann et al. [45], 2001	47/47	NR (18-63)	27/20	Focally increased uptake, exceeding that of the surrounding tissue and/or contralateral body regions	Two experienced nuclear medicine physicians
	Filmont et al. [46], 2003	78/78	57 (21-84)	46/32	NR	An experienced reader
	Mikhaeel et al. [47], 2000	45/45	NR	NR	Residual increased FDG uptake in previously diagnosed disease sites or the appearance of new uptake indicative of progressive disease	Two nuclear medicine physicians

Table 6. Continued

HD/NHL	Study and year	No. of patients/ scans	Mean or median age in years (range)	Sex (M/F)	Criteria for positivity	Interpreter(s)
<b>Mixed</b>						
	La Fougere et al. [39], 2006	50/50	NR (19-70)	24/26	-Regions of focally increased tracer uptake -Well-circumscribed areas of tracer uptake in the liver -Focal lung lesions identifiable on both attenuation-corrected and non-corrected images -In doubtful cases a $SUV_{max} \geq 2.0$	Two board-certified radiologists and nuclear medicine specialists with more than 10 years of experience in CT and PET
	Hernandez-Pampaloni et al. [40], 2006	16/21	NR	NR	A focus of increased activity, not corresponding to the known physiological distribution of FDG	Two experienced nuclear medicine physicians
	Reinhardt et al. [48], 2005	101/101	NR	72/29	All foci of elevated FDG uptake	NR
	Freudenberg et al. [49], 2004	27/27	46 (19-70)	16/11	A $SUV_{max} \geq 2.5$ in an area of focal tracer uptake	Two experienced nuclear medicine physicians
	Mikosch et al. [50], 2003*	93/121	NR	NR	Residual tracer uptake	NR
	Mikhaeel et al. [51], 2000*	32/32	NR	22/10	Residual tracer uptake	Two independent nuclear medicine physicians
	Bangerter et al. [52], 1999	36/36	31 (17-74)	16/20	Any foci of increased FDG uptake over background value that were not located in an area of physiologically increased uptake	Two independent investigators
	Bangerter et al. [53], 1999	58/58	NR	NR	Any clearly delineated uptake in the hilar and mediastinal regions	Two nuclear medicine physicians
	Stumpe et al. [54], 1998*	50/71	NR (17-88)	31/19	A focus of increased FDG uptake above the intensity of the background as long as it was outside the renal pelvis, urinary bladder and myocardium	At least two board-certified nuclear medicine physicians

**Abbreviations:** CT: computed tomography; FDG: 18F-fluoro-2-deoxyglucose; FDG-PET: 18F-fluoro-2-deoxyglucose positron emission tomography; HD: Hodgkin's disease; NHL: non-Hodgkin's lymphoma; NR: not reported;  $SUV_{max}$ : maximum standardised uptake value

\*This study allowed separate analysis of HD and NHL patients

**Table 7.** Characteristics of the 4 included studies investigating FDG-PET/CT fusion.

HD/NHL	Study and year	No. of patients/ scans	Mean or median age in years (range)	Sex (M/F)	Criteria for positivity	Interpreter(s)
<b>HD</b>	Schaefer et al. [55], 2007	66/66	35 (11-76)	46/20	NR	Two board-certified nuclear medicine physicians (6 and 3 years of PET experience) and two board-certified radiologists (10 and 6 years of CT experience)
<b>Mixed</b>	La Fougere et al. [39], 2006	50/50	59 (29-70)	40/10	A combination of the criteria mentioned in Tables 5 and 6 for this study	Two board-certified radiologists and nuclear medicine specialists with more than 10 years of experience in CT and PET
	Rhodes et al. [56], 2006	41/247	13 (3-18)	23/18	-Nonphysiologic focal FDG uptake -FDG uptake equal to or greater than that seen in the liver corresponding to a lymph node or abnormality on simultaneously performed diagnostic CT scan	NR
	Freudenberg et al. [49], 2004	27/27	46 (19-70)	16/11	A SUV <sub>max</sub> ≥2.5 in an area of focal tracer uptake and lymph nodes with a diameter >15 mm in the groin or >10 mm in all other regions	Two experienced nuclear medicine physicians and two radiologists

**Abbreviations:** HD: Hodgkin's disease; NHL: non-Hodgkin's lymphoma

**Table 8.** Quality assessment of the 3 included studies investigating CT.

Study and year	Criteria										Total scores			% of maximum score (IV and EV)	
	IV					EV					IV	EV	IV + EV		
	1	2	3	4	5	6	7	1	2	3					4
Rigacci et al. [38], 2005	+	-	-	-	-	+	+	-	+	+	+	-	3	3	50
La Fougere et al. [39], 2006	-	-	-	-	+	+	+	-	+	+	-	+	3	3	50
Hernandez-Pampaloni et al. [40], 2006	-	+	-	+	+	+	+	-	+	+	+	+	4	3	58

**Abbreviations:** IV: internal validity; EV: external validity

**Table 9.** Quality assessment of the 17 included studies investigating FDG-PET.

Study and year	Criteria										Total scores			% of maximum score (IV and EV)	
	IV					EV					IV	EV	IV + EV		
	1	2	3	4	5	6	7	1	2	3					4
Meany et al. [41], 2007	-	-	-	-	-	+	+	-	+	+	+	-	2	3	42
Bjurlberg et al. [42], 2006	-	-	-	-	-	+	+	-	+	+	+	-	2	3	42
Zinzani et al. [43], 2006	+	-	-	-	-	+	+	-	+	+	+	-	3	2	42
Rigacci et al. [38], 2005	+	-	-	-	-	+	+	-	+	+	+	-	3	3	50
Filmont et al. [44], 2004	-	-	+	-	+	+	+	+	+	+	-	-	4	3	58
Dittmann et al. [45], 2001	-	-	-	-	+	+	+	+	+	+	+	+	3	4	58
Filmont et al. [46], 2003	-	-	+	-	+	+	+	+	+	+	-	-	4	3	58
Mikhaeel et al. [47], 2000	-	-	-	-	+	+	+	-	+	+	+	+	3	3	50
La Fougere et al. [39], 2006	-	-	-	-	+	+	+	-	+	+	+	+	3	3	50
Hernandez-Pampaloni et al. [40], 2006	-	+	-	+	+	+	+	-	+	+	-	+	4	2	50
Reinhardt et al. [48], 2005	-	-	-	-	+	+	+	-	+	+	+	-	2	3	42
Freudenberg et al. [49], 2004	-	-	-	-	+	+	+	-	+	+	+	+	3	3	50
Mikosch et al. [50], 2003	-	+	-	-	+	+	+	-	+	+	+	-	4	2	50
Mikhaeel et al. [51], 2000	-	-	-	-	+	+	+	-	+	+	+	+	2	3	42
Bangerter et al. [52], 1999	+	-	+	-	+	+	+	+	+	+	+	-	4	3	58
Bangerter et al. [53], 1999	-	-	-	-	+	+	+	-	+	+	+	+	2	3	42
Stumpe et al. [54], 1998	-	-	-	-	+	+	+	-	+	+	+	+	2	3	42

**Abbreviations:** IV: internal validity; EV: external validity

**Table 10.** Quality assessment of the 4 included studies investigating FDG-PET/CT fusion.

Study and year	Criteria										Total scores		% of maximum score (IV and EV)		
	IV										IV	EV			
	1	2	3	4	5	6	7	1	2	3	4	5	IV	EV	
Schaefer et al. [55], 2007	-	-	-	-	+	+	+	+	+	+	+	+	3	5	67
La Fougere et al. [39], 2006	-	-	-	-	+	+	+	-	+	+	-	+	3	3	50
Rhodes et al. [56], 2006	-	-	-	-	+	+	-	+	+	+	+	+	2	5	58
Freudenberg et al. [49], 2004	-	-	-	-	+	+	+	-	+	-	+	+	3	3	50

**Abbreviations:** IV: internal validity; EV: external validity

**Table 11.** Results of the 3 included studies investigating CT.

HD/NHL	Study and year	Scoring system	Initial staging		Restaging	
			Sensitivity (95% CI)	Specificity (95% CI)	Sensitivity (95% CI)	Specificity (95% CI)
HD	La Fougere et al. [39], 2006	Region-based analysis (7 pre-defined regions)	87.5% (75.3-94.1)	85.6% (78.0-91.2)	85.7% (68.5-94.3)	75.6% (68.6-81.5)
Mixed	Hernandez-Pampaloni et al. [40], 2006	Patient-based analysis	-	-	100% (51.0-100)	58.8% (36.0-78.4)
	Rigacci et al. [38], 2005	Patient-based analysis	-	-	25% (4.6-70.0)	41.7% (24.5-61.2)

Table 12. Results of the 17 included studies investigating FDG-PET.

HD/NHL	Study and year	Scoring system	Initial staging Sensitivity (95% CI)	Specificity (95% CI)	Restaging Sensitivity (95% CI)	Specificity (95% CI)
<b>HD</b>	Meany et al. [41], 2007	Patient-based analysis	-	-	100% (34.2-100)	57.1% (36.6-75.5)
	Bjurlberg et al. [42], 2006	Patient-based analysis	-	-	91.7% (64.6-98.5)	95.2% (77.3-99.2)
	Zinzani et al. [43], 2006	Patient-based analysis	-	-	87.5% (52.9-97.8)	100% (89.0-100)
	Rigacci et al. [38], 2005	Patient-based analysis	-	-	100% (51.0-100)	83.3% (64.2-93.3)
	Filmont et al. [44], 2004	Patient-based analysis	-	-	100% (74.1-100)	85.7% (65.4-95.0)
	Mikosch et al. [50], 2003	Patient-based analysis	-	-	100% (87.1-100)	81.8% (65.6-91.4)
	Dirtmann et al. [45], 2001	Patient-based analysis	-	-	86.2% (69.4-94.5)	94.4% (74.2-99.0)
	Mikhaeel et al. [51], 2000	Patient-based analysis	-	-	100% (43.9-100)	91.7% (64.6-98.5)
	Stumpe et al. [54], 1998	Lesion-based analysis	87.5% (52.9-97.8)	100% (34.2-100)	85.0% (64.0-94.8)	95.7% (79.0-99.2)
	<b>NHL</b>	a Mikosch et al. [50], 2003	Patient-based analysis	-	-	81.5% (63.3-91.8)
b Filmont et al. [46], 2003		Patient-based analysis	-	-	87.0% (74.3-93.9)	93.8% (79.9-98.3)
c Mikhaeel et al. [47], 2000		Patient-based analysis	-	-	60.0% (35.8-80.2)	100% (88.7-100)
d Mikhaeel et al. [51], 2000		Patient-based analysis	-	-	71.4% (35.9-91.8)	100% (72.3-100)
e Stumpe et al. [54], 1998		Lesion-based analysis	83.3% (43.7-97.0)	100% (20.7-100)	100% (43.9-100)	100% (67.6-100)
<b>Mixed</b>	La Fougere et al. [39], 2006	Region-based analysis (7 pre-defined regions)	97.9% (89.1-99.6)*	98.1% (93.4-99.5)*	96.4% (82.3-99.4)*	99.4% (96.7-99.9)*
	Hernandez-Pampaloni et al. [40], 2006	Patient-based analysis	100% (87.5-100)**	100% (93.7-100)**	97.3% (90.8-99.3)**	98.4% (95.5-99.5)**
	Reinhardt et al. [48], 2005	Patient-based analysis	-	-	100% (51.0-100)	88.2% (65.7-96.7)
	Freudenberg et al. [48], 2004	Region-based analysis (5 predefined regions)	-	-	71.4% (52.9-84.8)	94.5% (86.7-97.9)
	Bangerter et al. [52], 1999	Patient-based analysis	-	-	78.3% (58.1-90.3)	98.2% (93.7-99.5)
	Bangerter et al. [53], 1999	Patient-based analysis	-	-	85.7% (60.1-96.0)	100% (77.2-100)
	Bangerter et al. [53], 1999	Patient-based analysis	-	-	71.4% (35.9-91.8)	86.2% (69.4-94.5)
	Bangerter et al. [53], 1999	Patient-based analysis	-	-	85.7% (48.7-97.4)	96.1% (86.8-98.9)

**Abbreviations:** HD: Hodgkin's disease; NHL: non-Hodgkin's lymphoma

**Notes:** \* Dedicated PET-scanner; \*\* FDG-PET portion of a combined FDG-PET/CT examination; **a**) Histologic subtype(s) of NHL not described; **b**) High-grade NHL in 51 patients; low-grade NHL in 11 patients, and unknown histological grade in 16 patients; **c**) All patients had aggressive NHL (diffuse mixed, diffuse large-cell, or large-cell immunoblastic lymphoma); **d**) Aggressive histology NHL (diffuse mixed, diffuse large-cell, and large-cell immunoblastic lymphoma); **e**) Nine with high-grade and six with low-grade NHL



**Table 13.** Results of the 4 included studies investigating FDG-PET/CT fusion.

HD/NHL	Study and year	Scoring system		Initial staging		Restaging	
		Sensitivity (95% CI)	Specificity (95% CI)	Sensitivity (95% CI)	Specificity (95% CI)	Sensitivity (95% CI)	Specificity (95% CI)
HD	Schaefer et al. [55], 2007	-	-	-	-	100% (85.7-100)**	90.7% (78.4-96.3)**
	La Fougere et al. [39], 2006	97.9% (89.1-99.6)*	100% (97.7-100)*	96.4% (82.3-99.4)*	100% (97.8-100)**	97.3% (90.8-99.3)**	99.5% (97.1-99.9)**
Mixed	Rhodes et al. [56], 2006	100% (87.5-100)**	100% (93.7-100)**	94.7% (75.4-99.1)***	-	91.3% (73.2-97.6)*	90.6% (85.3-94.1)***
		-	-	-	-	95.7% (79.0-99.2)**	99.1% (95.1-99.8)**
	Freudenberg et al. [49], 2004	-	-	-	-	92.9% (68.5-98.7)*	100% (77.2-100)**
	Patient-based analysis	-	-	-	-	92.9% (68.5-98.7)**	100% (77.2-100)**

**Abbreviations:** HD: Hodgkin's disease, NHL: non-Hodgkin's lymphoma

**Notes:** \* Side-by-side assessment of separately obtained CT and FDG-PET images; \*\* Hardware-oriented approach to image fusion; combined PET/CT; \*\*\* Both \* and \*\* were available

## Discussion

This systematic review included 19 studies, of which 3 studies investigated CT, 17 studies investigated FDG-PET, and 4 studies investigated FDG-PET/CT fusion for initial staging and/or restaging of malignant lymphoma. No WB-MRI studies were found eligible for inclusion. The number of included studies investigating CT, FDG-PET, or FDG-PET/CT fusion for initial staging of malignant lymphoma was scarce. Many of the included studies did not separately analyze HD and NHL patients, and/or mixed different histologic subtypes of NHL. Results of individual studies could not be meta-analyzed, because different scoring systems were used. Furthermore, none of the studies expressed their results according to the Ann Arbor staging system, which limits estimation of the therapeutic impact of each imaging modality.

The included studies had moderate methodological quality. Only one CT study was performed in a prospective fashion, and only one study explicitly mentioned that CT images were interpreted without knowledge of the reference test. None of the CT studies adequately described selection criteria, age, and sex of patients. Only 18% of the included FDG-PET studies was conducted prospectively, and only 29% of the studies explicitly mentioned that FDG-PET was interpreted without knowledge of the reference test. Up to 59% of the FDG-PET studies was potentially threatened by comparator review bias. Selection criteria, age and sex of patients were adequately described in only 24% of the FDG-PET studies. None of the FDG-PET/CT fusion studies was prospectively executed, and none of the studies explicitly mentioned that FDG-PET/CT fusion was interpreted without knowledge of the reference test. Selection criteria, age, and sex of patients were adequately described in only two FDG-PET/CT fusion studies. In addition, all CT, FDG-PET, and FDG-PET/CT fusion studies used follow-up as the standard of reference. As a consequence, incorporation bias and/or test review bias could have been present in almost all studies.

CT is the most commonly used imaging modality for staging malignant lymphoma because of its widespread availability and relatively low cost. The exact values of FDG-PET, FDG-PET/CT fusion, and WB-MRI in comparison to CT for initial staging of HD and NHL have not been determined yet. Therefore, CT remains the standard imaging modality for initial staging of malignant lymphoma. An important drawback of CT is its failure to detect pathologic changes in normal-sized structures and to detect lesions which have poor contrast with surrounding tissue. Another weakness of CT is that it is not reliable in the detection of bone marrow disease, which, if present, by definition indicates stage IV disease [16]. Furthermore, CT may not be able to differentiate residual viable tumor tissue from therapy-induced fibrosis; the three CT studies included in this review indeed reported a low to moderate specificity in restaging malignant lymphoma (**Table 11**) [39, 40]. Comparing current with previous CT scans may improve diagnostic reliability. Nevertheless, the utility of CT alone in

restaging malignant lymphoma can be limited. Another disadvantage of CT is exposure of the patient to ionizing radiation, which may induce second cancers. Each CT scan, covering the neck, thorax, abdomen, and pelvis, is associated with an effective dose of approximately 20-25 mSv [57, 58]. The Food and Drug Administration estimates that a CT examination with an effective dose of 10 mSv may be associated with an increased risk of developing fatal cancer for approximately one in 2000 patients, and the Biological Effects of Ionizing Radiation VII lifetime risk model predicts that with the same effective dose of 10 mSv, approximately one individual in 1000 will develop cancer [57, 58]. In patients with malignant lymphoma, imaging will repetitively be performed during follow-up, thereby increasing the risk [59]. This health risk caused by ionizing radiation is especially of concern in children, because they have a higher radiosensitivity than adults and they have more years ahead in which cancerous changes might occur [57]. In the present era, where HD can be cured in at least 80% of patients [3] and similar proceedings have been achieved in the treatment of certain types of NHLs [60, 61], prevention of second malignancies due to CT radiation is an important issue. Another disadvantage of CT is the administration of iodinated contrast agents, which may cause adverse reactions including rarely occurring but life-threatening contrast-induced nephrotoxicity and anaphylactic shock [62].

The main advantage of FDG-PET over anatomical imaging techniques, such as CT, is its ability to detect metabolic changes in areas involved with malignant lymphoma before structural changes become visible. A pretreatment FDG-PET scan may identify additional cases of focal bone marrow involvement that would be missed by bone marrow biopsy or CT. However, it is not clear yet whether this complementary information affects patient prognosis and is cost-effective [63]. It is also likely that FDG-PET surpasses CT in differentiating residual viable tumor tissue from therapy-induced fibrosis. Indeed, accuracy of FDG-PET in restaging of malignant lymphoma seems to be higher than that of CT (Tables 11 and 12). Routinely FDG avid malignant lymphomas (HD, diffuse large B-cell lymphoma, follicular lymphoma, and mantle cell lymphoma) are well visualized, both in initial staging and restaging [64, 65]. However, some subtypes of NHL, predominantly low-grade lymphomas, may have low or even no uptake of FDG. Nodal and extranodal marginal zone lymphomas [64-71], small lymphocytic lymphomas [64, 68, 72, 73], primary duodenal follicular lymphoma [64, 74], cutaneous T-cell lymphomas [64, 75], and peripheral T-cell lymphomas [65] have all been reported to be possibly FDG negative. Caution is warranted in these histologic subtypes of NHL because a negative FDG-PET scan does not necessarily rule out disease; complimentary anatomical imaging (CT or MRI) is mandatory to increase detection rate of lesions. It is also considered mandatory to perform a pre-treatment FDG-PET scan in these variably FDG avid NHLs; comparison of a post-treatment FDG-PET scan to a pre-treatment FDG-PET scan will lead to more accurate restaging [76]. Gastric marginal zone mucosa-associated lymphoid tissue (MALT)

lymphoma constitutes a special group and may not be visualized with either CT or FDG-PET [77]. In this instance, endoscopy and/or endoscopic ultrasonography may be of value. The included studies in this systematic review mixed patients with HD and NHL and/or mixed different histologic subtypes of NHL. Therefore, more studies are needed to determine the diagnostic performance of FDG-PET in staging the different histologic subtypes of NHL. A major drawback of FDG-PET is its lack of detailed anatomic information, which impedes precise localization of sites with FDG uptake and identification of other clinical problems such as spinal cord compression and ureteral, biliary, or central venous obstruction. Another disadvantage of FDG-PET is the possibility of FDG uptake in benign conditions with increased glycolysis such as infection, inflammation, and granulomatous disease. Additionally, high physiological uptake within the brain, myocardium, gastrointestinal tract, urinary tract, muscle, brown adipose tissue, salivary glands, lymphoid tissue, axillary skinfolds, apocrine sweat glands, and thymus may obscure or mimic the presence of tumour deposits. Caution is also warranted in patients receiving chemotherapy in conjunction with cytokines, such as granulocyte(-macrophage) colony stimulating factor, because these patients may have increased bone marrow FDG uptake up to 3 weeks after the last dose of cytokines. Another pitfall is that any process that stimulates the bone marrow, including bone marrow hyperplasia in HD or bone marrow hyperplasia as a consequence of recovery from a chemotherapeutic insult, may also result in increased FDG uptake. Similar effects can be seen in the spleen [78-80]. A careful evaluation of FDG-PET findings, along with an accurate patient's history and clinical examination is necessary to minimize the number of false positive interpretations. Another disadvantage of FDG-PET is exposure of the patient to ionizing radiation; the effective dose is approximately 3.3-7.6 mSv per examination [58].

FDG-PET/CT fusion, using a combined PET/CT scanner, allows more accurate localization of foci with increased FDG uptake than stand-alone PET, and this may reduce the problems of physiological FDG uptake being misinterpreted as pathological and false localization of disease. An additional advantage of combined PET/CT is the use of the CT images for attenuation correction of the PET emission data, which reduces whole-body scanning times by 25-40% to 30 minutes or less. This approach also provides low-noise attenuation correction factors, compared with those from standard PET transmission measurements using an external radiation source, and eliminates bias from emission contamination of postinjection transmission scans. A pitfall of CT-based attenuation correction, however, is that the use of concentrated CT contrast agents, CT beam-hardening artifacts due to metallic implants, and physiologic motion can result in alterations of standardized uptake values of lesions or in the appearance of artifactual lesions. Images without attenuation correction should also be evaluated to avoid misinterpretations [7, 8]. The limited evidence suggests FDG-PET/CT fusion to be superior to CT alone and FDG-PET alone in initial staging and

restaging of malignant lymphoma. However, more well-designed studies are needed to establish the additional value of FDG-PET/CT fusion compared to CT alone and FDG-PET alone in initial staging and restaging of malignant lymphoma. Future studies should also investigate whether the accuracy of FDG-PET/CT fusion is reproducible among the different histologic subtypes of malignant lymphoma. Radiation dose is a point of concern in FDG-PET/CT fusion. Although the CT portion of a PET/CT scan is usually performed at different settings than a standard diagnostic CT to decrease the radiation burden, the effective dose is still on the order of 25 mSv per examination [57, 81].

WB-MRI is a feasible technique for staging malignant lymphoma [82, 83]. However, no eligible WB-MRI studies were identified for inclusion in this systematic review. Large prospective trials are needed to determine the value of WB-MRI. WB-MRI may be of particular value for the assessment of bone marrow involvement [84]. In contrast to CT, FDG-PET, and FDG-PET/CT fusion, WB-MRI has the advantage of not exposing the patient to ionizing radiation, which is especially important in children. In addition, the safety profile of magnetic resonance contrast agents is favourable when compared with that of iodinated contrast with CT [85]. However, WB-MRI cannot be performed in patients with pacemakers, defibrillators, or other implanted electronic devices, and in case of claustrophobia. Other disadvantages of conventional (anatomical) WB-MRI are the lack of functional information which may result in failure to detect pathologic changes in normal-sized structures, and the large amounts of image data obtained which may result in the possibility of overlooking subtle pathological findings. Last mentioned drawbacks, however, may be overcome with recently developed functional WB-MRI techniques, such as diffusion-weighted imaging. Diffusion-weighted imaging highlights areas with restricted diffusion, such as occurs in many malignant tumors, including malignant lymphoma [86-88]. Additionally, superparamagnetic iron oxide nanoparticles, which are MRI-specific lymphographic agents, are currently under investigation and can potentially play a role in staging of malignant lymphoma by identifying involved lymph nodes independently of lymph node size [89].

Data on the cost-effectiveness of CT, FDG-PET, FDG-PET/CT fusion, and WB-MRI in staging malignant lymphoma are lacking. Only Klose et al. [90] attempted to address this issue and found an incremental cost-effectiveness ratio of FDG-PET versus CT of 3133 euros per correctly staged patient, in initial staging of malignant lymphoma [90]. However, this study included only a small number of patients, mixed patients with HD and NHL, did not apply an appropriate standard of reference in all patients, and did not take into account long-term patient outcomes [90].

In conclusion, the studies included in this systematic review were of moderate methodological quality and used different scoring systems to stage malignant lymphoma. CT remains the standard imaging modality for initial staging of malignant lymphoma, while FDG-PET has an essential role in restaging. Early results suggest

that FDG-PET/CT fusion outperforms both CT alone and FDG-PET alone. Data on the diagnostic performance of WB-MRI are lacking. Future well-designed studies, expressing their results according to the Ann Arbor staging system, are needed to determine which imaging modality is most accurate and cost-effective in staging malignant lymphoma.

## References

1. Jemal A, Siegel R, Ward E, Murray T, Xu J, Thun MJ. Cancer statistics, 2007. *CA Cancer J Clin* 2007;57:43-66
2. Armitage JO. Staging non-Hodgkin lymphoma. *CA Cancer J Clin* 2005;55:368-376
3. Connors JM. State-of-the-art therapeutics: Hodgkin's lymphoma. *J Clin Oncol* 2005;23:6400-6408
4. Lister TA, Crowther D, Sutcliffe SB, et al. Report of a committee convened to discuss the evaluation and staging of patients with Hodgkin's disease: Cotswolds meeting. *J Clin Oncol* 1989;7:1630-1636
5. Jhanwar YS, Straus DJ. The role of PET in lymphoma. *J Nucl Med*. 2006;47:1326-1334
6. Rohren EM, Turkington TG, Coleman RE. Clinical applications of PET in oncology. *Radiology* 2004;231:305-332
7. Blodgett TM, Meltzer CC, Townsend DW. PET/CT: form and function. *Radiology* 2007;242:360-385
8. Von Schulthess GK, Steinert HC, Hany TF. Integrated PET/CT: current applications and future directions. *Radiology* 2006;238:405-422
9. Lauenstein TC, Semelka RC. Emerging techniques: whole-body screening and staging with MRI. *J Magn Reson Imaging* 2006;24:489-498
10. Ladd SC, Zenge M, Antoch G, Forsting M. Whole-body MR diagnostic concepts. *Rofo* 2006;178:763-770
11. Rosenberg SA, Boiron M, DeVita VT Jr, et al. Report of the Committee on Hodgkin's Disease Staging Procedures. *Cancer Res* 1971;31:1862-1863
12. Kreef L. The EMI whole body scanner in the demonstration of lymph node enlargement. *Clin Radiol* 1976;27:421-429
13. Prokop M. Multislice CT: technical principles and future trends. *Eur Radiol* 2003;13 Suppl 5:S3-S13
14. Rydberg J, Buckwalter KA, Caldemeyer KS, et al. Multisection CT: scanning techniques and clinical applications. *Radiographics* 2000; 20:1787-1806
15. Lucey BC, Stuhlfaut JW, Soto JA. Mesenteric lymph nodes: detection and significance on MDCT. *AJR Am J Roentgenol* 2005;184:41-44
16. Vinnicombe SJ, Reznick RH. Computerised tomography in the staging of Hodgkin's disease and non-Hodgkin's lymphoma. *Eur J Nucl Med Mol Imaging* 2003;30 Suppl 1:S42-S55
17. Phelps ME, Hoffman EJ, Mullani NA, Ter-Pogossian MM. Application of annihilation coincidence detection to transaxial reconstruction tomography. *J Nucl Med* 1975;16:210-224
18. Paul R. Comparison of fluorine-18-2-fluorodeoxyglucose and gallium-67 citrate imaging for detection of lymphoma. *J Nucl Med* 1987;28:288-292
19. Moog F, Bangerter M, Diederichs CG, et al. Lymphoma: role of whole-body 2-deoxy-2-[F-18]fluoro-D-glucose (FDG) PET in nodal staging. *Radiology* 1997;203:795-800
20. De Wit M, Bumann D, Beyer W, Herbst K, Clausen M, Hossfeld DK. Whole-body positron emission tomography (PET) for diagnosis of residual mass in patients with lymphoma. *Ann Oncol* 1997;8 Suppl 1:S57-S60
21. Bangerter M, Griesshammer M, Binder T, et al. New diagnostic imaging procedures in Hodgkin's disease. *Ann Oncol* 1996;7 Suppl 4:S55-S59
22. Barrington SF, Carr R. Staging of Burkitt's lymphoma and response to treatment monitored by PET scanning. *Clin Oncol (R Coll Radiol)* 1995;7:334-335

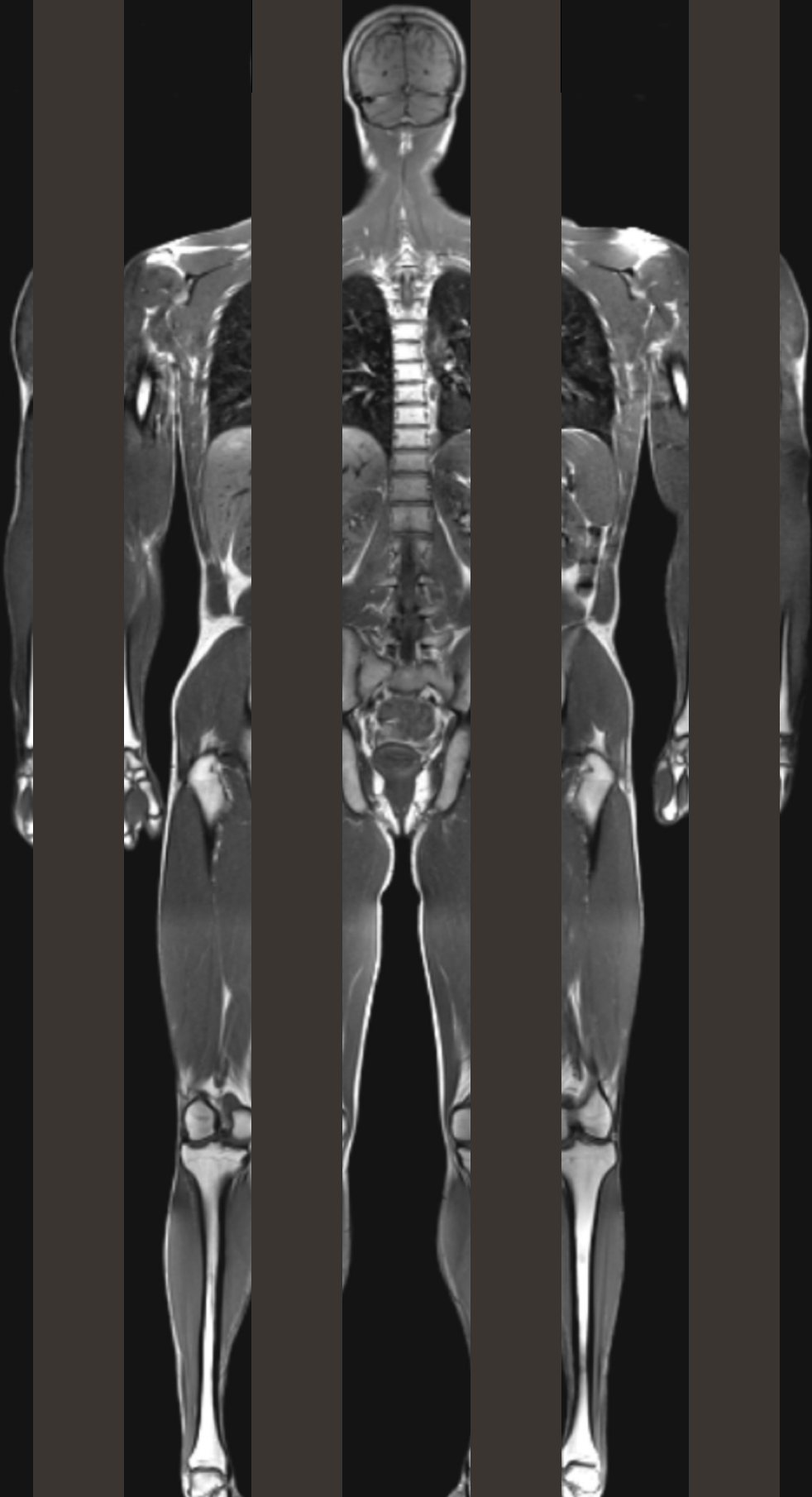
23. Zhang H, Tian M, Oriuchi N, Higuchi T, Tanada S, Endo K. Oncological diagnosis using positron coincidence gamma camera with fluorodeoxyglucose in comparison with dedicated PET. *Br J Radiol* 2002;75:409-416
24. Tatsumi M, Kitayama H, Sugahara H, et al. Whole-body hybrid PET with 18F-FDG in the staging of non-Hodgkin's lymphoma. *J Nucl Med* 2001;42:601-608
25. Boren EL Jr, Delbeke D, Patton JA, Sandler MP. Comparison of FDG PET and positron coincidence detection imaging using a dual-head gamma camera with 5/8-inch NaI(Tl) crystals in patients with suspected body malignancies. *Eur J Nucl Med* 1999;26:379-387
26. Shreve PD, Steventon RS, Deters EC, Kison PV, Gross MD, Wahl RL. Oncologic diagnosis with 2-[fluorine-18] fluoro-2-deoxy-D-glucose imaging: dual-head coincidence gamma camera versus positron emission tomographic scanner. *Radiology* 1998;207:431-437
27. Wahl RL. To AC or not to AC: that is the question. *J Nucl Med* 1999;40:2025-2028
28. Kellogg GJ, Sullivan DM, Wilson W, et al. FDG-PET Lymphoma Demonstration Project Invitational Workshop. *Acad Radiol* 2007;14:330-339
29. Coleman M, Kostakoglu L. Early 18F-labeled fluoro-2-deoxy-D-glucose positron emission tomography scanning in the lymphomas: changing the paradigms of treatments? *Cancer* 2006;107:1425-1428
30. Gallamini A, Hutchings M, Rigacci L, et al. Early interim 2-[18F]fluoro-2-deoxy-D-glucose positron emission tomography is prognostically superior to international prognostic score in advanced-stage Hodgkin's lymphoma: a report from a joint Italian-Danish study. *J Clin Oncol* 2007;25:3746-3752
31. Damadian R. Field focusing n.m.r. (FONAR) and the formation of chemical images in man. *Philos Trans R Soc Lond B Biol Sci* 1980;289:489-500
32. Lauterbur PC. Progress in n.m.r. zeugmatography imaging. *Philos Trans R Soc Lond B Biol Sci* 1980;289:483-487
33. Schmidt GP, Wintersperger B, Graser A, Baur-Melnyk A, Reiser MF, Schoenberg SO. High-resolution whole-body magnetic resonance imaging applications at 1.5 and 3 Tesla: a comparative study. *Invest Radiol* 2007;42:449-459
34. Schick F. Whole-body MRI at high field: technical limits and clinical potential. *Eur Radiol* 2005;15:946-959
35. Kelly S, Berry E, Roderick P, et al. The identification of bias in studies of the diagnostic performance of imaging modalities. *Br J Radiol* 1997;70:1028-1035
36. Whiting P, Rutjes AW, Reitsma JB, Bossuyt PM, Kleijnen J. The development of QUADAS: a tool for the quality assessment of studies of diagnostic accuracy included in systematic reviews. *BMC Med Res Methodol* 2003;3:25
37. Whiting PF, Weswood ME, Rutjes AW, Reitsma JB, Bossuyt PN, Kleijnen J. Evaluation of QUADAS, a tool for the quality assessment of diagnostic accuracy studies. *BMC Med Res Methodol* 2006;6:9
38. Rigacci L, Castagnoli A, Dini C, et al. 18FDG-positron emission tomography in post treatment evaluation of residual mass in Hodgkin's lymphoma: long-term results. *Oncol Rep* 2005;14:1209-1214
39. La Fougere C, Hundt W, Brockel N, et al. Value of PET/CT versus PET and CT performed as separate investigations in patients with Hodgkin's disease and non-Hodgkin's lymphoma. *Eur J Nucl Med Mol Imaging* 2006;33:1417-1425
40. Hernandez-Pampaloni M, Takalkar A, Yu JQ, Zhuang H, Alavi A. F-18 FDG-PET imaging and correlation with CT in staging and follow-up of pediatric lymphomas. *Pediatr Radiol* 2006;36:524-531



41. Meany HJ, Gidvani VK, Minniti CP. Utility of PET scans to predict disease relapse in pediatric patients with Hodgkin lymphoma. *Pediatr Blood Cancer* 2007;48:399-402
42. Bjurberg M, Gustavsson A, Ohlsson T, Brun E. FDG-PET in the detection of residual disease and relapse in patients with Hodgkin's lymphoma. Experience from a Swedish centre. *Acta Oncol* 2006;45:743-749
43. Zinzani PL, Tani M, Fanti S, et al. Early positron emission tomography (PET) restaging: a predictive final response in Hodgkin's disease patients. *Ann Oncol* 2006;17:1296-1300
44. Filmont JE, Yap CS, Ko F, et al. Conventional imaging and 2-deoxy-2-[(18)F]fluoro-D-glucose positron emission tomography for predicting the clinical outcome of patients with previously treated Hodgkin's disease. *Mol Imaging Biol* 2004;6:47-54
45. Dittmann H, Sokler M, Kollmannsberger C, et al. Comparison of 18FDG-PET with CT scans in the evaluation of patients with residual and recurrent Hodgkin's lymphoma. *Oncol Rep* 2001;8:1393-1399
46. Filmont JE, Vranjesevic D, Quon A, et al. Conventional imaging and 2-deoxy-2-[18F]fluoro-D-glucose positron emission tomography for predicting the clinical outcome of previously treated non-Hodgkin's lymphoma patients. *Mol Imaging Biol* 2003;5:232-239
47. Mikhaeel NG, Timothy AR, O'Doherty MJ, Hain S, Maisey MN. 18-FDG-PET as a prognostic indicator in the treatment of aggressive Non-Hodgkin's Lymphoma-comparison with CT. *Leuk Lymphoma* 2000;39:543-553
48. Reinhardt MJ, Herkel C, Althoefer C, Finke J, Moser E. Computed tomography and 18F-FDG positron emission tomography for therapy control of Hodgkin's and non-Hodgkin's lymphoma patients: when do we really need FDG-PET? *Ann Oncol* 2005;16:1524-1529
49. Freudenberg LS, Antoch G, Schutt P, et al. FDG-PET/CT in re-staging of patients with lymphoma. *Eur J Nucl Med Mol Imaging* 2004;31:325-329
50. Mikosch P, Gallowitsch HJ, Zinke-Cerwenka W, et al. Accuracy of whole-body 18F-FDP-PET for restaging malignant lymphoma. *Acta Med Austriaca* 2003;30:41-47
51. Mikhaeel NG, Timothy AR, Hain SF, O'Doherty MJ. 18-FDG-PET for the assessment of residual masses on CT following treatment of lymphomas. *Ann Oncol* 2000;11 Suppl 1:S147-S150
52. Bangerter M, Moog F, Griesshammer M, et al. Role of whole body FDG-PET imaging in predicting relapse of malignant lymphoma in patients with residual masses after treatment. *Radiography* 1999;5:155-163
53. Bangerter M, Kotzerke J, Griesshammer M, Elsner K, Reske SN, Bergmann L. Positron emission tomography with 18-fluorodeoxyglucose in the staging and follow-up of lymphoma in the chest. *Acta Oncol* 1999;38:799-804.
54. Stumpe KD, Urbinelli M, Steinert HC, Glanzmann C, Buck A, von Schulthess GK. Whole-body positron emission tomography using fluorodeoxyglucose for staging of lymphoma: effectiveness and comparison with computed tomography. *Eur J Nucl Med* 1998;25:721-728
55. Schaefer NG, Taverna C, Strobel K, Wastl C, Kurrer M, Hany TF. Hodgkin disease: diagnostic value of FDG PET/CT after first-line therapy – is biopsy of FDG-avid lesions still needed? *Radiology* 2007;244:257-262
56. Rhodes MM, Delbeke D, Whitlock JA, et al. Utility of FDG-PET/CT in follow-up of children treated for Hodgkin and non-Hodgkin lymphoma. *J Pediatr Hematol Oncol* 2006;28:300-306
57. Semelka RC, Armao DM, Elias J Junior, Huda W. Imaging strategies to reduce the risk of radiation in CT studies, including selective substitution with MRI. *J Magn Reson Imaging* 2007;25:900-909

58. Barentsz J, Takahashi S, Oyen W, et al. Commonly used imaging techniques for diagnosis and staging. *J Clin Oncol* 2006;24:3234-3244
59. Executive Summary Board on Radiation Effects Research – Division on Earth and Life Studies editor. *Health Risks from Exposure to Low Levels of Ionizing Radiation: BEIR VII – Phase 2*. Washington, DC: National Academy Press; 2005
60. Ansell SM, Armitage J. Non-Hodgkin lymphoma: diagnosis and treatment. *Mayo Clin Proc* 2005;80:1087-1097
61. Hennessy BT, Hanrahan EO, Daly PA. Non-Hodgkin lymphoma: an update. *Lancet Oncol* 2004;5:341-353
62. Namasivayam S, Kalra MK, Torres WE, Small WC. Adverse reactions to intravenous iodinated contrast media: a primer for radiologists. *Emerg Radiol* 2006;12:210-215
63. Pakos EE, Fotopoulos AD, Ioannidis JP. 18F-FDG PET for evaluation of bone marrow infiltration in staging of lymphoma: a meta-analysis. *J Nucl Med* 2005;46:958-963
64. Tsukamoto N, Kojima M, Hasegawa M, et al. The usefulness of (18)F-fluorodeoxyglucose positron emission tomography ((18)F-FDG-PET) and a comparison of (18)F-FDG-pet with (67)gallium scintigraphy in the evaluation of lymphoma: relation to histologic subtypes based on the World Health Organization classification. *Cancer* 2007;110:652-659
65. Elstrom R, Guan L, Baker G, et al. Utility of FDG-PET scanning in lymphoma by WHO classification. *Blood* 2003;101:3875-3876
66. Hoffmann M, Wohrer S, Becherer A, et al. 18F-Fluoro-deoxy-glucose positron emission tomography in lymphoma of mucosa-associated lymphoid tissue: histology makes the difference. *Ann Oncol* 2006;17:1761-1765
67. Alinari L, Castellucci P, Elstrom R, et al. 18F-FDG PET in mucosa-associated lymphoid tissue (MALT) lymphoma. *Leuk Lymphoma* 2006;47:2096-2101
68. Karam M, Novak L, Cyriac J, Ali A, Nazeer T, Nugent F. Role of fluorine-18 fluoro-deoxyglucose positron emission tomography scan in the evaluation and follow-up of patients with low-grade lymphomas. *Cancer* 2006;107:175-183
69. Beal KP, Yeung HW, Yahalom J. FDG-PET scanning for detection and staging of extranodal marginal zone lymphomas of the MALT type: a report of 42 cases. *Ann Oncol* 2005;16:473-480
70. Hoffmann M, Kletter K, Becherer A, Jager U, Chott A, Raderer M. 18F-fluorodeoxyglucose positron emission tomography (18F-FDG-PET) for staging and follow-up of marginal zone B-cell lymphoma. *Oncology* 2003;64:336-340
71. Hoffmann M, Kletter K, Diemling M, et al. Positron emission tomography with fluorine-18-2-fluoro-2-deoxy-D-glucose (F18-FDG) does not visualize extranodal B-cell lymphoma of the mucosa-associated lymphoid tissue (MALT)-type. *Ann Oncol* 1999;10:1185-1189
72. Najjar F, Hustinx R, Jerusalem G, Fillet G, Rigo P. Positron emission tomography (PET) for staging low-grade non-Hodgkin's lymphomas (NHL). *Cancer Biother Radiopharm* 2001;16:297-304
73. Jerusalem G, Beguin Y, Najjar F, et al. Positron emission tomography (PET) with 18F-fluorodeoxyglucose (18F-FDG) for the staging of low-grade non-Hodgkin's lymphoma (NHL). *Ann Oncol* 2001;12:825-830
74. Hoffmann M, Chott A, Puspok A, Jager U, Kletter K, Raderer M. 18F-fluorodeoxyglucose positron emission tomography (18F-FDG-PET) does not visualize follicular lymphoma of the duodenum. *Ann Hematol* 2004;83:276-278

75. Valencak J, Becherer A, Der-Petrossian M, Trautinger F, Raderer M, Hoffmann M. Positron emission tomography with [18F] 2-fluoro-D-2- deoxyglucose in primary cutaneous T-cell lymphomas. *Haematologica* 2004;89:115-116
76. Juweid ME, Stroobants S, Hoekstra OS, et al. Use of positron emission tomography for response assessment of lymphoma: consensus recommendations of the Imaging Subcommittee of the International Harmonization Project in Lymphoma. *J Clin Oncol* 2007;25:571-578
77. Perry C, Herishanu Y, Metzger U, et al. Diagnostic accuracy of PET/CT in patients with extranodal marginal zone MALT lymphoma. *Eur J Haematol* 2007;79:205-209
78. Castellucci P, Nanni C, Farsad M, et al. Potential pitfalls of 18F-FDG PET in a large series of patients treated for malignant lymphoma: prevalence and scan interpretation. *Nucl Med Commun* 2005;26:689-694
79. Castellucci P, Zinzani P, Pourdehnad M, et al. 18F-FDG PET in malignant lymphoma: significance of positive findings. *Eur J Nucl Med Mol Imaging* 2005;32:749-756
80. Barrington SF, O'Doherty MJ. Limitations of PET for imaging lymphoma. *Eur J Nucl Med Mol Imaging* 2003;30 Suppl 1:S117-S127
81. Brix G, Lechel U, Glatting G, et al. Radiation exposure of patients undergoing whole-body dual-modality 18F-FDG PET/CT examinations. *J Nucl Med* 2005;46:608-613
82. Brennan DD, Gleeson T, Coate LE, Cronin C, Carney D, Eustace SJ. A comparison of whole-body MRI and CT for the staging of lymphoma. *AJR Am J Roentgenol* 2005;185:711-716
83. Kellenberger CJ, Miller SF, Khan M, Gilday DL, Weitzman S, Babyn PS. Initial experience with FSE STIR whole-body MR imaging for staging lymphoma in children. *Eur Radiol* 2004;14:1829-1841
84. Schmidt GP, Reiser MF, Baur-Melnyk A. Whole-body imaging of the musculoskeletal system: the value of MR imaging. *Skeletal Radiol* 2007;36:1109-1119
85. Runge VM. Safety of magnetic resonance contrast media. *Top Magn Reson Imaging* 2001;12:309-314
86. Murtz P, Krautmacher C, Traber F, Gieseke J, Schield HH, Willinek WA. Diffusion-weighted whole-body MR imaging with background body signal suppression: a feasibility study at 3.0 Tesla. *Eur Radiol* 2007;17:3031-3037
87. Koh DM, Collins DJ. Diffusion-weighted MRI in the body: applications and challenges in oncology. *AJR Am J Roentgenol* 2007;188:1622-1635
88. Takahara T, Imai Y, Yamashita T, Yasuda S, Nasu S, Van Cauteren M. Diffusion weighted whole body imaging with background body signal suppression (DWIBS): technical improvement using free breathing, STIR and high resolution 3D display. *Radiat Med* 2004;22:275-282
89. Will O, Purkayastha S, Chan C, et al. Diagnostic precision of nanoparticle-enhanced MRI for lymph-node metastases: a meta-analysis. *Lancet Oncol* 2006;7:52-60
90. Klose T, Leidl R, Buchmann I, Brambs HJ, Reske SN. Primary staging of lymphomas: cost-effectiveness of FDG-PET versus computed tomography. *Eur J Nucl Med* 2000;27:1457-1464



# Chapter 3

## Radiation exposure and mortality risk from CT and PET imaging of patients with malignant lymphoma

Quarles van Ufford HME, Kwee TC, Bierings MB, Ludwig I, Nievelstein RA,  
De Klerk JMH, Beek FJ, Mali WP, De Bruin PW, Geleijns J

In submission

## Abstract

### Objective

Imaging plays a vital role in the management of patients with malignant lymphoma (Hodgkin lymphoma [HL] and non-Hodgkin Lymphoma [NHL]). Imaging is generally performed by computed tomography (CT) and more recently also by positron emission tomography (PET) using  $^{18}\text{F}$ -FDG. Both CT and  $^{18}\text{F}$ -FDG PET are associated with a certain mortality risk resulting from the exposure to ionizing radiation. The aim of this study was to perform accurate radiation risk assessment for imaging of patients with malignant lymphoma.

### Subjects and Methods

To quantify radiation exposure and risk, first organ doses were assessed for a typical work-up in children with HL and adults with NHL. Subsequently, life tables were constructed for assessment of radiation risks, also taking into account the disease-related mortality.

### Results

In children with HD, cumulative effective dose from medical imaging reached 66 mSv (newborn), 69 mSv (1-year-old), 80 mSv (5-year-old), 90 mSv (10-year-old), and 113 mSv (15-year-old). In adults with NHL cumulative effective dose from medical imaging was 97 mSv. For children with HL and adults with NHL, average fractions of radiation-induced deaths were 0.4% for boys and 0.07% for males; 0.7% for girls and 0.09% for females.

### Conclusion

The disease-related reduction in life expectancy of patients diagnosed with malignant lymphoma must be taken into account for achieving accurate assessment of radiation risk. The modest radiation risk that results from imaging with CT and  $^{18}\text{F}$ -FDG PET is considered as justified, but imaging should be performed with care.

## Introduction

Imaging plays a vital role in the management of patients with malignant lymphoma (Hodgkin lymphoma [HL] and non-Hodgkin lymphoma [NHL]). Accurate imaging is important for determining the initial stage of disease which guides the treatment strategy. Furthermore, the initial stage influences the prognosis. Imaging is also important for assessing response to therapy, and detecting tumor persistence or recurrence [1-3]. Computed tomography (CT) and more recently positron emission tomography (PET) with  $^{18}\text{F}$ -FDG have become indispensable tools in oncological imaging [1, 4-8]. However, CT and PET result in radiation exposure of the patient, and imaging with ionising radiation is associated with a carcinogenic risk and the possible induction of malignant lesions.

There is a worldwide growing concern about radiation exposure in medical imaging. Estimates of the National Council on Radiation Protection & Measurements (NCRP) Scientific Committee in the United States in 2006 show an almost six fold increase of the per capita dose from medical exposure to about 3 mSv compared to 1982. CT and nuclear medicine examinations are the largest contributors [9].

Therapeutic advances have dramatically improved survival of patients with malignant lymphoma over the past decades [10-12]. Therefore, current treatment strategies not only aim at maximizing curative success, but also at minimizing (late) toxicity, such as infertility, premature menopause, cardiac disease, and most importantly, risk of second neoplasms [10-12]. In this context, the potential hazard of ionising radiation that is associated with diagnostic CT and PET scanning in patients with malignant lymphoma is an increasingly important issue.

Most of the quantitative information regarding the risks of radiation-induced cancer comes from studies of survivors of the atomic bombs dropped on Japan in 1945 [13]. In the subgroup of atomic-bomb survivors who received low doses of radiation, ranging from 5 to 150 mSv (with a mean dose of 40 mSv), there was a significant increase in the overall risk of cancer [14-16].

Performing dose and risk assessment should be prioritized for circumstances with high cumulative radiation exposure for individual patients and better survival rates. This is particularly true when patients are young, such as children with HL, and when the cumulative radiation dose from imaging is expected to fall in the range from 5 to 150 mSv, such as during follow-up of patients treated for malignant lymphoma [17-19].

The aim of this study was to perform accurate radiation risk assessment for imaging of patients with malignant lymphoma. To achieve our goal, the radiation exposure of CT and  $^{18}\text{F}$ -FDG PET was calculated for a typical work-up for children with HL in different age categories and for adults with NHL. We expected that disease-related mortality would have a significant effect on the assessment of radiation risk in patients with malignant lymphoma and that disease-related mortality would be much higher

compared to radiation-induced mortality. Advanced radiation risk assessment, based on the demographic methodology of life tables, was developed to take into account these effects.

## Materials and Methods

### Clinical practice of imaging

Malignant lymphomas are a heterogeneous group of diseases, differing with regard to histology, treatment, and outcome. It is beyond the scope of this study to encompass all different entities. Instead we focus on the most common types of malignant lymphoma in children and adults: HL and diffuse large B-cell lymphoma, respectively [20-23]. The most typical imaging strategy for children with HL (age <18 years) and for adults with NHL (DLBCL) was used in this study. In children with HL, the imaging strategy was based on the protocol according to the Children's Oncology Group [COG]. In adults with DLBCL, the imaging strategy was based on the Dutch HOVON 84 trial (**Table 1**).

Imaging with ultrasound and chest radiography was not considered in this study, since ultrasound is not associated with radiation exposure, and the radiation exposure from chest radiography is negligible compared to CT and  $^{18}\text{F}$ -FDG PET scans.

**Table 1.** Imaging strategies for children with HL and adults with DLBCL

	Children with HL	Adults with DLBCL
Most common group	Intermediate Risk Strategy: stage I-A bulky disease, I-AE, IB, II-A bulky disease, II-AE, II-B, III-A, III-AE, III-AS, III-AE+S, IV-A en IV-AE	Stage II - IV
Initial diagnostic	1 CT scan of neck-chest-abdomen 1 whole-body PET scan 1 chest X-ray	1 CT scan of neck-thorax-abdomen 1 chest X-ray
Therapeutic phase	2 CT scans of neck-chest-abdomen 1 whole-body PET scan (direct after therapy) 2 chest X-ray	2 CT scans of neck-chest-abdomen 1 whole-body PET scan
Follow-up	2 CT scans of neck-chest-abdomen 7 CT scans of neck and chest (for most common supradiaphragmatic stage I and II disease) 4 chest X-ray	4 CT scans of neck-chest-abdomen 2 chest X-ray
Timing of CT scans during follow-up	at 3,6,9,12,15,18,24,36 and 60 months	at 6,12,18 and 24 months



## Radiation exposure from CT

There was no information available that allowed for assessment of organ doses in pediatric patients undergoing CT. Therefore, we created Medical Internal Radiation Dose (MIRD) pediatric patient models in five general categories according to age and weight: newborn (3.6 kg), 1-year-old (9.7 kg), 5-year-old (19.8 kg), 10-year-old (33.2 kg), and 15-year-old (56.8 kg). The adult MIRD patient model represents an average-sized patient of 74 kg. All these hermaphrodite patient models (MIRD V) are described by spheres, ellipsoids and cones, as illustrated in **Figure 1** [24]. For assessment of radiation exposure from CT we used these patient models in combination with an algorithm for Monte Carlo dose calculations (ImpactMC software, version 1.0, VAMP, Erlangen, Germany) [25]. The manufacturer of the Aquilion CT scanner (Toshiba Medical Systems) disclosed two measured X-ray spectra (100 kV and 120 kV) and information about the design of the CT scanner. This information was implemented in the Monte Carlo simulation. A MatLab script (The MathWorks, Natick, Massachusetts, USA) was used to extract organ doses from the calculated dose distributions within the MIRD mathematical phantoms.

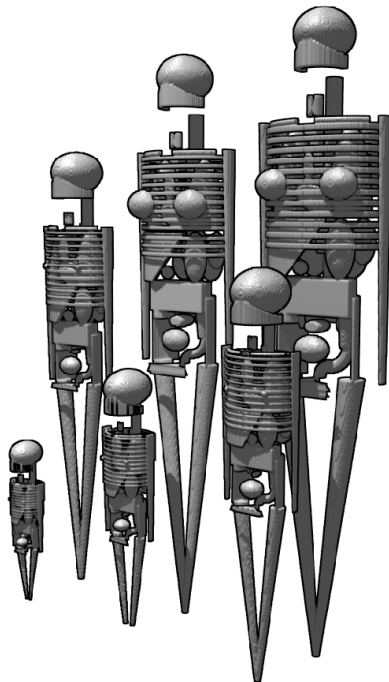


**Figure 1.** The mathematical hermaphrodite MIRD patient models, their body, skeleton and organs are described by spheres, ellipsoids and cones. The pediatric patient models are divided into five categories according to their age and weight: newborn (3.6 kg, left first row); 1-year-old (9.7 kg); 5-year-old (19.8 kg); 10-year-old (33.2 kg); 15-year old (56.8 kg). The adult model represents an average-sized patient of 74 kg (right second row).

In CT it is common practice to adjust acquisition parameters to the size of the patient. We derived the following clinical CT acquisition parameters. For small children a tube voltage of 100 kV is used (weight < 30kg); for larger children and adults a tube voltage of 120 kV is used ( $\geq$  30kg). Radiation output of the CT scanner is expressed as the Volume Computed Tomography Dose Index (CTDIvol) [26]. The clinically applied tube current, rotation time and pitch factor are associated with a CTDIvol of respectively 2.1 mSv (newborn, 3.6kg); 2.9 mSv (1-year-old, 9.7kg); 4.1 mSv (5-year-old, 19.8kg); 4.6 (10-year-old, 33.2kg); 7.1 (15-year-old, 56.8kg); and 9.5 mSv (adult, 74kg). Dose calculations that were performed for the MIRD phantoms with the Monte Carlo software yielded organ doses, total body dose, and effective dose according to ICRP 103. Dose assessment was performed for 12 CT acquisitions, i.e. for whole-body CT scans (including neck, chest and abdomen), and for CT scans of the neck and chest only, in all six age categories.

#### Radiation exposure from PET

Different positron-emitting tracers on a biologically active molecule can be administered intravenously into the body. In patients with malignant lymphoma,  $^{18}\text{F}$ -FDG is the established tracer for PET imaging. An important advantage of  $^{18}\text{F}$ -FDG PET is the high contrast resolution between tumors and normal tissues, making it sensitive for lesion detection.

For assessment of organ dose and effective dose from PET scans, published tables were used that provide information about organ dose and effective dose per MBq of administered  $^{18}\text{F}$ -FDG activity. The ICRP provides information for 1-, 5-, 10-, 15-year-old-children, and for adults [27]. Ruotsalainen et al. [28] published tables for estimation of radiation dose to the newborn in  $^{18}\text{F}$ -FDG PET studies. For the PET scan a dose of 3 MBq of  $^{18}\text{F}$ -FDG per kg body weight was assumed to be administered. The 5 different age categories in children that are being analysed in this study correspond to  $^{18}\text{F}$ -FDG doses of 10 MBq (newborn), 30 MBq (1-year-old), 60 MBq (5-year-old); 100 MBq (10-year-old), and 170 MBq (15-year-old), respectively. In adults, administration of 220 MBq  $^{18}\text{F}$ -FDG was assumed.

#### Risk assessment

We performed risk assessment in five age categories of male and female pediatric patients diagnosed with HL (newborns, and children at the age of 1, 5, 10, and 15 years), and in three age categories for adult male and female patients diagnosed with DLBCL at the age of 55, 65, and 75 years.

The BEIR VII excess relative risk (ERR) model was used for calculating organ-specific radiation risk [29]. In the BEIR VII model, the organ-specific solid cancer mortality is expressed, relative to the gender- and age-dependent risk of background cancer mortality for specific organs. This background is the naturally occurring mortality,

not the mortality that is induced due to radiation exposure during medical imaging. Data on the risk of naturally occurring cancer mortality according to organ, gender, and attained age were derived from ICRP Publication 103 (Euro-American cancer mortality rates by age and site) [30]. Subsequently, according to the BEIR VII model, an overall ERR function depending on organ dose, gender, age at exposure, and attained age was calculated for male and female patients. Organ dose was incorporated into the risk model as a function of attained age; this was required because patients have different weights (and ages) and thus receive different associated radiation exposures during diagnosis, treatment, and surveillance of malignant lymphoma. In addition to radiation risk, mortality rates that are typical for the young patient group with HL and the adult patient group with DLBCL could be taken into account; i.e. the overall 10-year survival for HL (94%) and 5-year survival for DLBCL (58%) [20-23]. Calculations were performed with and without taking into account the disease-related mortality. Life tables are used in demography for measuring and modelling population processes. These tables allow calculation of the fraction of radiation-induced deaths, the reduction of life expectancy, and the survival rate. The radiation-induced, age, gender, and dose-dependent overall mortality that was calculated with the BEIR VII model was incorporated into life tables, together with the mortality risks that are typical for patients with malignant lymphoma (HL- and DLBCL-related mortality rates). In addition, background mortality, that is typical for the asymptomatic population (gender- and age-specific probability of dying) was derived for the European population at large, based on the Eurostat database, and included in the lifetables [31].

## Results

### Radiation exposure from CT and FDG PET scans

The radiation exposure from a whole-body CT scan, from a CT scan of neck and chest, and from a whole-body <sup>18</sup>F-FDG PET scan for children (HL) according to the five pediatric age categories and for adults (DLBCL) are presented in **Table 2**. Linear interpolation of dose values was performed to yield dose estimations at different ages. Appropriate organ doses and the effective dose were thus calculated for the year of diagnosis and treatment and for the following years of surveillance. Effective dose increased gradually with age from 5.5 mSv to 13.3 mSv (whole-body CT); and from 3.4 mSv to 7.9 mSv (neck-chest CT). For PET examinations the variations in effective dose were smaller, ranging from 2.8 mSv to 4.3 mSv. In CT the highest organ doses were observed for lung and thyroid, but variations in organ dose were modest for organs lying entirely within the scanned range. In PET the highest organ dose by far was observed for the bladder.

**Table 2.** Radiation exposure doses in mSv (total body dose (only CT), effective dose, and organ doses) for children with HL according to the five age and weight categories and for adults with DLBCL, for a whole-body CT scan (WB-CT), a CT scan of neck and thorax (CT neck-chest), and a PET scan, respectively.

	0 years old / 3.6kg			1 years old / 9.7kg			5 years old / 19.8kg		
	WB-CT	CT neck-chest	PET	WB-CT	CT neck-chest	PET	WB-CT	CT neck-chest	PET
Total body	4.8	2.6	n.a.	5.7	3.0	n.a.	6.9	3.3	n.a.
Effective dose	5.5	3.4	3.8	6.6	4.0	2.8	8.3	4.5	3.0
Bone marrow	2.2	0.9	3.1	2.7	1.2	1.8	4.1	1.7	1.9
Stomach	6.2	4.6	2.3	7.5	5.0	2.0	9.3	4.0	2.1
Colon	6.0	0.5	2.2	7.1	0.5	2.2	8.6	0.3	2.4
Liver	6.2	4.6	4.4	7.4	5.2	2.0	9.1	4.6	2.2
Lung	6.7	6.5	2.2	8.1	7.9	1.9	10.1	9.7	2.0
Breast	5.6	5.5	2.3	6.6	6.3	1.6	8.4	8.0	1.7
Prostate	5.3	0.1	2.7	5.9	0.0	2.0	7.1	0.0	2.1
Uterus	6.1	0.3	4.0	7.3	0.2	2.9	9.0	0.1	3.3
Ovary	6.0	0.3	3.3	7.0	0.3	2.4	8.5	0.1	2.6
Bladder	6.0	0.1	11.1	7.2	0.1	17.2	9.0	0.0	19.0
Other solid cancers	4.8	2.6	3.8	5.7	3.0	2.8	6.9	3.3	3.0
Thyroid	6.4	6.4	2.2	8.7	8.6	2.0	11.4	11.3	2.1

Table 2. Continued

	0 years old / 3.6kg		1 years old / 9.7kg		5 years old / 19.8kg	
	WB-CT	CT neck-chest	PET	WB-CT	CT neck-chest	PET
	10 years old / 33.2kg		15 years old / 56.8kg		Adult / 74kg	
	WB-CT	CT neck-chest	PET	WB-CT	CT neck-chest	PET
Total body	6.9	3.5	n.a.	9.0	4.4	n.a.
Effective dose	8.6	5.1	3.6	11.0	6.2	4.3
Bone marrow	6.2	2.9	2.2	10.4	5.0	2.4
Stomach	9.4	5.5	2.2	11.8	5.0	2.4
Colon	8.7	0.4	2.7	10.8	0.2	2.9
Liver	9.1	6.1	2.2	11.2	6.3	2.4
Lung	10.1	9.9	2.1	12.4	12.1	2.4
Breast	8.1	8.1	1.8	9.1	9.0	1.9
Prostate	7.0	0.0	2.2	8.6	0.0	2.4
Uterus	9.1	0.1	3.9	11.6	0.1	4.4
Ovary	8.6	0.1	3.0	10.6	0.1	3.4
Bladder	9.3	0.0	27.9	12.2	0.0	35.8
Other solid cancers	6.9	3.5	3.6	9.0	4.4	4.3
Thyroid	12.8	12.7	2.1	19.4	19.5	2.2
				24.8	24.8	2.2

n.a. not available

\*) this acquisition is not part of the clinical protocols

Neonates and children with HL undergo seven whole-body CT scans, five CT scans of neck and chest, and two  $^{18}\text{F}$ -FDG PET scans during a period of 5 years. Adults with DLBCL undergo seven whole-body CT scans and one  $^{18}\text{F}$ -FDG PET scan during a period of two and a half years. Due to the intensive use of X-ray imaging the effective dose accumulates rapidly in patients with malignant lymphoma. In children with HL, cumulative effective dose reaches 66 mSv (newborn at diagnosis), 69 mSv (1 year old at diagnosis), 80 mSv (5 year old at diagnosis), 90 mSv (10 year old at diagnosis), and 113 mSv (15 year old at diagnosis). Differences between these pediatric age categories are due to differences in patient size and due to the patient size-specific acquisition protocols for both the CT and  $^{18}\text{F}$ -FDG PET scans. In adults with DLBCL cumulative effective dose reaches 97 mSv two and a half years after diagnosis.

#### Risk assessment

Demographic and risk-related parameters were derived from the life tables for neonates and children (with HL) corresponding with the five different age and weight categories. The pediatric categories are identified by the age at diagnosis (**Table 3**) and for adult patients (with DLBCL) the categories were 55, 65 and 75 years of age at diagnosis of the disease (**Table 4**).

Calculations were performed with and without the disease-related mortality rates typical for the patient cohorts (**Table 3**). Risk assessment, also taking into account the effects of disease-related mortality, resulted in a substantially lower fraction of radiation-induced deaths, and shorter associated reduction of life expectancy.

The calculations which included disease-related mortality resulted in an average 10-year survival of 94% (range 93 – 94%) for the young patient group with HL. For the adult patient group with DLBCL, the calculated average 5-year survival was 55% (range 46 – 59%). Within the pediatric patient group, the average fraction of radiation-induced deaths was 0.4% for males and 0.7% for females. Within the adult group these values were even smaller; 0.07% for males and 0.09% for females. The average radiation-induced reduction of life expectancy in the pediatric group with HL is 21 days for males and 45 days for females. In the adults suffering from DLBCL, the average reduction is 1.5 for males and 2.0 days for females.

**Table 3.** Risk assessment for 5 categories of children with HL based on a demographic methodology and life tables with and without correction for disease related mortality. Quantification of cumulative patient radiation dose and associated mortality risk, for patients with different age at time of diagnosis.

	0 years old				1 year old			
	Male	Female	Male	Female	Male	Female	Male	Female
	no	no	yes	yes	no	no	yes	yes
Corrected for disease related mortality	0.005	0.010	0.003	0.007	0.006	0.011	0.004	0.007
Fraction radiation induced deaths	76	82	60	64	76	81	60	63
Life expectancy at year of diagnosis (year)	29	64	19	41	30	68	20	43
Radiation induced reduction of life expectancy (days)	n.a.	n.a.	5841	6560	n.a.	n.a.	5731	6440
Disease related reduction of life expectancy (days)	29	64	5859	6601	30	68	5750	6483
Total reduction of life expectancy (days)	99	99	93	94	100	100	94	94
10 year survival after diagnosis (percentage)								
5 year old								
	Male	Female	Male	Female	Male	Female	Male	Female
Corrected for disease related mortality	no	no	yes	yes	no	no	yes	yes
Fraction radiation induced deaths	0.006	0.011	0.004	0.007	0.006	0.011	0.004	0.007
Life expectancy at year of diagnosis (year)	72	77	58	61	67	72	54	58
Radiation induced reduction of life expectancy (days)	32	71	21	46	32	68	22	46
Disease related reduction of life expectancy (days)	n.a.	n.a.	5205	5881	n.a.	n.a.	4577	5213
Total reduction of life expectancy (days)	32	71	5226	5928	32	68	4598	5259
10 year survival after diagnosis (percentage)	100	100	94	94	100	100	94	94
10 year old								
	Male	Female	Male	Female	Male	Female	Male	Female
Corrected for disease related mortality	no	no	yes	yes	no	no	yes	yes
Fraction radiation induced deaths	0.007	0.012	0.005	0.008				
Life expectancy at year of diagnosis (year)	62	67	51	55				
Radiation induced reduction of life expectancy (days)	35	74	25	51				
Disease related reduction of life expectancy (days)	n.a.	n.a.	3985	4578				
Total reduction of life expectancy (days)	35	74	4009	4629				
10 year survival after diagnosis (percentage)	99	100	93	94				
n.a. Not applicable								





## Discussion

This study shows that the effect of disease-related mortality on radiation risk assessment for patients with malignant lymphoma is substantial. By taking into account disease-related mortality the assessment of the fraction of radiation-induced deaths decreased between 30% to 40% for HL, and between 50% to 80% for DLBCL. The assessment of radiation-induced reduction of life expectancy reduced with similar percentages. Our methodology, that integrates a model for organ dose assessment and risk assessment in one demographic model, showed that radiation-induced reduction of life expectancy is only a small fraction compared to the disease-related reduction of life expectancy, namely a fraction between 0.003 and 0.011 for HL (children); and between 0.0003 and 0.0006 for DLBCL (adults). This reflects that the radiation-related risk is a late risk with its expression up to decades after the actual exposure and has therefore less effect on the reduction of life expectancy. Our methodology for radiation risk assessment is an improvement compared to the usual standard of practice where disease-related mortality is not considered. The observed cumulative effective doses are relatively high for imaging patients with malignant lymphoma; however, the associated estimated radiation risks are still modest.

Within the pediatric patient group, it is estimated that on average 0.4% male and 0.7% female patients die eventually due to the radiation exposure associated with medical imaging. For adult patients diagnosed with DLBCL, it is estimated that 0.07% male and 0.09% female patients die due to the radiation exposure. The higher values for females result mainly from the relative high sensitivity of the female breast for radiation exposure [32].

This study has some limitations. Malignant lymphomas are a heterogeneous group of entities, with more than 40 subtypes [33]. The two major entities are HL and NHL, with DLBCL being the most common type of NHL. With regard to radiation exposure, age is an important factor. Therefore, we chose to analyze the risk of radiation exposure in only two types of lymphoma, being pediatric patients with HL and adult patients with DLBCL. Another limitation is that although assumed 10- and 5-year survival rates of HL and DLBCL were derived from recent literature [20-23], these numbers may actually underestimate current survival rates, given the continuous improvements in treatment. Furthermore, this study only focused on the mortality risk caused by the radiation exposure of the patient. The morbidity risk induced by the radiation exposure was not considered. It can be assumed that not all patients with a radiation-induced malignancy die due to this malignancy, and more patients suffer from radiation-induced diseases than the number of patients expressed in the mortality risk. With the implementation of integrated PET-CT scanners, a low-dose CT scan is performed additionally to the PET scan, as it is used for attenuation correction in PET imaging. This low-dose CT scan was not included in this study. Two or one additional

low-dose CT scan(s) would have been performed for children with HL and for adults with DLBCL, respectively, with each low-dose CT scan causing an extra radiation exposure of approximately 3 mSv [34]. However, by combining PET and CT the PET scan may be performed with less  $^{18}\text{F}$ -FDG which would result in a dose reduction. The low-dose CT scans will hardly influence the estimated radiation risks. Finally, it should be recognised that there are considerable uncertainties in the radiation risk model of BEIR, especially regarding the risk at the low dose levels as encountered in CT [35]. The available evidence is not conclusive, primarily because of the absence of definitive epidemiological data at low dose levels. Radiation risk estimates for low radiation doses is still a controversial topic.

In order to establish the most efficient imaging strategy and limit the radiation exposure in malignant lymphoma patients, there are different options. It may be sufficient to use only the low-dose whole-body CT scan (along with  $^{18}\text{F}$ -FDG PET) during and after therapy instead of the diagnostic whole-body CT scan. Another possibility is to use whole-body magnetic resonance imaging (MRI) as a radiation-free alternative to CT and/or  $^{18}\text{F}$ -FDG PET for staging malignant lymphoma. Whole-body MRI has evolved into a clinically feasible technique with respect to image quality and examination time. Furthermore, the introduction of newer sequences that provide more functional tissue information, particularly diffusion-weighted imaging (DWI), may facilitate the staging of malignant lymphoma. Although more research is certainly necessary, the first studies show that whole-body MRI, including DWI, is a promising alternative to ( $^{18}\text{F}$ -FDG PET)/CT [36-38].

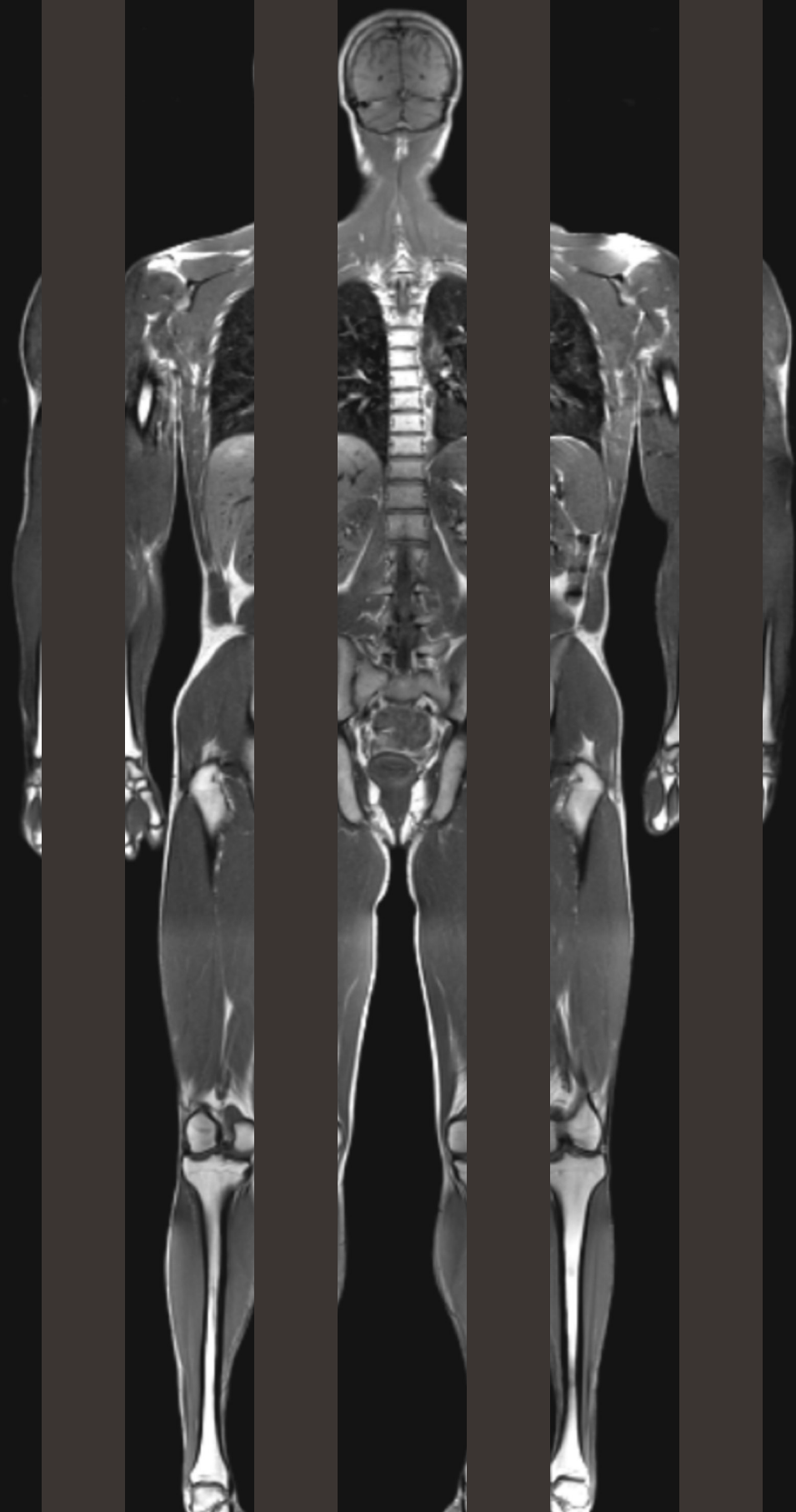
In conclusion, the disease-related reduction in life expectancy of patients diagnosed with malignant lymphoma must be taken into account for achieving accurate assessment of radiation risk. Although cumulative effective dose from medical imaging is high, the actual calculated radiation risks are modest. The radiation exposure that results from imaging with CT and  $^{18}\text{F}$ -FDG PET is considered as justified, but should still be performed with care. Ongoing studies have to establish the most efficient imaging strategies for the different subtypes of malignant lymphoma.

## References

1. Hoskin PJ. PET in lymphoma: what are the oncologist's needs? *Eur J Nucl Med Mol Imaging* 2003;30 Suppl 1:S37-S41
2. Carbone PP, Kaplan HS, Musshoff K, Smithers DW, Tubiana M. Report of the Committee on Hodgkin's Disease Staging Classification. *Cancer Res* 1971;31:1860-1861
3. Armitage JO. Staging non-Hodgkin lymphoma. *CA Cancer J Clin* 2005;55:368-376
4. Hoh CK, Glaspy J, Rosen P, et al. Whole-body FDG-PET imaging for staging of Hodgkin's disease and lymphoma. *J Nucl Med* 1997;38:343-348
5. Buchmann I, Reinhardt M, Elsner K, et al. 2-(fluorine-18)fluoro-2-deoxy-D-glucose positron emission tomography in the detection and staging of malignant lymphoma. A bicenter trial. *Cancer* 2001;91:889-899
6. Seam P, Juweid ME, Cheson BD. The role of FDG-PET scans in patients with lymphoma. *Blood* 2007;110:3507-3516
7. Juweid ME, Stroobants S, Hoekstra OS, et al. Use of positron emission tomography for response assessment of lymphoma: consensus of the Imaging Subcommittee of International Harmonization Project in Lymphoma. *J Clin Oncol* 2007;25:571-578
8. Cheson BD, Pfistner B, Juweid ME, et al. Revised response criteria for malignant lymphoma. *J Clin Oncol* 2007;25:579-586
9. Mettler FA, Jr, Thomadsen BR, Bhargavan M, et al. Medical radiation exposure in the U.S. in 2006: preliminary results. *Health Phys* 2008;95:502-507
10. Connors JM. State-of-the-art therapeutics: Hodgkin's lymphoma. *J Clin Oncol* 2005;23:6400-6408
11. Ansell SM, Armitage J. Non-Hodgkin lymphoma: diagnosis and treatment. *Mayo Clin Proc* 2005;80:1087-1097
12. Hennessy BT, Hanrahan EO, Daly PA. Non-Hodgkin lymphoma: an update. *Lancet Oncol* 2004;5:341-353
13. Executive Summary Board on Radiation Effects Research—Division on Earth and Life Studies editor. *Health Risks from Exposure to Low Levels of Ionizing Radiation: BEIR VII—Phase 2*. Washington, DC, National Academy Press, 2005
14. Preston DL, Shimizu Y, Pierce DA, Suyama A, Mabuchi K. Studies of mortality of atomic bomb survivors. Report 13: Solid cancer and noncancer disease mortality: 1950-1997. *Radiat Res* 2003;160:381-407
15. Pierce DA, Preston DL. Radiation-related cancer risks at low doses among atomic bomb survivors. *Radiat Res* 2000;154:178-186
16. Preston DL, Ron E, Tokuoka S, et al. Solid cancer incidence in atomic bomb survivors: 1958-1998. *Radiat Res* 2007;168:1-64
17. Brenner D, Elliston C, Hall E, Berdon W. Estimated risks of radiation-induced fatal cancer from pediatric CT. *AJR Am J Roentgenol* 2001;176:289-296
18. Brenner DJ, Elliston CD. Estimated radiation risks potentially associated with full-body CT screening. *Radiology* 2004;232:735-738
19. Linton OW, Mettler FA, Jr. National conference on dose reduction in CT, with an emphasis on pediatric patients. *AJR Am J Roentgenol* 2003;181:321-329

20. Von der Weid NX. Adult life after surviving lymphoma in childhood. *Support Care Cancer* 2008;16:339-345
21. Chow LM, Nathan PC, Hodgson DC, et al. Survival and late effects in children with Hodgkin's lymphoma treated with MOPP/ABV and low-dose, extended-field irradiation. *J Clin Oncol* 2006;24:5735-5741
22. Illidge T, Tolan S. Current treatment approaches for diffuse large B-cell lymphoma. *Leuk Lymphoma* 2008;49:663-676
23. Feugier P, Van HA, Sebban C, et al. Long-term results of the R-CHOP study in the treatment of elderly patients with diffuse large B-cell lymphoma: a study by the Groupe d'Etude des Lymphomes de l'Adulte. *J Clin Oncol* 2005;23:4117-4126
24. Cristy M. Mathematical phantoms representing children of various ages for use in estimates of internal dose. U.S. Nuclear Regulatory Commission Rep. NUREG/CR-1159 (also Oak Ridge National Laboratory Rep. ORNL/NUREG/TM-367), 1980
25. Deak P, van SM, Shrimpton PC, Zankl M, Kalender WA. Validation of a Monte Carlo tool for patient-specific dose simulations in multi-slice computed tomography. *Eur Radiol* 2008;18:759-772
26. Nit-Gray MF. AAPM/RSNA Physics Tutorial for Residents: Topics in CT. Radiation dose in CT. *Radiographics* 2002;22:1541-1553
27. Valentin DJ. Radiation dose to patients from radiopharmaceuticals (Addendum 2 to ICRP Publication 53). *Ann ICRP* 1998;28:1
28. Ruotsalainen U, Suhonen-Polvi H, Eronen E, et al. Estimated radiation dose to the newborn in FDG-PET studies. *J Nucl Med* 1996;37:387-393
29. NAS/NRC. Health risks from exposure to low levels of ionising radiation: BEIR VII phase 2. Board on Radiation Effects Research National Research Council of the National Academies. Washington DC, 2006
30. The 2007 Recommendations of the International Commission on Radiological Protection. ICRP publication 103. *Ann ICRP* 2007;37:1-332
31. Eurostat. <http://epp.eurostat.ec.europa.eu/>, 2007.
32. De Bruin ML, Sparidans J, van't Veer MB, et al. Breast Cancer Risk in Female Survivors of Hodgkin's Lymphoma: Lower Risk After Smaller Radiation Volumes. *J Clin Oncol* 2009;27:4239-4246
33. Swerdlow S, Campo E, Harris N. WHO Classification of Tumours of Haematopoietic and Lymphoid Tissues (4th ed.). Lyon, France: International Agency for Research on Cancer, 2008
34. Brix G, Lechel U, Glatting G, et al. Radiation exposure of patients undergoing whole-body dual-modality 18F-FDG PET/CT examinations. *J Nucl Med* 2005;46:608-613
35. Uncertainties in fatal cancer risk estimates used in radiation protection. Report 126. National Council on Radiation Protection and Measurements.
36. Kwee TC, van Ufford HM, Beek FJ, et al. Whole-body MRI, including diffusion-weighted imaging, for the initial staging of malignant lymphoma: comparison to computed tomography. *Invest Radiol* 2009;44:683-690
37. Punwani S, Taylor SA, Bainbridge A, et al. Pediatric and adolescent lymphoma: comparison of whole-body STIR half-Fourier RARE MR imaging with an enhanced PET/CT reference for initial staging. *Radiology* 2010;255:182-190

38. Lin C, Luciani A, Itti E, et al. Whole-body diffusion-weighted magnetic resonance imaging with apparent diffusion coefficient mapping for staging patients with diffuse large B-cell lymphoma. *Eur Radiol* 2010;20:2027-2038



# Chapter 4<sup>1</sup>

Diffusion-weighted whole-body  
imaging with background body  
signal suppression (DWIBS):  
features and potential  
applications in oncology

Kwee TC, Takahara T, Ochiai R, Nieuvelstein RA, Lijten PR

*Eur Radiol* 2008;18:1937-1952

## Abstract

Diffusion-weighted magnetic resonance imaging (DWI) provides functional information and can be used for the detection and characterization of pathologic processes, including malignant tumors. The recently introduced concept of “diffusion-weighted whole-body imaging with background body signal suppression” (DWIBS) now allows acquisition of volumetric diffusion-weighted images of the entire body. This new concept has unique features different from conventional DWI and may play an important role in whole-body oncological imaging. This review describes and illustrates the basics of DWI, the features of DWIBS, and its potential applications in oncology.



## Introduction

Cancer is the second leading cause of death in developed countries, is among the three leading causes of death for adults in developing countries, and is responsible for 12.5% of all deaths worldwide [1]. Once a malignant tumor is detected, determination of disease extent (staging) is important for appropriate treatment planning and determining prognosis. Imaging plays a pivotal role in cancer staging. Furthermore, imaging is of great importance in monitoring response to therapy and in the detection of tumor recurrence.

Diffusion-weighted magnetic resonance imaging (DWI) provides functional information and can be used for the detection and characterization of pathologic processes, including malignant tumors; it may therefore be of value in staging and follow-up imaging of malignant tumors. DWI using single-shot echo-planar imaging (EPI) is a well-established method to examine the brain. Extracranial DWI, however, did not become clinical standard because the use of EPI was complicated by magnetic susceptibility artifacts and severe image distortion in the body [2-6]. Recently introduced parallel imaging techniques, such as SENSitivity Encoding (SENSE) [7, 8], and the development of stronger gradients and multichannel coils have largely overcome this problem; DWI of adequate quality can now be performed in the body, at high b-value [9, 10]. Despite above-mentioned breakthroughs in DWI, breathhold or respiratory triggered scanning was still considered necessary since it was widely accepted that respiratory motion was an impediment for DWI of (moving) visceral organs [11-15].

Then, in 2004, Takahara et al. [16] reported a unique concept of whole-body DWI, called "diffusion-weighted whole-body imaging with background body signal suppression" (DWIBS). This technique intentionally uses free breathing scanning rather than breathholding or respiratory triggering to visualize (moving) visceral organs and their lesions. In a later published article, Ballon et al. [17] also reported whole-body DWI during free breathing. Ballon et al.'s study [17] aimed to visualize metastatic lesions in static tissue (bone marrow) [17]; this was in agreement with the accepted theory at that time. However, they additionally found that visceral organs such as the spleen and kidneys were also visualized [17]. The feasibility of the free breathing approach could initially not be explained, but was clarified later; it can be understood with knowledge of the relationship between the motion probing gradients (MPGs) and the type (coherence) of motion, as will be described in a later section. This concept offers a wide range of potential applications in whole-body oncological imaging.

The first purpose of this review is to acquaint the reader with the features of DWIBS. Second, although evidence regarding its effectiveness is still limited, the potential applications of DWIBS in oncology will be described and illustrated. Finally, drawbacks, limitations, and future considerations of DWIBS will be discussed.

## Basics of DWI

As introduced by Stejskal and Tanner [18], the most common approach to render MRI sensitive to diffusion is to place two strong symmetrical gradient lobes (so-called MPGs) on either side of the 180° refocusing pulse in a spin echo sequence (**Figures 1-3**). The degree of signal attenuation in DWI depends both on the magnitude of diffusion (also referred to as intravoxel “incoherent” motion [19-21]) and the amount of diffusion weighting. It should be realized that only intravoxel “incoherent” motion leads to signal decrease, whereas intravoxel “coherent” motion, irrespective of its magnitude, does not affect signal, as will be explained in a later section. The amount of diffusion weighting is determined by the so-called b-value (b) and is calculated as follows:

$$b = \gamma^2 G^2 \delta^2 (\Delta - \delta/3),$$

where  $\delta$  is the duration of one MPG,  $\Delta$  is the interval between the leading edges of the MPGs,  $G$  is the strength of the MPG (**Figure 1**), and  $\gamma$  is the gyromagnetic ratio (the ratio of the magnetic moment to the angular momentum of a particle, 42.58 MHz/T for hydrogen) [7, 18].

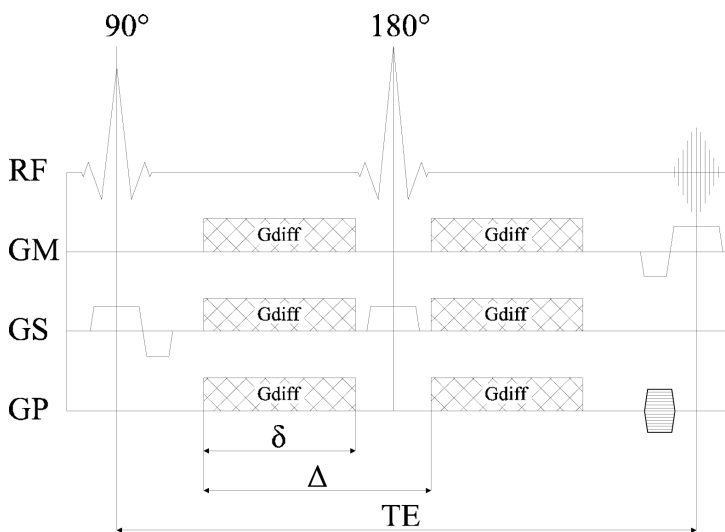


**Figure 1.** The Stejskal-Tanner sequence [5] (RF, radio frequency; GM, readout direction; GP, phase encoding direction; GS section select direction; MPG, motion probing gradient;  $\delta$ , duration of one MPG;  $\Delta$ , time interval between the leading edges of the MPGs; TE, echo time).

In biological tissue, diffusion is expressed and quantified by means of an effective or apparent diffusion coefficient (ADC). If two or more images with different b-values are acquired, the ADC of a selected region-of-interest (ROI) can be calculated as follows:

$$ADC = (1/b_1 - b_0) \ln(S[b_1]/S[b_0]),$$

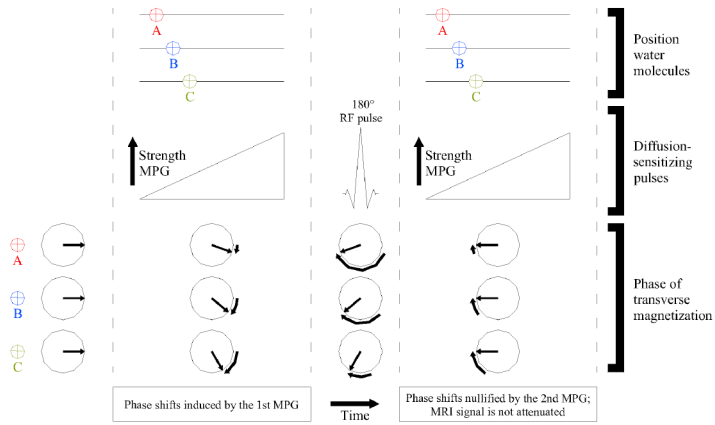


**Figure 2.** Three stationary water molecules (A,B,C) in one voxel. Phase shifts induced by the first motion probing gradient (MPG) are nullified by the second MPG. Because of the maintained phase coherence among the three water molecules, MRI signal is not attenuated (MPG, motion probing gradient; RF, radio frequency).

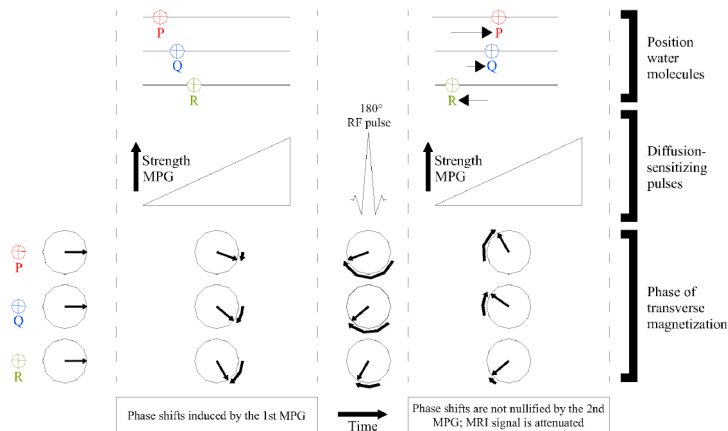


**Figure 3.** Three water molecules (P,Q,R) in one voxel, undergoing diffusion. Phase shifts induced by the first motion probing gradient (MPG) are not nullified by the second MPG. Because of the resulting phase dispersion among the three water molecules, MRI signal is attenuated (MPG, motion probing gradient; RF, radio frequency).

where  $b_1$  and  $b_0$  represent two different b-values,  $S[b_1]$  the signal intensity of the selected ROI on the slice level acquired with b-value  $b_1$ , and  $S[b_0]$  the signal intensity of the same ROI on the same slice level acquired with b-value  $b_0$ . A pixel by pixel map (so-called ADC map), whose intensity yields quantitative estimation of the regional ADC, can be obtained by post-processing [22].

DWI has potential in the field of oncological imaging. Malignant tumors may exhibit either restricted or increased diffusion, depending on their micro-architecture. For example, tumors with a high cellular density possess more cellular membranes per volume unit, which impedes the mobility of water molecules and restricts diffusion. Failure of the  $\text{Na}^+/\text{K}^+$  ATPase pump during necrotic cell death (similar to acute ischemic stroke) may also lead to restricted diffusion. Restricted diffusion has been reported for most malignant tumors [9, 10, 23]. On the other hand, loss of cell membrane integrity in necrotic tumors and decrease in tumor cellularity due to necrosis and/or apoptotic processes may result in increased diffusion, unless the necrotic fluid itself possesses high viscosity. In addition, intratumoral edema and cystic tumor components also increase diffusion because of increased water content [9, 10, 23].

For a more in-depth overview of the current status of conventional (breathhold or respiratory triggered) DWI, we refer the reader to the articles of Thoeny and De Keyzer [9], and Koh and Collins [10].

## Concept of DWIBS

When DWI was applied to the chest and abdominal region, another important problem was encountered: respiratory motion. It was known that T2-weighted image contrast could be maintained in T2-weighted imaging during free breathing. Nevertheless, breathholding or respiratory triggering was preferred to avoid image blurring. Similar rules seem to apply to DWI, but with a different underlying theory. Most people believed that diffusion-weighted image contrast would largely be lost in DWI during free breathing, because respiratory motion is tremendously larger than diffusion. Thus, DWI during free breathing seemed to be impossible and breathholding or respiratory triggering was strongly recommended, mainly to avoid signal loss rather than image blurring. Because of its limited scanning time, only a limited number of slices with relatively large slice thickness could be obtained in each examination, similar to incremental computed tomography (CT). As a result, signal-to-noise ratio (SNR) is low and lesion conspicuity may be diminished. Respiratory triggered scanning improves SNR, but at the expense of an approximate threefold increase in scanning time.

As described previously, Takahara et al. [16] developed the concept of DWIBS and proved the feasibility of DWI during free breathing. They also observed that SNR of DWI during free breathing considerably surpassed that of breathhold scanning [16]. These observations were in contradiction with the general assumption at that

time. They extended the possibilities of DWI: scanning time is no more limited (as in breathhold scanning) and image acquisition time is no more confined to a particular phase of the breathing cycle (as in respiratory triggered scanning), images with multiple b-values including high b-values around  $1000 \text{ s/mm}^2$  can be acquired, thin slices can be obtained, and multiple signal averaging is possible. Furthermore, these advances enable volumetric (3D) image processing including maximum intensity projections (MIPs), volume rendering, and multiplanar reformatting (MPR) in any plane (Figures 4 and 5).

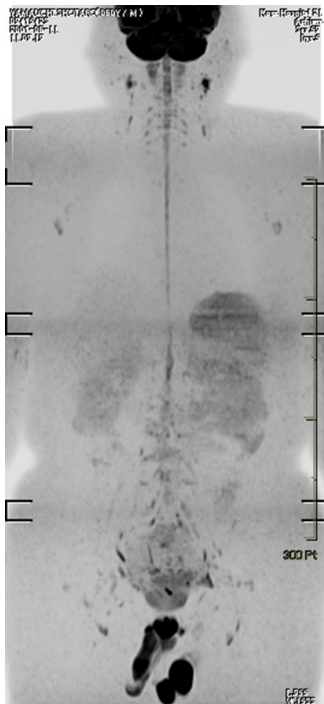


**Figure 4.** Coronal maximum intensity projection DWIBS image (inverted black-and-white gray scale) of a healthy 60-year-old **male** volunteer. Normal high signal intensity (black on this image) can be seen in the brain, spinal cord, nerves of the brachial plexus, prostate, testis, penis, spleen, and cervical, axillary, pelvic, and inguinal lymph nodes.

### Reason for the feasibility of free breathing in DWI

Sensitivity of DWI to microscopic diffusion (in the order of several micrometers) is maintained even during free breathing. To understand the feasibility of free breathing in DWIBS, two types of motion should be distinguished; intravoxel “incoherent” motion and intravoxel “coherent” motion. Intravoxel “incoherent” motion refers to the incoherent motion of water molecules within a voxel (i.e. diffusion) [19-21]. Intravoxel “coherent” motion refers to the coherent motion of water molecules within a voxel. Since the two MPG in a diffusion-weighted sequence (**Figure 1**) are applied within a very small time interval (in the order of 50 ms), additional respiratory

motion can indeed be regarded as coherent motion. The two MPGs only lead to signal decrease in case of intravoxel “incoherent” motion (i.e. diffusion), whereas signal is not affected by intravoxel “coherent” motion caused by additional respiratory motion. In other words, because DWIBS employs single-shot EPI, the acquired phase shift due to respiratory motion is equal in each phase encoding step and therefore does not affect image formation (**Figure 6**) [7].

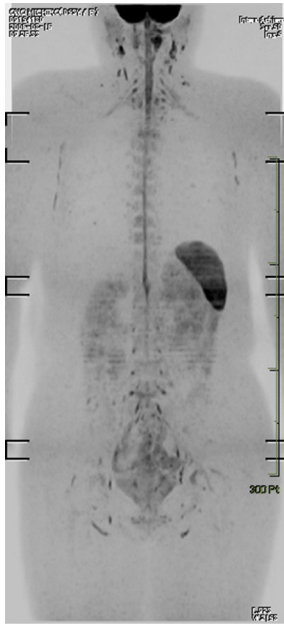


**Figure 5.** Coronal maximum intensity projection DWIBS image (inverted black-and-white gray scale) of a healthy 53-year-old **female** volunteer. Normal high signal intensity (black on this image) can be seen in the brain, spinal cord, nerves of the brachial and lumbosacral plexus, vertebral bone marrow, endometrium, spleen, and cervical, axillary, pelvic, and inguinal lymph nodes.

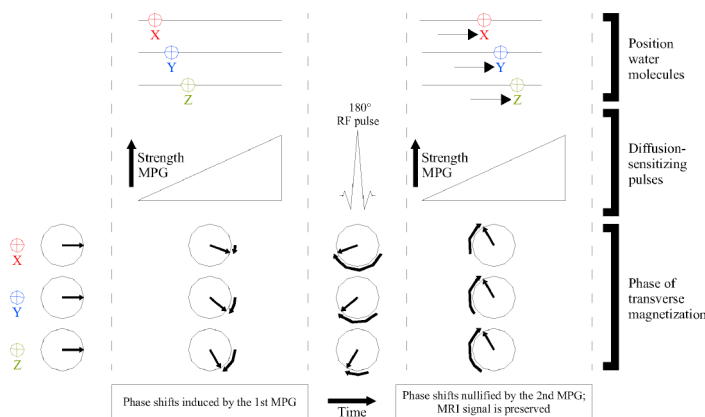


**Figure 6.** Three stationary water molecules (X,Y,Z) in one voxel, undergoing respiratory motion. Respiratory motion induces a linear phase shift but does not cause phase dispersion. Because of the maintained phase coherence among the three water molecules, MRI signal is preserved (MPG, motion probing gradient; RF, radio frequency).

Thus, DWI can be regarded as equal to T2-weighted imaging with respect to respiratory motion. In other words, diffusion-weighted image contrast is maintained during free breathing, while breathholding or respiratory triggering reduces image blurring. However, SNR in DWI is significantly less than in T2-weighted imaging. Therefore, instead of aiming to reduce image blurring, it can be more advantageous to improve SNR in DWI by means of free breathing scanning, which allows thin slice acquisitions and multiple slice excitations for volumetric imaging.

## Practical implementation of DWIBS

Suggested sequences for DWIBS at 1.5 T are listed in **Table 1**. It is currently recommended to obtain axial slices in DWIBS, to minimize image distortion. Because DWIBS allows obtaining thin axial slices (up to 4 mm), high quality reformatted images can subsequently be created in any plane. DWIBS is combined with either a short inversion time inversion recovery (STIR) pre-pulse or a frequency-selective (chemical shift selective [CHESS]) pre-pulse for fat suppression. STIR theoretically gives superior global fat suppression over an extended field of view, compared to CHESS, because of its insensitivity to magnetic field inhomogeneities [24]. Therefore, STIR can be used everywhere in the body. In addition, STIR may be useful in suppressing bowel signal, which may have a short T1 value, similar to that of fat. However, one of the main disadvantages of STIR, compared to CHESS, is decreased SNR because of partial loss of proton signal during the inversion time [24]. Since abdominal organs usually do not suffer significantly from magnetic field inhomogeneities, CHESS can be used in this area, both to increase SNR and to reduce image acquisition time. Continuous whole-body imaging, however, usually requires the use of STIR because of the presence of magnetic field inhomogeneities in the neck, shoulder, lungs, and lower extremities. On the other hand, it is possible to optimize a whole-body examination by imaging each station with the most appropriate fat suppression technique (either STIR or CHESS). The b-value determines the degree of background body signal suppression; b-values in the range of 800-1000 s/mm<sup>2</sup> generally result in good background body signal suppression for tumor detection. It should be realized that the use of a certain b-value combined with STIR is more effective in background body signal suppression than a combination of the same b-value with CHESS. For homogeneous organs like the liver and pancreas, background body signal suppression is of less importance, and a b-value of 500 s/mm<sup>2</sup> is sufficient for tumor detection in the majority of cases, while reducing image acquisition time. On the other hand, for tumor detection in organs with an already (normal) high signal intensity in DWIBS, such as the prostate, b-values in the order of 1500-2000 s/mm<sup>2</sup> can be applied. For signal reception in DWIBS, either a built-in-body coil or a surface coil can be used. Advantages of a built-in body coil are patient comfort and large coverage. However, although it has been reported that image quality is clear enough for the detection of lesions [25], contrast-to-noise ratio (CNR)

**Table 1.** Suggested sequences for DWIBS at 1.5 T.

Name	DWIBS-STIR	DWIBS-CHESS
<b>Main characteristics</b>	-Most suitable for organs and body regions suffering from large magnetic field inhomogeneities -Useful in suppressing bowel signal -Relatively lower SNR than DWIBS-CHESS -Relatively more time-consuming than DWIBS-CHESS	-Most suitable for organs and body regions without significant magnetic field inhomogeneities -Relatively higher SNR than DWIBS-STIR -Relatively less time-consuming than DWIBS-STIR
<b>Suitability</b>		
Neck and shoulder	++	-
Chest	++	-
Abdomen and pelvis		
-Liver, pancreas, spleen	+	++
-Colon	++	+
-Kidneys	++	+
-Uterus, bladder	+	++
-Prostate	+	+
Extremities	++	-
<b>Imaging parameters</b>		
Fat suppression	STIR	CHESS
B-value (s/mm <sup>2</sup> )	1000 <sup>a,b</sup>	1000 <sup>a,b</sup>
Direction of MPGs	Phase, frequency, and slice	Phase, frequency, and slice
TR (ms)	10205	7679
TE (ms)	70	70
TI (ms)	180	NA
Parallel imaging factor	2	2
Halfscan factor	0.6	0.6
EPI factor	47	47
Slice orientation	Axial	Axial
No. of slices	60	60
Slice thickness/gap (mm)	4/0	4/0
FOV (mm)	400	400
RFOV (%)	70	70
Matrix	160	160
Scan percentage (%)	70	70
Actual voxel size (mm <sup>3</sup> )	2.5 x 3.6 x 4.0	2.5 x 3.6 x 4.0
Calculated voxel size (mm <sup>3</sup> )	1.6 x 1.6 x 4.0	1.6 x 1.6 x 4.0
No. of signals averaged	10	10
Scan time	7 min 8 s	2 min 56 s

<sup>a</sup> For imaging of the upper abdomen (including liver, spleen, and pancreas), a b-value of 500 s/mm<sup>2</sup> can be applied, if necessary combined with respiratory triggered scanning

<sup>b</sup> For tumor detection in the prostate, b-values in the order of 1500-2000 s/mm<sup>2</sup> can be applied

**Legend:** ++ Very good; + Good; +/- Moderate; - Poor; -- Very poor

**Abbreviations:** CHESS: chemical shift selective; DWIBS: Diffusion-weighted whole-body imaging with background body signal suppression; EPI: echo-planar imaging; FOV: field of view; MPGs: motion probing gradients; NA: not applicable; RFOV: rectangular field of view; SNR: signal-to-noise ratio; STIR: short inversion time inversion recovery; TE: echo time; TI: inversion time; TR: repetition time



is inferior to that of a surface coil. One approach to obtain whole-body images using a surface coil, is the use of a so-called whole-body surface coil design. A whole-body surface coil design combines a large number of seamlessly integrated coil elements and independent radiofrequency channels, which offers large anatomical coverage (in the order of 200 cm) and allows image acquisition without any time loss due to patient or coil repositioning. However, it is also possible to perform a time-efficient whole-body examination using only one surface coil with limited coverage. In order to perform such an examination, an additional table platform should be mounted on top of the original patient table. Furthermore, spacers should be placed between both tables to create space to move the lower part of the surface coil from one station to the next. As a result, the patient can remain in the same position, repositioning of the surface coil to image the next station requires only little additional time (< 1 minute per station), and 3D alignment among the imaged stations is maintained. After completion of the examination, separately imaged stations can be merged with sophisticated software, creating the whole-body image (**Figure 7**). Image acquisition time for DWBS is typically on the order of 5-7 minutes per 25 cm coverage, when using STIR and a b-value of 1000 s/mm<sup>2</sup>. Inverting the gray scale of DWBS images makes them resemble position emission tomography (PET)-like images (**Figures 4 and 5**). DWBS can be performed on state-of-the-art MRI systems supplied by all major vendors, including GE Healthcare, Hitachi Medical Systems, Philips Healthcare, Siemens Medical Solutions, and Toshiba Medical Solutions.

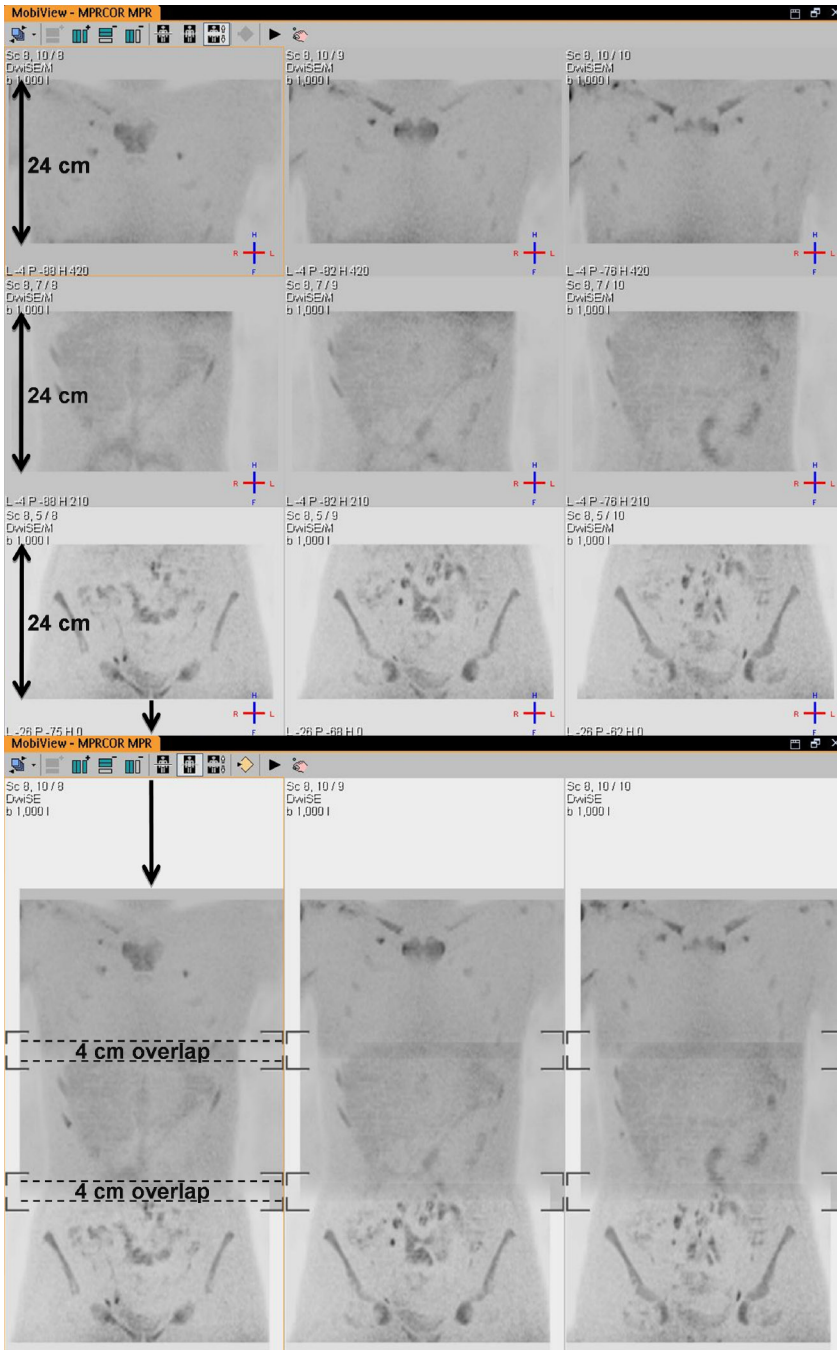


**Figure 7.** Separately imaged stations can be merged with sophisticated software, creating the whole-body image.

## Potential applications of DWIBS in oncology

### Staging

Primary tumors and distant metastases exhibiting restricted diffusion can be identified with DWIBS. DWIBS may especially be useful to detect relatively small lesions, because of its high CNR. It should be noted, however, that evaluation of areas close to the heart and the diaphragm may be hampered in DWIBS because of signal loss and artifacts due to incoherent tissue motion. Nevertheless, overall, DWIBS may be a very useful adjunct to anatomical MRI or CT, where small lesions may be obscured or overlooked because of the large amount of image data, and lesions in normal-sized organs may be missed (**Figure 8**).

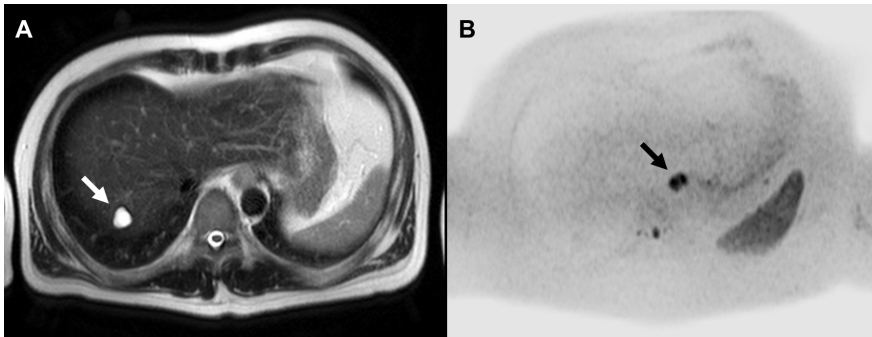


**Figure 8.** 41-year-old man with distal esophageal cancer shown by DWIBS but inconspicuous on T2-weighted MRI. (A) Axial T2-weighted image shows a small high signal intensity lesion in segment 7 of the liver (arrow), consistent with a cyst. No other conspicuous lesions can be identified. (B) Axial DWIBS image (inverted black-and-white gray scale) at the same level shows abnormal signal intensity in the lower part of the esophagus (arrow), consistent with esophageal carcinoma.

Accurate assessment of nodal status has important therapeutic and prognostic significance in patients with newly diagnosed cancers. Current cross-sectional imaging modalities rely on insensitive size and morphologic criteria and, thus, lack the desired accuracy for characterizing lymph nodes [26]. DWIBS may be a valuable tool for the identification and characterization of lymph nodes; normal lymph nodes have a relatively restricted diffusion because of their high cellular density and are well visualized with DWIBS, while surrounding fat tissue is suppressed (Figures 4 and 5). Metastatic lymph nodes may have increased cellular density or necrotic areas, which further restricts or increases diffusion, respectively. However, it is still unknown whether it is possible to differentiate healthy lymph nodes or benign lymphadenopathy from malignant lymph nodes using DWIBS with calculation of ADCs. Nevertheless, DWIBS is an outstanding tool to identify lymph nodes, irrespective of their histological composition. DWIBS, for example, may be complimentary to nanoparticle-enhanced MRI, which has proven to be very useful for characterization of lymph nodes [27] but may have difficulties in tracing them.

## Monitoring response to therapy

Another potential application of DWIBS is in the assessment of radiation and/or chemotherapy efficacy. Currently, CT and anatomical MRI are the most commonly used means for the follow-up of cancer patients. Serial measurements of tumor dimensions are made, and criteria, such as the World Health Organization (WHO) or Response Evaluation Criteria in Solid Tumors (RECIST) criteria are applied to assess therapeutic efficacy [28]. DWIBS can similarly be applied and its ability to obtain (automated) total volume measurements may especially be useful (**Figure 9**). In the near future, it is expected that the further development of multichannel coils and accelerated parallel imaging will allow acquisition of true isotropic high-resolution volume data sets.

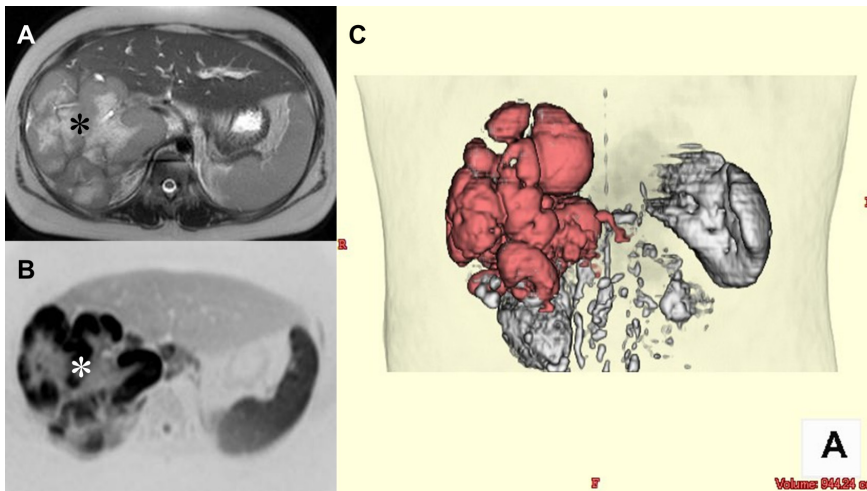


**Figure 9.** Volume measurement of a primary hepatic diffuse large B-cell lymphoma in a 10-year-old girl using DWIBS. (A) Axial respiratory-gated T2-weighted image shows a bulky mass occupying most of the right lobe of the liver (asterisk). (B) Axial DWIBS image (inverted black-and-white gray scale) at the same level clearly visualizes the tumor with excellent contrast between the tumor and surrounding tissue (asterisk). (C) Volume-rendered image using thin slice (4 mm, no gap) DWIBS dataset shows the three-dimensional shape of the tumor (colored red) and allows for tumor volume measurement.

A disadvantage of the current approach of obtaining repetitive tumor size measurements on CT or MRI is that it cannot be used to give an early assessment of the effectiveness of radiation and/or chemotherapy. Early identification of patients who are likely to show a poor response to a certain treatment can be of great advantage: it provides the opportunity to adjust individual treatment regimes more rapidly, and sparing patients unnecessary morbidity, expense and delay in initiation of effective treatment. PET is a promising functional imaging modality for the early

assessment of response to therapy for various tumors [29], but DWIBS, which is less expensive and does not require any patient preparation, may also be of value. Similar to PET, DWIBS is able to detect functional changes in areas involved with tumor before structural changes become visible (**Figure 10**). In addition, the recently introduced functional diffusion map (fDM \ currently referred to as parametric response mapping of diffusion) allows calculation and visualization of tumor ADC changes during treatment and takes into account spatial heterogeneity of tumor response; it has proved to be useful to predict treatment response in brain tumor patients [30-32] and its feasibility for evaluating treatment response of metastatic bone disease from prostate cancer has recently been presented [33]. Extracranial application of fDM analysis in a DWIBS examination would be very attractive, but is technologically challenging and requires further investigation. The accuracy and reproducibility of ADC mapping and measurements in DWIBS, which are the primary requisites for fDM analysis, should first be investigated.

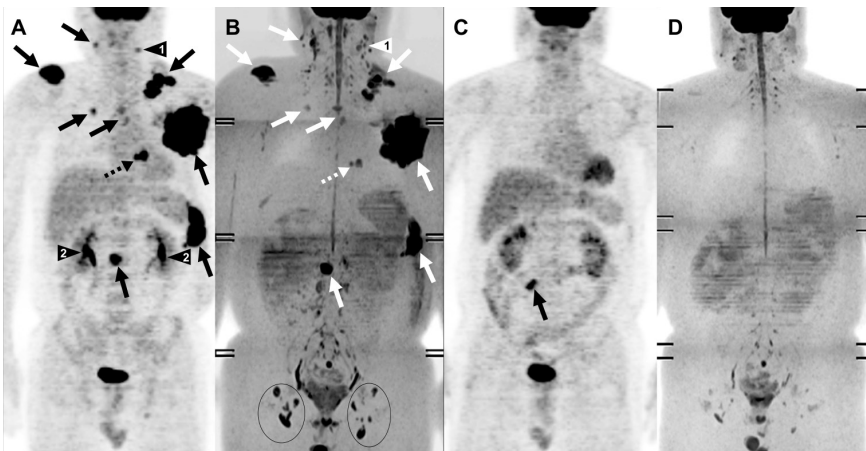


**Figure 10.** Comparison of pre- and post-chemotherapy FDG-PET and DWIBS images in a 44-year-old man with diffuse large B-cell lymphoma. (A) Coronal maximum intensity projection FDG-PET and (B) coronal maximum intensity projection DWIBS images before initiation of chemotherapy. Both images show cervical, bilateral supra/infraclavicular, mediastinal, left axillary, para-aortic lymph node, and splenic involvement (arrows), and cardiac involvement (dashed arrow). (C) FDG-PET and (D) DWIBS images at the end of treatment show resolution of all pre-existing lesions.

(A, B) A limitation of DWIBS is that discrimination between normal and metastatic lymph nodes is still based on size criteria; the FDG-PET positive left cervical lymph node (arrowhead 1) cannot conclusively be identified as malignant on DWIBS (arrowhead 1). DWIBS also shows prominent bilateral inguinal lymph nodes (within the circles) which are normal according to FDG-PET. On the other hand, thanks to its higher spatial resolution, DWIBS visualizes two separate cardiac lesions (dashed arrow), whereas FDG-PET shows only one large cardiac lesion (dashed arrow). DWIBS also allows better evaluation of the urinary tract than FDG-PET, where potential lesions can be obscured because of FDG accumulation (arrowheads 2). (C) Note the physiological FDG uptake in the large intestine (arrow), which should not be confused with persistent malignant lymphoma.

Detection of tumor persistence or recurrence

Differentiating persistent or recurrent tumor tissue from nontumoral posttherapeutic change is of great importance for correct patient management, but is often difficult with CT or anatomical MRI. Functional imaging techniques, such as PET [34] may allow better differentiation. The less expensive DWIBS may also be of value. It can be hypothesized that persistent or recurrent tumor tissue will show a more restricted diffusion than treatment-related changes, mainly because of higher cellular density. However, whether or not it is possible to differentiate persistent or recurrent tumor tissue from nontumoral posttherapeutic change using DWIBS still has to be determined.

### Initial results of DWIBS in oncology

The few clinical studies on DWIBS (i.e. DWI using high b-value [1000 s/mm<sup>2</sup>], the application of a fat suppression pre-pulse, image acquisition during free breathing, and multiple signal averaging) investigated only a small number of patients, and their results have to be considered as preliminary.

Ichikawa et al. [35] evaluated the usefulness of DWIBS in the detection of colorectal adenocarcinoma. Thirty-three consecutive patients with 33 endoscopic colonoscopically proven colorectal cancers and another 15 controls with a negative endoscopic colonoscopy were included. Visual assessment of the DWIBS images resulted in high sensitivity (91%, 20/22) and specificity (100%, 15/15). However, because no benign pathologies were included, specificity of DWIBS might have been overestimated [35].

Ichikawa et al [36] also investigated the value of DWIBS in the detection of pancreatic adenocarcinoma. Twenty-six patients with pathologically proven pancreatic adenocarcinoma and another 23 controls with either chronic pancreatitis (n = 20) or intraductal papillary mucinous tumors (n = 3), without any evidence of pancreatic adenocarcinoma during a minimum of 12 months of clinicoradiological follow-up, underwent DWIBS. Visual assessment of the DWIBS images resulted in high sensitivity (96.2%, 75/78) and specificity (98.6%, 68/69).

Tsushima et al. [37] investigated the value of DWIBS, T2-weighted MRI, and DWIBS/T2-weighted MRI fusion as a screening tool for the detection of abdominal malignancies. Thirty-seven patients with a malignant tumor (5 renal cell carcinomas, 4 advanced gastric carcinomas, 4 metastatic liver tumors, 3 pancreatic carcinomas, 2 hepatocellular carcinomas, 2 cholangiocarcinomas, 1 bone lesion of lymphoma, 1 transverse colon carcinoma, 5 rectal carcinomas, 3 ovarian carcinomas, 2 prostate carcinomas, 2 metastatic bone tumors, 1 peritoneal dissemination, 1 recurrent colon carcinoma, and 1 ascending colon carcinoma) and 73 patients without a malignant tumor were retrospectively analyzed. Malignant tumors had pathologically been verified and the



absence of a malignancy in the controls was confirmed by clinical and radiological (conventional MRI and contrast-enhanced CT) findings. The areas under the receiver operating characteristic curves for the visual detection of malignant lesions of DWIBS/T2-weighted MRI fusion (0.904) was significantly higher than those of DWIBS (0.720,  $P < 0.01$ ) and T2-weighted MRI (0.822,  $P < 0.05$ ). Both sensitivity and specificity were higher in DWIBS/T2-weighted MRI fusion (89.5% and 81.9%, respectively) compared with those of DWIBS (72.4% and 59.0%;  $P < 0.01$  and  $P < 0.001$ , respectively), and the specificity of DWIBS/T2-weighted MRI fusion (81.9%) was significantly higher than that of T2-weighted MRI (68.8%,  $P < 0.01$ ). Limitations of this study are its retrospective design, the presence of selection bias, the use of an imperfect reference standard, and the heterogeneity of the patient population [37].

Komori et al. [38] compared the lesion detection rates of DWIBS and  $^{18}\text{F}$ -fluoro-2-deoxyglucose (FDG)-PET/CT in 16 consecutive patients with a total of 27 malignant lesions (15 lung cancers, 5 pulmonary metastases of parathyroid cancer, 3 pulmonary metastases of lung cancer, 3 colon cancers, and 1 breast cancer). The lesions were confirmed to be malignant by means of biopsy, surgery, or a minimum clinical follow-up of six months. In addition, seven regions showing slight accumulation of FDG (standardized uptake value  $< 2.5$ ) were selected as reference organs, and their ADCs (in  $\times 10^{-3} \text{ mm}^2/\text{s}$ ) were measured and compared with those of the malignant lesions. Twenty-five (92.6%) of 27 malignant lesions were detected visually with DWIBS, in contrast to 22 malignant lesions (81.5%) with FDG-PET/CT. However, there was no significant difference between the mean ADCs of the reference organs ( $n = 7$ ,  $1.54 \pm 0.24 \text{ SD}$ ) and the malignant lesions ( $n = 25$ ,  $1.18 \pm 0.70 \text{ SD}$ ). Unfortunately, diagnostic performance of DWIBS in terms of sensitivity and specificity was not assessed in this study. Furthermore, the heterogeneity of the patient population may have led to overlapping ADCs in reference organs and malignant lesions. Another drawback of this study is that it was not clear whether the readers were blinded to the reference standard and FDG-PET/CT when interpreting the DWIBS images [38].

Tamai et al. [39] performed DWIBS in 18 consecutive females with surgically proven endometrial cancer and 12 cervical cancer patients with pathologically confirmed normal endometrium. All endometrial cancers and the normal endometria appeared hyperintense on DWIBS images. The mean ADC (in  $\times 10^{-3} \text{ mm}^2/\text{s}$ ) of endometrial cancer ( $0.88 \pm 0.16 \text{ SD}$ ) was significantly lower ( $P < 0.01$ ) than that of normal endometrium ( $1.53 \pm 0.10 \text{ SD}$ ), without any overlap between them. The mean ADC for each histologic grade was  $0.93 \pm 0.16 \text{ SD}$  (grade 1),  $0.92 \pm 0.13 \text{ SD}$  (grade 2), and  $0.73 \pm 0.09 \text{ SD}$  (grade 3). The ADC of grade 3 tumors was significantly lower than that of grade 1 tumors ( $P < 0.05$ ). This study proved DWIBS to be feasible in demonstrating endometrial cancer and suggests that ADC measurement has a potential ability to differentiate between normal and cancerous tissue in the endometrium. Estimation of histologic grade based on ADCs seems difficult because of considerable overlap.

A limitation of this study is that no benign endometrial pathologies were included. Therefore, it is still unclear whether it is possible to differentiate malignant from non-malignant endometrial lesions using ADC measurements in DWIBS. ADCs of the normal endometrium may vary according to menstrual cycle in premenopausal women, but menstrual phase of the patients was not taken into consideration in analyzing the ADCs of the normal endometrium in the control group. Another drawback of this study was the fact that readers were not completely blinded when analyzing the images of the control group [39].

Tamai et al. [40] also performed DWIBS in 43 surgically treated patients with 58 myometrial tumors, including seven uterine sarcomas (five leiomyosarcomas and two endometrial stromal sarcomas) and 51 benign leiomyomas (43 ordinary leiomyomas, two cellular leiomyomas and six degenerated leiomyomas), in addition to conventional non-enhanced and postcontrast MRI sequences. Both uterine sarcomas and cellular leiomyomas exhibited high signal intensity on DWIBS images, whereas ordinary leiomyomas and most degenerated leiomyomas showed low signal intensity. The mean ADC (in  $\times 10^{-3} \text{ mm}^2/\text{s}$ ) of sarcomas ( $1.17 \pm 0.15 \text{ SD}$ ) was lower than those of the normal myometrium ( $1.62 \pm 0.11 \text{ SD}$ ) and degenerated leiomyomas ( $1.70 \pm 0.11 \text{ SD}$ ) without any overlap; however, they overlapped with those of ordinary leiomyomas and cellular leiomyomas. This study suggests that, in addition to morphological features, DWIBS may be able to distinguish uterine sarcomas from benign leiomyomas, although ADC measurement may have a limited role due to a large overlap between sarcomas and benign leiomyomas. A disadvantage of this study is the nonconsecutive enrollment of patients. Furthermore, menstrual phase of the patients was not taken into account in the assessment of the ADC of the normal myometrium [40].

Ballon et al. [17] investigated the feasibility of monitoring response to therapy using DWIBS. Examples presented in their study include the evaluation of therapeutic response in bone marrow during cytotoxic therapy for leukemia and metastatic prostate cancer, and during cytokine administration for marrow mobilization prior to stem cell harvest [17].

## Drawbacks and limitations of DWIBS

### General

Although DWIBS offers many potential applications in oncological imaging, it may suffer from several drawbacks. First, DWIBS does not exclusively visualize malignant tumors. Benign pathologies with restricted diffusion, such as abscesses, will also exhibit high signal on DWIBS source images (**Figure 11**) [41]. Furthermore, DWIBS not only visualizes pathological areas of restricted diffusion, but also several normal structures; brain, salivary glands, tonsils, spleen, gallbladder, small intestine/small intestinal contents, colon, adrenal glands, prostate, testes, penis, endometrium, ovaries, spinal



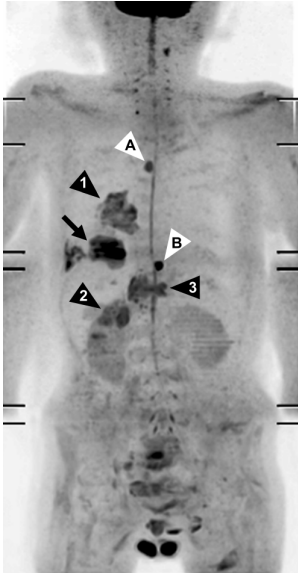


**Figure 11.** 78-year-old man with metastatic lung cancer and two benign lesions visualized with DWIBS. Coronal maximum intensity projection DWIBS image shows an area with restricted diffusion in the right lower lobe, consistent with lung cancer (arrow). In addition, DWIBS image shows ipsilateral hilar lymph node metastasis (arrowhead 1), retroperitoneal/adrenal metastasis (arrowhead 2), and vertebral metastasis (arrowhead 3). DWIBS image also shows restricted diffusion in a thoracic vertebra (arrowhead A). T1- and T2-weighted images (not shown), however, indicate this “lesion” to be a (benign) cavernous hemangioma, instead of a vertebral metastasis. Furthermore, DWIBS image shows a well-circumscribed area of restricted diffusion in the epigastric region (arrowhead B); physical examination reveals a (benign) sebaceous cyst to be responsible for this area of restricted diffusion.

cord, peripheral nerves, lymph nodes, and bone marrow may all exhibit high signal intensity on DWIBS source images (Figures 4, 5, and 10). High signal intensities within these organs do not necessarily indicate pathologic states, whereas true lesions within these organs may be obscured. Visibility of the spleen is highly variable and probably dependent on its iron content (and consequent signal loss). T2 shine-through and insufficiently suppressed fat signal may also hinder image interpretation. Although at the expense of prolonged acquisition time, T2 shine-through effects can be removed by performing ADC mapping, provided that ADC mapping is accurate and feasible in DWIBS. Another limitation of DWIBS is its suppression of background body signals, as a result of which sufficient anatomical information is lacking. Standard T1- and T2-weighted sequences therefore remain indispensable to act as an anatomical reference frame for the DWIBS images, in order to exactly localize lesions. DWIBS and anatomical (whole-body) MRI can be viewed side-by-side, or fused with commercially available software (Figure 12). An additional advantage of DWIBS/anatomical MRI fusion may be increased sensitivity and specificity [37]. Finally, although DWIBS images can be post-processed to create MIPs and PET-like images, which are very attractive for demonstration purposes (Figures 4, 5, and 10), source images should always be consulted, because subtle lesions may be missed or obscured in projected images.

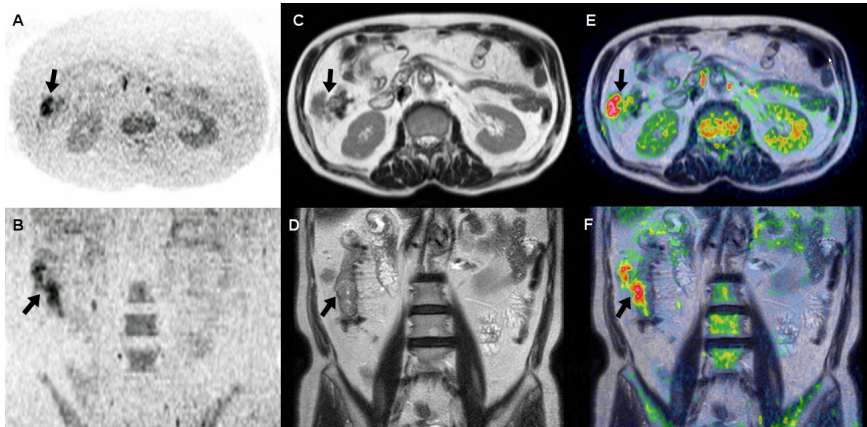


**Figure 12.** Fusion of a DWIBS image and a T2-weighted image in a 64-year-old man with ascending colon cancer. (A) Axial and (B) coronally reformatted DWIBS images show abnormal signal in the area of the ascending colon. (C) Axial and (D) coronal T2-weighted images show a large mass of intermediate signal intensity in the ascending colon, extending beyond the serosa. (E) Fused axial and (F) coronal DWIBS/T2-weighted images, highlighting the lesion.

#### ADC measurements in DWIBS

Signal intensity is directly related to the degree of diffusion and the ADC is the quantitative measure of diffusion in DWI. Both signal intensity and ADCs are mainstays in the identification and characterization of lesions in DWI. However, because of the allowance of respiratory motion in DWIBS, slice levels of images obtained with different b-values may not be identical. In addition, because DWIBS employs multiple slice excitations, slices levels of images obtained with the same b-value may be different. Consequently, ADC measurements of moving organs in DWIBS may be less accurate, less reproducible, and different from conventional (breathhold or respiratory triggered) DWI. In other words, DWIBS images of moving organs are possibly more suitable for visual nonquantitative evaluation than quantitative analysis. In their phantom study, Muro et al. [42] reported that ADCs of slowly moving phantoms, simulating respiratory motion, were no more than 10% different from ADCs of static phantoms, if the ROIs were placed (and remained) within the homogeneous phantom. However, if the ROIs covered the edge of the phantom, ADCs were markedly different [42]. Thus, the results of this study indicate that ADC measurements of homogeneous tissue appear to be accurate, whereas ADC measurements of heterogeneous tissue or small lesions (e.g. pulmonary nodules or small liver lesions) may be unreliable in DWIBS. Nasu et al. [43] compared ADCs of hepatic malignant tumors in both respiratory triggered DWI and DWIBS. Thirty patients with liver metastasis or hepatocellular carcinoma in the right hepatic lobe were examined. The mean measured ADC in respiratory triggered DWI was  $1.36 (\pm 0.33 \text{ SD})$ , whereas the mean measured ADC in DWIBS was  $1.47 (\pm 0.61$

SD). The statistical difference between both mean ADCs was not clear ( $P=0.050$ ). The individual ADCs in DWIBS were more scattered than those in respiratory triggered DWI and there was no regular pattern in individual ADC differences [43]. It should be noted, however, that the comparison between respiratory triggered DWI and DWIBS was (clinically) not fair, since roughly estimated scanning time of respiratory triggered DWI was approximately 1.3-2 times longer [43]. It should be noted that in a similar investigation with accurate time measurements, scanning time in respiratory triggering was even nearly three times longer [44]. More in vivo research is needed to determine the accuracy and reproducibility of ADC measurements in DWIBS.

### Future considerations of DWIBS

More studies with large sample sizes are needed to establish the value of DWIBS and to develop criteria for differentiation between malignant and non-malignant lesions. Future research is also warranted to optimize the sequence for DWIBS. An important issue in DWIBS is the optimization of background body signal suppression, while maintaining high signal from areas with restricted diffusion. Fat suppression is essential for lymph node and lesion conspicuity in DWIBS. Takahara et al. [16] reported STIR to be superior to CHESS for fat suppression in the neck/upper chest region in DWIBS at 1.5 T. In addition, STIR has the potential advantage to avoid false positive results because of intestinal contents. However, there is no report yet which technique is better for detecting intestinal (e.g. colonic) tumors. Whether STIR or CHESS should be preferred for DWIBS of the trunk at 1.5 T requires further systematic investigation. Additionally, the utility of using negative oral contrast agents should be investigated; the use of a negative oral contrast agent may further aid in the suppression of bowel signal [45], which is especially important when evaluating (possible) gastrointestinal/ intra-abdominal malignancies. DWIBS at 3.0 T potentially offers higher SNR, since SNR increases linearly with increasing field strength. Susceptibility artifacts, on the other hand, increase exponentially with increasing field strength, which will degrade DWIBS images [46]. A recent feasibility study indeed reported DWIBS at 3.0 T to provide a better lesion-to-bone tissue contrast, compared to DWIBS at 1.5 T [47]. STIR proved to offer the best fat suppression in all body regions at 3.0 T [47]. However, larger susceptibility-induced image distortions and signal intensity losses, stronger blurring artifacts, and more pronounced motion artifacts degraded the image quality at 3.0 T [47]. Thus, further investigations concerning DWIBS at 3.0 T should be undertaken. Image acquisition during free breathing is the hallmark and the driving force behind the DWIBS sequence. A disadvantage of this free breathing approach, however, is the possibility of image blurring due to the periodic displacement of the diaphragm (**Figure 13A**), which may hamper adequate visualization of small lesions near the diaphragm, such as in the liver. Respiratory triggering may be used to reduce image blurring

(**Figure 13B**), but increases image acquisition time. The recently introduced tracking only navigator (TRON) technique, however, adequately deals with both problems. As the name implies, the navigator-echo in TRON is not used to create a gating window (in other words, data acquired during the entire breathing cycle can be used for image formation), but is only used to track and correct for displacements. Consequently, displaced organs and lesions near the diaphragm can be visualized with less blurring and with only minimal prolongation of scan time (**Figure 13C**) [44]. TRON is a very promising tool for DWIBS of paradiaphragmatic organs and lesions, but its technical performance (i.e. whether it routinely results in anatomically reliable, reproducible images) still needs to be investigated.

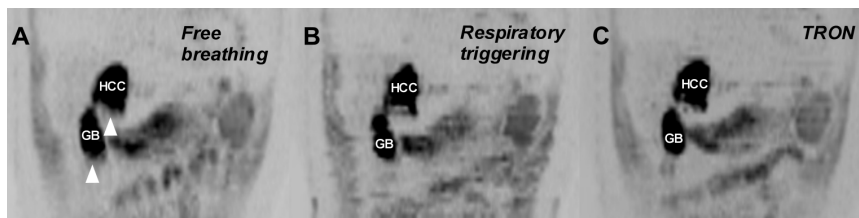


**Figure 13.** Comparison of DWIBS images obtained (1) during free breathing, (2) with respiratory triggering and (3) with TRON, in a 48-year-old male with hepatocellular carcinoma and hemochromatosis. (A) Coronally reformatted DWIBS image obtained during free breathing shows an area with restricted diffusion in segment IV of the liver; biopsy proved this lesion to be a hepatocellular carcinoma (HCC). Bile in the gallbladder (GB) also shows restricted diffusion. Note significant blurring of the hepatocellular carcinoma and the gallbladder, especially at their lower boundaries (arrowheads). (B) Coronally reformatted DWIBS image obtained with respiratory triggering results in reduced blurring of the hepatocellular carcinoma (HCC) and the gallbladder (GB), but introduces stepladder-like artifacts due to gating error. Furthermore, image acquisition time is approximately 2.5 times prolonged in comparison to (A). (C) Coronally reformatted DWIBS image obtained with TRON shows slight gating error, but offers good delineation of the hepatocellular carcinoma (HCC) and the gallbladder (GB). Image acquisition time is only slightly (approximately 1.2 times) increased in comparison to (A).

## Summary

Image acquisition during free breathing, multiple signal averaging, and background body signal suppression by means of a fat suppression pre-pulse and heavy diffusion weighting, are the main features of DWIBS. DWIBS is a diffusion-weighted sequence, but its (image) characteristics are different from conventional (breathhold or respiratory triggered) DWI. DWIBS highlights areas with restricted diffusion, such as occurs in many malignant primary and metastatic tumors, and provides an outstanding visualization of lymph nodes. Although the exact value of DWIBS still has to be established, it has potential use in tumor staging, monitoring response to cancer therapy, and in the detection of tumor persistence or recurrence.

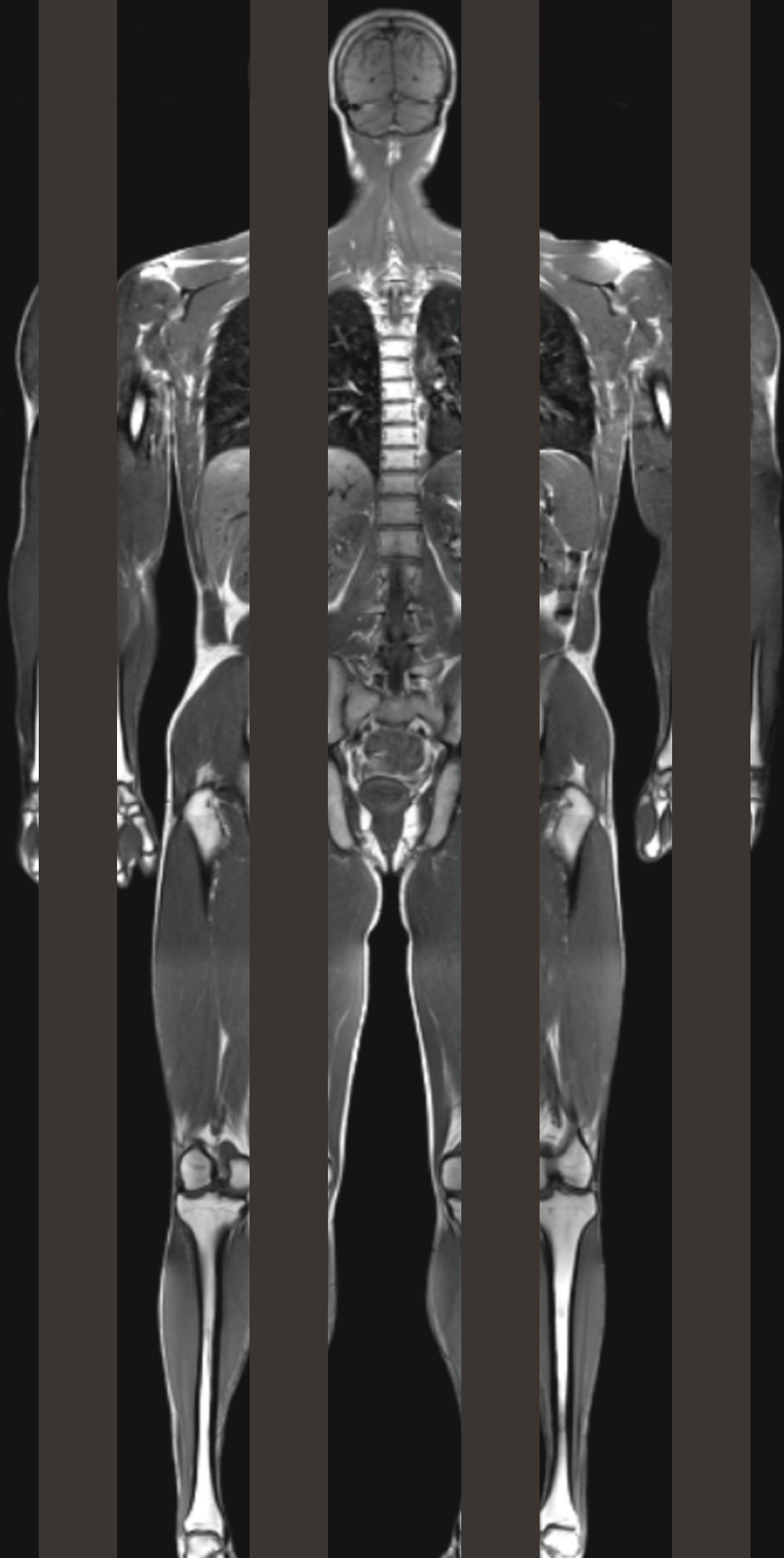
## References

1. World Health Organization. International Union Against Cancer. Global action against cancer. Geneva: WHO Press, 2005
2. Ichikawa T, Haradome H, Hachiya J, Nitatori T, Araki T. Diffusion-weighted MR imaging with single-shot echo-planar imaging in the upper abdomen: preliminary clinical experience in 61 patients. *Abdom Imaging* 1999;24:456-461
3. Ichikawa T, Haradome H, Hachiya J, Nitatori T, Araki T. Diffusion-weighted MR imaging with a single-shot echoplanar sequence: detection and characterization of focal hepatic lesions. *AJR Am J Roentgenol* 1998;170:397-402
4. Muller MF, Prasad P, Siewert B, et al. Abdominal diffusion mapping with use of a whole-body echo-planar system. *Radiology* 1994;190:475-478
5. Muller MF, Prasad P, Bimmler D, et al. Functional imaging of the kidney by means of measurement of the apparent diffusion coefficient. *Radiology* 1994;193:711-715
6. Edelman RR, Gaa J, Wedeen VJ, et al. In vivo measurement of water diffusion in the human heart. *Magn Reson Med* 1994;32:423-428
7. Bammer R. Basic principles of diffusion-weighted imaging. *Eur J Radiol* 2003;45:169-184
8. Glockner JF, Hu HH, Stanley DW, Angelos L, King K. Parallel MR imaging: a user's guide. *Radiographics* 2005;25:1279-1297
9. Thoeny HC, De Keyzer F. Extracranial applications of diffusion-weighted magnetic resonance imaging. *Eur Radiol* 2007;17:1385-1393
10. Koh DM, Collins DJ. Diffusion-weighted MRI in the body: applications and challenges in oncology. *AJR Am J Roentgenol* 2007;188:1622-1635
11. Low RN, Gurney J. Diffusion-weighted MRI (DWI) in the oncology patient: value of breathhold DWI compared to unenhanced and gadolinium-enhanced MRI. *J Magn Reson Imaging* 2007;25:848-858.
12. Nasu K, Kuroki Y, Nawano S, et al. Hepatic metastases: diffusion-weighted sensitivity-encoding versus SPIO-enhanced MR imaging. *Radiology* 2006;239:122-130
13. Yoshikawa T, Kawamitsu H, Mitchell DG, et al. ADC measurement of abdominal organs and lesions using parallel imaging technique. *AJR Am J Roentgenol* 2006;187:1521-1530
14. Nasu K, Kuroki Y, Kuroki S, Murakami K, Nawano S, Moriyama N. Diffusion-weighted single shot echo planar imaging of colorectal cancer using a sensitivity-encoding technique. *Jpn J Clin Oncol* 2004;34:620-626
15. Taouli B, Martin AJ, Qayyum A, et al. Parallel imaging and diffusion tensor imaging for diffusion-weighted MRI of the liver: preliminary experience in healthy volunteers. *AJR Am J Roentgenol* 2004;183:677-680
16. Takahara T, Imai Y, Yamashita T, Yasuda S, Nasu S, Van Cauteren M. Diffusion weighted whole body imaging with background body signal suppression (DWIBS): technical improvement using free breathing, STIR and high resolution 3D display. *Radiat Med* 2004;22:275-282
17. Ballon D, Watts R, Dyke JP, et al. Imaging therapeutic response in human bone marrow using rapid whole-body MRI. *Magn Reson Med* 2004;52:1234-1238

18. Stejskal EO, Tanner JE. Spin diffusion measurements: spin echoes in the presence of a time-dependent field gradient. *J Chem Phys* 1965;42:288-292
19. Turner R, Le Bihan D, Maier J, et al. Echo-planar imaging of intravoxel incoherent motion. *Radiology* 1990;177:407-414
20. Le Bihan D, Breton E, Lallemand D, Aubin ML, Vignaud J, Laval-Jeantet M. Separation of diffusion and perfusion in intravoxel incoherent motion MR imaging. *Radiology* 1988;168:497-505
21. Le Bihan D, Breton E, Lallemand D, Grenier P, Cabanis E, Laval-Jeantet M. MR imaging of intravoxel incoherent motions: application to diffusion and perfusion in neurological disorders. *Radiology* 1986;161:401-407
22. Le Bihan D. Molecular diffusion nuclear magnetic resonance imaging. *Magn Reson Q* 1991;7:1-30
23. Provenzale JM, Mukundan S, Barboriak DP. Diffusion-weighted and perfusion MR imaging for brain tumor characterization and assessment of treatment response. *Radiology* 2006;239:632-649
24. Delfaut EM, Beltran J, Johnson G, Rousseau J, Marchandise X, Cotten A. Fat suppression in MR imaging: techniques and pitfalls. *Radiographics* 1999;19:373-382
25. Li S, Sun F, Jin ZY, Xue HD, Li ML. Whole-body diffusion-weighted imaging: technical improvement and preliminary results. *J Magn Reson Imaging* 2007;26:1139-1144
26. Torabi M, Aquino SL, Harisinghani MG. Current concepts in lymph node imaging. *J Nucl Med* 2004;45:1509-1518
27. Will O, Purkayastha S, Chan C, et al. Diagnostic precision of nanoparticle-enhanced MRI for lymph-node metastases: a meta-analysis. *Lancet Oncol* 2006;7:52-60
28. Jaffe CC. Measures of response: RECIST, WHO, and new alternatives. *J Clin Oncol* 2006;24:3245-3251
29. Weber WA. Positron emission tomography as an imaging biomarker. *J Clin Oncol* 2006;24:3282-3292
30. Hamstra DA, Rehemtulla A, Ross BD. Diffusion magnetic resonance imaging: a biomarker for treatment response in oncology. *J Clin Oncol* 2007;25:4104-4109
31. Hamstra DA, Chenevert TL, Moffat BA, et al. Evaluation of the functional diffusion map as an early biomarker of time-to-progression and overall survival in high-grade glioma. *Proc Natl Acad Sci U S A* 2005;102:16759-16764
32. Moffat BA, Chenevert TL, Lawrence TS, et al. Functional diffusion map: a noninvasive MRI biomarker for early stratification of clinical brain tumor response. *Proc Natl Acad Sci U S A* 2005;102:5524-5529
33. Lee KC, Bradley DA, Hussain M, et al. A feasibility study evaluating the functional diffusion map as a predictive imaging biomarker for detection of treatment response in a patient with metastatic prostate cancer to the bone. *Neoplasia* 2007;9:1003-1011
34. Rohren EM, Turkington TG, Coleman RE. Clinical applications of PET in oncology. *Radiology* 2004;231:305-332
35. Ichikawa T, Erturk SM, Motosugi U, et al. High-B-value diffusion-weighted MRI in colorectal cancer. *AJR Am J Roentgenol* 2006;187:181-184
36. Ichikawa T, Erturk SM, Motosugi U, et al. High-b value diffusion-weighted MRI for detecting pancreatic adenocarcinoma: preliminary results. *AJR Am J Roentgenol* 2007;188:409-414
37. Tsushima Y, Takano A, Taketomi-Takahashi A, Endo K. Body diffusion-weighted MR imaging using high b-value for malignant tumor screening: usefulness and necessity of referring to T2-weighted images and creating fusion images. *Acad Radiol* 2007;14:643-650

38. Komori T, Narabayashi I, Matsumura K, et al. 2-[Fluorine-18]-fluoro-2-deoxy-D-glucose positron emission tomography/computed tomography versus whole-body diffusion-weighted MRI for detection of malignant lesions: initial experience. *Ann Nucl Med* 2007;21:209-215
39. Tamai K, Koyama T, Saga T, et al. Diffusion-weighted MR imaging of uterine endometrial cancer. *J Magn Reson Imaging* 2007;26:682-687
40. Tamai K, Koyama T, Saga T, et al. The utility of diffusion-weighted MR imaging for differentiating uterine sarcomas from benign leiomyomas. *Eur Radiol* 2008;18:723-730
41. Stadnik TW, Demaerel P, Luypaert RR, et al. Imaging tutorial: differential diagnosis of bright lesions on diffusion-weighted MR images. *Radiographics* 2003;23:e7
42. Muro I, Takahara T, Horie T, et al. Influence of respiratory motion in body diffusion weighted imaging under free breathing (examination of a moving phantom). *Nippon Hoshasen Gijutsu Gakkai Zasshi* 2005;61:1551-1558
43. Nasu K, Kuroki Y, Sekiguchi R, Nawano S. The effect of simultaneous use of respiratory triggering in diffusion-weighted imaging of the liver. *Magn Reson Med Sci* 2006;5:129-136
44. Takahara T, Ogino T, Okuaki T, et al. Respiratory gated body diffusion weighted imaging avoiding prolongation of scan time: tracking only navigator echo (TRON) technique. Presented at the Joint Annual Meeting ISMRM-ESMRMB, Berlin, Germany, May 19-25, 2007
45. Laghi A, Paolantonio P, Iafrate F, Altomari F, Miglio C, Passariello R. Oral contrast agents for magnetic resonance imaging of the bowel. *Top Magn Reson Imaging* 2002;13:389-396
46. Kuhl CK, Textor J, Gieseke J, et al. Acute and subacute ischemic stroke at high-field-strength (3.0-T) diffusion-weighted MR imaging: intraindividual comparative study. *Radiology* 2005;234:509-516
47. Murtz P, Krautmacher C, Traber F, Gieseke J, Schield HH, Willinek WA. Diffusion-weighted whole-body MR imaging with background body signal suppression: a feasibility study at 3.0 Tesla. *Eur Radiol* 2007;17:3031-3037







# Chapter 4<sup>2</sup>

## Whole-body diffusion-weighted magnetic resonance imaging

Kwee TC, Takahara T, Ochiai R, Katahira K, Van Cauteren M, Imai Y, Nievelstein RA, Lijten PR

*Eur J Radiol* 2009;70:409-417

## Abstract

Diffusion-weighted magnetic resonance imaging (DWI) provides information on the diffusivity of water molecules in the human body. Technological advances and the development of the concept of diffusion-weighted whole-body imaging with background body signal suppression (DWIBS) have opened the path for routine clinical whole-body DWI. Whole-body DWI allows detection and characterization of both oncological and non-oncological lesions throughout the entire body. This article reviews the basic principles of DWI and the development of whole-body DWI, illustrates its potential clinical applications, and discusses its limitations and challenges.

## Introduction

Computed tomography (CT) is one of the technologies that came to dominate the cross-sectional imaging of human anatomy in clinical practice. However, functional or metabolic pathologic changes can occur in the absence of any corresponding anatomical changes, and are not visualized by anatomical imaging. Furthermore, posttherapeutic changes may be difficult to be discriminated from residual disease by CT alone. Functional imaging techniques, including single photon emission computed tomography (SPECT) and positron emission tomography (PET), are complementary to anatomical imaging, and multimodality scanners which are able to acquire coregistered structural and functional information, such as SPECT/CT and PET/CT, play an increasingly important role in the evaluation of human disease [1]. Disadvantages of SPECT/CT and PET/CT, however, are a relatively long preparation time for the examination and exposure of the patient and examiner to ionizing radiation. Magnetic resonance imaging (MRI) does not have these disadvantages. Furthermore, MRI is able to provide both anatomical and functional information within a single examination. In particular, the development and clinical application of whole-body diffusion-weighted MRI (DWI) is under active investigation. Whole-body DWI provides functional information (i.e. diffusivity of water molecules) and is able to highlight both oncological and non-oncological lesions throughout the entire body. Whole-body DWI may be a powerful adjunct to anatomical whole-body MRI, by detecting subtle lesions and pathologic changes in normal-sized structures, and reducing image interpretation time. Moreover, anatomical whole-body MRI and whole-body DWI can be performed in the same scanner, without patient repositioning (unlike in SPECT/CT and PET/CT), which reduces the probability of a mismatch between anatomical and functional datasets. Furthermore, practical implementation of whole-body DWI is relatively easy, since it can be performed on most modern MRI scanners and does not require any contrast agent administration. This article reviews the basic principles of DWI and the development of whole-body DWI, illustrates its potential clinical applications, and discusses its limitations and challenges.

## Basic principles of DWI

Diffusion in biological tissue

DWI allows visualization and measurement of the random (Brownian) extra-, intra-, and transcellular motion of water molecules, driven by their internal thermal energy. The signal intensity in DWI is a function of the Brownian motion of an ensemble of water molecules [2, 3]. For water molecules in the bulk phase, the probability distribution of displacements due to Brownian motion is Gaussian and symmetrically disposed about their original position [2, 4]. In biological tissue, however, the presence of restricting barriers (such as cell membranes, fibers, and macromolecules) interferes

with the free displacement (diffusion) of water molecules. Consequently, in biological tissue the signal intensity in DWI depends on the separation and permeability of these restricting boundaries. More specifically, water diffusion in biological tissue is thought to be composed of diffusing water molecules in the intracellular spaces, diffusing water molecules in the extracellular spaces, and diffusing water molecules across the cell membrane (i.e. from the intracellular to extracellular spaces, and vice versa) (**Figure 1**). Intravascular water molecules may also contribute to signal intensity in DWI, but these perfusion effects are nullified when strong diffusion-weighting is employed [5, 6], such as is common in whole-body DWI. Water diffusion in the intracellular spaces is considered to be more impeded than that in the extracellular spaces, since intracellular spaces contain more natural barriers. Pathophysiological processes which alter the volume ratio between the intracellular space and the extracellular space, or pathological processes which alter the physical nature of the impeding barriers within the intracellular or extracellular spaces, or cell membrane itself, affect the diffusivity of the water molecules, which can be visualized with DWI and measured by the apparent diffusion coefficient (ADC) [4]. Besides cellular structure, it should be noted that viscosity also influences water diffusivity, according to an inverse relationship [2]. Thus, in summary, the visualization and measurement of the diffusivity of water molecules in the human body by DWI represents a fingerprint of cellular characteristics. The first successful clinical application of DWI was in diagnosing acute ischemic stroke. Failure of the  $\text{Na}^+/\text{K}^+$  ATPase pump in ischemic stroke leads to a net translocation of water from the extracellular to the intracellular space. As a result, intracellular/extracellular volume ratio increases, corresponding to a more restricted diffusion [7]. DWI may also be used for tumor detection and characterization throughout the body. For example, tumors with a high cellular density have a relatively higher intracellular/extracellular space volume ratio, and consequently a relatively impeded diffusion (**Figure 1**). Failure of the  $\text{Na}^+/\text{K}^+$  ATPase pump during necrotic cell death in tumors (similar to acute ischemic stroke) may also lead to an impeded diffusion. An impeded diffusion has been reported for most malignant tumors [8, 9]. On the other hand, loss of cell membrane integrity in necrotic tumors (i.e. increase in the diffusion of water molecules from the intracellular to extracellular spaces, and vice versa) and decrease in tumor cellularity (i.e. decrease in the intracellular/extracellular space volume ratio) due to necrosis and/or apoptotic processes may result in increased diffusivity. In addition, intratumoral edema and cystic tumor components also increase diffusivity because of increased water content [8, 9]. Finally, DWI may be used to detect and characterize various non-oncological lesions, such as inflammatory lesions, infections/abscesses, and intravascular thrombi [10, 11]. For example, inflammatory lesions and infections may exhibit an impeded diffusion due to cellular swelling (which decreases the intracellular/extracellular space volume ratio), and abscesses and thrombi are believed to decrease the diffusivity of water molecules because of their hyperviscous nature.

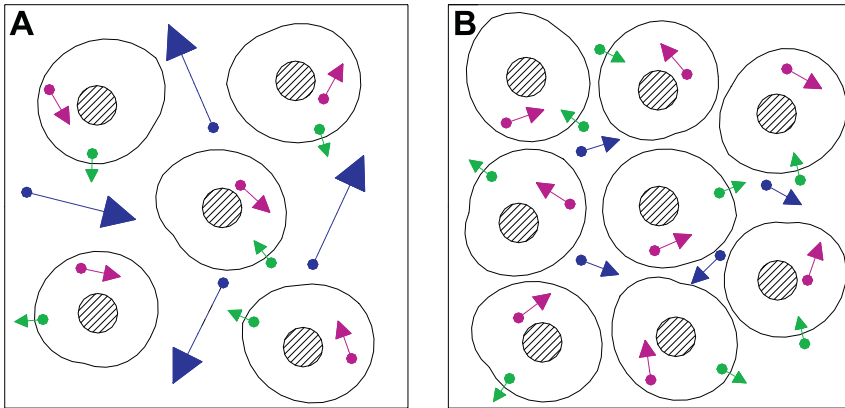


**Figure 1.** Schematic representation of diffusing water molecules in the intracellular spaces (purple arrows), diffusing water molecules in the extracellular spaces (blue arrows), and diffusing water molecules from the intracellular to extracellular spaces, and vice versa (green arrows). (A) Normal tissue; the largest amount of water diffusion takes place in the extracellular spaces (blue arrows). (B) Tissue with increased cellular density (e.g. tumor tissue) has relatively less water diffusion in the extracellular spaces (blue arrows), and consequently an overall more restricted diffusion.

#### DWI sequence

The most common approach for a DWI acquisition is the use of a T2-weighted spin echo sequence, with two strong motion probing gradients (MPGs) on either side of the 180° refocusing pulse, which is also known as the Stejskal-Tanner sequence (**Figure 2**) [12]. Stationary water molecules within a voxel acquire a phase shift by the first MPG, which is nullified by the second MPG. The resultant signal intensity of that voxel is equal to its signal intensity on an image obtained with the same sequence without the MPGs. However, water molecules within a voxel undergoing diffusion acquire a phase shift by the first MPG, which is not nullified by the second MPG because of a positional difference of the water molecules between the moment of the application of the first MPG and the moment of the application of the second MPG; as a result, signal is attenuated. The resultant signal intensity (SI) of a voxel containing diffusing water molecules is equal to its intensity on a T2-weighted image decreased by an amount related to the degree of diffusion:

$$SI = SI_0 \times \exp(-b \times D), \quad (1)$$

where  $SI_0$  is the signal intensity on the T2-weighted (or  $b = 0$  s/mm<sup>2</sup>) image,  $D$  is the diffusion coefficient, and  $b$  is the b-value (which expresses the degree of diffusion weighting) which is calculated as follows:

$$b = \gamma^2 \times G^2 \times \delta^2 (\Delta - \delta/3), \quad (2)$$

where  $\delta$  is the duration of one MPG,  $\Delta$  is the interval between the leading edges of the MPGs,  $G$  is the strength of the MPG (**Figure 2**), and  $\gamma$  is the gyromagnetic ratio (the ratio of the magnetic moment to the angular momentum of a particle, 42.58 MHz/T for hydrogen) [3, 12].

DWI is usually performed with MPGs in three orthogonal directions. However, fewer or more MPG directions may also be used, depending on the presence of diffusional isotropy (i.e. equal limitations to diffusion in all directions) or diffusional anisotropy (i.e. unequal limitations to diffusion in certain directions) of the tissue of interest and the investigator's interest. For example, DWI in the brain or kidney may preferably be performed with MPGs in at least three directions, because of their anisotropic nature [13, 14].

Since the Stejskal-Tanner sequence is based on a T2-weighted spin echo sequence, the acquired diffusion-weighted image also has T2-weighted contrast, which is referred to as T2 shine-through. T2 shine-through may be mistaken for impeded diffusion. To differentiate between potential areas of T2 shine-through and areas with an impeded diffusion, and to allow quantification of diffusion by means of the ADC, two or more images with different b-values should be acquired; the ADC ( $D$ ) of a selected region-of-interest (ROI) can then be calculated as follows:

$$D = (1/(b_1 - b_0)) \ln (S[b_0]/S[b_1]), \quad (3)$$

where  $b_1$  and  $b_0$  represent two different b-values,  $S[b_1]$  the signal intensity of the selected ROI on the image acquired with b-value  $b_1$ , and  $S[b_0]$  the signal intensity of the same ROI on the image acquired with b-value  $b_0$ . A pixel by pixel map (so-called ADC map), whose intensity yields quantitative estimation of the regional ADC, can be obtained by post-processing and applying the equations described above [15, 16]. It should be noted that T2 shine-through does not necessarily hinder image interpretation, but, in fact, often even increases conspicuity of lesions, since many lesions have both a prolonged T2 and an impeded diffusion.

## Development of whole-body DWI

### MRI technology

By the end of the 1990s, DWI became a well-established method for brain imaging, mainly because of its exquisite sensitivity to ischemic stroke [7]. This clinical rise of DWI can primarily be attributed to the development of high-performance magnetic field gradients, allowing for ultrafast single-shot echo-planar imaging (EPI), which is necessary for DWI. With EPI, the complete image is formed after the application of a single radiofrequency (RF) excitation pulse (or a 90-180° RF-pulse combination [**Figure 2**]) within a fraction of a second [17]. However, the long train of gradient echoes

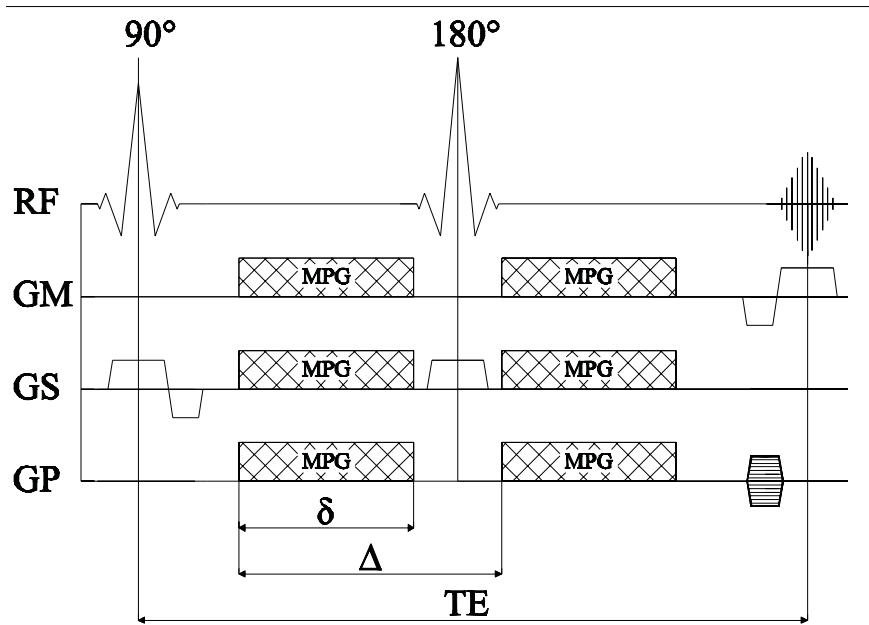


**Figure 2.** The Stejskal-Tanner sequence [12] (RF radio frequency, GM readout direction, GP phase encoding direction, GS section select direction, MPG motion probing gradient,  $\delta$  duration of one MPG,  $\Delta$  time interval between the leading edges of the MPGs, TE echo time). Note that the Stejskal-Tanner sequence is basically a T2-weighted spin echo sequence if the MPGs are not applied.

in the EPI-readout results in T2\*-decay, which can markedly limit the maximum attainable spatial resolution. In addition, EPI has only a very small bandwidth per pixel along the phase encoding direction. Consequently, EPI is very susceptible to main field inhomogeneities, local susceptibility gradients, and chemical shift, which all may lead to severe image degradation. These artifacts occur in case of tissue heterogeneity, especially at air-tissue and bone-tissue boundaries [3, 18]. Because of the heterogeneous tissue in the trunk with its many air-tissue boundaries (e.g. in the vicinity of the lungs and bowels, and at the surface of the body) and because of the high likelihood of motion artifacts in the trunk, whole-body DWI was previously not clinically feasible yet. However, relatively recently introduced parallel imaging techniques, such as SENSitivity Encoding (SENSE), can reduce the train of gradient echoes in the EPI-readout in combination with a faster  $k$ -space traversal per unit time. The resultant increased bandwidth per pixel in the phase-encoding direction and the shortened EPI train significantly decrease image distortion [3, 19]. The advent of these parallel imaging techniques, and the continuing development of stronger gradients and multichannel coils have finally enabled whole-body DWI.

## Conceptualization of whole-body DWI

Until recently, breathholding or respiratory triggering were considered necessary for DWI outside the brain, in order to minimize artifacts from physiological motion and to maintain sensitivity to diffusion (which is on the order of several micrometers). DWI under free breathing was considered to be impossible, because it was assumed that respiratory motion would lead to loss of diffusion-weighted image contrast. However, neither breathholding nor respiratory triggering allow clinically acceptable whole-body DWI. Breathhold scanning only allows obtaining thick-sliced diffusion-weighted images with relatively low signal-to-noise ratio (SNR), without the possibility to perform three-dimensional image processing (such as multiple planar reformatting [MPR], maximum intensity projection [MIP], and volume rendering [VR]). As a result, lesion conspicuity is likely diminished. Although respiratory triggered scanning allows obtaining thin-sliced high-quality diffusion-weighted images, its prolonged examination time (image acquisition takes only place within a particular phase of the respiratory cycle) is a serious impediment for routine clinical whole-body DWI.

In 2004, Takahara et al. [20] overcame the problems inherent to breathholding and respiratory triggering, by showing the feasibility of whole-body DWI under free breathing. This concept is also known as diffusion-weighted whole-body imaging with background body signal suppression (DWIBS). To understand the feasibility of DWIBS, knowledge of the concepts of intravoxel incoherent motion (IVIM) and intravoxel coherent motion (IVCM) is important. IVIM refers to the incoherent, random motion of water molecules within a voxel (diffusion equals IVIM). IVIM implies a change in the spatial relationship among water molecules within a voxel. IVCM refers to the coherent, synchronous motion of water molecules within a voxel [15, 16]. IVCM implies bulk tissue motion which does not affect the spatial relationship among water molecules within a voxel. Four combinations of intravoxel motion of water molecules can be encountered (**Figure 3** and **Table 1**). In case of no IVIM (i.e. no diffusion), only T2-weighted contrast is observed in DWI, with slight image blurring in case of concomitant IVCM; this was known before the development of DWIBS. In case of IVIM without IVCM, as is well-known, both diffusion-weighted contrast and T2-weighted contrast are observed. Most importantly, in case of IVIM and IVCM, diffusion-weighted image contrast is maintained, with only slight image blurring (**Table 1**). The reason why IVCM does not affect diffusion-weighted image contrast is the fact that the acquired phase shift of coherently moving water molecules induced by the two MPGs in the Stejskal-Tanner sequence is equal in each phase-encoding step and, therefore, does not affect image formation. Since respiratory motion can be regarded as coherent motion during the small period in which the two MPGs are applied (usually < 50 ms), DWI under free breathing (i.e. the concept of DWIBS) is feasible. As mentioned previously, slight image blurring occurs in case of DWI under free breathing (free breathing equals IVCM). However, as a trade-off, scanning time is



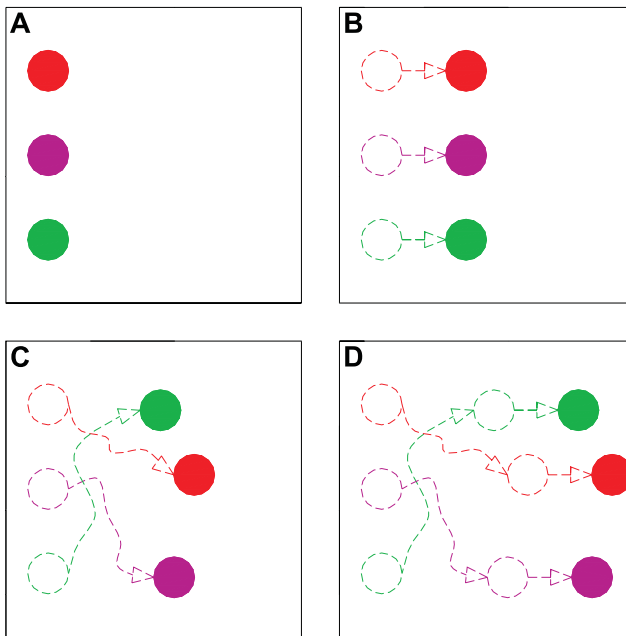


**Figure 3.** Schematic representation of three water molecules in a voxel, undergoing four different types of motion. (A) No intravoxel coherent motion (IVIM) and no intravoxel coherent motion (IVCM). (B) IVCM, but no IVIM. (C) IVIM, but no IVCM. (D) IVIM with concomitant IVCM.

**Table 1.** Four combinations of intravoxel motion of water molecules and their effect on image contrast and image quality in DWI.

No.	IVIM	IVCM	Image contrast	Image quality
1	No	No	T2-weighted only	No blurring
2	No	Yes	T2-weighted only	Slight blurring
3	Yes	No	Diffusion-weighted and T2-weighted	No blurring
4	Yes	Yes	Diffusion-weighted and T2-weighted	Slight blurring

IVIM: intravoxel incoherent motion; IVCM: intravoxel coherent motion

unlimitedly available (unlike in breathholding) and the use of the available scanning time is extremely efficient (unlike in respiratory triggering); this allows thin-sliced DWI with multiple signal averagings (to increase SNR and allowing for MPR, MIP, and VR), within a clinically acceptable examination time. Thus, DWIBS has become the approach to perform whole-body DWI.

Practical implementation of whole-body DWI

Practical implementation of whole-body DWI, using the DWIBS concept, is relatively easy, since it can be performed on most modern MRI scanners and does not require any contrast agent administration. Furthermore, compared to SPECT/CT and PET/

CT, MRI scanners are more widely available, and whole-body DWI is less expensive. Besides a free breathing approach, DWIBS is further characterized by heavily diffusion-weighting (b-values of up to 1000-1500 s/mm<sup>2</sup> are applied) and the application of either a short inversion time inversion recovery (STIR) pre-pulse or a frequency selective [chemical shift selective (CHESS)] pre-pulse for fat suppression, in order to optimize background body signal suppression and improve lesion conspicuity. Note that fat suppression is also required to avoid image degradation due to severe chemical shift when using EPI. The choice for the degree of diffusion-weighting and the method of fat suppression depend on the organ/body region under examination. However, for whole-body scanning, generally a b-value of 1000 s/mm<sup>2</sup> is selected, combined with STIR for robust fat suppression over an extended field of view (which is especially important in the neck, shoulder, lungs, and lower extremities, areas which are prone to significant magnetic field inhomogeneities) [21]. Nevertheless, CHESS may be selected for scanning the abdominopelvic part (which usually does not suffer significantly from magnetic field homogeneities) of a whole-body DWI examination, in order to increase SNR and decrease image examination time [21]. On the other hand, if bowel signal suppression is an important issue, STIR may be preferred for the abdominopelvic region as well [21]. It is currently recommended to obtain axial slices in DWIBS, with the phase-encoding in the anterior-posterior direction, in order to minimize image distortion. Typical image acquisition parameters for whole-body DWI at 1.5 T are: repetition time/echo time/inversion time of 10205/70/180 ms, number of slices of 60, slice thickness/gap of 4/0 mm, cranio-caudal coverage of 24 cm for each station, field of view (FOV) of 43 cm, rectangular FOV of 80%, acquisition matrix of 160, scan percentage (phase encoding reduction) of 70%, half scan factor of 0.6, EPI factor (echo train length) of 47, image acquisition in the axial plane, MPGs in three orthogonal axes, b values of 0 and 1000 s/mm<sup>2</sup>, 10 signals averaged, parallel imaging SENSE factor of 2, actual voxel size of 2.5 × 3.6 × 4.0 mm<sup>3</sup>, calculated voxel size of 1.6 × 1.6 × 4.0 mm<sup>3</sup>, and total acquisition time of 7 minutes and 8 s for each station. If a CHESS pre-pulse is selected instead of a STIR pre-pulse for fat suppression, and if 6 instead of 10 signals are averaged, image acquisition time of one station can be reduced to approximately 3 minutes. Obtained axial DWIBS images can be post-processed for MPR, MIP, and VR. Usually, grayscale inversion is applied, which makes the DWIBS images resemble PET images.

Whole-body DWI is currently best performed at 1.5 T, using a surface coil for signal reception. Whole-body DWI at 3.0 T potentially offers higher SNR, and is feasible [22], but is technologically challenging due to the higher risk of susceptibility artifacts. Whole-body DWI can be performed using only one surface coil with limited coverage. In order to perform such an examination, an additional table platform should be mounted on top of the original patient table. Furthermore, spacers should be placed between both tables to create space to move the lower part of the surface

coil from one station to the next. As a result, the patient can remain in the same position, repositioning of the surface coil to image the next station requires only little additional time (<1 minute per station), and 3D alignment among the imaged stations is maintained. After completion of the examination, separately imaged stations can be merged with sophisticated software, creating the whole-body image. Another, more advanced approach to perform whole-body DWI is the use of a so-called whole-body surface coil design. A whole-body surface coil design combines a large number of seamlessly integrated coil elements and independent radiofrequency channels, which offers large anatomical coverage (in the order of 200 cm) and allows image acquisition without any time loss due to patient or coil repositioning.

## Potential clinical applications of whole-body DWI

### Oncological

Whole-body DWI enables visualization of various primary and metastatic tumors exhibiting an impeded diffusion throughout the entire body (**Figures 4-7**). Whole-body DWI, using the concept of DWIBS, may be a powerful adjunct to anatomical whole-body MRI, by detecting subtle lesions and pathologic changes in normal-sized structures, thanks to its high contrast-to-noise ratio (CNR). Furthermore, whole-body DWI immediately directs the eye of the investigator to all potential lesions, which reduces image interpretation time of anatomical whole-body MRI alone. However, whole-body DWI should always be evaluated together with other (anatomical) whole-body MRI sequences, in order to avoid false-positive results. This was also confirmed in a recent study by Ohno et al. [23], who investigated 203 patients with non-small cell lung cancer for M-stage assessment; specificity and accuracy of whole-body T1-weighted in-phase imaging with and without contrast enhancement, T1-weighted opposed-phase imaging, and STIR imaging, with (specificity,  $P=0.02$ ; accuracy,  $P<0.01$ ) and that without whole-body DWI (specificity,  $P=0.02$ ; accuracy,  $P=0.01$ ) were significantly higher than those of whole-body DWI alone. Similarly, Tsushima et al. [24] investigated the value of DWIBS and DWIBS/T2-weighted MRI fusion as a screening tool for the detection of abdominal malignancies in 37 patients, and found that sensitivity and specificity of DWIBS/T2-weighted MRI fusion (89.5% and 81.9%) were significantly higher ( $P<0.01$  and  $P<0.001$ ) than those of DWIBS alone (72.4% and 59.0%).

Determination of nodal status is of crucial importance for appropriate treatment planning and determining prognosis in patients with cancer. Current cross-sectional imaging modalities, however, rely on insensitive size and morphologic criteria and, thus, lack the desired accuracy for characterizing lymph nodes [25]. Whole-body DWI, using the concept of DWIBS, may also be a valuable tool for the identification and characterization of lymph nodes throughout the entire body. Normal lymph nodes

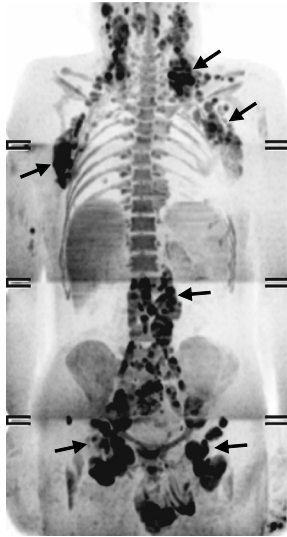


**Figure 4.** A 60-year-old man with stage III diffuse large B-cell non-Hodgkin lymphoma. Coronal maximum intensity projection whole-body DWI shows widespread supra- and infradiaphragmatic lymphadenopathy (arrows).

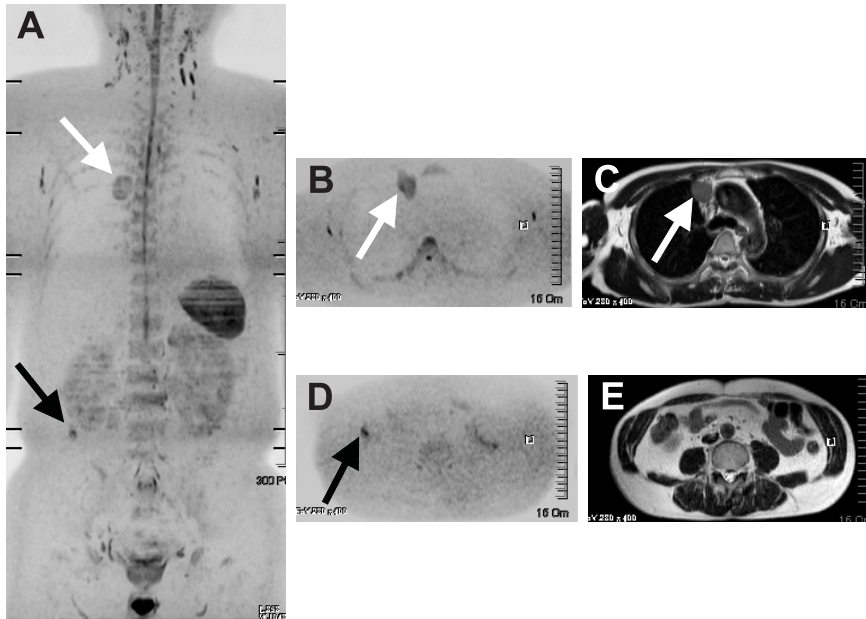


**Figure 5.** A 63-year-old asymptomatic male who underwent whole-body DWI for health screening, with a thymoma and a moderately differentiated submucosal ascending colon cancer. (A) Coronal maximum intensity projection whole-body DWI shows the thymoma (white arrow) and the ascending colon cancer (black arrow). (B) Corresponding axial DWI and (C) axial T2-weighted image also show the thymoma (white arrows). (D) Corresponding axial DWI shows the ascending colon cancer (black arrow), but (E) axial T2-weighted image does not depict the lesion.

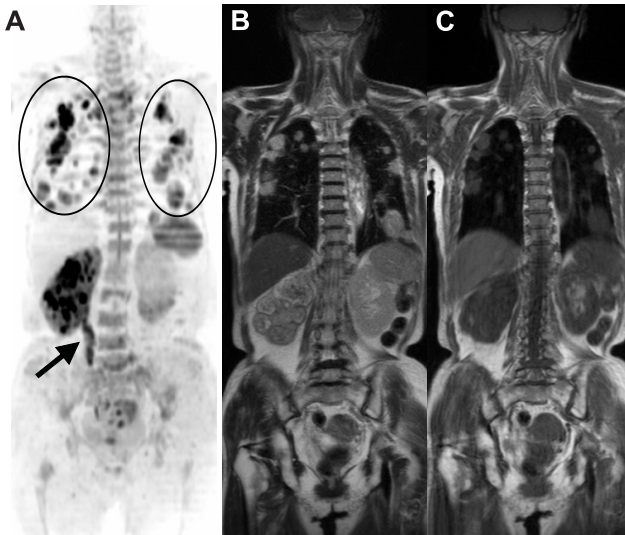


**Figure 6.** A 75-year-old female with metastatic transitional cell carcinoma of the right ureter. (A) Coronal maximum intensity projection whole-body DWI showing the right ureteral tumor with diffuse renal involvement (arrow) and multiple lung metastases (encircled). (B) Corresponding coronal T2 weighted whole-body image and (C) corresponding coronal T1-weighted whole-body image.

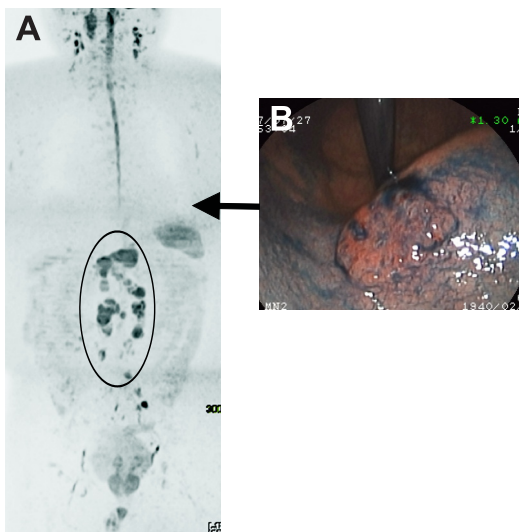


**Figure 7.** A 67-year-old asymptomatic male who underwent whole-body DWI for health screening, with a moderately differentiated gastric cancer and lymph node metastasis. (A) Coronal maximum intensity projection whole-body DWI shows pathologically enlarged lymph nodes (encircled). The gastric cancer itself, however, is not visualized. This may be due to the relative close proximity of the stomach to the heart, which may result in signal loss because of intravoxel incoherent heart motion. Air in the stomach (which may lead to susceptibility artefacts), peristalsis, and the size of the gastric cancer (limited to the muscularis propria, maximum diameter of 3 cm) may also play a role. (B) Gastroscopic image showing the primary gastric cancer.

have a relatively impeded diffusion (low ADC) because of their high cellular density. Metastatic lymph nodes may have increased cellular density or necrotic areas, which further impedes or increases diffusion, respectively. Initial reports show that ADCs of metastatic lymph nodes are significantly lower than those of non-metastatic lymph nodes [26, 27]. ADC measurements may thus be helpful in discriminating malignant from non-malignant lymph nodes, although further research on this topic is certainly required. It should also be noted that ADCs obtained in different centers may vary, because of different ways of ADC measurements (e.g. measurement of the entire lymph node will result in a higher ADC than in a measurement in which necrotic regions are excluded) and different image acquisition parameters (e.g. lower field strengths and lower b-values reduce image distortion and improve SNR on the ADC). Therefore, each center may need to establish its own reference values until further data are available [28]. Besides lymph node characterization, DWI is an outstanding tool to identify lymph nodes, irrespective of their histological composition. DWI, for example, may be complimentary to nanoparticle-enhanced MRI, which has proven to be very useful for characterization of lymph nodes [29] but may have difficulties in tracing them.

Whole-body DWI, using the concept of DWIBS, may also be very useful for monitoring response to cancer therapy. First of all, it allows for tumor volume measurements, thanks to its high CNR. Secondly, and most importantly, changes in tumor diffusion due to successful radiation and/or chemotherapy (which induce changes in cellularity, necrosis, and/or apoptosis) may occur earlier than significant changes in tumor size. These early changes in tumor diffusion can be visualized with whole-body DWI, which potentially allows early discrimination of responders and nonresponders to cancer therapy. Consequently, individual treatment regimes can be adjusted more rapidly, and patients can be spared unnecessary morbidity, expense and delay in initiation of effective treatment.

Finally, posttherapeutic changes may be difficult to discriminate from residual or recurrent disease by anatomical imaging alone in cancer patients. Whole-body DWI may also play an important role in these cancer patients; residual or recurrent tumor may have a higher cellular density (i.e. a relatively higher intracellular/extracellular space volume ratio) and consequently more restricted diffusion than posttherapeutic changes, which can be visualized using whole-body DWI.

#### Non-oncological

Although many of its potential clinical applications lie in oncological imaging, whole-body DWI may also be of value in detecting and evaluating various non-oncological pathologies. Inflammatory lesions, infections/abscesses, and intravascular thrombi may have a restricted diffusion and are well depicted by whole-body DWI (**Figure 8**) [10, 11]. Another high potential non-oncological application of whole-body DWI

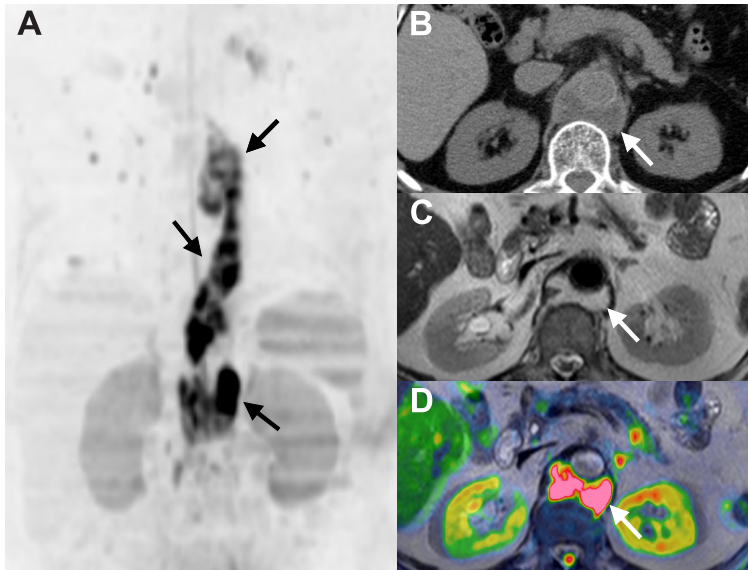


**Figure 8.** A 80-year-old female with a retroperitoneal abscess. (A) Coronal maximum intensity projection whole-body DWI clearly shows the lesion along the central part of the body. (B) Axial non-enhanced CT-scan, (C) axial T2-weighted image, and (D) fused axial DWI/T2-weighted image, show ballooning of the diaphragmatic crus and the lesion in the retroaortic area (arrows).

is the visualization of the peripheral nervous system. Normal peripheral nerves have a relatively restricted diffusion and are well-visualized with DWI (**Figure 9**). In a feasibility study, Takahara et al. [30] showed the potential of DWI in visualizing the brachial plexus. Eventually, it is expected that it will be possible to visualize the entire peripheral nervous system with a single whole-body DWI examination.

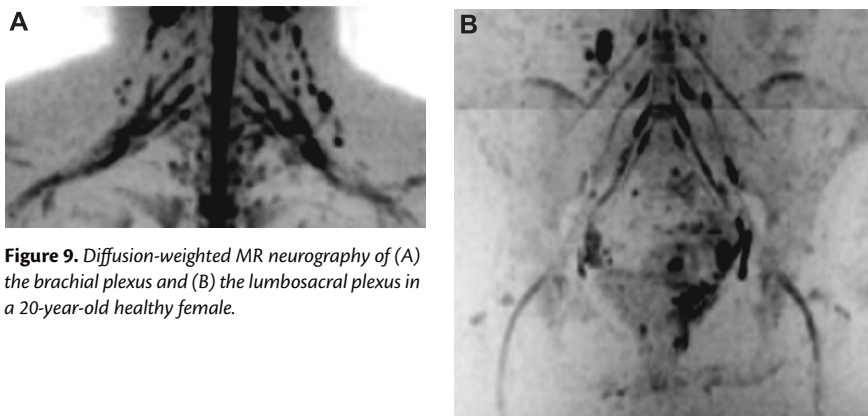


**Figure 9.** Diffusion-weighted MR neurography of (A) the brachial plexus and (B) the lumbosacral plexus in a 20-year-old healthy female.



## Limitations and challenges of whole-body DWI

The fact that whole-body DWI shows all areas with restricted diffusion throughout the entire body is also one of its main limitations, since an impeded diffusion is neither confined to pathologic conditions only (several normal structures also exhibit an impeded diffusion), nor to a specific pathologic condition only (both oncological and various non-oncological lesions) exhibit an impeded diffusion) (**Table 2**). Therefore, a careful evaluation of whole-body DWI findings, along with other (anatomical) whole-body MRI sequences [23, 24], a patient's accurate history, and clinical examination, is necessary to minimize the number of false-positive interpretations.

**Table 2.** Visualized normal tissues and pathologic conditions in whole-body DWI.

Visualized normal tissues*	Visualized pathologic conditions
- <i>Nervous system</i>	-Tumors
Brain, spinal cord, peripheral nerves	-Inflammatory lesions
- <i>Gastrointestinal system</i>	-Infections/abscesses
Salivary glands, gallbladder, small intestinal and colonic contents	-Thrombi, hematoma
- <i>Lymphatic system</i>	
Tonsils, spleen, lymph nodes	
- <i>Genitourinary system</i>	
Kidneys, adrenal glands, prostate, testis, penis, endometrium, ovaries	
-Bone marrow	

\*The number and signal intensity of visualized normal tissues in whole-body DWI varies per individual and is also dependent on the applied imaging protocol (e.g. more normal tissues with higher signal intensity are visualized when applying lower b-values, and when using a CHESS pre-pulse instead of a STIR pre-pulse for fat suppression)

Furthermore, whole-body DWI may have difficulty in depicting areas with an impeded diffusion close to the heart because of signal loss due to incoherent intravoxel heart motion (**Figure 7**). Another drawback of whole-body DWI, using the concept of DWIBS, is slight image blurring (slight image blurring is accepted in exchange for an unlimitedly available scanning time, allowing for thin-sliced DWI with multiple signal averagings). Therefore, respiratory triggering may still be necessary for visualization of small objects near the diaphragm (such as small liver lesions), but this is at the expense of a two- to threefold increase in scanning time. The recently developed TRacking Only Navigator (TRON) technique, however, may successfully deal with both problems. In contrast to conventional navigator echo-based respiratory gating, the navigator echo in TRON is only used for tracking (i.e. correction of displacements) and not for gating (i.e. only acceptance of data during a narrow window). Consequently, TRON may offer sharp images of moving objects, with only slight prolongation of scanning time [31]. TRON is a very promising tool, but still needs to be clinically investigated. Another

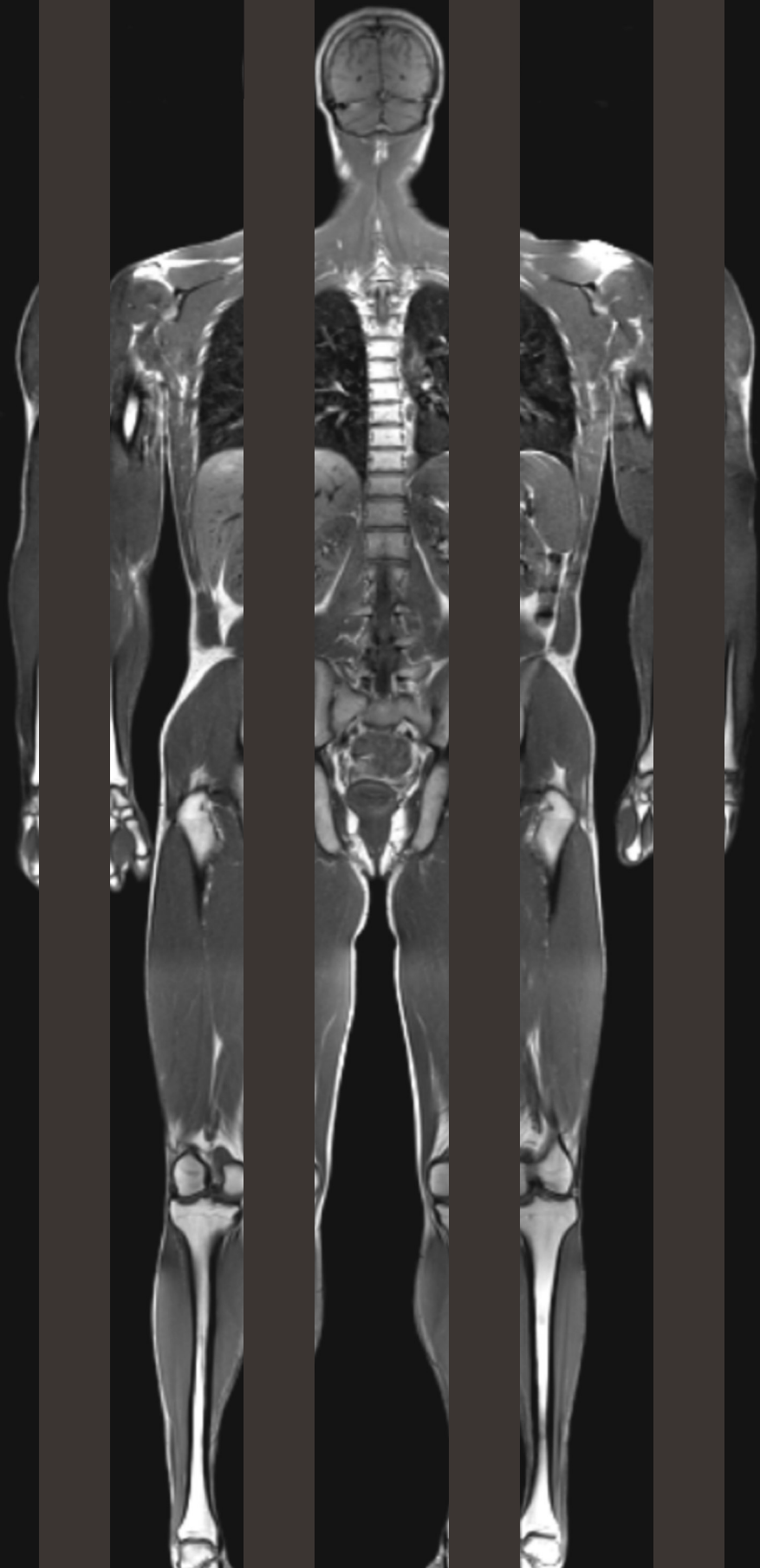


issue is that ADC measurements of small or heterogeneous lesions, especially near the diaphragm, may be inaccurate in whole-body DWI, using the concept of DWIBS. This is due to the fact that slice levels of diffusion-weighted images obtained with different excitations (using the same or different b-values) may be different in areas undergoing respiratory motion. Therefore, breathholding or respiratory triggering may still be necessary for accurate ADC measurement of small or heterogeneous moving objects [32]. Finally, although whole-body DWI has high clinical potential, more research is needed to establish the value of whole-body DWI in comparison to other whole-body imaging modalities (such as SPECT/CT and PET/CT), in the evaluation of various oncological and non-oncological pathologies.

## References

1. Townsend DW. Multimodality imaging of structure and function. *Phys Med Biol* 2008;53:R1-R39
2. Einstein A. Investigations on the theory of the Brownian motion. Dover, New York, 1956
3. Bammer R. Basic principles of diffusion-weighted imaging. *Eur J Radiol*. 2003;45:169-184
4. Sotak CH. Nuclear magnetic resonance (NMR) measurement of the apparent diffusion coefficient (ADC) of tissue water and its relationship to cell volume changes in pathological states. *Neurochem Int* 2004;45:569-582
5. Koh DM, Scurr E, Collins DJ, et al. Colorectal hepatic metastases: quantitative measurements using single-shot echo-planar diffusion-weighted MR imaging. *Eur Radiol* 2006;16:1898-1905
6. Yamada I, Aung W, Himeno Y, Nakagawa T, Shibuya H. Diffusion coefficients in abdominal organs and hepatic lesions: evaluation with intravoxel incoherent motion echo-planar MR imaging. *Radiology* 1999;210:617-623
7. Schaefer PW, Grant PE, Gonzalez RG. Diffusion-weighted MR imaging of the brain. *Radiology* 2000;217:331-345
8. Thoeny HC, De Keyser F. Extracranial applications of diffusion-weighted magnetic resonance imaging. *Eur Radiol* 2007;17:1385-1393
9. Provenzale JM, Mukundan S, Barboriak DP. Diffusion-weighted and perfusion MR imaging for brain tumor characterization and assessment of treatment response. *Radiology* 2006;239:632-649
10. Takahara T. Whole body volumetric diffusion-weighted imaging (DWI). Presented at the ISMRM 16<sup>th</sup> Scientific Meeting and Exhibition, Toronto, Ontario, Canada, May 3-9, 2008
11. Nakahashi M, Sato N, Tsushima Y, Amanuma M, Endo K. Diffusion-weighted magnetic resonance imaging of the body in venous thrombosis: a report of four cases. *Abdom Imaging*. 2008;33:353-356
12. Stejskal EO, Tanner JE. Spin diffusion measurements: spin echoes in the presence of a time-dependent field gradient. *J Chem Phys* 1965;42:288-292
13. Sakuma H, Nomura Y, Takeda K, et al. Adult and neonatal human brain: diffusional anisotropy and myelination with diffusion-weighted MR imaging. *Radiology* 1991;180:229-233
14. Fukuda Y, Ohashi I, Hanafusa K, et al. Anisotropic diffusion in kidney: apparent diffusion coefficient measurements for clinical use. *J Magn Reson Imaging* 2000;11:156-160
15. Le Bihan D, Breton E, Lallemand D, Grenier P, Cabanis E, Laval-Jeantet M. MR imaging of intravoxel incoherent motions: application to diffusion and perfusion in neurologic disorders. *Radiology* 1986;161:401-407
16. Le Bihan D, Breton E, Lallemand D, Aubin ML, Vignaud J, Laval-Jeantet M. Separation of diffusion and perfusion in intravoxel incoherent motion MR imaging. *Radiology* 1988;168:497-505
17. Poustchi-Amin M, Mirowitz SA, Brown JJ, McKinstry RC, Li T. Principles and applications of echo-planar imaging: a review for the general radiologist. *Radiographics* 2001;21:767-779
18. Liu C, Ogawa S. EPI image reconstruction with correction of distortion and signal losses. *J Magn Reson Imaging* 2006;24:683-689
19. Glockner JF, Hu HH, Stanley DW, Angelos L, King K. Parallel MR imaging: a user's guide. *Radiographics* 2005;25:1279-1297
20. Takahara T, Imai Y, Yamashita T, Yasuda S, Nasu S, Van Cauteren M. Diffusion weighted whole body imaging with background body signal suppression (DWIBS): technical improvement using free breathing, STIR and high resolution 3D display. *Radiat Med* 2004;22:275-282

21. Delfaut EM, Beltran J, Johnson G, Rousseau J, Marchandise X, Cotten A. Fat suppression in MR imaging: techniques and pitfalls. *Radiographics* 1999;19:373-382
22. Mürtz P, Krautmacher C, Träber F, Gieseke J, Schild HH, Willinek WA. Diffusion-weighted whole-body MR imaging with background body signal suppression: a feasibility study at 3.0 Tesla. *Eur Radiol* 2007;17:3031-3037
23. Ohno Y, Koyama H, Onishi Y, et al. Non-small cell lung cancer: whole-body MR examination for M-stage assessment-utility for whole-body diffusion-weighted imaging compared with integrated FDG PET/CT. *Radiology* 2008;248:643-654
24. Tushima Y, Takano A, Taketomi-Takahashi A, Endo K. Body diffusion-weighted MR imaging using high b-value for malignant tumor screening: usefulness and necessity of referring to T2-weighted images and creating fusion images. *Acad Radiol* 2007;14:643-650
25. Torabi M, Aquino SL, Harisinghani MG. Current concepts in lymph node imaging. *J Nucl Med* 2004;45:1509-1518
26. Kim JK, Kim KA, Park BW, Kim N, Cho KS. Feasibility of diffusion-weighted imaging in the differentiation of metastatic from nonmetastatic lymph nodes: early experience. *J Magn Reson Imaging* 2008;28:714-719
27. Akduman El, Momtahn AJ, Balci NC, Mahajann N, Havlioglu N, Wolverson MK. Comparison between malignant and benign abdominal lymph nodes on diffusion-weighted imaging. *Acad Radiol* 2008;15:641-646
28. King AD, Ahuja AT, Yeung DK, et al. Malignant cervical lymphadenopathy: diagnostic accuracy of diffusion-weighted MR imaging. *Radiology* 2007;245:806-813
29. Will O, Purkayastha S, Chan C, et al. Diagnostic precision of nanoparticle-enhanced MRI for lymph-node metastases: a meta-analysis. *Lancet Oncol* 2006;7:52-60
30. Takahara T, Hendrikse J, Yamashita T, Mali WPTM, Kwee TC, Imai Y, Luijten PR. Diffusion-weighted MR neurography of the brachial plexus: feasibility study. *Radiology* 2008;249:653-660
31. Takahara T, Ogino T, Okuaki T et al. Respiratory gated body diffusion weighted imaging avoiding prolongation of scan time: tracking only navigator echo (TRON) technique. Presented at the Joint Annual Meeting ISMRM-ESMRMB, Berlin, Germany, May 19–25, 2007
32. Muro I, Takahara T, Horie T, et al. Influence of respiratory motion in body diffusion weighted imaging under free breathing (examination of a moving phantom). *Nippon Hoshasen Gijutsu Gakkai Zasshi* 2005;61:1551-1558



# Chapter 4<sup>3</sup>

## Whole-body diffusion-weighted imaging for staging malignant lymphoma in children

Kwee TC, Takahara T, Vermoolen MA, Bierings MB, Mali WP, Nievelstein RA

Pediatr Radiol; 2010;40:1592-1602

## Abstract

Computed tomography (CT) is currently the mainstay in staging malignant lymphoma in children, but the risk of second neoplasms due to ionizing radiation associated with CT is non-negligible. Whole-body magnetic resonance imaging (MRI) techniques, and whole-body diffusion-weighted imaging (DWI) in particular, may be a good radiation-free alternative to CT. DWI is characterized by a high sensitivity for the detection of lesions and allows quantitative assessment of diffusion, which may aid in the evaluation of malignant lymphomas. This article will review whole-body MRI techniques for staging malignant lymphoma, with emphasis on whole-body DWI. Furthermore, future considerations and challenges in whole-body DWI will be discussed.

## Introduction

Cancer is the second most common cause of death among children aged 0-14 years, surpassed only by accidents [1]. Of all childhood cancers, the malignant lymphomas (Hodgkin's disease [HD] and non-Hodgkin lymphoma [NHL]), rank third in incidence, with an age-standardized incidence rate of 15.5 per million [2]. Furthermore, in adolescents (aged 15-19 years), the malignant lymphomas are the leading cause of cancer, with an age-standardized incidence of 47.4 per million [2]. Once a malignant lymphoma has been diagnosed histologically, extent of disease has to be assessed (i.e. staging), because this determines treatment planning and prognosis, and knowing all sites of involvement allows monitoring the effect of therapy [3, 4]. Malignant lymphomas are staged using the Ann Arbor staging system [3, 4], except for pediatric NHLs which are staged using the Murphy staging system [5, 6]. Initial staging (i.e. staging of patients with newly diagnosed malignant lymphoma) and restaging (i.e. staging after onset or completion of therapy, or staging in case of disease recurrence) are usually done by means of computed tomography (CT) or combined  $^{18}\text{F}$ -fluoro-2-deoxyglucose positron emission tomography (FDG-PET)/CT [7, 8]. FDG-PET/CT has a central role in the management of pediatric HD. However, FDG-PET does not form part of the standard imaging protocol in pediatric NHL, although it is often performed in an ad hoc fashion. A disadvantage of (FDG-PET)/CT is exposure of the patient to ionizing radiation, which may lead to the development of second neoplasms in later life [9]. This is especially important in children and adolescents, because they are inherently more radiosensitive than adults, and because they have more remaining years of life during which a radiation-induced cancer could develop [9]. Over the past decades, outcome of pediatric patients with malignant lymphoma has improved considerably, with long-term event-free survival rates of >90% in pediatric HD [10] and >80% in pediatric NHL [11]. Current treatment strategies for malignant lymphoma aim at maximizing chance of cure, while minimizing (late) toxicity such as infertility, premature menopause, cardiac disease, and, most importantly, risk of second neoplasms [10, 11]. Therefore, addressing the radiation risks from CT is an important issue in this patient population. Using dedicated low-dose CT protocols in children may reduce the risk of radiation-induced fatal cancer from CT [12]. An alternative solution is to replace (FDG-PET)/CT by other, radiation-free imaging modalities, such as ultrasound or magnetic resonance imaging (MRI) [12]. In the context of staging of malignant lymphoma, whole-body MRI may be an excellent alternative to (FDG-PET)/CT, because it allows cross-sectional imaging of the entire body, provides a high soft-tissue contrast, and offers a wide arsenal of anatomical and functional sequences. With regard to the latter, whole-body diffusion-weighted imaging (DWI) has recently been introduced as a potentially useful functional imaging modality to evaluate malignant lymphomas [13, 14]. Since some centres already perform MRI for staging, DWI may

be added to the routine MRI protocol as a potentially valuable adjunct. In this article, whole-body MRI techniques for staging malignant lymphoma, and whole-body DWI in particular, will be described and illustrated. Furthermore, future considerations and challenges in whole-body DWI will be discussed.

## Whole-body MRI techniques for staging malignant lymphoma

### Conventional whole-body MRI

Although there is no standard protocol for whole-body MRI, and the definition of “whole-body MRI” is rather arbitrary, whole-body MRI is usually performed or displayed in the coronal plane, with a field of view that provides a coverage of at least the area from the head/neck to the upper thighs (**Figures 1 and 2**) [15-18].

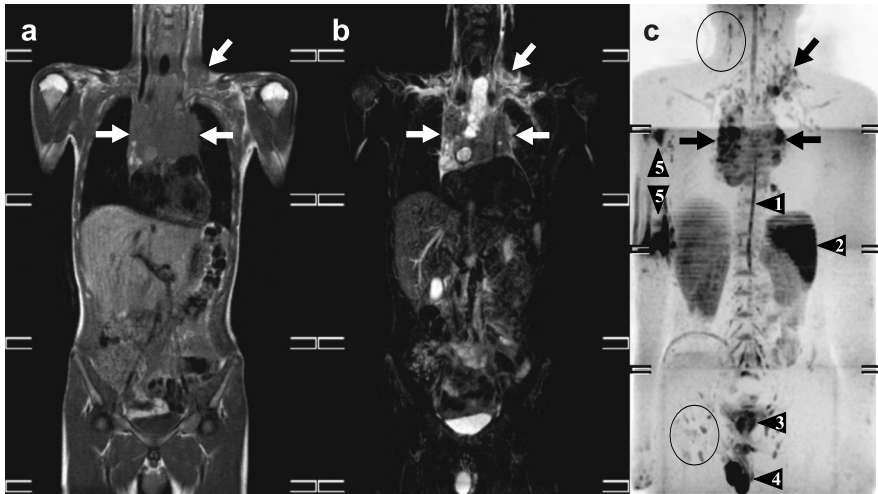


**Figure 1.** A 15-year-old male with stage II nodular sclerosing Hodgkin's disease. Coronal whole-body T1-weighted (a), STIR (b) and grayscale inverted MIP diffusion-weighted images (c) show cervical and mediastinal lymph node involvement (arrows). Note normal high signal intensity of the spinal cord (arrowhead 1), spleen (arrowhead 2), prostate (arrowhead 3) and testes (arrowhead 4) at whole-body DWI (c). Also note insufficiently suppressed fat (arrowheads 5), not to be mistaken for pathologic lesions. Normal lymph nodes (encircled) are also visualized at whole-body DWI.

Previously, separate body regions were imaged by repeatedly repositioning the patient [19]. However, this approach was time-consuming, and uncomfortable to both the examiner and the patient. At present, this limitation has been overcome by the widespread availability of sliding table platforms which allow sequential movement of the patient through the bore of the magnet without patient repositioning [20]. Commonly applied sequences for whole-body MRI include (contrast-enhanced) T1-



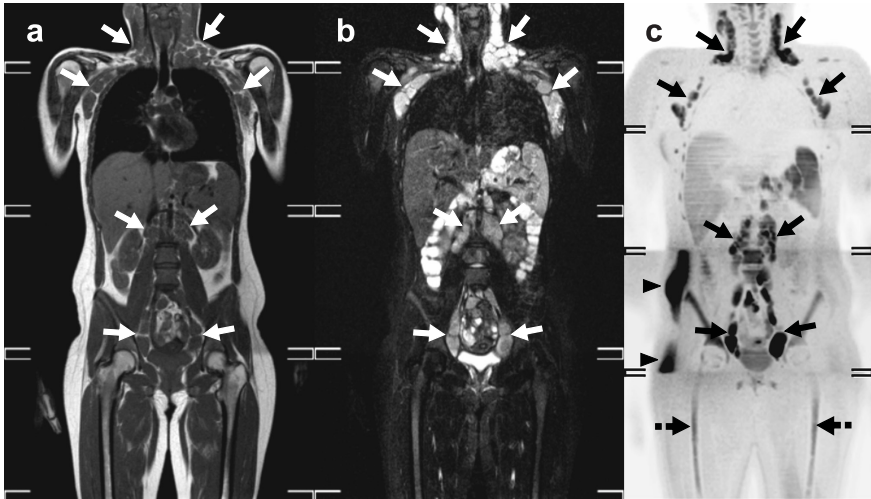


**Figure 2.** A 17-year-old female with unspecified widespread lymphoproliferative disease. Coronal whole-body T1-weighted (a), STIR (b) and grayscale inverted diffusion-weighted images (c) show extensive (bilateral) cervical, axillary, paraaortic, mesenteric, and pelvic lymph node involvement (continuous arrows). Note relatively high signal intensity of the bone marrow (e.g. in both femoral diaphyses (dashed arrows) suggestive of bone marrow hyperplasia (reconversion). Also note insufficiently suppressed fat in the right flank and buttock (arrowheads).

weighted and (fat-suppressed) T2-weighted imaging, but there is no consensus yet which (combination of) sequence(s) provide(s) the highest diagnostic accuracy while being time-efficient. Nonetheless, previous studies [16-18] have shown the particular utility of short inversion time inversion recovery (STIR) whole-body MRI for staging malignant lymphoma. STIR is a sensitive method for the detection of parenchymal and bone marrow lesions, which are generally highlighted as high signal intensity structures on this sequence [16-18, 21]. However, malignant lymph nodes cannot be differentiated from non-malignant nodes on the basis of signal intensity yet, neither on T1-weighted nor on T2-weighted sequences. Thus, assessment of nodal involvement is still based on size criteria on conventional MRI. So far, only three studies [16-18] have investigated the value of conventional whole-body MRI for the staging of malignant lymphoma. Brennan et al. [16] performed a study in 23 adults that presented either for initial staging or restaging of HD or NHL and reported that whole-body MRI using STIR enables disease staging and that it compared favorably with CT for the detection of lymph nodes larger than 12 mm in short-axis diameter and for the detection of bone marrow involvement. Kellenberger et al. [17] performed a small study in 8 children for initial staging and restaging of HD or NHL and reported that whole-body MRI using STIR is a sensitive technique for staging malignant lymphoma and that it is superior to blind bone marrow biopsy and conventional imaging (including CT, gallium-67 scintigraphy, and bone scintigraphy) for the detection of bone marrow

involvement, at initial diagnosis. However, whole-body MRI using STIR was reported to lack specificity for diagnosing recurrent or residual disease [17]. Finally, Kwee et al. [18] compared whole-body MRI using both T1-weighted and STIR sequences to CT for the initial staging of 31 patients with HD or NHL. Staging results of whole-body MRI were equal to those of CT in 74% (23/31), higher in 26% (8/31), and lower in 0% (0/31) of patients, with correct/incorrect/unresolved overstaging relative to CT in 3, 2, and 1 patient(s), respectively, and incorrect staging of both modalities in 1 patient [18]. Results of these studies [16-18] suggest that staging of malignant lymphoma using whole-body MRI is feasible and promising, but definitive conclusions regarding its value in the diagnostic management of malignant lymphoma cannot be made yet.

#### Rationale for DWI

A disadvantage of conventional (T1-weighted or T2-weighted) whole-body MRI is the large amount of data that has to be evaluated, including data from a lot of normal structures such as fat, muscles, and vascular structures. Consequently, image interpretation can be time-consuming and subtle lesions may be overlooked. DWI, also known as intravoxel incoherent motion imaging, may overcome this disadvantage of conventional whole-body MRI. The most common approach to render MRI sensitive to diffusion is by using a spin-echo sequence and placing two strong gradients (so-called motion-probing gradients [MPGs]) on either side of the 180° refocusing pulse [22]. DWI is basically a T2-weighted sequence, but the application of two strong MPGs results in a decrease in signal intensity of all structures. Importantly, the amount of signal intensity decrease induced by the MPGs is not similar for all structures, but depends on the degree of apparent diffusion that occurs between the MPGs; structures with a relatively low diffusivity are less suppressed than tissues with a relatively high degree of diffusion or perfusion (e.g. vascular structures, cerebrospinal fluid, and urinary bladder contents). Since most lesions (both benign and malignant) exhibit a relatively impeded diffusion, they generally lose less signal than surrounding normal background structures at DWI, resulting in a high lesion-to-background contrast. Furthermore, fat suppression (which is inherently necessary in echo-planar imaging [EPI] to avoid image degradation due to severe chemical shift) also improves lesion-to-background contrast. Thus, DWI may increase lesion detection rate while decreasing image interpretation time. As mentioned previously, DWI is basically a T2-weighted sequence; consequently, residual T2 components (also known as T2 shine-through) can be seen on diffusion-weighted images, which may mimic areas of impeded diffusion. For this reason, it is often recommended to review a corresponding apparent diffusion coefficient (ADC) map, which does not contain any residual T2 components and allows quantifying diffusion; this is especially important in diagnosing acute ischemic stroke [23]. However, in order to create an ADC map, at least two datasets with different degrees of diffusion-weighting (i.e. b-values) have to

be acquired. Furthermore, lesion-to-background contrast on the ADC map is poor, and misregistration of the different datasets obtained with different b-values may occur (e.g. due to patient motion or image distortion). Moreover, and perhaps more importantly, T2 shine-through should not always be regarded as a disadvantage. In fact, many lesions exhibit both a prolonged T2 value and an impeded diffusion; both components contribute to the high conspicuity of lesions at DWI.

DWI: from the brain to the body

Since the mid-1990s, DWI has developed into a well-accepted method for the diagnosis of acute ischemic stroke [23]. Of note, in acute ischemic stroke, apparent diffusion is (most likely) impeded due to cytotoxic edema [23, 24], which gives high signal at DWI. Previously, however, DWI outside the brain was not routinely feasible, because the use of EPI, which is necessary for ultrafast imaging, could lead to severe image distortion in the magnetically inhomogeneous body. This limitation has relatively recently been overcome by the development of stronger and faster gradients, and, most importantly, parallel acquisition techniques [25], which allow shortening of the echo-train length in EPI, thereby reducing image distortion.

Whole-body DWI with background body signal suppression: DWIBS

Previously, it was thought that diffusion-weighted contrast could not be maintained during bulk tissue motion, and in particular respiratory motion, because diffusion takes place over several micrometers during the period in which the MPGs are applied, whereas respiratory motion takes place on the order of centimeters. Thus, breathhold or respiratory triggered DWI was considered necessary for DWI of the chest and abdomen. However, in breathhold DWI, only thick slices (usually 8 to 10 mm) with relatively low signal-to-noise ratio (SNR) can be obtained, which cannot be used to create multiplanar reformats (MPRs) or 3D displays such as maximum intensity projections (MIPs). Respiratory triggered DWI does not have these disadvantages, but can considerably prolong the scan time. Thus, both breathhold and respiratory triggered DWI are not suitable for a whole-body DWI examination. A major breakthrough for whole-body DWI was the proof of the feasibility of DWI under free breathing [13, 14]. The fact that a free breathing acquisition is feasible can be explained by the fact that respiratory motion can be regarded as coherent motion during the period in which the MPGs are applied, and as such does not affect intravoxel incoherent motion (i.e. diffusion) [13, 14]. The concept of DWI under free breathing was called Diffusion-weighted Whole-body Imaging with Background body Signal suppression (DWIBS). The free breathing approach allows obtaining thin slices (typically 4-5 mm) with multiple signal averages (to increase SNR) in a practically acceptable scan time, and the acquired dataset can be used to create multiplanar reformats and 3D displays. Furthermore, in DWIBS, high b-values (typically 1000 s/

mm<sup>2</sup>) are applied to ensure sufficient suppression of background body signals, while highlighting lesions. Inverting the grayscale of DWIBS images gives them the typical appearance of PET-like images (Figures 1 to 4). Further details about the concept of DWIBS, including its practical implementation and parameter settings, can be read elsewhere [14]. Currently, a whole-body DWI examination can be performed in approximately 20-30 minutes. When adding conventional (T1- and T2-weighted) whole-body MRI, total examination time can be approximately 45 minutes. Suggested sequences for whole-body MRI/DWI at 1.5T are listed in **Table 1**. In our experience, children aged 8 years and older tolerate such an examination very well, without the need for any sedation (of note, most pediatric malignant lymphomas occur in older children and adolescents [2]). One recent study [18] compared a combination of conventional whole-body MRI (T1-weighted and STIR sequences) and whole-body DWI (without using any ADC mapping) to CT for the staging of 28 patients with newly diagnosed HD or NHL. Staging results of combined conventional whole-body MRI and whole-body DWI were equal to those of CT in 75% (21/28), higher in 25% (7/28), and lower in 0% (0/28) of patients, with correct/incorrect overstaging relative to CT in 6 and 1 patient(s), respectively. Interestingly, the combination of conventional whole-body MRI with whole-body DWI correctly upstaged four of 28 patients compared to conventional whole-body MRI alone, which well reflects the potential additional diagnostic value of DWI [18]. Nevertheless, although these initial results appear very promising compared to CT, more studies with larger sample sizes are needed. Furthermore, whole-body DWI has not yet been compared to FDG-PET(/CT).

## Whole-body DWI for staging malignant lymphoma; specific considerations

### Nodal pathology

One of the first observations that were made when DWI was applied in the entire body was the clear visualization of lymph nodes, which appear as high signal intensity structures, while surrounding background (including fat) is suppressed (Figures 1 to 4) [13]. For this reason, it was thought that one promising application of whole-body DWI could be in staging of malignant lymphoma. However, one important limitation of DWI is that it visualizes both non-malignant and malignant lymph nodes (**Figure 1**). This is because normal lymph nodes already have a relatively low diffusivity (probably due to high cellularity) and long T2 value. Several studies [26-30] have reported that lymphomatous lymph nodes have lower ADCs than metastatic lymph nodes or benign lymphadenopathy (probably due to increased cellularity). However, these studies [26-30] only included pathologically enlarged lymph nodes without considering (normal-sized) "healthy" lymph nodes. Therefore, the value of ADC measurements in discriminating (normal-sized) "healthy" lymph nodes from (normal-sized) lymphomatous lymph nodes is still unknown. In addition, one recent

**Table 1.** Suggested sequences for whole-body MRI/DWI at 1.5T

Parameter	T1-weighted	STIR	DWI-SFS <sup>1</sup>	DWI-STIR <sup>1</sup>
Pulse sequence	Single-shot turbo spin-echo		Single-shot spin-echo echo-planar imaging	
Repetition time (ms)	537	2444	6962	8612
Echo time (ms)	18	64	78	-
Inversion time (ms)	-	165	180	-
Receiver bandwidth (Hz)	460.1	487.9	30.2	-
Slice orientation	Coronal		Axial <sup>2</sup>	
Slice thickness (mm)	6.0		4.0	
Slice gap (mm)	1.0		0.0	
No. of slices per station	30		60	
Cranio-caudal coverage per station (mm)	265		240	
Field of view (mm <sup>2</sup> )	530 × 265	530 × 265	450 × 360	
Acquisition matrix	208 × 287	336 × 120	128 × 81	
Directions of motion probing gradients	-		Phase, frequency, and slice	
B-values (s/mm <sup>2</sup> )	-		0 and 1000 <sup>3</sup>	
No. of signals averaged	1	2	3	
Partial Fourier acquisition (%)	-		0.651	
Parallel acceleration factor	-		2	
Echo-planar imaging factor	-		43	
Respiratory motion compensation techniques	Breath holding or respiratory gating are recommended when scanning the chest and abdomen		Image acquisition under free breathing	
Acquired voxel size (mm <sup>3</sup> )	1.27 × 1.85 × 6.00	1.58 × 2.21 × 6.00	3.52 × 4.50 × 4.00	
Reconstructed voxel size (mm <sup>3</sup> )	1.04 × 1.04 × 6.00	1.04 × 1.04 × 6.00	1.76 × 1.76 × 4.00	
Effective scan time per station <sup>4</sup>	47 s	44 s	3 min 20 s	4 min 4 s
Total no. of stations	7	-	3 (+1) <sup>5</sup>	4
Total effective scan time <sup>4</sup>	5 min 48 s	5 min 13 s	14 min 4 s <sup>5</sup>	16 min 26 s

**Abbreviations:** SFR: spectral fat saturation; STIR: short inversion time inversion recovery

**Notes:**

<sup>1</sup>DWI can be combined with either spectral fat saturation (DWI-SFS) or a short inversion time inversion recovery pre-pulse (DWI-STIR) for fat suppression. DWI-SFR offers higher SNR and is relatively less time-consuming than DWI-STIR. However, DWI-STIR offers more robust fat suppression over an extended field of view than DWI-SFR, because STIR is less sensitive to magnetic field inhomogeneities. Because the head, neck, and shoulder regions usually suffer from considerable magnetic field inhomogeneities, it is recommended to use DWI-STIR for these body regions. In addition, DWI-STIR may be useful in suppressing bowel signal, which often has a short T1 relaxation time, similar to that of fat.

<sup>2</sup>At present, it is recommended to perform DWI in the axial plane and to coronally reformat the acquired dataset afterwards, because direct coronal scanning may still suffer from considerable image distortion due to the need for a larger field of view

<sup>3</sup>A b-value of 1000 s/mm<sup>2</sup> is effective in suppressing background body signals while highlighting lesions throughout the entire body. Therefore, a b-value of 1000 s/mm<sup>2</sup> can be recommended for whole-body imaging. The relatively low signal at a b-value of 1000 s/mm<sup>2</sup> can be increased by acquiring multiple signal averages. The additional acquisition of a b-value of 0 s/mm<sup>2</sup> allows quantitative diffusion measurements.

<sup>4</sup>Effective scan time without taking into account the time needed for acquiring survey scans, breath holding, respiratory gating, table movements, and coil repositioning.

<sup>5</sup>Using DWI-SFR for three stations covering the pelvis, abdomen, and chest, and using DWI-STIR for the station that covers the head, neck, and shoulder.

study [31] performed an inter- and intra-observer reproducibility study regarding ADC measurements of normal-sized lymph nodes. In this study [31], ranges of mean ADC difference  $\pm$  limits of agreement (in  $10^{-3}$  mm<sup>2</sup>/s) for inter-observer agreement were  $-0.03$  to  $0.02 \pm 0.15$  to  $0.31$ . In addition, ranges of mean ADC difference  $\pm$  limits of agreement (in  $10^{-3}$  mm<sup>2</sup>/s) for intra-observer agreement were  $0.00$  to  $0.04 \pm 0.13$  to  $0.32$  [31]. Given this relatively large variability, inter- and intra-observer reproducibility of ADC measurements of normal-sized lymph nodes appears to be rather poor. Thus, the detection of lymphomatous lymph nodes in whole-body DWI is still based on size criteria. Nonetheless, compared to conventional (T1-weighted and T2-weighted) whole-body MRI, whole-body DWI provides a faster and more straightforward evaluation of the amount and distribution of (pathologically enlarged) lymphomatous lymph nodes. There are some potential pitfalls and drawbacks that have to be taken into account when evaluating whole-body DWI with respect to the evaluation of nodal/lymphoid pathology. First, DWI, and in particular DWIBS (which is used for whole-body DWI), highlights lymph nodes while suppressing surrounding normal structures. Because of the lack of an anatomical reference, size measurements of lymph nodes at DWI are highly dependent on the applied window level and window width. In addition, there are no published studies comparing nodal measurements at DWI with those at conventional imaging (either CT or T1- and T2-weighted images). Thus, at present, it is recommended that sizes of lymph nodes that are suspicious for malignancy at DWI are measured on conventional T1-weighted or T2-weighted images for verification. Nevertheless, the efficacy of such an approach is still unknown. Another issue is that, unlike respiratory motion, cardiac motion may result in non-rigid body motion and signal loss of structures close to the heart [32, 33]. Consequently, the evaluation of mediastinal lymph nodes may be affected by cardiac motion. Nevertheless, relatively large mediastinal masses can readily be identified at DWI (**Figure 1**).

#### Extranodal pathology

DWI is a very sensitive method for the detection of extranodal lymphomatous lesions, which generally exhibit high signal intensity at DWI (due to a low diffusivity and long T2) (**Figure 3**). Importantly, several benign conditions (including inflammatory and infectious lesions) also have high signal intensity at DWI. To minimize the number of false-positive results, DWI should be interpreted along with other sequences, and patient's history and findings on clinical examination should be known when interpreting the images. Although there are yet no established criteria for classifying lesions as negative or positive for lymphomatous involvement, a signal intensity higher than that of the spinal cord has often been proposed as suggestive for malignancy [33-36]. On the other hand, diffusivity may be increased in case of necrosis (provided no hemorrhagic components are present), which can be visualized as areas of relatively low signal intensity at DWI. Another important issue is that several normal extranodal

structures (including brain, salivary glands, Waldeyer's ring, thymus, spleen, gallbladder, adrenal glands, prostate, testes, penis, endometrium, ovaries, spinal cord, peripheral nerves, and bone marrow) (may) also exhibit high signal intensity at DWI [13, 14], due to their relatively low diffusivity and long T2 value (**Figure 1**). In our experience, Waldeyer's ring in particular may appear very hyperintense at DWI (Figures 3 and 4). Detection of abnormality in this organ based on differences in signal intensity may be difficult, although an asymmetrical appearance may suggest the presence of lymphomatous involvement (**Figure 4**).

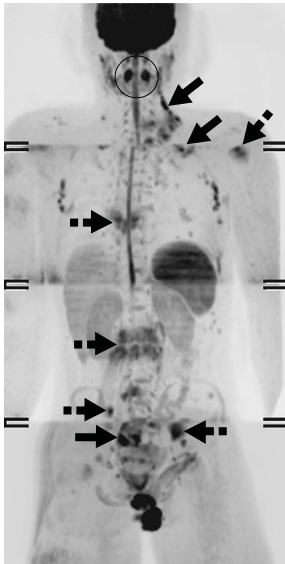


**Figure 3.** A 16-year-old male with stage IV nodular sclerosing Hodgkin's disease. Coronal whole-body grayscale inverted MIP diffusion-weighted image shows left cervical, infraclavicular, and pelvic lymph node involvement (continuous arrows), and left humeral, vertebral, and pelvic bone marrow involvement (dashed arrows). Note that both pharyngeal tonsils (encircled) also exhibit high signal intensity, but this is a normal finding.

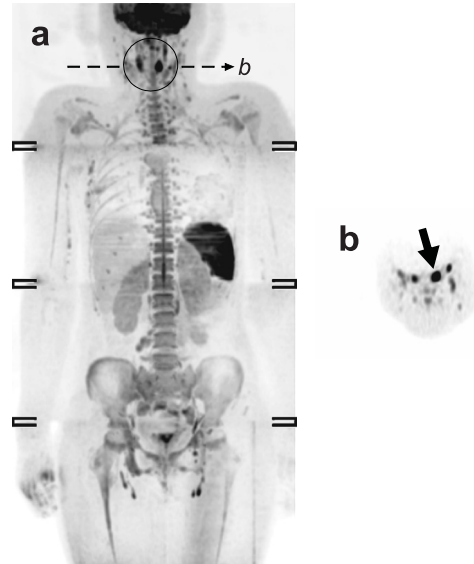


**Figure 4.** A 12-year-old female with stage I diffuse large B-cell lymphoma arising in the pharyngeal tonsils (histologically proven). Coronal whole-body grayscale inverted MIP diffusion-weighted image (a) shows no obvious nodal or extranodal pathology, except for striking high signal intensity in both pharyngeal tonsils (encircled). Although the normal Waldeyer's ring often exhibits a high signal intensity (as can also be seen in **Figure 3**), a corresponding axial image (b) shows size asymmetry of the pharyngeal tonsils.

Another lymphoid organ that often appears very hyperintense at DWI is the spleen (Figures 1 to 4). Consequently, abnormality in this organ may be obscured. On the other hand, visibility of the spleen is variable and probably dependent on its iron content (and consequent signal loss). Similarly, the visibility of the liver is related to its iron content, although this organ usually appears relatively hypointense at high



b-values (i.e.  $\geq 1000$  s/mm<sup>2</sup>). A potential pitfall in DWI is in the evaluation of the bone marrow. During skeletal maturation, hematopoietic (red) marrow is converted to fatty (yellow) marrow [37]. At DWI, yellow marrow appears hypointense thanks to the use of fat suppression. On the other hand, red bone marrow appears as hyperintense at DWI, probably due to its high cellularity which has a relatively impeded diffusion [38]. Residual or reconverted red bone marrow (islands) may resemble lymphomatous bone marrow involvement (**Figure 2**). Thus, signal intensities of normal and lymphomatous bone marrow may overlap at DWI [39]. Nevertheless, additional conventional (T1-weighted or T2-weighted) MRI sequences may increase the diagnostic performance of DWI alone in the assessment of the bone marrow. Despite its imperfect specificity, DWI may have a role in ruling out bone marrow involvement and guiding bone marrow biopsy [39, 40]. Other important body regions that require special consideration are the liver and the lung. Similar to bone marrow involvement, liver or lung involvement, which are not uncommon in malignant lymphoma [41, 42] represent stage IV disease [3, 4]. Usually, DWI of the liver is acquired under breathholding or respiratory triggering [43]. Especially the suppression of liver vessels in DWI is an advantage over conventional MRI sequences, which increases sensitivity for the detection of lesions [44]. However, as mentioned previously, whole-body DWI is acquired under free breathing. Despite the fact that the breathing approach introduces slight image blurring due to diaphragmatic motion, liver lesions can generally be well depicted thanks to thin slice acquisition and the high degree of signal averaging [45]. DWI of the lung is a particular challenge; besides cardiac and respiratory motion artifacts, susceptibility-induced image distortion and signal loss due to the many air-tissue interfaces may occur. Nevertheless, although sensitivity of CT still outperforms that of MRI/DWI in the lung, studies in patients with pulmonary nodules have shown that DWI is able to detect lung lesions up to 5 mm in diameter [34-36]. Moreover, unlike CT, DWI is able to provide functional tissue information, which may aid in the differentiation between benign and malignant pulmonary lesions [34-36]. Of note, DWI has been shown to diagnostically outperform FDG-PET in the characterization of pulmonary nodules/masses [36]. Despite its promise, the diagnostic performance of DWI in the detection of lymphomatous lung lesions requires further investigation.

### Role of imaging beyond staging

Imaging plays a crucial role in staging of malignant lymphoma, but may also be of value in the (early) assessment of response to therapy. Early assessment of response to therapy will allow applying a more individualized therapy, which will maximize the chance of cure while minimizing risk of (late) toxicity. However, anatomic imaging modalities such as CT, ultrasound, and conventional (T1-weighted and T2-weighted) MRI sequences may not be sufficiently accurate in discriminating residual disease from fibrosis or scar tissue [46-48]. FDG-PET, on the other hand, provides functional



tissue information, and may be superior to conventional imaging modalities in this context. A recent study by Furth et al. [48] has indeed shown that FDG-PET is superior to conventional imaging methods (i.e. contrast-enhanced MRI of neck, abdomen, and pelvis; ultrasound examinations of all lymph node regions; as well as contrast-enhanced CT of the chest) with regard to specificity in early (i.e. after two cycles of chemotherapy) and late response assessment (i.e. after completion of chemotherapy) in pediatric patients with HD (68% vs. 3%, and 78% vs. 11%, respectively; both  $P < .001$ ). Specificity of early therapy response assessment by FDG-PET was improved to 97% by quantitative analysis of maximal standardized uptake value reduction using a cutoff value of 58%. These data [48] suggest that FDG-PET should not be omitted either for staging or response assessment. At present it is still highly speculative whether DWI can replace FDG-PET in the diagnostic management of malignant lymphoma. Interestingly, a voxel-based quantitative DWI approach [functional diffusion mapping, currently referred to as parametric response mapping of diffusion (PRM<sub>ADC</sub>)] has recently shown promise to give an early prediction of survival in patients with high-grade gliomas [49, 50]. However, whole-body quantitative DWI techniques still have to be developed and subsequently compared to FDG-PET, which is currently the functional imaging modality of choice in malignant lymphoma.

## Future considerations and challenges

### Reducing image blurring

Diffusion-weighted contrast is maintained under free breathing acquisition (i.e. DWIBS), although at the expense of slight image blurring. Image blurring may affect interpretation of paradiaphragmatic organs, such as the liver. An effective approach to reduce image blurring in DWIBS may be the use of a navigator echo technique that allows continuous real-time slice tracking and position correction, without the use of any gating window. Consequently, image blurring is reduced without considerably prolonging scan time [45, 51] Implementing such a technique in a whole-body DWI sequence for staging malignant lymphoma may be attractive, since it can improve visualization of peridiaphragmatic organs.

### Whole-body DWI at 3.0T

Whole-body DWI is currently best performed at 1.5T, using a phased-array receiver surface coil. Nevertheless, SNR in DWI is relatively low, even though a high number of signal averages can be acquired when using the concept of DWIBS. SNR is increased when performing DWI at higher field strength, since SNR increases linearly with field strength [52]. This, in turn, may improve staging accuracy in malignant lymphoma. A recent feasibility study indeed showed that DWIBS at 3.0T offers higher SNR compared to that at 1.5T, but the former still suffers from a higher risk of B0 and B1

inhomogeneities and susceptibility artifacts [53]. Therefore, the further development of multi-source radiofrequency (RF) transmission technology [54] (which will be discussed later) and non-EPI-based DWI techniques [55] is important to solve these problems. Another challenge at high field strength is fat suppression; inadequately suppressed fat may hinder image interpretation. Compared to a frequency selective (spectral fat saturation) pre-pulse, a short inversion time inversion recovery (STIR) pre-pulse has shown to offer the best fat suppression in all body regions at 3.0T [53], since the latter is less sensitive to B<sub>0</sub> inhomogeneities. However, the use of STIR inherently yields lower SNR than the use of spectral fat saturation [56]. Furthermore, both spectral fat saturation and STIR require additional RF and/or gradient pulses, thereby increasing the specific absorption rate (SAR) and prolonging scan time [56]. Thus, the development of new fat suppression techniques is important to exploit the full potential of whole-body DWI at higher field strength. In this respect, the reintroduction of the slice-selection gradient reversal (SSGR) technique is very promising [57, 58]. The SSGR technique uses two slice-selection gradients of opposing polarity for the 90° excitation pulse and the 180° refocusing pulse in a spin-echo EPI sequence for diffusion sensitization. The SSGR technique exploits the high sensitivity of EPI to chemical shift artifacts (water-fat shift) in the phase-encoding direction due to the relatively low bandwidth in that orientation; water signal will completely be preserved, but only fat signal that was exposed to both the excitation pulse and the refocusing pulse in the center of the water slice will contribute to image formation. Since chemical shift artifacts are more pronounced at higher field strengths, fat signal can tremendously be reduced or even completely be eliminated using the SSGR technique at field strengths  $\geq 3.0T$ . Furthermore, unlike spectral fat saturation and STIR, the SSGR technique does not prolong scan time, nor does it increase SAR [57, 58]. Another promising development that was recently implemented at a clinical 3.0T-system is the multi-source RF transmission technology [54]. Using this technology, independent RF pulses are sent; this improves image uniformity and consistency compared to single-source RF transmission, which may suffer from dielectric resonance effects at high field strength. Furthermore, local RF deposition (SAR) can be reduced, allowing for faster scanning [54]. Thus, although 1.5T-systems still provide the best and most reproducible image quality, eventually it is expected that whole-body DWI at 3.0T will become possible in routine clinical practice.

Shifting gears in whole-body molecular imaging

The discrimination between normal-sized non-malignant lymph nodes and normal-sized lymphomatous lymph nodes is still an unsolved issue in DWI. This is because both normal and malignant lymph nodes are highlighted at DWI, and ADC measurements have not shown yet to be able to discriminate [31]. Ultrasmall superparamagnetic iron oxide (USPIO)-enhanced MRI was introduced in the early 1990s as a promising

imaging modality for evaluating lymph nodes [59, 60], allowing for the identification of malignant nodal infiltration independent of lymph node size. Intravenously administered USPIOs are taken up by macrophages in the reticuloendothelial system, predominantly within the lymph nodes, but also in Waldeyer's ring, spleen and bone marrow. Normal homogeneous uptake of USPIOs in nonmetastatic lymph nodes shortens the T2 and T2\* values, turning these lymph nodes hypointense on T2- and T2\*-weighted images, whereas malignant lymph nodes lack uptake and remain hyperintense [60]. USPIO-enhanced lymphography has shown to achieve higher diagnostic precision than conventional, unenhanced MRI for the detection of lymph nodes metastases of various tumors [61]. However, conspicuity and detectability of lymph nodes is relatively low in USPIO-enhanced MRI. Consequently, image interpretation can be very time consuming, and malignant lymph nodes of small size may be missed. Furthermore, one image dataset before and one image dataset after USPIO administration has to be obtained, which poses an extra burden on the patient, and on logistic and financial resources. Performing DWI after USPIO administration may overcome disadvantages of DWI and conventional (T2- or T2\*-weighted) USPIO-enhanced MRI alone. Theoretically, in USPIO-enhanced DWI only malignant lymph nodes will be highlighted; the high lymph node-to-background contrast will reduce image interpretation time and will obviate the need to acquire an additional dataset of images before USPIO administration. The feasibility of this new concept has recently been proven in patients with urinary bladder and prostate cancer [62] (although attention should be paid to possible oversuppression by USPIOs as a result of which micrometastases may be missed); an extension of this concept to the entire body (i.e. USPIO-enhanced whole-body DWI) may provide a highly accurate method for the determination of extent of nodal involvement in patients with malignant lymphoma. An important additional advantage of USPIO-enhanced whole-body DWI over whole-body DWI alone is suppression of signal from the normal Waldeyer's ring, spleen and normal or hyperplastic red bone marrow, against which lymphomatous lesions in these organs will theoretically be highlighted [63].

Another promise for the future is the development of whole-body PET/MRI systems [64]. Although several technological difficulties have to be solved for designing a fully integrated whole-body PET/MRI system (including the issues of electromagnetic interference between the two systems and MRI-based attenuation correction), and its high (development) costs have to be taken into account [64], the integrated use of whole-body DWI and FDG-PET may be of interest in (pediatric) patients with malignant lymphoma. For example, FDG-PET may increase diagnostic performance of DWI alone in several areas, including (normal-sized) lymph nodes [7], spleen [65], and bone marrow [66]. Furthermore, FDG-PET may be a powerful adjunct to whole-body MRI/DWI in restaging malignant lymphoma; restaging performance of whole-body MRI/DWI is still unknown, but FDG-PET has already proven to be of value in

diagnosing persistent or recurrent disease [7, 67, 68]. On the other hand, an area where DWI may clearly be of advantage compared to FDG-PET is the urinary tract. Normal FDG accumulation in the renal collecting system, ureters, and bladder may limit the use of FDG-PET in the evaluation of renal, paraortic, and pelvic lesions [69], whereas DWI does not have this disadvantage. Another advantage of DWI over (FDG-) PET is its superior spatial resolution. Furthermore, although most pediatric NHLs are FDG-avid, DWI allows visualizing certain subtypes of NHLs that are not FDG-avid [7, 8].

## Conclusion

Whole-body MRI, and whole-body DWI in particular, provides a radiation-free alternative for staging malignant lymphoma in children. Whole-body DWI may potentially facilitate image interpretation and increase sensitivity of conventional (T1- and T2-weighted) whole-body MRI alone. Nevertheless, there is a strong need for comparative studies with (FDG-PET)/CT before definitive conclusions can be made regarding its value in the diagnostic management of malignant lymphoma. Integrating whole-body DWI with other molecular imaging strategies, including USPIO-enhanced imaging and FDG-PET, is expected to further increase its staging performance in malignant lymphoma.

---

## Acknowledgement

This work was supported by ZonMw Program for Health Care Efficiency Research (grant number 80-82310-98-08012).

## References

1. Jemal A, Siegel R, Ward E, Hao Y, Xu J, Thun MJ. Cancer statistics, 2009. *CA Cancer J Clin* 2009;59:225-249
2. Steliarova-Foucher E, Stiller C, Kaatsch P, et al. Geographical patterns and time trends of cancer incidence and survival among children and adolescents in Europe since the 1970s (the ACCIS project): an epidemiological study. *Lancet* 2004;364:2097-2105
3. Connors JM. State-of-the-art therapeutics: Hodgkin's lymphoma. *J Clin Oncol* 2005;23:6400-6408
4. Armitage JO. Staging non-Hodgkin lymphoma. *CA Cancer J Clin* 2005;55:368-376
5. Murphy SB. Classification, staging and end results of treatment of childhood non-Hodgkin's lymphomas: dissimilarities from lymphomas in adults. *Semin Oncol* 1980;7:332-339
6. Murphy SB, Fairclough DL, Hutchison RE, Berard CW. Non-Hodgkin's lymphomas of childhood: an analysis of the histology, staging, and response to treatment of 338 cases at a single institution. *J Clin Oncol* 1989;7:186-193
7. Kwee TC, Kwee RM, Nievelstein RA. Imaging in staging of malignant lymphoma: a systematic review. *Blood* 2008;111:504-516
8. Juweid ME, Stroobants S, Hoekstra OS, et al; Imaging Subcommittee of International Harmonization Project in Lymphoma. Use of positron emission tomography for response assessment of lymphoma: consensus of the Imaging Subcommittee of International Harmonization Project in Lymphoma. *J Clin Oncol* 2007;25:571-578
9. Brenner DJ, Hall EJ. Computed tomography--an increasing source of radiation exposure. *N Engl J Med* 2007;357:2277-2284
10. Hodgson DC, Hudson MM, Constine LS. Pediatric hodgkin lymphoma: maximizing efficacy and minimizing toxicity. *Semin Radiat Oncol* 2007;17:230-242
11. Gross TG, Termuhlen AM. Pediatric non-Hodgkin's lymphoma. *Curr Oncol Rep* 2007;9:459-465
12. Semelka RC, Armao DM, Elias J Jr, Huda W. Imaging strategies to reduce the risk of radiation in CT studies, including selective substitution with MRI. *J Magn Reson Imaging* 2007;25:900-909
13. Takahara T, Imai Y, Yamashita T, Yasuda S, Nasu S, Van Cauteren M. Diffusion weighted whole body imaging with background body signal suppression (DWIBS): technical improvement using free breathing, STIR and high resolution 3D display. *Radiat Med* 2004;22:275-282
14. Kwee TC, Takahara T, Ochiai R, Nievelstein RA, Luijten PR. Diffusion-weighted whole-body imaging with background body signal suppression (DWIBS): features and potential applications in oncology. *Eur Radiol* 2008;18:1937-1952
15. Schmidt GP, Baur-Melnyk A, Herzog P, et al. High-resolution whole-body magnetic resonance image tumor staging with the use of parallel imaging versus dual-modality positron emission tomography-computed tomography: experience on a 32-channel system. *Invest Radiol* 2005;40:743-753
16. Brennan DD, Gleeson T, Coate LE, Cronin C, Carney D, Eustace SJ. A comparison of whole-body MRI and CT for the staging of lymphoma. *AJR Am J Roentgenol* 2005;185:711-716
17. Kellenberger CJ, Miller SF, Khan M, Gilday DL, Weitzman S, Babyn PS. Initial experience with FSE STIR whole-body MR imaging for staging lymphoma in children. *Eur Radiol* 2004;14:1829-1841

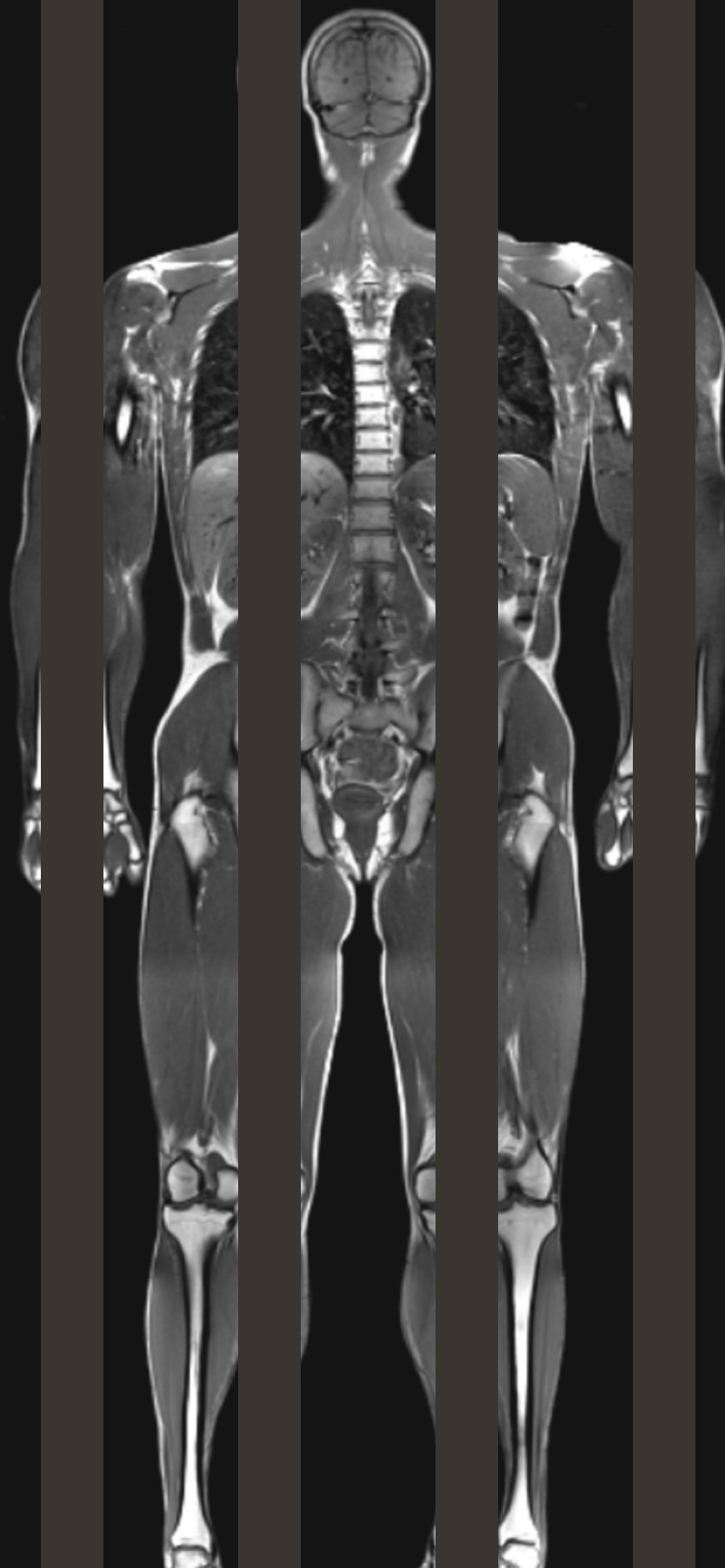
18. Kwee TC, Quarles van Ufford HM, Beek FJ, et al. Whole-Body MRI, including diffusion-weighted imaging, for the initial staging of malignant lymphoma: comparison to computed tomography. *Invest Radiol* 2009;44:683-690
19. Walker R, Kessar P, Blanchard R, et al. Turbo STIR magnetic resonance imaging as a whole-body screening tool for metastases in patients with breast carcinoma: preliminary clinical experience. *J Magn Reson Imaging* 2000;11:343-350
20. Kavanagh E, Smith C, Eustace S. Whole-body turbo STIR MR imaging: controversies and avenues for development. *Eur Radiol* 2003;13:2196-2205
21. Kellenberger CJ, Epelman M, Miller SF, Babyn PS. Fast STIR whole-body MR imaging in children. *Radiographics* 2004;24:1317-1330
22. Stejskal EO, Tanner JE. Spin diffusion measurements: spin echoes in the presence of a time-dependent field gradient. *J Chem Phys* 1965;42:288-292
23. Schaefer PW, Grant PE, Gonzalez RG. Diffusion-weighted MR imaging of the brain. *Radiology* 2000;217:331-345
24. Sevick RJ, Kanda F, Mintorovitch J, et al. Cytotoxic brain edema: assessment with diffusion-weighted MR imaging. *Radiology* 1992;185:687-690
25. Pruessmann KP, Weiger M, Scheidegger MB, Boesiger P. SENSE: sensitivity encoding for fast MRI. *Magn Reson Med* 1999;42:952-962
26. Holzapfel K, Duetsch S, Fauser C, Eiber M, Rummeny EJ, Gaa J. Value of diffusion-weighted MR imaging in the differentiation between benign and malignant cervical lymph nodes. *Eur J Radiol* 2009;72:381-387
27. King AD, Ahuja AT, Yeung DK, et al. Malignant cervical lymphadenopathy: diagnostic accuracy of diffusion-weighted MR imaging. *Radiology* 2007;245:806-813
28. Abdel Razek AA, Soliman NY, Elkhamary S, Alsharaway MK, Tawfik A. Role of diffusion-weighted MR imaging in cervical lymphadenopathy. *Eur Radiol* 2006;16:1468-1477
29. Sumi M, Van Cauteren M, Nakamura T. MR microimaging of benign and malignant nodes in the neck. *AJR Am J Roentgenol* 2006;186:749-757
30. Sumi M, Sakihama N, Sumi T, et al. Discrimination of metastatic cervical lymph nodes with diffusion-weighted MR imaging in patients with head and neck cancer. *AJNR Am J Neuroradiol* 2003;24:1627-1634
31. Kwee TC, Takahara T, Luijten PR, Nieuvelstein RA. ADC measurements of lymph nodes: Inter- and intra-observer reproducibility study and an overview of the literature. *Eur J Radiol* 2010;75:215-220
32. Norris DG. Implications of bulk motion for diffusion-weighted imaging experiments: effects, mechanisms, and solutions. *J Magn Reson Imaging* 2001;13:486-495
33. Sakurada A, Takahara T, Kwee TC, et al. Diagnostic performance of diffusion-weighted magnetic resonance imaging in esophageal cancer. *Eur Radiol* 2009;19:1461-1469
34. Uto T, Takehara Y, Nakamura Y, et al. Higher sensitivity and specificity for diffusion-weighted imaging of malignant lung lesions without apparent diffusion coefficient quantification. *Radiology* 2009;252:247-254
35. Satoh S, Kitazume Y, Ohdama S, Kimura Y, Taura S, Endo Y. Can malignant and benign pulmonary nodules be differentiated with diffusion-weighted MRI? *AJR Am J Roentgenol* 2008;191:464-470
36. Mori T, Nomori H, Ikeda K, et al. Diffusion-weighted magnetic resonance imaging for diagnosing malignant pulmonary nodules/masses: comparison with positron emission tomography. *J Thorac Oncol* 2008;3:358-364

37. Laor T, Jaramillo D. MR imaging insights into skeletal maturation: what is normal? *Radiology* 2009;250:28-38
38. Nonomura Y, Yasumoto M, Yoshimura R, et al. Relationship between bone marrow cellularity and apparent diffusion coefficient. *J Magn Reson Imaging* 2001;13:757-760
39. Yasumoto M, Nonomura Y, Yoshimura R et al. MR detection of iliac bone marrow involvement by malignant lymphoma with various MR sequences including diffusion-weighted echo-planar imaging. *Skeletal Radiol* 2002;31:263-269
40. Kwee TC, Kwee RM, Verdonck LF, Bierings MB, Nievelstein RA. Magnetic resonance imaging for the detection of bone marrow involvement in malignant lymphoma. *Br J Haematol* 2008;141:60-68
41. Baumhoer D, Tzankov A, Dirnhofer S, Tornillo L, Terracciano LM. Patterns of liver infiltration in lymphoproliferative disease. *Histopathology* 2008;53:81-90
42. Berkman N, Breuer R, Kramer MR, Polliack A. Pulmonary involvement in lymphoma. *Leuk Lymphoma* 1996;20:229-237
43. Naganawa S, Kawai H, Fukatsu H, et al. Diffusion-weighted imaging of the liver: technical challenges and prospects for the future. *Magn Reson Med Sci* 2005;4:175-186
44. Parikh T, Drew SJ, Lee VS, et al. Focal liver lesion detection and characterization with diffusion-weighted MR imaging: comparison with standard breath-hold T2-weighted imaging. *Radiology* 2008;246:812-822
45. Kwee TC, Takahara T, Ogino T, et al. Diffusion-weighted MR imaging (DWI) using TRacking only Navigator Echo (TRON): initial clinical evaluation and comparison to respiratory triggered and free breathing DWI. Presented at the ISMRM 17<sup>th</sup> Scientific Meeting & Exhibition, Honolulu, Hawai'i, USA, April 18–24, 2009
46. Radford JA, Cowan RA, Flanagan M, et al. The significance of residual mediastinal abnormality on the chest radiograph following treatment for Hodgkin's disease. *J Clin Oncol* 1988;6:940-946
47. Jerusalem G, Beguin Y, Fassotte MF, et al. Whole-body positron emission tomography using 18F-fluorodeoxyglucose for posttreatment evaluation in Hodgkin's disease and non-Hodgkin's lymphoma has higher diagnostic and prognostic value than classical computed tomography scan imaging. *Blood* 1999;94:429-433
48. Furth C, Steffen IG, Amthauer H, et al. Early and late therapy response assessment with [18F] fluorodeoxyglucose positron emission tomography in pediatric Hodgkin's lymphoma: analysis of a prospective multicenter trial. *J Clin Oncol* 2009;27:4385-4391
49. Hamstra DA, Galbán CJ, Meyer CR, et al. Functional diffusion map as an early imaging biomarker for high-grade glioma: correlation with conventional radiologic response and overall survival. *J Clin Oncol* 2008;26:3387-94
50. Hamstra DA, Rehemtulla A, Ross BD. Diffusion magnetic resonance imaging: a biomarker for treatment response in oncology. *J Clin Oncol* 2007;25:4104-4109
51. Takahara T, Ogino T, Okuaki T, et al. Respiratory gated body diffusion weighted imaging avoiding prolongation of scan time: tracking only navigator echo (TRON) technique. Presented at the Joint Annual Meeting ISMRM-ESMRMB, Berlin, Germany, May 19–25, 2007
52. Schick F. Whole-body MRI at high field: technical limits and clinical potential. *Eur Radiol* 2005;15:946-959
53. Mürtz P, Krautmacher C, Träber F, Gieseke J, Schild HH, Willinek WA. Diffusion-weighted whole-body MR imaging with background body signal suppression: a feasibility study at 3.0 Tesla. *Eur Radiol* 2007;17:3031-3037

54. Willinek WA, Gieseke J, Kukuk G. Parallel RF transmission in body MRI for reduced dielectric shading, improved B1 homogeneity and accelerated imaging at 3.0T: Initial clinical experience in 40 patients using MultiTransmit. Presented at the ISMRM 17<sup>th</sup> Scientific Meeting & Exhibition, Honolulu, Hawai'i, USA, April 18–24, 2009
55. Deng J, Miller FH, Salem R, Omary RA, Larson AC. Multishot diffusion-weighted PROPELLER magnetic resonance imaging of the abdomen. *Invest Radiol* 2006;41:769-775
56. Delfaut EM, Beltran J, Johnson G, Rousseau J, Marchandise X, Cotten A. Fat suppression in MR imaging: techniques and pitfalls. *Radiographics* 1999;19:373-382
57. Nagy Z, Weiskopf N. Efficient fat suppression by slice-selection gradient reversal in twice-refocused diffusion encoding. *Magn Reson Med* 2008;60:1256-1260
58. Takahara T, Zwanenburg J, Visser F et al. Fat suppression with Slice-Selection Gradient Reversal (SSGR) revisited. Presented at the ISMRM 17<sup>th</sup> Scientific Meeting & Exhibition, Honolulu, Hawai'i, USA, April 18–24, 2009
59. Weissleder R, Elizondo G, Wittenberg J, Rabito CA, Bengele HH, Josephson L. Ultrasmall superparamagnetic iron oxide: characterization of a new class of contrast agents for MR imaging. *Radiology* 1990;175:489-493
60. Weissleder R, Elizondo G, Wittenberg J, Lee AS, Josephson L, Brady TJ. Ultrasmall superparamagnetic iron oxide: an intravenous contrast agent for assessing lymph nodes with MR imaging. *Radiology* 1990;175:494-498
61. Will O, Purkayastha S, Chan C, et al. Diagnostic precision of nanoparticle-enhanced MRI for lymph-node metastases: a meta-analysis. *Lancet Oncol* 2006;7:52-60
62. Thoeny HC, Triantafyllou M, Birkhaeuser FD, et al. Combined Ultrasmall Superparamagnetic Particles of Iron Oxide-Enhanced and Diffusion-Weighted Magnetic Resonance Imaging Reliably Detect Pelvic Lymph Node Metastases in Normal-Sized Nodes of Bladder and Prostate Cancer Patients. *Eur Urol* 2009;55:761-769
63. Senéterre E, Weissleder R, Jaramillo D, et al. Bone marrow: ultrasmall superparamagnetic iron oxide for MR imaging. *Radiology* 1991;179:529-533
64. Von Schulthess GK, Schlemmer HP. A look ahead: PET/MR versus PET/CT. *Eur J Nucl Med Mol Imaging* 2009;36 Suppl 1:S3-9
65. De Jong PA, van Ufford HM, Baarslag HJ, et al. CT and 18F-FDG PET for noninvasive detection of splenic involvement in patients with malignant lymphoma. *AJR Am J Roentgenol* 2009;192:745-753
66. Pakos EE, Fotopoulos AD, Ioannidis JP. 18F-FDG PET for evaluation of bone marrow infiltration in staging of lymphoma: a meta-analysis. *J Nucl Med* 2005;46:958-963
67. Zijlstra JM, Lindauer-van der Werf G, Hoekstra OS, Hooft L, Riphagen II, Huijgens PC. 18F-fluoro-deoxyglucose positron emission tomography for post-treatment evaluation of malignant lymphoma: a systematic review. *Haematologica* 2006;91:522-529
68. Terasawa T, Nihashi T, Hotta T, Nagai H. 18F-FDG PET for posttherapy assessment of Hodgkin's disease and aggressive Non-Hodgkin's lymphoma: a systematic review. *J Nucl Med* 2008;49:13-21
69. Cook GJ, Fogelman I, Maisey MN. Normal physiological and benign pathological variants of 18-fluoro-2-deoxyglucose positron-emission tomography scanning: potential for error in interpretation. *Semin Nucl Med* 1996;26:308-314







# Chapter 5

## Whole-body MRI using a sliding table and repositioning surface coil approach

Takahara T, Kwee TC, Kifune S, Ochiai R, Sakamoto T, Niwa T, Van Cauteren M, Luijten PR

*Eur Radiol* 2010;20:1366-1373

## Abstract

### Objective

To introduce and assess a new way of performing whole-body MRI using a non-integrated surface coil approach as available on most clinical MRI systems worldwide.

### Methods:

Ten consecutive asymptomatic subjects prospectively underwent whole-body MRI for health screening. Whole-body MRI included T1-, T2- and diffusion-weighted sequences, and was performed using a non-integrated surface coil to image four different stations without patient repositioning. The four separately acquired stations were merged, creating seamless coronal whole-body T1-, T2- and diffusion-weighted images. Anatomical alignment, image quality at the boundaries of adjacent stations, and overall image quality of all stations were qualitatively assessed.

### Results:

The average time ( $\pm$  SD) taken to change the surface coil from one station to the next station was 53.8 ( $\pm$  7.1) s. The average total extra examination time  $\pm$  SD was 2 minutes 41.4 s ( $\pm$  15.3) s. Anatomical alignment, image quality at the boundaries of adjacent stations, and overall image quality of all stations of T1-, T2- and diffusion-weighted whole-body MRI were overall graded as “good” to “excellent”.

### Conclusion:

This study shows that a time-efficient and high-quality whole-body MRI examination can easily be performed by using a non-integrated sliding surface coil approach.

## Introduction

Magnetic resonance imaging (MRI) offers high spatial resolution and excellent soft-tissue contrast, making it an ideal tool for the detection of parenchymal and osseous lesions. Furthermore, MRI does not use any potentially harmful radiation. MRI may therefore be an attractive technique for the detection and characterisation of disease throughout the entire body [1, 2]. Previously, whole-body MRI was hampered by severe limitations. Repositioning of the patient and the surface coils to image the separate stations of the whole-body MRI examination led to exceedingly long examination times. Furthermore, anatomical alignment between separately imaged stations was not maintained using this approach. This limitation has been overcome by the development of the sliding table platform, which allows sequential movement of the patient through the bore of the magnet without patient repositioning, while signal is received by either an integrated body coil or by a (more recently introduced) whole-body surface coil design [1-3]. A whole-body surface coil design yields superior signal-to-noise ratio (SNR) and spatial resolution compared with an integrated transmit-receive body coil. Moreover, the use of surface coils allows for parallel imaging, which may be necessary for scan time reduction and for acquiring certain types of MRI sequences, such as diffusion-weighted MRI (DWI). Of note, DWI has recently been implemented in a whole-body MRI examination and is a potentially powerful tool for the detection and characterisation of various oncological and non-oncological lesions [4]. Thus, the use of a whole-body surface coil design is preferred to perform a whole-body MRI examination. The interest in the clinical application of whole-body MRI is rapidly increasing, as is well illustrated by the large number of publications in this field over the past few years [5-16]. Furthermore, whole-body MRI may be an excellent alternative to whole-body PET/CT [5-7, 9, 11, 12], given its wider availability [17] and the lack of ionising radiation [18]. However, most MR systems in routine clinical practice may not yet be equipped with an integrated whole-body surface coil design. Moreover, for a large number of these systems, an easily available upgrade towards fully integrated whole-body surface coil technology may not be available (yet). On the other hand, non-integrated surface coils (some of which are capable of parallel imaging) are widely available. These surface coils, however, have only a limited anatomical coverage. Nevertheless, it may still be possible to perform a whole-body MRI examination using a non-integrated surface coil. The aim of this study was therefore to introduce and qualitatively assess a new and easy approach to performing a time-efficient and high-quality whole-body MRI examination (including DWI) using a non-integrated surface coil.

## Subjects and Methods

### Asymptomatic subjects

Institutional review board approval was waived because MRI examinations were performed as part of routine patient care. Ten consecutive asymptomatic subjects (5 men and 5 women; mean age, 61.6 years [range, 52–79 years]; mean height, 160.2 cm [range, 154–167 cm]; mean weight 55.6 kg [range, 44–62 kg]; mean body mass index 21.6 kg/m<sup>2</sup> [range, 18.3–24.2 kg/m<sup>2</sup>]) who underwent whole-body MRI for health screening were prospectively included. Subjects with a general contraindication for MRI (including implanted pacemaker and claustrophobia) were excluded from participation.

### Table preparation

In order to perform a whole-body MRI examination using a non-integrated surface coil, four spacers (each with a height of 5 cm) were placed on the original patient table. Subsequently, an additional table platform (Table top extender, Philips Healthcare, Best, The Netherlands) was mounted on top of these four spacers. In this way, sufficient space was created to freely move the lower part of a surface coil over a distance of approximately 110 cm along the z-axis, without the need to reposition the subject who is lying on top of the additional table platform (**Figure 1**). As a trade-off, the use of spacers and an additional table platform reduced the available vertical bore diameter by 6.5 cm.

### MRI

All subjects were examined by 1.5-T MRI (Achieva, Philips Healthcare, Best, The Netherlands), using a 4-element phased-array surface coil (SENSE body, Philips Healthcare, Best, The Netherlands), in the head-first position. Four different anatomical stations (station 1 = head/neck; station 2 = chest; station 3 = abdomen; station 4 = pelvis) were separately imaged, using T1-, T2- and diffusion-weighted sequences. Geometries among the different stations of the T1-, T2- and diffusion-weighted sequences were coupled using software implemented in the standard operating console (Geolinks, Philips Healthcare, Best, The Netherlands). After imaging one station, the operator entered the examination room, moved the surface coil to the next station, and repositioned the center of the coil at the isocenter of the magnet (three station changes in total), without repositioning the subject (Movie clip 1). In this way, 3D alignment among the imaged stations was maintained. Of note, the operator was outside the examination room during scanning. The positions and overlaps of the four stations in DWI are shown in **Figure 2**. To maintain sufficient SNR in the periphery of the field of view (FOV) of each station in the z-direction, a 3-cm overlap between two adjacent stations was applied. Furthermore, a 7-cm overlap was applied between stations 1 and 2, in order to maintain robust fat suppression in

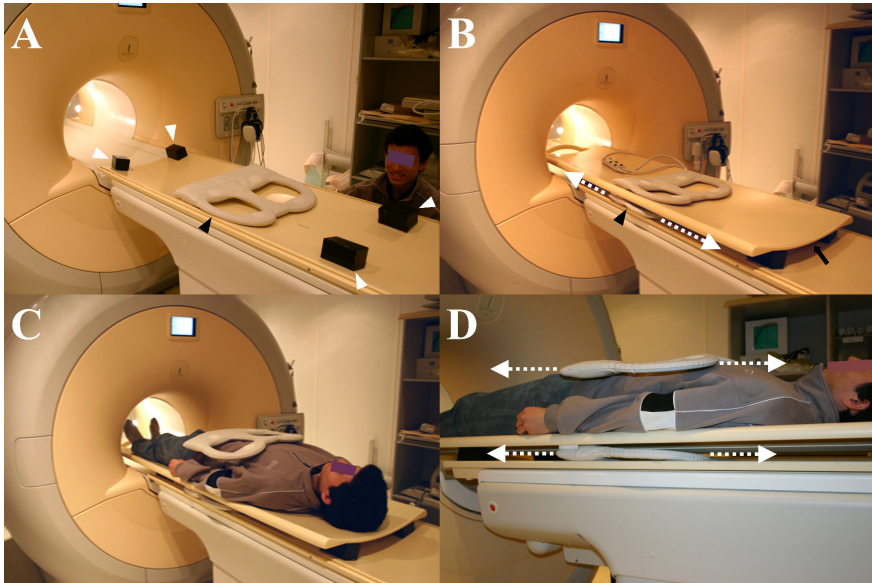


**Figure 1.** Table preparation for whole-body MRI using a sliding surface coil approach. (A) Spacers (white arrowheads) are placed on top of the original patient table to create space for the lower part of the surface coil (black arrowhead). (B) An additional table platform is mounted on top of the spacers (arrow). The lower part of the surface coil (black arrow head) can be moved freely below the additional table platform (dashed arrows). (C, D) Patient is lying on top of the additional table platform; the surface coil can be moved freely without patient repositioning (dashed arrows).

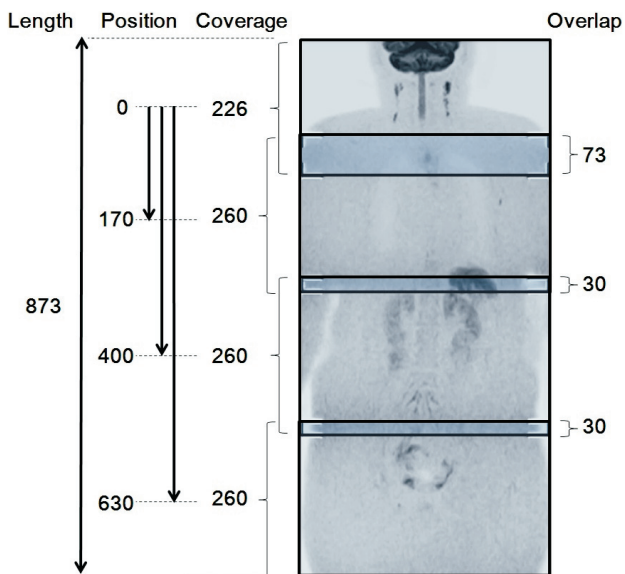


**Figure 2.** Positions and overlaps of the four stations in DWI, with explanatory measures (in mm). Imaging length of DWI was 87.3 cm, and aimed to cover the body from the level of the ear to the inguinal region

the neck/shoulder region, an area which may suffer considerably from magnetic field heterogeneity. Because of the gradient design, no corrections for non-linear gradient behaviour had to be applied.

T1-weighted gradient-echo imaging was performed with the following sequence parameters per station: repetition time (TR)/echo time (TE) of 187/2.3 (in-phase) and 4.6 (out-of-phase) ms, image acquisition in the coronal plane, slice thickness/gap of 7.0/1.0 mm, number of slices of 25, FOV of 400 mm<sup>2</sup>, acquisition matrix of 224, 1 signal average, imaging percentage (phase encode reduction) of 65%, actual pixel size of 1.79 × 2.74 mm<sup>2</sup>, reconstructed pixel size of 1.25 × 1.25 mm<sup>2</sup>, image acquisition under (end-inspiratory) breath-holding, and total imaging time 28 s per station.

T2-weighted turbo spin-echo imaging was performed with the following sequence parameters per station: TR/TE of 1000/82 ms, image acquisition in the coronal plane, slice thickness/gap of 7.0/1.0 mm, number of slices of 25, FOV of 400 mm<sup>2</sup>, acquisition matrix of 320, 1 signal average, imaging percentage (phase encode reduction) of 96%, half image factor of 0.525, parallel imaging (SENSitivity Encoding [SENSE]) factor of 2.0, actual pixel size of 1.25 × 1.31 mm<sup>2</sup>, reconstructed pixel size of 0.78 × 0.78 mm<sup>2</sup>, image acquisition under (end-inspiratory) breath-holding, and total imaging time of 25 s per station.

Diffusion-weighted single-shot echo-planar imaging (EPI) was performed in the transverse plane with slice overlaps in station 1 (head/neck), because station 1 is relatively more prone to image distortion. No slice overlaps were used for DWI of stations 2-4 (chest, abdomen, and pelvis). Station 1: TR/TE/inversion time of 5320/68/180 ms, slice thickness/gap of 4.0/-1.0 mm, number of packages of 2, number of slices of 75, 4 signal averages, and total imaging time of 191 s. Stations 2-4: TR/TE/inversion time of 9249/68/180 ms, slice thickness/gap of 4.0/0 mm, number of packages of 1, number of slices of 65, 5 signal averages, and total imaging time of 212 s per station. The remaining parameters for DWI were the same in all stations: FOV of 400 mm<sup>2</sup>, rectangular FOV of 70%, acquisition matrix of 160, motion probing gradients in three orthogonal axes, number of b-values of 2 (0 and 1000 s/mm<sup>2</sup>), imaging percentage (phase encode reduction) of 80%, half scan factor of 0.6, parallel imaging (SENSitivity Encoding [SENSE]) factor of 2.0 (of note, to enable parallel imaging, each station needed separate preparatory imaging), EPI factor of 47, actual pixel size of 2.50 × 3.19 mm<sup>2</sup>, reconstructed pixel size of 1.56 × 1.56 mm<sup>2</sup>, and image acquisition under free breathing.

Diffusion-weighted images were coronally reformatted, with a slice thickness/gap of 5.0/0mm, and displayed using grey-scale inversion. Subsequently, the four separately acquired stations were merged by software implemented in the standard operating console (MobiView, Philips Healthcare, Best, The Netherlands), for each of the coronal T1-weighted, coronal T2-weighted and coronal reformatted DWI datasets. In this way, seamless coronal whole-body T1-weighted, T2-weighted and diffusion-weighted images were created, each covering the area from at least the neck to the inguinal area (**Figure 3**).



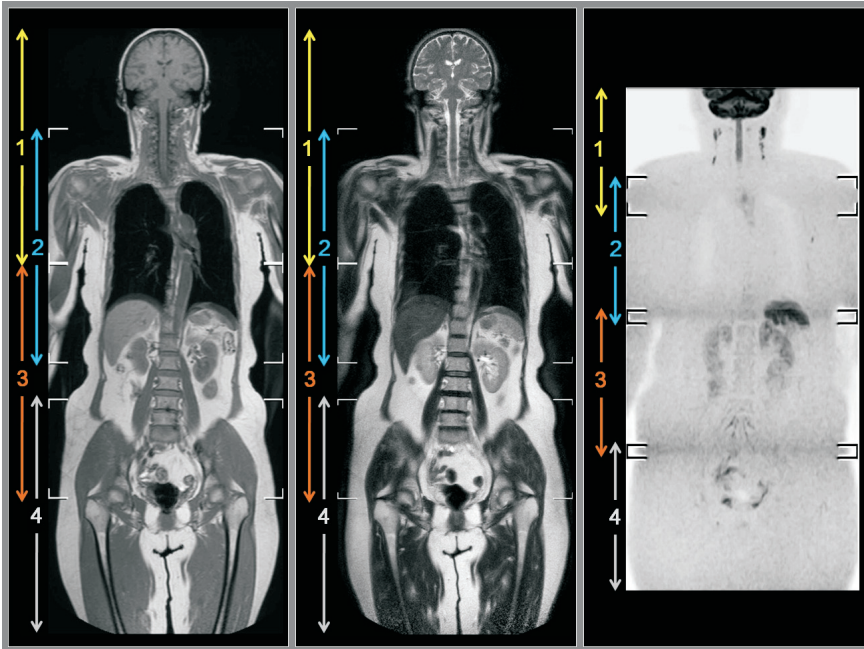


**Figure 3.** Representative examples of whole-body T1-weighted (A), T2-weighted (B) and diffusion-weighted (C) images, acquired using the sliding surface coil approach, in an asymptomatic subject without abnormal findings (case 2). Note that anatomical alignment and image quality at the boundaries between the head/neck and chest stations, and between the boundaries of the abdominal and pelvic stations are good to excellent, whereas those at the boundaries between the chest and abdominal stations are moderate to good (arrowheads).

#### Data analysis

Time required to change the surface coil from one station to the next station was measured for each of the three station changes, in each asymptomatic subject. Average time  $\pm$  SD to change the surface coil from one station to the next station and average total extra examination time  $\pm$  SD were calculated.

Subsequently, the coronal whole-body T1-, T2- and diffusion-weighted images were reviewed independently by two board-certified radiologists (T.T. and T.N., with 20 and 12 years experience in MRI interpretation, respectively). Anatomical alignment between adjacent stations in each sequence was assessed using a five-point grading scale (1 = very poor, anatomical alignment completely lacking; 2 = poor, anatomical alignment differs by more than 20 mm; 3 = moderate, anatomical alignment differs by more than 5 mm, but less than 20 mm; 4 = good, anatomical alignment differs by less than 5 mm; 5 = excellent, exact anatomical alignment). Furthermore, both image quality at the boundaries of adjacent stations and overall image quality of all stations in each sequence were assessed using a four-point grading scale (1 = inadequate image

quality with marked artifacts; 2 = adequate image quality with diagnostically relevant artifacts; 3 = good image quality with slight, diagnostically irrelevant artifacts; 4 = excellent image quality without artifacts).

Median scores regarding anatomic alignment between adjacent stations, image quality at the boundaries of different adjacent stations, and overall image quality of all different stations were calculated for each sequence. The Kruskal-Wallis test was used to test for overall equality of medians in each data group. When significant differences occurred, independent samples were compared by using the Mann-Whitney U test. Differences were considered significant when *P* values were less than 0.05. Statistical analyses were executed using Statistical Package for the Social Sciences (SPSS) software version 16.0 (SPSS, Chicago, Ill, USA).

## Results

All subjects tolerated this whole-body MRI protocol well (including breath-holding for T1- and T2-weighted imaging), without any claustrophobic events. Average total scan time  $\pm$  SD was 38 minutes 10 s  $\pm$  2 minutes 16 s. Average effective room time  $\pm$  SD was 41 minutes 8 s  $\pm$  2 minutes 18 s. Average time  $\pm$  SD to change the surface coil from one station to the next station was 53.8  $\pm$  7.1 s (range, 35-67 s). Average total extra examination time  $\pm$  SD for imaging four stations (corresponding to three coil repositionings) was 2 minutes 41.4 s  $\pm$  15.3 s (range, 2 minutes 16 s-3 minutes 1 s).

Median scores regarding anatomical alignment were 5 (excellent) between all stations on all sequences, and were not significantly different from each other, for both observers (**Table 1**).

**Table 1.** Overall comparison of scores regarding anatomical alignment between different stations

Sequence	Observer	Median score (range)			P value
		Stations 1 $\leftrightarrow$ 2	Stations 2 $\leftrightarrow$ 3	Stations 3 $\leftrightarrow$ 4	
T1-weighted	1	5 (-)	5 (-)	5 (-)	1.000
	2	5 (4-5)	5 (4-5)	5 (4-5)	1.000
T2-weighted	1	5 (-)	5 (-)	5 (-)	1.000
	2	5 (-)	5 (-)	5 (-)	1.000
DWI	1	5 (-)	5 (-)	5 (-)	1.000
	2	5 (-)	5 (3-5)	5 (-)	0.126

Scoring system: 1 = very poor, anatomical alignment completely lacking; 2 = poor, anatomical alignment differs by more than 20 mm; 3 = moderate, anatomical alignment differs by more than 5 mm, but less than 20 mm; 4 = good, anatomical alignment differs by less than 5 mm; 5 = excellent, exact anatomical alignment

Median scores regarding image quality were 4 (excellent) at all station boundaries of T1- and T2-weighted images, and were not significantly different from each other, for both observers (**Table 2**). However, although median scores regarding image quality

at the boundaries of different stations of diffusion-weighted images were 3 (good) or 4 (excellent), they were significantly different from each other, for both observers (**Table 2**). Pairwise comparisons revealed that quality of diffusion-weighted images at the boundaries of stations 1 and 2 (head/neck and chest) was significantly better ( $P \leq 0.001$  for both observers) than that at the boundaries of stations 2 and 3 (chest and abdomen) and stations 3 and 4 (abdomen and pelvis), without any significant differences between the other stations.

**Table 2.** Comparison of scores regarding image quality at the boundaries of different stations

Sequence	Observer	Median score (range)			P value
		Stations 1↔2	Stations 2↔3	Stations 3↔4	
T1-weighted	1	4 (-)	4 (-)	4 (-)	1.000
	2	4 (-)	4 (-)	4 (-)	1.000
T2-weighted	1	4 (-)	4 (-)	4 (-)	1.000
	2	4 (-)	4 (-)	4 (-)	1.000
DWI	1	4 (-)	3 (2-4)	3 (-)	< 0.001
	2	4 (-)	3 (2-4)	3 (2-4)	< 0.001

Scoring system: 1 = inadequate image quality with marked artifacts; 2 = adequate image quality with diagnostically relevant artifacts; 3 = good image quality with slight, diagnostically irrelevant artifacts; 4 = excellent image quality without artifacts

Median scores regarding overall image quality were either 3 (good) or 4 (excellent) for all stations of all sequences and for both observers, but these scores were almost always significantly different from each other (**Table 3**). Pairwise comparisons first revealed that overall quality of T1-weighted images of stations 1 (head/neck), 3 (abdomen), and 4 (pelvis) was significantly better ( $P = 0.030$ ) than that of station 2 (chest) for observer 1, without any significant differences between the other stations. Findings of observer 2 were slightly different; overall quality of T1-weighted images of station 1 (head/neck) was significantly better ( $P < 0.03$ ) than that of all other stations,

**Table 3.** Comparison of scores regarding overall image quality of each station

Sequence	Observer	Median score (range)				P value
		Station 1	Station 2	Station 3	Station 4	
T1-weighted	1	4 (-)	4 (2-4)	4 (-)	4 (-)	0.005
	2	4 (-)	3 (2-4)	3 (-)	4 (3-4)	< 0.001
T2-weighted	1	4 (-)	3.5 (2-4)	4 (-)	4 (-)	0.001
	2	4 (-)	3 (2-4)	4 (2-4)	4 (3-4)	< 0.001
DWI	1	4 (-)	4 (-)	4 (3-4)	4 (-)	0.392
	2	4 (-)	3.5 (3-4)	3 (2-4)	3.5 (3-4)	0.012

Scoring system: 1 = inadequate image quality with marked artifacts; 2 = adequate image quality with diagnostically relevant artifacts; 3 = good image quality with slight, diagnostically irrelevant artifacts; 4 = excellent image quality without artifacts

and overall quality of T1-weighted images of station 4 (pelvis) was significantly better ( $P = 0.004$ ) than that of station 3 (abdomen), without any significant differences between other stations. Second, overall quality of T2-weighted images of stations 1 (head/neck), 3 (abdomen), and 4 (pelvis) were significantly better ( $P = 0.012$  for observer 1 and  $P < 0.001$  for observer 2) than that of station 2 (chest), without any significant differences between the other stations. Third, although median scores regarding overall quality of diffusion-weighted images of all stations were not significantly different from each other for observer 1, this was the case for observer 2; pairwise comparisons revealed that overall quality of diffusion-weighted images of station 1 (head/neck) was significantly better ( $P = 0.012$ ) than that of all other stations, without any significant differences between the other stations.

A representative example of a whole-body T1-weighted, a T2-weighted and a diffusion-weighted image using a non-integrated sliding surface coil approach can be seen in **Figure 3**.

One subject had a high suspicion of lung cancer because of a high signal intensity area in the lung at DWI, which was histopathologically confirmed. No abnormal findings were detected in any of the other nine subjects.

## Discussion

Whole-body MRI has evolved into a clinically feasible technique over the past few years [1-16]. In MRI, and especially in whole-body MRI, there is always a trade-off between image quality and scan time. Regardless of type of MRI sequence used and the scan speed itself, handling of the patient through the MRI system to obtain a whole-body examination has always been a major issue. Streamlining this process will yield both a reduction in total examination time and an increase in image quality. Previously, whole-body MRI was performed by repeatedly repositioning the patient in order to image the separate stations of the whole-body MRI examination; this significantly increased total examination time. Furthermore, anatomical alignment between separately imaged stations was not maintained using this approach; acquired images of separate stations had to be adjusted and aligned manually to create the visually appealing whole-body image [3]. Then, the moving table platform was introduced, allowing for sequential movement of the patient through the bore of the magnet during imaging; patient repositioning was no longer required and total examination time was reduced. Furthermore, the slice selection gradients match exactly at each station, as a result of which anatomical alignment between separate stations is maintained [3]. Post-processing software capable of automatically aligning the different stations and fusing them into one seamless whole-body image has been developed; this significantly reduced the time required for processing the images after the examination. However, signal in whole-body MRI was still acquired using an integrated body coil, which yields

inferior SNR and spatial resolution compared with a surface coil [3]. Recently, whole-body surface coil technology (combining a large number of seamlessly integrated coil elements and independent radiofrequency channels) was introduced, which offers whole-body coverage and overcomes the problem of compromised image quality inherent to signal reception using an integrated body coil [1, 2]. Furthermore, a whole-body surface coil design allows for parallel imaging, which may be necessary for imaging time reduction and for DWI [4]. On the other hand, non-integrated surface coils such as those still being used on most of the currently installed systems are widely available, yield excellent image quality and allow for parallel imaging. However, their limited anatomical coverage may be a practical issue.

The present study shows that it is feasible to perform a time-efficient and high-quality whole-body MRI examination (including DWI), using a non-integrated surface coil. Using the sliding surface coil approach, average extra examination time was only less than three minutes (161.4 s) for acquiring four separate stations. Furthermore, anatomical alignment between adjacent stations, image quality at the boundaries of adjacent stations, and overall image quality of all stations were graded as “good” to “excellent” overall. Quality of diffusion-weighted images at the boundaries of the chest and abdominal station, and at the boundaries of the abdominal and pelvic stations were relatively poorer (although still graded as “good” overall). In addition, quality of both T1-, T2- and diffusion-weighted images of the head/neck station tended to be better than that of the chest, abdominal, and pelvic stations (although still graded as “good” overall). This finding can be explained by the fact that the chest, abdominal, and pelvic regions are more prone to breathing artifacts (i.e. the continuously changing position of the diaphragm, paradiaphragmatic, and abdominal organs during image acquisition and between the two imaging procedures may result in slight image blurring) than the head/neck region. It should be noted that this problem is most likely not related to the sliding surface coil approach, and would also have occurred when using a whole-body surface coil design. Nonetheless, it may potentially hinder image interpretation and decrease lesion conspicuity.

Using the sliding surface coil approach, sufficient space was created to freely move the lower part of a surface coil over a distance of approximately 110 cm along the z-axis. However, true whole-body imaging was not performed, because the upper extremities were just outside the FOV, while the lower extremities were not examined at all. Nevertheless, the region from the head to pelvis, the most essential part of the body when performing whole-body imaging studies (e.g. in cases of oncological staging) could easily be covered in all subjects.

Another relative drawback of the proposed sliding surface coil approach is narrowing of the bore diameter in the vertical direction by 6.5 cm because of the use of spacers and an additional table platform. Especially in the Western world, where the prevalence of obesity and the number of large-sized patients is increasing, this

may be an issue [19]. Furthermore, narrowing of the bore diameter may increase the risk of claustrophobic events, although all subjects in the present study tolerated the whole-body MRI examination well. Another drawback is the need to prepare the MRI table. However, this requires only a negligible amount of extra time (less than five minutes). Additionally, in the present study, a surface coil with a relatively small anatomical coverage (24 cm in the z-axis) was used. The use of a surface coil with larger anatomical coverage may even further decrease extra examination time, because fewer coil repositionings will be required. For example, a surface coil with 48 cm coverage (which is currently widely available for routine clinical use) allows up to 96 cm of imaging along the z-axis (with maintenance of anatomical alignment), with only one coil repositioning. Eventually, it is expected that the availability of whole-body surface coil designs will increase and that they will become the method of choice when performing a whole-body MRI examination. Until then, the sliding surface coil approach is an excellent alternative for performing a whole-body MRI examination. A relative study limitation is the fact that slice thickness of acquired coronal T1- and T2-weighted images (slice thickness/gap of 7.0/1.0 mm) did not match that of coronally reformatted diffusion-weighted images (slice thickness/gap of 5.0/0.0 mm). However, it would be impractical to acquire thinner T1- and T2-weighted slices, because this would considerably improve scan time and decrease SNR. Furthermore, the acquired axial diffusion-weighted dataset was reformatted into thin coronal slices rather than into thicker slices, because the former theoretically allows better lesion evaluation. In conclusion, the present study showed that a time-efficient, high-quality whole-body MRI examination can easily be performed by using a sliding surface coil approach.

## Acknowledgements

We thank Ms. Naoko Tsutsumi, Ms. Satomi Yano, and Ms. Asaka Obuchi for technical assistance in scanning. This work was funded (T.T.) by Nederandse Organisatie voor Wetenschappelijk Onderzoek (NWO) and the Japanese Society of Magnetic Resonance in Medicine (JSMRM).

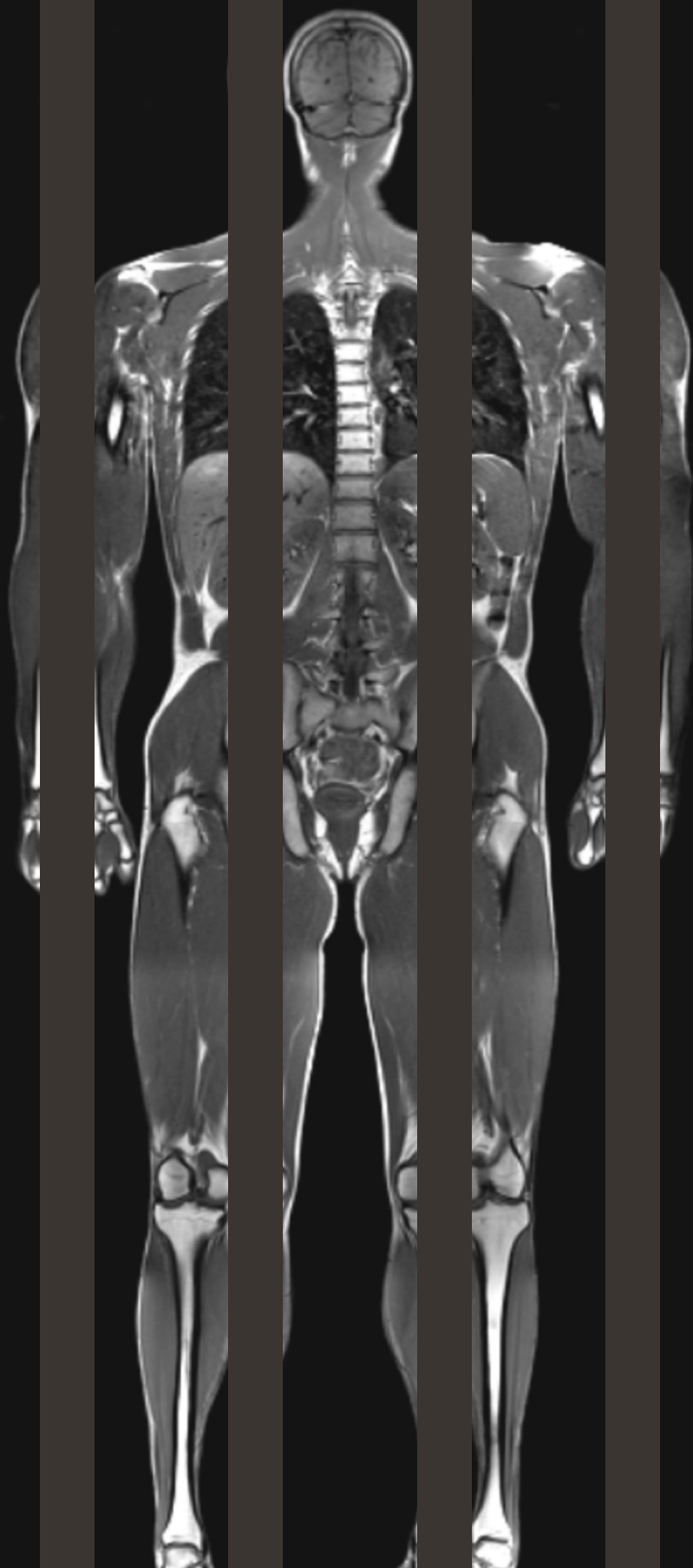
## References

1. Lauenstein TC, Semelka RC. Whole-body magnetic resonance imaging. *Top Magn Reson Imaging* 2005;16:15-20
2. Lauenstein TC, Semelka RC. Emerging techniques: whole-body screening and staging with MRI. *J Magn Reson Imaging* 2006;24:489-498
3. Hargaden G, O'Connell M, Kavanagh E, Powell T, Ward R, Eustace S. Current concepts in whole-body imaging using turbo short tau inversion recovery MR imaging. *AJR Am J Roentgenol* 2003;180:247-252
4. Kwee TC, Takahara T, Ochiai R, Nievelstein RA, Luijten PR. Diffusion-weighted whole-body imaging with background body signal suppression (DWIBS): features and potential applications in oncology. *Eur Radiol* 2008;18:1937-1952
5. Yi CA, Shin KM, Lee KS, et al. Non-small cell lung cancer staging: efficacy comparison of integrated PET/CT versus 3.0-T whole-body MR imaging. *Radiology* 2008;248:632-642
6. Ohno Y, Koyama H, Onishi Y, et al. Non-small cell lung cancer: whole-body MR examination for M-stage assessment--utility for whole-body diffusion-weighted imaging compared with integrated FDG PET/CT. *Radiology* 2008;248:643-654
7. Plathow C, Aschoff P, Lichy MP, et al. Positron emission tomography/computed tomography and whole-body magnetic resonance imaging in staging of advanced nonsmall cell lung cancer--initial results. *Invest Radiol* 2008;43:290-297
8. Brauck K, Zenge MO, Vogt FM, et al. Feasibility of whole-body MR with T2- and T1-weighted real-time steady-state free precession sequences during continuous table movement to depict metastases. *Radiology* 2008;246:910-916
9. PfannenberG C, Aschoff P, Schanz S, et al. Prospective comparison of 18F-fluorodeoxyglucose positron emission tomography/computed tomography and whole-body magnetic resonance imaging in staging of advanced malignant melanoma. *Eur J Cancer* 2007;43:557-564
10. Mürtz P, Krautmacher C, Träber F, Gieseke J, Schild HH, Willinek WA. Diffusion-weighted whole-body MR imaging with background body signal suppression: a feasibility study at 3.0 Tesla. *Eur Radiol* 2007;17:3031-3037
11. Lichy MP, Aschoff P, Plathow C, et al. Tumor detection by diffusion-weighted MRI and ADC-mapping--initial clinical experiences in comparison to PET-CT. *Invest Radiol* 2008;42:605-613
12. Schmidt GP, Schoenberg SO, Schmid R, et al. Screening for bone metastases: whole-body MRI using a 32-channel system versus dual-modality PET-CT. *Eur Radiol* 2007;17:939-949
13. Schmidt GP, Baur-Melnyk A, Herzog P, et al. High-resolution whole-body magnetic resonance image tumor staging with the use of parallel imaging versus dual-modality positron emission tomography-computed tomography: experience on a 32-channel system. *Invest Radiol* 2005;40:743-753
14. Schlemmer HP, Schäfer J, PfannenberG C, et al. Fast whole-body assessment of metastatic disease using a novel magnetic resonance imaging system: initial experiences. *Invest Radiol* 2005;40:64-71
15. Lauenstein TC, Goehde SC, Herborn CU, et al. Whole-body MR imaging: evaluation of patients for metastases. *Radiology* 2004;233:139-148
16. Antoch G, Vogt FM, Freudenberg LS, et al. Whole-body dual-modality PET/CT and whole-body MRI for

- tumor staging in oncology. *JAMA* 2003;290:3199-3206
17. Ahmad MN, Zafar AM, Nadeem N. Where there is no PET/CT. *Eur J Radiol* 2009;70:463-454
  18. Huang B, Law MW, Khong PL. Whole-body PET/CT scanning: estimation of radiation dose and cancer risk. *Radiology* 2009;251:166-174
  19. Uppot RN, Sahani DV, Hahn PF, Gervais D, Mueller PR. Impact of obesity on medical imaging and image-guided intervention. *AJR Am J Roentgenol* 2007;188:433-440







# Chapter 6<sup>1</sup>

ADC measurements of lymph nodes: inter- and intraobserver reproducibility study and an overview of the literature

Kwee TC, Takahara T, Luijten PR, Nieuwstein RA

Eur J Radiol;75:215-220

## Abstract

### Purpose

Apparent diffusion coefficient (ADC) measurements in diffusion-weighted magnetic resonance imaging (DWI) may be of value in discriminating malignant from non-malignant lymph nodes, provided that they are reproducible. The aim of this study was to determine the inter- and intraobserver reproducibilities of ADC measurements of lymph nodes and to provide an overview of the current literature on ADC measurements in the characterization of lymph nodes.

### Materials and Methods

Twenty healthy volunteers underwent DWI of the head and neck region and the pelvic region, at b-values of 0 s/mm<sup>2</sup> and 1000 s/mm<sup>2</sup>. Two observers independently and blindly measured ADCs of lymph nodes. Inter- and intraobserver reproducibilities were assessed using the Bland-Altman method.

### Results

Mean ADCs of normal lymph nodes (in 10<sup>-3</sup> mm<sup>2</sup>/s) varied between 1.15 and 1.18. Ranges of mean ADC difference ± limits of agreement (in 10<sup>-3</sup> mm<sup>2</sup>/s) for interobserver agreement were -0.03-0.02 ± 0.15-0.31. Ranges of mean ADC difference ± limits of agreement (in 10<sup>-3</sup> mm<sup>2</sup>/s) for intraobserver agreement were 0.00-0.04 ± 0.13-0.32.

### Conclusion

In light of previously reported data, the results of the present study suggest that ADC measurements may not always be sufficiently reproducible to discriminate malignant from non-malignant lymph nodes. Future studies which directly compare the ADCs of different nodal pathologies/conditions are required to further investigate the inter- and intraobserver reproducibilities of ADC measurements of lymph nodes.

## Introduction

Cancer is the second leading cause of death in developed countries, is among the three leading causes of death for adults in developing countries, and is responsible for 12.5% of all deaths worldwide [1]. Once a malignant tumor is detected, determination of nodal status is of crucial importance for appropriate treatment planning and determining prognosis. Current cross-sectional imaging modalities, however, rely on insensitive size and morphologic criteria and, thus, lack the desired accuracy for characterizing lymph nodes [2].

Diffusion-weighted magnetic resonance (MR) imaging (DWI) is a functional imaging modality, allowing for the detection and characterization of lesions exhibiting restricted diffusion. Recent technological advances, including the development of high-performance magnetic field gradients and parallel imaging, have expanded the application of DWI from the brain to the body [3]. Along with the development of the concept of Diffusion-weighted Whole-body Imaging with background body signal Suppression (DWIBS), which aims to obtain wide coverage and (near) volumetric scanning, this allows obtaining a high quality and time-efficient whole-body DWI examination [4, 5]. Furthermore, in contrast to computed tomography, single photon emission computed tomography, and positron emission tomography, DWI does not expose the patient to ionizing radiation and does not require administering any contrast agents. The main clinical application of DWI in the brain is in the diagnosis of acute ischemic stroke, but DWI in the body has particular potential in the detection and characterization of primary tumors and metastases [3-5]. DWI may also be a valuable tool for the identification and characterization of lymph nodes; DWI highlights both normal and pathologic lymph nodes and enables measuring diffusion in lymph nodes by means of the apparent diffusion coefficient (ADC) [4, 5]. Normal lymph nodes have a relatively restricted diffusion (low ADC) because of their high cellular density [6]. Metastatic lymph nodes may have increased cellular density or necrotic areas, which further restricts or increases diffusion, respectively [4]. ADC measurements may thus allow discriminating malignant from non-malignant lymph nodes. Several studies have investigated whether ADC measurements are helpful in lymph node characterization [7-14]. Inter- and intraobserver reproducibilities of ADC measurements of lymph nodes in DWI, however, are still unknown. Serial measurements must be accurate and reproducible, or clinical utility will inevitably be limited [15]. We therefore performed this study to assess the inter- and intraobserver reproducibilities of ADC measurements of lymph nodes in DWI, in healthy volunteers. In addition, an update of the literature on ADC measurements in the characterization of lymph nodes is given.

## Materials and Methods

### Study participants

This study was approved by the local institutional review board and written informed consent was obtained from all participants. Twenty healthy adult volunteers (10 men and 10 women; mean age, 22.7 years; age range, 18–37 years) were prospectively included. Volunteers who underwent surgery in the past, volunteers who had a malignancy in the past, volunteers who have been or are suffering from a chronic inflammation or infection, volunteers using medication at present, volunteers who suffered from a transient infection within the past two months, volunteers with symptoms possibly indicating an active inflammation or infection (e.g. fever, chills, night sweats, malaise, weight loss, fatigue, rhinorrhoe, coughing, throat ache, nausea, vomiting, diarrhea, etc.), and volunteers with a general contraindication for MR imaging (including implanted pacemaker and claustrophobia) were excluded from participation.

### MR imaging

All volunteers were examined with a 1.5-T MR scanner (Achieva, Philips Healthcare, Best, The Netherlands) using a four-element phased array surface coil (SENSE body coil, Philips Medical Systems, Best, The Netherlands). In all volunteers, DWI scans of the head and neck region and the pelvic region were obtained, using a Stejskal-Tanner sequence [16] with single-shot echo-planar imaging (EPI). Applied sequence parameters for DWI of the head and neck region were as follows: repetition time (TR)/echo time/inversion time of 8612/ 78/180 ms, number of slices of 60, slice thickness/gap of 4/0 mm, cranio-caudal coverage of 240 mm, field of view (FOV) of 450×366 mm<sup>2</sup>, rectangular FOV of 81.3%, acquisition matrix of 256, scan percentage (phase encoding reduction) of 78.2%, half scan factor of 0.651, EPI factor (echo train length) of 43, bandwidth of 1874.3 Hz, image acquisition in the axial plane, motion probing gradients (MPGs) in three orthogonal axes, b-values of 0 and 1000 s/mm<sup>2</sup> (the highest b-value was chosen based on practical experience), 3 averages, parallel imaging (SENSitivity Encoding [SENSE]) factor of 2, image acquisition under free breathing, actual voxel size of 3.52 x 4.50 x 4.00 mm<sup>3</sup>, reconstructed voxel size of 1.76 x 1.76 x 4.00 mm<sup>3</sup>, image acquisition time of 4 minutes and 44 s. Applied sequence parameters for DWI of the pelvic region were identical, except for a TR of 6962 ms, a chemical shift selective (CHESS) pre-pulse instead of an IR pre-pulse for fat suppression, and an image acquisition time of 3 minutes and 50 s. Axial trace ADC maps were created of all obtained images, using the b-values of 0 and 1000 s/mm<sup>2</sup>.

### Image analysis

MR images were transferred to a workstation (ViewForum; Philips Medical Systems, Best, The Netherlands). One of the authors (T.C.K.) reviewed the images and randomly

selected one lymph node with a short-axis diameter of 5 mm or less and one lymph node with a short-axis diameter exceeding 5 mm, in both the head and neck region and the pelvic region, in each of the 20 volunteers. The locations and slice numbers of the selected lymph nodes were recorded for further analysis. Subsequently, a board-certified radiologist (observer 1, R.A.J.N., with 13 years of experience in MR imaging) and a research physician (observer 2, T.C.K.) independently and blindly performed ADC measurements of all selected lymph nodes, as follows: regions of interest (ROIs) were placed manually in the selected lymph nodes, on the images obtained at a b-value of 1000 s/mm<sup>2</sup>. Each ROI was variable in shape and size, so that it included as much of the nodal parenchyma as possible. The ROIs were then copied and pasted onto the ADC maps, and ADCs of lymph nodes were automatically calculated (**Figure 1**). All measurements were done twice by each of the two readers, with a wash-out period of two weeks between the first and second series of measurements.

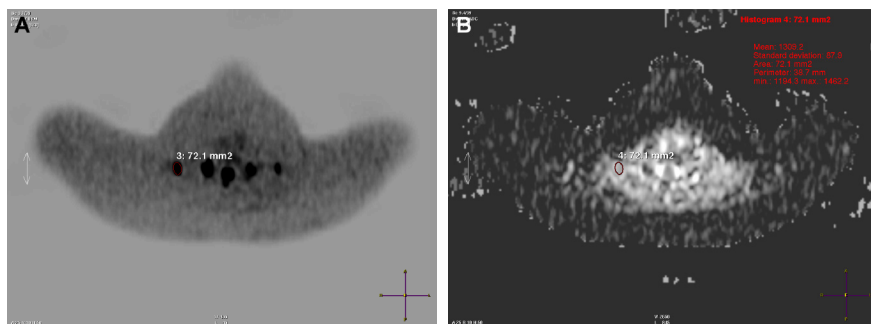


**Figure 1.** Example of ADC measurement of a lymph node in the head and neck region. (A) A region of interest (ROI) was placed manually in the selected lymph node, on the image obtained at a b-value of 1000 s/mm<sup>2</sup>. The ROI was then copied and pasted onto the ADC map, and the ADC of the lymph node was automatically calculated.

### Statistical Analysis

First, mean ADCs  $\pm$  SDs of normal lymph nodes were calculated for each reader, for each series of measurements. Second, inter- and intraobserver reproducibility of ADC measurements of lymph nodes were determined as mean absolute difference (bias) and 95% confidence interval of the mean difference (limits of agreement), according to the methods of Bland and Altman [15]. Reproducibility analyses were separately done for lymph nodes with a short axis diameter  $>$  5 mm and lymph nodes with a short axis diameter  $\leq$  5 mm.

Statistical analyses were executed using Statistical Package for the Social Sciences version 12.0 software (SPSS, Chicago, IL, USA) and MedCalc Software (MedCalc, Mariakerke, Belgium).

## Results

Mean ADCs of normal lymph nodes varied between  $1.15 \times 10^{-3} \text{ mm}^2/\text{s}$  and  $1.18 \times 10^{-3} \text{ mm}^2/\text{s}$  (Table 1). The mean biases and limits of agreement for inter- and intraobserver measurements according to lymph node short-axis diameter are summarized in Tables 2 and 3, and the corresponding Bland-Altman plots are displayed in Figures 2 and 3.

**Table 1.** ADCs of normal lymph nodes

Observer	Measurement	Mean ADC $\pm$ SD (in $10^{-3} \text{ mm}^2/\text{s}$ )
1	1	$1.17 \pm 0.27$
	2	$1.15 \pm 0.27$
2	1	$1.18 \pm 0.28$
	2	$1.15 \pm 0.28$

**Table 2.** Interobserver reproducibility of ADC measurements of lymph nodes

Lymph node short-axis diameter	Series of measurements	Mean bias (in $10^{-3} \text{ mm}^2/\text{s}$ )	Limits of agreement (in $10^{-3} \text{ mm}^2/\text{s}$ )
>5 mm	1	-0.01	$\pm 0.31$
	2	0.02	$\pm 0.15$
$\leq 5$ mm	1	-0.01	$\pm 0.19$
	2	-0.03	$\pm 0.30$

**Table 3.** Intraobserver reproducibility of ADC measurements of lymph nodes

Lymph node short-axis diameter	Observer	Mean bias (in $10^{-3} \text{ mm}^2/\text{s}$ )	Limits of agreement (in $10^{-3} \text{ mm}^2/\text{s}$ )
>5 mm	1	0.02	$\pm 0.20$
	2	0.04	$\pm 0.25$
$\leq 5$ mm	1	0.02	$\pm 0.32$
	2	0.00	$\pm 0.13$



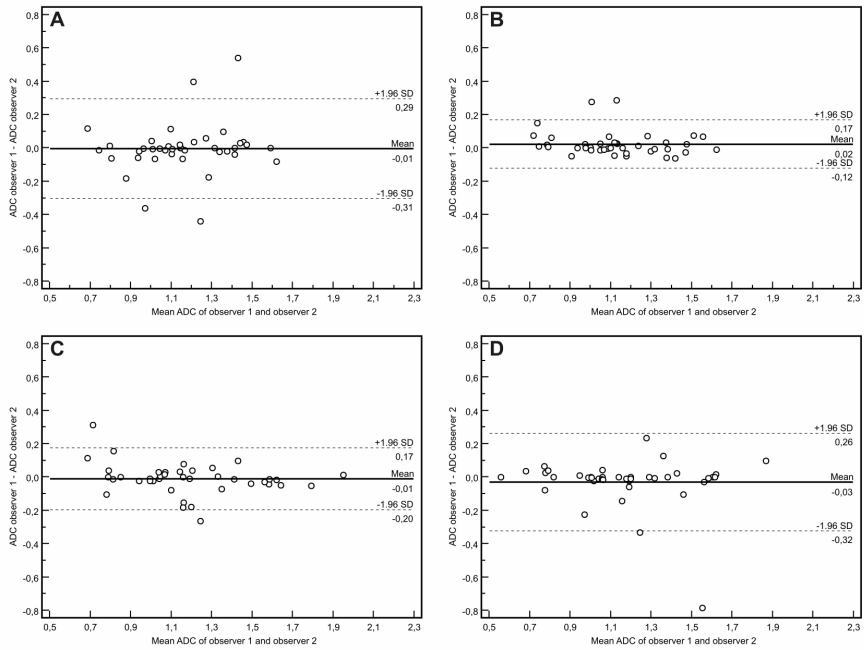


**Figure 2.** Interobserver reproducibility of ADC measurements of lymph nodes in DWIBS. Bland-Altman plots of difference of ADC measurements (y-axis) against mean ADC measurement (x-axis), with mean absolute difference (bias) (continuous line) and 95% confidence interval of the mean difference (limits of agreement) (dashed lines) for (A) the first series of measurement of lymph nodes with a short axis diameter > 5 mm, (B) the second series of measurements of lymph nodes with a short axis diameter > 5 mm, (C) the first series of measurements of lymph nodes with a short axis diameter  $\leq$  5 mm, and (D) the second series of measurements of lymph nodes with a short axis diameter  $\leq$  5 mm.

Interobserver reproducibility between lymph nodes with a short-axis diameter > 5 mm and lymph nodes with a short axis diameter  $\leq$  5 mm was comparable, with mean bias between two ADC measurements varying between  $-0.03 \times 10^{-3}$  and  $0.02 \times 10^{-3}$   $\text{mm}^2/\text{s}$ , and limits of agreement varying between  $\pm 0.15 \times 10^{-3}$  and  $\pm 0.31 \times 10^{-3}$   $\text{mm}^2/\text{s}$  (Table 2 and Figure 2). Intraobserver reproducibility between lymph nodes with a short-axis diameter > 5 mm and lymph nodes with a short-axis diameter  $\leq$  5 mm was also comparable, with mean bias between two ADC measurements varying between  $0.00 \times 10^{-3}$   $\text{mm}^2/\text{s}$  and  $0.04 \times 10^{-3}$   $\text{mm}^2/\text{s}$ , and limits of agreement varying between  $\pm 0.13 \times 10^{-3}$   $\text{mm}^2/\text{s}$  and  $\pm 0.32 \times 10^{-3}$   $\text{mm}^2/\text{s}$  (Table 3 and Figure 3).

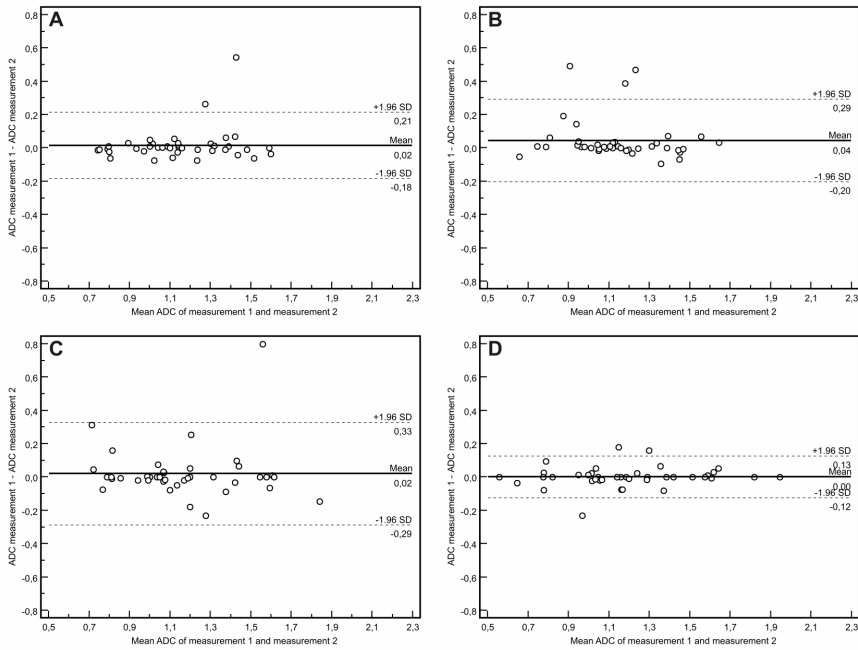


**Figure 3.** Intraobserver reproducibility of ADC measurements of lymph nodes in DWIBS. Bland-Altman plots of difference of ADC measurements (y-axis) against mean ADC measurement (x-axis), with mean absolute difference (bias) (continuous line) and 95% confidence interval of the mean difference (limits of agreement) (dashed lines) for (A) the first series of measurement of lymph nodes with a short axis diameter > 5 mm, (B) the second series of measurements of lymph nodes with a short axis diameter > 5 mm, (C) the first series of measurements of lymph nodes with a short axis diameter ≤ 5 mm, and (D) the second series of measurements of lymph nodes with a short axis diameter ≤ 5 mm.

## Discussion

Technological advances and the introduction of the concept of DWIBS have opened the path for routine clinical whole-body DWI [3-5]. Tissues which have a long T2 value and a restricted diffusion, such as many malignant tumors, are visualized in DWI. DWI is also a powerful tool to identify lymph nodes throughout the entire body, but may also be used to characterize them through ADC measurements [4, 5]. Several studies have calculated the ADCs of different nodal pathologies/conditions in various body regions and investigated whether they were effective in differentiating these different nodal pathologies (Table 4) [7-14]. Six of eight previously reported studies [7-10, 12, 13] indicated that ADC measurements may be useful in nodal characterization, while two of eight studies [11, 14] indicated that ADC measurements were not effective in discriminating malignant from non-malignant lymph nodes (Table 4).

**Table 4.** Previously reported ADCs of different nodal pathologies/conditions per study

Study and year	Field strength (T) / b-values (s/mm <sup>2</sup> )	Nodal pathology/condition (N)	Mean ADC ± SD (in x 10 <sup>-3</sup> mm <sup>2</sup> /s)	Statistical differences in mean ADCs	Absolute differences in mean ADCs (in x 10 <sup>-3</sup> mm <sup>2</sup> /s)
Sumi et al. [7], 2003	1.5 / 500, 1000	1. Metastatic (25) <sup>a</sup>	0.410 ± 0.105	1 vs. 2; P<0.01	1 - 2; 0.108
		2. Benign lymphadenopathy (25)	0.302 ± 0.062	1 vs. 3; P<0.01	1 - 3; 0.187
		3. Lymphoma (5) <sup>b</sup>	0.223 ± 0.056	2 vs. 3; P<0.05	2 - 3; 0.079
Sumi et al. [8], 2006	1.5 / 500, 1000	1. Metastatic (24) <sup>a</sup>	1.167 ± 0.447	1 vs. 2; P<0.001	1 - 2; 0.515
		2. Benign lymphadenopathy (35)	0.652 ± 0.101	1 vs. 3; P<0.001	1 - 3; 0.566
		3. Lymphoma (14) <sup>c</sup>	0.601 ± 0.427	2 vs. 3; P<0.01	2 - 3; 0.051
Abdel-Razek [9], 2006	1.5 / 0, 1000	1. Metastatic (51) <sup>a</sup>	1.09 ± 0.11	1 vs. 2; P<0.04	1 - 2; 0.555
		2. Benign lymphadenopathy (15)	1.64 ± 0.16	1 vs. 3; NS	1 - 3; 0.12
		3. Lymphoma (21) <sup>c</sup>	0.97 ± 0.27	2 vs. 3; P<0.04	2 - 3; 0.67
King et al. [10], 2007	1.5 / 0, 100, 200, 300, 400, 500	1. Metastatic (51) <sup>a</sup>	1.057 ± 0.169	1 vs. 2; P<0.001	1 - 2; 0.255
		2. Metastatic (15) <sup>d</sup>	0.802 ± 0.128	1 vs. 3; P<0.001	1 - 3; 0.393
		3. Lymphoma (21) <sup>c</sup>	0.664 ± 0.071	2 vs. 3; P<0.04	2 - 3; 0.138
Lin et al. [11], 2008	3.0 / 0, 1000	1. Metastatic (12) <sup>e</sup>	0.83 ± 0.15	1 vs. 2; P=0.639	1 - 2; 0.08
		2. Non-malignant (71) <sup>f</sup>	0.75 ± 0.19		
Akduman et al. [12], 2008	1.5 / 0, 600	1. Metastatic (16) <sup>g</sup>	1.84 ± 0.37	1 vs. 2; P<0.0005	1 - 2; 0.54
		2. Non-malignant (40) <sup>h</sup>	2.38 ± 0.29		
Kim et al. [13], 2008	1.5 / 0, 1000	1. Metastatic (30) <sup>e</sup>	0.7651 ± 0.1137	1 vs. 2; P<0.001	1 - 2; 0.237
		2. Non-malignant (220) <sup>f</sup>	1.0021 ± 0.1859		
Nakai et al. [14], 2008	1.5 / 0, 800	1. Metastatic (7) <sup>e</sup>	1.4 ± 0.4	1 vs. 2; P=0.28	1 - 2; 0.1
		2. Non-malignant (134) <sup>f</sup>	1.3 ± 0.24		

<sup>a</sup> Metastatic lymph nodes from primary squamous cell carcinoma in the head and neck region; <sup>b</sup> Non-Hodgkin lymphoma; <sup>c</sup> Non-Hodgkin lymphoma and Hodgkin disease  
<sup>d</sup> Metastatic lymph nodes from nasopharyngeal carcinoma; <sup>e</sup> Metastatic lymph nodes from cervical or uterine cancer; <sup>f</sup> Non-malignant lymph nodes (not further specified) in patients with cervical or uterine cancer; <sup>g</sup> Metastatic lymph nodes in patients with various abdominal malignancies or lung cancer; <sup>h</sup> Non-malignant lymph nodes (not further specified) in patients with various abdominal malignancies or lung cancer  
 NS: not significant

Attention should be paid to the unique characteristics of normal lymph nodes. In contrast to many other normal tissues, normal lymph nodes are densely packed with cells, which explains their relatively low ADC [6]. Many malignant tumors also have a high cellular density, and, when metastasized to a lymph node, may not always further decrease its ADC. This may explain why ADC measurements may not always be able to discriminate malignant from non-malignant lymph nodes [11, 14]. In contrast, when the metastatic tumor has a higher cellular density than a normal lymph node (i.e. relatively lower diffusion), or when the metastatic tumor contains necrotic areas (i.e. relatively higher diffusion), ADC measurements may allow discriminating malignant from non-malignant lymph nodes [7-10, 12, 13]. Remarkably, previously reported ADCs within the groups metastatic lymph nodes (range,  $0.410\text{-}1.84 \times 10^{-3} \text{ mm}^2/\text{s}$ ), malignant lymphoma (range,  $0.223\text{-}0.97 \times 10^{-3} \text{ mm}^2/\text{s}$ ), benign lymphadenopathy ( $0.302\text{-}1.64 \times 10^{-3} \text{ mm}^2/\text{s}$ ), and non-malignant lymph nodes (range,  $0.75\text{-}2.38 \times 10^{-3} \text{ mm}^2/\text{s}$ ) vary widely (Table 5) [7-14].

**Table 5.** Previously reported ADCs per nodal pathology/condition by different studies

Nodal pathology/condition	Study	Mean ADC $\pm$ SD (in $10^{-3} \text{ mm}^2/\text{s}$ )
Metastatic lymph nodes	Sumi et al. [7]	$0.410 \pm 0.105^a$
	Kim et al. [13]	$0.7651 \pm 0.1137^b$
	King et al. [10]	$0.802 \pm 0.128^c$
	Lin et al. [11]	$0.83 \pm 0.15^b$
	Sumi et al. [8]	$1.167 \pm 0.447^a$
	Abdel-Razek et al. [9]	$1.09 \pm 0.11^a$
	King et al. [10]	$1.057 \pm 0.169^a$
	Nakai et al. [14]	$1.4 \pm 0.4^c$
	Akduman et al. [12]	$1.84 \pm 0.37^d$
Lymphoma	Sumi et al. [7]	$0.223 \pm 0.056^e$
	Sumi et al. [8]	$0.601 \pm 0.427^f$
	King et al. [10]	$0.664 \pm 0.071^e$
	Abdel-Razek et al. [9]	$0.97 \pm 0.27^f$
Benign lymphadenopathy	Sumi et al. [7]	$0.302 \pm 0.062$
	Sumi et al. [8]	$0.652 \pm 0.101$
	Abdel-Razek et al. [9]	$1.64 \pm 0.16$
Non-malignant lymph nodes	Lin et al. [11]	$0.75 \pm 0.19^g$
	Kim et al. [13]	$1.0021 \pm 0.1859^g$
	Nakai et al. [14]	$1.3 \pm 0.24^g$
	Akduman et al. [12]	$2.38 \pm 0.29^h$

<sup>a</sup> Metastatic lymph nodes from primary squamous cell carcinoma in the head and neck region; <sup>b</sup> Metastatic lymph nodes from cervical or uterine cancer; <sup>c</sup> Metastatic lymph nodes from nasopharyngeal carcinoma; <sup>d</sup> Metastatic lymph nodes in patients with various abdominal malignancies or lung cancer; <sup>e</sup> Non-Hodgkin lymphoma; <sup>f</sup> Non-Hodgkin lymphoma and Hodgkin disease; <sup>g</sup> Non-malignant lymph nodes (not further specified) in patients with cervical or uterine cancer; <sup>h</sup> Non-malignant lymph nodes (not further specified) in patients with various abdominal malignancies or lung cancer

These differences may be explained by the inclusion of different histological subtypes (which may have different ADCs due to differences in cellular architecture) and different ways of ADC measurements (e.g. measurement of the entire lymph node will result in a higher ADC than in a measurement in which necrotic regions are excluded). Furthermore, a number of instrumental factors can give rise to random or systematic errors in estimates of the ADC. Random errors can arise from image noise and motion artifacts. Systematic errors can arise from incorrect values used for the diffusion gradient amplitudes, the presence of imaging, susceptibility, or eddy current gradient cross-terms unaccounted for in the b-value calculation, errors in the b-value calculation, image noise, and gradient calibration inaccuracy [17].

The mean ADC of normal lymph nodes, as was found in the present study, varied between  $1.15 \times 10^{-3}$  and  $1.18 \times 10^{-3}$  mm<sup>2</sup>/s, and overlapped with several previously reported ADCs of different nodal pathologies/conditions (**Table 5**) [7-14]. Despite this overlap, ADC measurements may still be useful in nodal characterization, since our ADC measurements may vary from those obtained in other centers because of previously mentioned reasons. More importantly, this study is the first to investigate the inter- and intraobserver reproducibilities of ADC measurements of lymph nodes; limits of agreement with regard to interobserver reproducibility varied between  $\pm 0.15 \times 10^{-3}$  and  $\pm 0.31 \times 10^{-3}$  mm<sup>2</sup>/s, and limits of agreement with regard to intraobserver reproducibility varied between  $\pm 0.13 \times 10^{-3}$  mm<sup>2</sup>/s and  $\pm 0.32$  mm<sup>2</sup>/s (with no apparent differences between lymph nodes with a short-axis diameter > 5 mm and lymph nodes with a short-axis diameter  $\leq$  5 mm). To obtain a gross estimation of the clinical acceptability of these limits of agreements, they should be compared to previously reported absolute differences in mean ADCs between different nodal pathologies/conditions (**Table 4**, last column). This comparison shows that the limits of agreements with regard to inter- and intraobserver reproducibilities of ADC measurements frequently exceed the absolute difference in mean ADCs between two nodal pathologies/conditions (**Table 4**, last column). In other words, this suggests that ADC measurements may not always be sufficiently reproducible to differentiate between different nodal pathologies and to discriminate between malignant and non-malignant lymph nodes.

A limitation of the present study is that only healthy volunteers were included, as a result of which only normal-sized lymph nodes were evaluated. Inter- and intraobserver reproducibilities of ADC measurements of pathologically enlarged lymph nodes may be different, and may still be of value in histological characterization of pathologically enlarged lymph nodes. Nevertheless, there is particular interest in the ability of DWI to differentiate normal-sized malignant from normal-sized non-malignant lymph nodes, which is a major unsolved clinical problem [2, 4, 5]. It was therefore justified to perform this study in a healthy study population, with normal-sized lymph nodes. Another issue is the moderate reproducibility of the ADC measurements in the

present study. This reproducibility may become better if thinner slices with a higher spatial resolution are acquired. It should be noted, however, that the applied slice thickness and spatial resolution in the present study are similar to the ones commonly used for a time-efficient whole-body DWI examination [4]. Another drawback of this study is that relatively young volunteers were included. Although the ADC of normal lymph nodes in a young population is not expected to be different from that in an older population, we can not exclude this.

## Conclusion

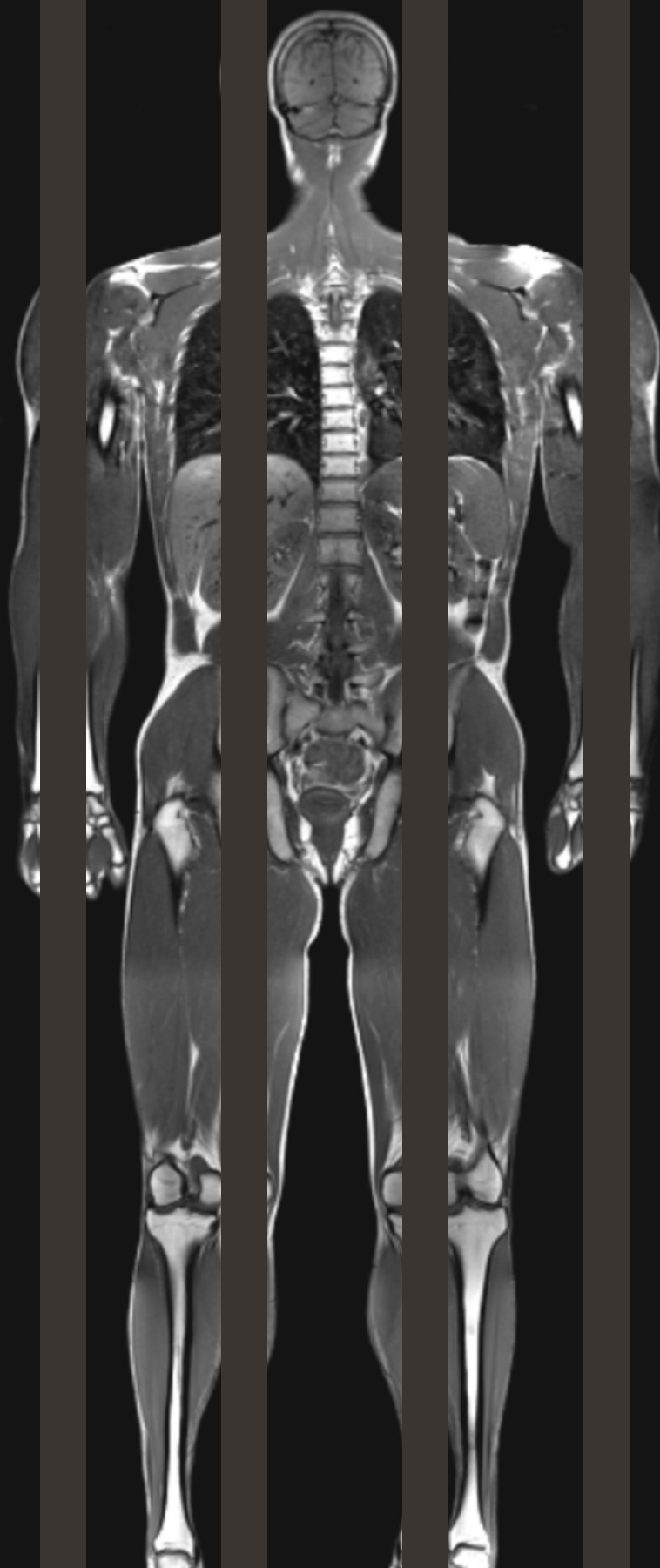
In light of previously reported data, the results of the present study suggest that ADC measurements may not always be sufficiently reproducible to differentiate between malignant and non-malignant lymph nodes. Future studies which directly compare the ADC different nodal pathologies are required to further investigate the inter- and intraobserver reproducibilities of ADC measurements of lymph nodes.

## Acknowledgement

The authors would like to thank Professor Willem P.Th.M. Mali (University Medical Center Utrecht, Department of Radiology) for reading the manuscript and giving valuable comments.

## References

1. World Health Organization and International Union Against Cancer. Global action against cancer. Geneva: WHO Press, 2005
2. Torabi M, Aquino SL, Harisinghani MG. Current concepts in lymph node imaging. *J Nucl Med* 2004;45:1509-1518
3. Koh DM, Collins DJ. Diffusion-weighted MRI in the body: applications and challenges in oncology. *AJR Am J Roentgenol* 2007;188:1622-1635
4. Kwee TC, Takahara T, Ochiai R, Nievelstein RAJ, Luijten PR. Diffusion-weighted whole-body imaging with background body signal suppression (DWIBS): features and potential applications in oncology. *Eur Radiol* 2008;18:1937-1952
5. Takahara T, Imai Y, Yamashita T, Yasuda S, Nasu S, Van Cauteren M. Diffusion weighted whole body imaging with background body signal suppression (DWIBS): technical improvement using free breathing, STIR and high resolution 3D display. *Radiat Med* 2004;22:275-282
6. Willard-Mack CL. Normal structure, function, and histology of lymph nodes. *Toxicol Pathol* 2006;34:409-424
7. Sumi M, Sakihama N, Sumi T, et al. Discrimination of metastatic cervical lymph nodes with diffusion-weighted MR imaging in patients with head and neck cancer. *AJNR Am J Neuroradiol* 2003;24:1627-1634
8. Sumi M, Van Cauteren M, Nakamura T. MR microimaging of benign and malignant nodes in the neck. *AJR Am J Roentgenol* 2006;186:749-757
9. Abdel Razek AA, Soliman NY, Elkhamary S, Alsharaway MK, Tawfik A. Role of diffusion-weighted MR imaging in cervical lymphadenopathy. *Eur Radiol* 2006;16:1468-1477
10. King AD, Ahuja AT, Yeung DK, et al. Anteroposterior Hippocampal Metabolic Heterogeneity: Three-dimensional Multivoxel Proton 1H MR Spectroscopic Imaging--Initial Findings. *Radiology* 2007;245:806-813
11. Lin G, Ho KC, Wang JJ, et al. Detection of lymph node metastasis in cervical and uterine cancers by diffusion-weighted magnetic resonance imaging at 3T. *J Magn Reson Imaging* 2008;28:128-135
12. Akduman EI, Momtahan AJ, Balci NC, Mahajann N, Havlioglu N, Wolverson MK. Comparison between malignant and benign abdominal lymph nodes on diffusion-weighted imaging. *Acad Radiol* 2008;15:641-646
13. Kim JK, Kim KA, Park BW, Kim N, Cho KS. Feasibility of diffusion-weighted imaging in the differentiation of metastatic from nonmetastatic lymph nodes: early experience. *J Magn Reson Imaging* 2008;28:714-719
14. Nakai G, Matsuki M, Inada Y, et al. Detection and evaluation of pelvic lymph nodes in patients with gynecologic malignancies using body diffusion-weighted magnetic resonance imaging. *J Comput Assist Tomogr* 2008;32:764-768
15. Bland JM, Altman DG. Statistical methods for assessing agreement between two methods of clinical measurement. *Lancet* 1986;1:307-310
16. Stejskal EO, Tanner JE. Spin diffusion measurements: spin echoes in the presence of a time-dependent field gradient. *J Chem Phys* 1965;42:288-292
17. Tofts PS, Lloyd D, Clark CA, et al. Test liquids for quantitative MRI measurements of self-diffusion coefficient in vivo. *Magn Reson Med* 2000;43:368-374





# Chapter 6<sup>2</sup>

## ADC measurements in the evaluation of lymph nodes in patients with non-Hodgkin lymphoma: feasibility study

Kwee TC, Ludwig I, Uiterwaal CS, Quarles van Ufford HME,  
Vermoolen MA, Fijnheer R, Bierings MB, Nievelstein RA

MAGMA 2011; 24:1-8

## Abstract

### Object

To determine whether apparent diffusion coefficient (ADC) measurements allow discrimination of normal lymph nodes from lymphomatous lymph nodes, and indolent lymphomas from aggressive lymphomas in patients with non-Hodgkin lymphoma (NHL).

### Materials and Methods

Eighteen healthy volunteers and thirty-two patients with newly diagnosed NHL (indolent: n=16; aggressive: n=16) underwent diffusion-weighted imaging. ADCs of normal lymph nodes were compared to those of lymphomatous lymph nodes, and ADCs of indolent lymphomas were compared to those of aggressive lymphomas. Receiver Operating Characteristic (ROC) analysis was performed when ADCs were significantly different between two of aforementioned groups.

### Results

ADCs (in  $10^{-3}$  mm<sup>2</sup>/s) of lymphomatous lymph nodes ( $0.70 \pm 0.22$ ) were significantly lower ( $P < 0.0001$ ) than those of normal lymph nodes ( $1.00 \pm 0.15$ ). Area under the ROC curve was 0.865. Sensitivity and specificity were 78.1% and 100% when using an optimal cut-off ADC value of 0.80. On the other hand, ADCs of indolent lymphomas ( $0.67 \pm 0.21$ ) were not significantly different ( $P = 0.2997$ ) from those of aggressive lymphomas ( $0.74 \pm 0.23$ ).

### Conclusion

ADC measurements show promise as a highly specific tool for discrimination of normal lymph nodes from lymphomatous lymph nodes, but appear to be of no utility in differentiating indolent from aggressive lymphomas.

## Introduction

Non-Hodgkin lymphomas (NHLs) comprise approximately 4% to 5% of all malignancies and are the fourth to fifth most frequently occurring type of cancer in the Western world [1]. In 2009, an estimated 65 980 new cases of NHL will be diagnosed in the United States [1]. Once a NHL has been diagnosed histologically, extent of disease has to be assessed, because this determines prognosis and treatment planning [2,3]. Recently, whole-body diffusion-weighted magnetic resonance (MR) imaging (DWI) was introduced as a new imaging modality for staging malignant lymphoma [4-6]. Both normal and lymphomatous lymph nodes exhibit high signal intensity at DWI [4-6]. Therefore, detection of lymphomatous lymph nodes at DWI still depends on size criteria which are regarded as imperfect [7]. On the other hand, DWI allows quantifying diffusion in lymph nodes by means of apparent diffusion coefficient (ADC) measurements, and this may aid in the characterization of lymph nodes. It is expected that malignant tissue, including metastatic lymph nodes, generally exhibits hypercellularity, increased nucleus-to-cytoplasm ratios, and an increased amount of macromolecular proteins [8], resulting in an decreased diffusion in the extra- and intracellular compartments (i.e. lower ADC) compared to normal lymph nodes [9]. Previous studies [10-15] have shown that ADCs of lymphomatous lymph nodes are generally lower than those of metastatic lymph nodes and benign lymphadenopathy. However, these studies [10-15] exclusively investigated pathologic lymph nodes with different histologies, and did not compare ADCs of lymphomatous lymph nodes to those of normal lymph nodes. Furthermore, although some studies [16-21] have shown that ADCs of metastatic lymph nodes are significantly different from those of normal lymph nodes, these studies did not include lymphomatous lymph nodes. Moreover, results of different studies are generally not comparable due to the use of different b-values, a different number of b-values, and different ADC measurement methods. Therefore, it is still unknown whether ADC measurements can be used for discriminating normal lymph nodes from lymphomatous lymph nodes in the staging work-up of patients with NHL.

Many subtypes of NHLs exist, but they can grossly be divided into a group of indolent lymphomas and a group of aggressive lymphomas [2,3,22]. Indolent lymphomas are characterized by slow growth, and are generally considered incurable, although median survival is relatively long. On the other hand, aggressive lymphomas are characterized by rapid growth, and can be treated curatively with relatively high survival rates [2,3]. If transformation from indolent to aggressive lymphoma (which eventually occurs in 40% of patients with an indolent lymphoma [2,3]) is clinically suspected, a biopsy should be performed for histological confirmation. However, the lymphomatous site that contains the tumor cells with the highest malignancy grade can be missed by biopsy, as a result of which multiple or repeated biopsies may sometimes be needed.

If DWI can predict which lymphomatous lesions contain the tumor cells with the highest malignancy grade, the number of biopsies and associated patient morbidity can be reduced. It can be hypothesized that differences in (sub)cellular structures between indolent and aggressive lymphomas may lead to different degrees of diffusivity. For example, grade I and II follicular lymphomas, which are the most common of the indolent lymphomas, consist of small- to intermediate-sized neoplastic cells that are closely packed [8] thus having a high cellular density. On the other hand, diffuse large b-cell lymphomas (which are the most common of the high-grade lymphomas) consist of larger neoplastic cells [8], which may correspond to a relatively lower cellular density. Since lesions with a higher cellularity are known to have a lower diffusivity than lesions with a lower cellularity [23-25], ADC measurements may also be of utility in predicting malignancy grade in patients with lymphoma.

The purposes of this study were to investigate whether ADC measurements allow discrimination of normal lymph nodes from lymphomatous lymph nodes, and indolent from aggressive lymphomas in patients with NHL.

## Materials and Methods

### Study participants

This study was approved by the institutional review board of the University Medical Center Utrecht. All participants were enrolled after they had been properly informed and provided written informed consent. Eighteen healthy adult volunteers (9 men and 9 women; mean age, 22.9 years; age range, 19-37 years) were prospectively included, in order to determine ADCs of normal lymph nodes. Exclusion criteria for this volunteer study were: previous surgery or malignancy, chronic or acute inflammation or infection, and current use of medicine. Furthermore, twenty-two consecutive patients with newly diagnosed NHL (21 men and 11 women; median age, 61.5 years; age range, 22-75 years; 16 indolent lymphomas, 16 aggressive lymphomas) were prospectively included, in order to determine ADCs of lymphomatous lymph nodes. All patients had undergone at least one excisional biopsy to histologically confirm the diagnosis of NHL. Biopsies had been examined by board-certified pathologists with expertise in lymphoma diagnosis, and NHLs had been classified as indolent or aggressive according to the recent WHO classification [22]. Characteristics of included patients are displayed in **Table 1**.

**Table 1.** Patient characteristics.

No.	Age (years)	Gender (M/F)	Lymphoma classification	Indolent/aggressive
1	29	M	Diffuse large B-cell lymphoma	Aggressive
2	67	M	Follicular lymphoma grade I-II	Indolent
3	60	M	Diffuse large B-cell lymphoma	Aggressive
4	61	F	Diffuse large B-cell lymphoma	Aggressive
5	44	F	Diffuse large B-cell lymphoma	Aggressive
6	64	F	Diffuse large B-cell lymphoma	Aggressive
7	58	M	Diffuse large B-cell lymphoma	Aggressive
8	62	F	Diffuse large B-cell lymphoma	Aggressive
9	56	M	Small lymphocytic lymphoma	Indolent
10	66	F	Follicular lymphoma grade I-II	Indolent
11	62	M	Diffuse large B-cell lymphoma	Aggressive
12	22	M	Anaplastic large cell lymphoma	Aggressive
13	59	M	Diffuse large B-cell lymphoma	Aggressive
14	74	M	Diffuse large B-cell lymphoma	Aggressive
15	47	M	Diffuse large B-cell lymphoma	Aggressive
16	58	M	Nodal marginal zone lymphoma	Indolent
17	47	M	Follicular lymphoma	Indolent
18	71	F	Lymphoplasmacytic lymphoma	Indolent
19	72	F	Nodal marginal zone lymphoma	Indolent
20	55	M	Follicular lymphoma grade I-II	Indolent
21	60	F	Diffuse large B-cell lymphoma	Aggressive
22	64	M	Follicular lymphoma grade I-II	Indolent
23	62	F	Extranodal marginal zone lymphoma	Indolent
24	68	M	Low-grade B-cell lymphoma	Indolent
25	75	M	Diffuse large B-cell lymphoma	Aggressive
26	54	M	Follicular lymphoma grade I-II	Indolent
27	47	M	Diffuse large B-cell lymphoma	Aggressive
28	71	M	Follicular lymphoma grade I-II	Indolent
29	72	F	Follicular lymphoma grade I-II	Indolent
30	54	M	Extranodal marginal zone lymphoma	Indolent
31	72	F	Angioimmunoblastic T-cell lymphoma	Aggressive
32	67	M	Follicular lymphoma grade I-II	Indolent

### MR imaging

MR imaging was performed using a 1.5-T system (Achieva, Philips Healthcare, Best, The Netherlands) with a 4-element phased-array surface coil for signal reception in all body regions. In the volunteers, axial diffusion-weighted images of the head/neck and pelvis were acquired. In the patients, axial diffusion-weighted images of the head/neck, chest, abdomen, and pelvis were obtained. Note that DWI of the chest and abdomen was not acquired in the volunteers, because, in our experience, normal lymph nodes in these regions are usually not depicted at DWI. Applied sequence parameters for

DWI were as follows: single-shot spin-echo echo-planar imaging, repetition time/echo time/inversion time of 8612/78/180 ms, slice thickness/gap of 4/0 mm, number of slices of 60, field of view of  $450 \times 360 \text{ mm}^2$ , acquisition matrix of  $128 \times 81$ , motion probing gradients in three orthogonal axes, b-values of 0 and  $1000 \text{ s/mm}^2$ , number of signal averages of 3, half scan factor of 0.651, parallel imaging (SENSitivity Encoding) factor of 2, echo train length of 43, acquired voxel size of  $3.52 \times 4.50 \times 4.00 \text{ mm}^3$ , reconstructed voxel size of  $1.76 \times 1.76 \times 4.00 \text{ mm}^3$ , image acquisition under free breathing, and scan time of 4 minutes and 4 s for each of the four stations. Of note, at a high b-value of  $1000 \text{ s/mm}^2$ , ADC measurements are relatively perfusion insensitive and theoretically more reflective of tissue cellularity and the integrity of cellular membranes [9]. Furthermore, a b-value of  $1000 \text{ s/mm}^2$  yields good background body signal suppression while highlighting lymphomatous lesions [4-6]. Axial trace ADC maps were created by signals obtained from images with the two b-values (0 and  $1000 \text{ s/mm}^2$ ). In all patients, axial CT images of the neck, chest, abdomen, and pelvis, and coronal T1-weighted and short inversion time inversion recovery (STIR) whole-body MR images were acquired in addition to axial DWI.

#### Image analysis

All MR images were transferred to a workstation (ViewForum; Philips Healthcare, Best, The Netherlands). One observer (R.A.J.N., with fourteen years of experience in MR imaging) reviewed the images of the volunteers, and another observer (T.C.K., with more than two years of experience in DWI) reviewed the images of the patients. Both observers knew that they were evaluating scans from either healthy subjects or patients with NHL. However, each observer was blinded to the results of the other observer. Furthermore, the second observer was blinded to the lymphoma type of the patients, other clinical and imaging information, and follow-up findings. In the volunteers, the largest normal lymph node was identified, and a region of interest (ROI) was placed in this lymph node on the image that was obtained at a b-value of  $1000 \text{ s/mm}^2$ . This ROI was placed on the slice containing the largest portion of the lymph node, in order to minimize partial volume averaging effects. Each ROI was variable so that it included as much of the nodal parenchyma as possible, but edges of the lymph node were not included. Accurate localisation of the ROI was checked on the image obtained at a b-value of  $0 \text{ s/mm}^2$ . The ROI was then copied and pasted onto the ADC map, and the mean ADC of the lymph node was automatically calculated. In the patients, lymph nodes were considered lymphomatous in case their short-axis diameter clearly exceeded 10 mm on CT, T1-weighted, and STIR whole-body MR images, as is common in the evaluation of malignant lymphoma [26]. Furthermore, the lymph nodes with a short-axis diameter larger than 10 mm also had to be positive at pretherapy  $^{18}\text{F}$ -fluoro-2-deoxy-D-glucose positron emission tomography (FDG-PET) or decrease in size on follow-up CT studies after therapy (minimum follow-up time of 6 months) if pretherapy FDG-PET was not performed. Decrease in size on follow-up CT studies was defined as an at least 50% decrease in the sum of the product of the

perpendicular diameters of the involved lymph node from baseline (**Figure 1**), which is partly in line with the recently revised response criteria for lymphoma [27]. In each patient, the largest lymphomatous lymph node was identified on the CT, T1-weighted, and STIR whole-body MR images, and its ADC was measured as described previously. When lymph nodes showed heterogeneous signal intensity on native ( $b=1000$  s/mm<sup>2</sup>) diffusion-weighted images, only the solid-appearing portions (i.e. high signal intensity)

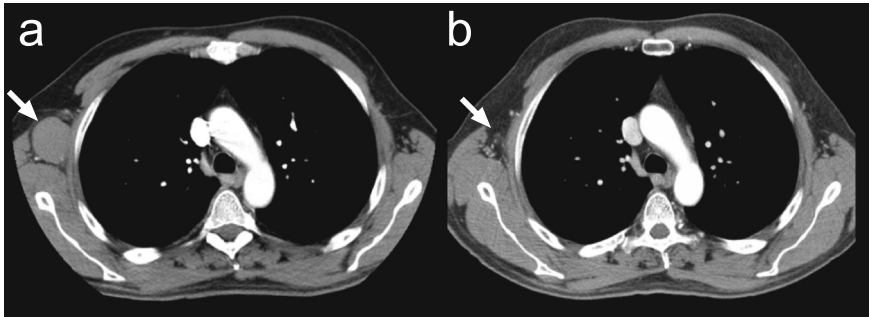


**Figure 1.** Baseline (pretherapy) CT (a) and 6-month posttherapy CT (b) in a 54-year-old male with follicular lymphoma. Baseline CT (a) shows a pathologically enlarged right axillary lymph node (3.5 cm × 3.5 cm) (arrow) that was selected for ADC analysis. At 6-month posttherapy CT (b), only small axillary lymph nodes with perpendicular diameters less than 1.0 cm are visible (arrow), which confirms that the right axillary lymph node at baseline CT was indeed lymphomatous.

were included in the ROI, while obvious necrotic components (i.e. low signal intensity) were excluded from the ROI. Of note, only the largest lymph node in each healthy volunteer and the largest lymphomatous lymph node in each patient were analyzed in order to avoid selection and clustering bias [28]. Selecting the largest lymph node in both populations also reduced inaccuracies in ADC measurements due to partial volume effects. Representative examples of ADC measurements are shown in **Figures 2 and 3**.

#### Statistical analysis

Kolmogorov-Smirnov tests were used to check whether ADCs of the different groups were normally distributed. ADCs of normal lymph nodes were compared to those of lymphomatous lymph nodes, and ADCs of indolent lymphomas were compared to those of aggressive lymphomas, using unpaired two-tailed *t* tests. In case the unpaired *t* tests revealed a significant difference in ADCs between two of the aforementioned groups, additional Receiver Operating Characteristic (ROC) analysis was performed to determine the area under the ROC curve and the optimal cut-off ADC value with corresponding sensitivity and specificity. *P* values less than 0.05 were considered to indicate a statistically significant difference. Statistical analyses were executed using MedCalc version 10.4.5.0 software (MedCalc, Mariakerke, Belgium).

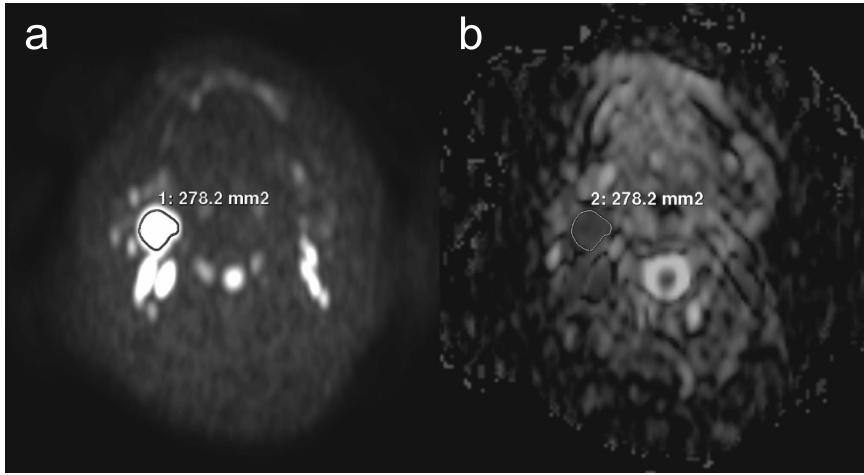


**Figure 2.** Example of an ADC measurement of a lymphomatous cervical lymph node in a 60-year-old female with diffuse large B-cell lymphoma. A freehand ROI was placed in the lymphomatous cervical lymph node, on the image obtained at a b-value of 1000 s/mm<sup>2</sup> (a). The ROI was then copied and pasted the ADC map, and the ADC of the lymphomatous lesion (in this case  $0.74 \times 10^{-3}$  mm<sup>2</sup>/s) was automatically calculated.

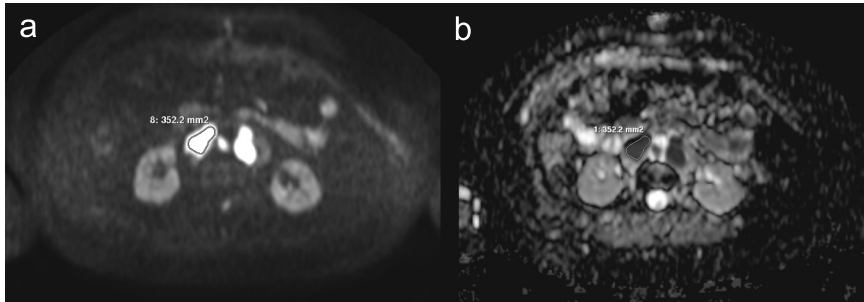


**Figure 3.** Example of an ADC measurement of a lymphomatous para-aortic lymph node in a 72-year-old female with nodal marginal zone lymphoma. A freehand ROI was placed in the lymphomatous para-aortic lymph node, on the image obtained at a b-value of 1000 s/mm<sup>2</sup> (a). The ROI was then copied and pasted onto the ADC map, and the ADC of the lymphomatous lesion (in this case  $0.51 \times 10^{-3}$  mm<sup>2</sup>/s) was automatically calculated.

## Results

All diffusion-weighted images were of diagnostic quality, without any disturbing (susceptibility or motion) artifacts (**Figures 2 and 3**). ROIs for ADC measurements of normal lymph nodes in the volunteers were placed in left cervical (n=6), right cervical (n=6), right axillary (n=1), left inguinal (n=1), and right inguinal (n=4) lymph nodes. Mean size of ROIs in the volunteers was 56 mm<sup>2</sup> (standard deviation, 19 mm<sup>2</sup>; range, 28–87 mm<sup>2</sup>). ROIs for ADC measurements of lymphomatous lymph nodes in the patients



were placed in left cervical (n=4), right cervical (n=2), left axillary (n=4), right axillary (n=6), paraaortic (n=8), mesenteric (n=2), left perirenal (n=1), left inguinal (n=2), and right inguinal (n=3) lymph nodes. Lymphomatous involvement of these lymph nodes was confirmed by pretherapy FDG-PET in 18 patients and by follow-up CT studies in 14 patients. Mean size of ROIs in the patients was 908 mm<sup>2</sup> (standard deviation, 1144 mm<sup>2</sup>; range, 120-4134 mm<sup>2</sup>). Kolmogorov-Smirnov tests confirmed that the ADCs of the different groups were normally distributed, justifying comparisons by means of unpaired *t* tests.

ADCs (in 10<sup>-3</sup> mm<sup>2</sup>/s) of lymphomatous lymph nodes (mean ± SD, 0.70 ± 0.22) were significantly lower (*P*<0.0001) than those of normal lymph nodes (mean ± SD, 1.00 ± 0.15). Box-and-whisker plots with ADCs according to nodal status (normal vs. lymphomatous) are shown in **Figure 4**. Area under the ROC curve was 0.865 (95% CI: 0.738-0.945). The ROC curve is displayed in **Figure 5**. Sensitivity was 78.1% (95% CI: 60.0-90.7%) and specificity was 100% (95% CI: 81.5-100%) when using an optimal cut-off ADC value of 0.80.

ADCs of indolent lymphomas (mean ± SD, 0.67 ± 0.21) were not significantly different (*P*=0.3691) from those of aggressive lymphomas (mean ± SD, 0.74 ± 0.23). Box-and-whisker plots with ADCs according to lymphoma type (indolent vs. aggressive) are shown in **Figure 6**.

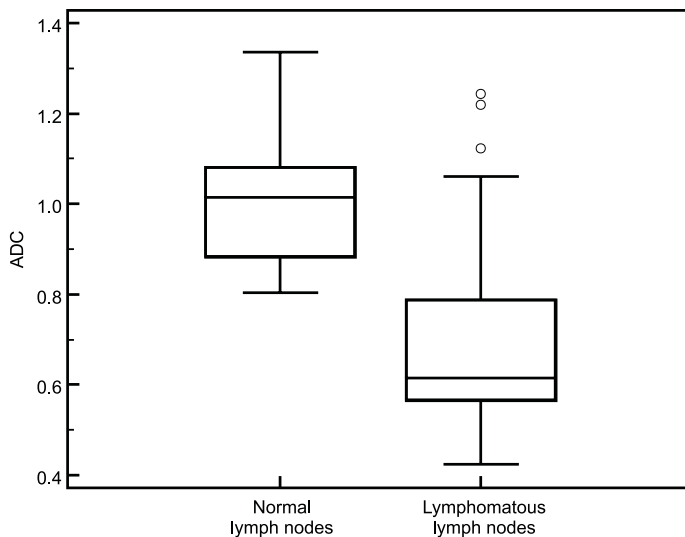


**Figure 4.** Box-and-whisker plots show median (middle line of box), quartiles (top and bottom lines of box), upper extreme value (upper whisker), lower extreme value (lower whisker), and outliers (circles) for ADCs (in 10<sup>-3</sup> mm<sup>2</sup>/s) according to nodal status (normal vs. lymphomatous). ADCs of lymphomatous lymph nodes (mean ± SD, 0.70 ± 0.22) were significantly lower (*P*=<0.0001) than those of normal lymph nodes (mean ± SD, 1.00 ± 0.15).

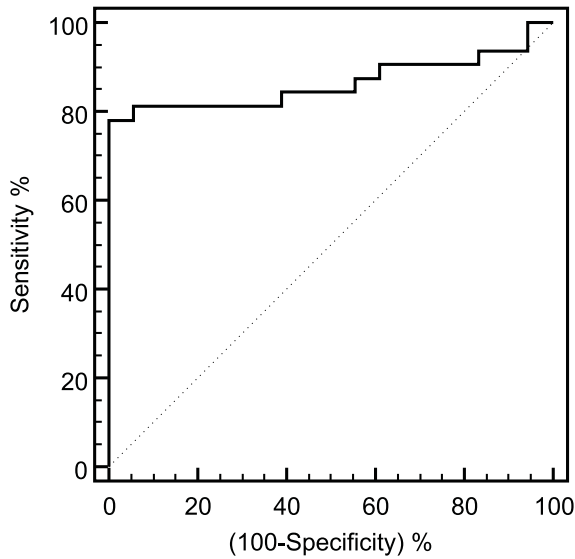


**Figure 5.** ROC curve for ADC measurements for the determination of nodal status (normal vs. lymphomatous). Area under the ROC curve was 0.865 (95% CI: 0.738-0.945).

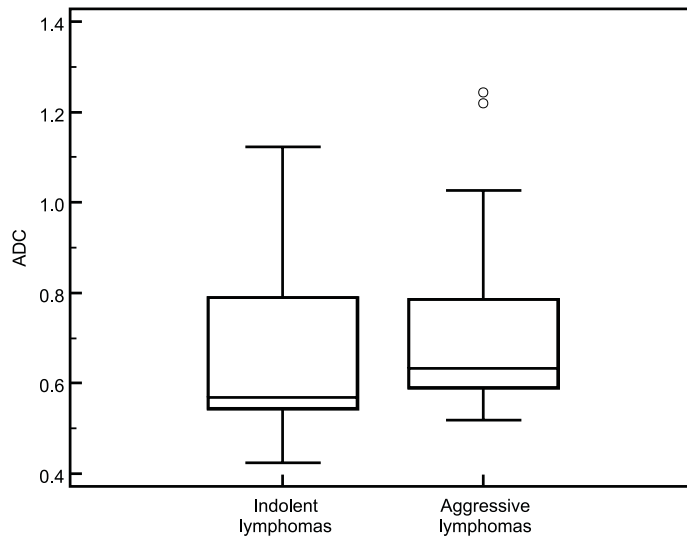


**Figure 6.** Box-and-whisker plots show median (middle line of box), quartiles (top and bottom lines of box), upper extreme value (upper whisker), lower extreme value (lower whisker), and outliers (circles) for ADCs (in  $10^{-3} \text{ mm}^2/\text{s}$ ) according to lymphoma type (indolent vs. aggressive). ADCs of indolent lymphomas (mean  $\pm$  SD,  $0.67 \pm 0.21$ ) were not significantly different ( $P=0.2997$ ) from those of aggressive lymphomas (mean  $\pm$  SD,  $0.74 \pm 0.23$ ).

## Discussion

Accurate assessment of spread of nodal disease in patients with NHL is important for determining prognosis and treatment planning [2,3]. The relatively recent development of whole-body DWI [29,30] made it a feasible technique for staging NHL [4-6]. DWI not only allows visualizing anatomic abnormalities, but it also provides functional information in that it allows quantification of the random motion of water molecules (i.e. diffusion) by means of ADC measurements [31]. The ADC may provide a reflection of anatomical and functional cellular characteristics. For example, the ADC has shown to be inversely correlated to the tissue cellularity and the integrity of cell membranes [23-25]. As such, it may aid in the characterization of lesions [9], including the assessment of lymph nodes in patients with NHL. Previous studies in patients presenting with cervical lymphadenopathy have reported ADCs (in  $10^{-3}$  mm<sup>2</sup>/s) of lymphomatous lymph nodes of  $0.223 \pm 0.056$  [10],  $0.449 \pm 0.096$  (without nodal necrosis) [11],  $0.601 \pm 0.427$  [12],  $0.64 \pm 0.09$  [15],  $0.664 \pm 0.071$  [14],  $0.97 \pm 0.27$  [13], and  $1.091 \pm 0.405$  (with nodal necrosis) [11]. Note that reported ADCs of lymphomatous lymph nodes vary widely, which can be explained by different ways of ADC measurements (e.g. measurement of the entire lymph node will result in a higher ADC than in a measurement in which necrotic regions are excluded) and the use of different b-values. Nevertheless, all previous studies [10-15] reported that ADCs of lymphomatous lymph nodes are generally lower than those of metastatic lymph nodes and benign lymphadenopathy. However, the utility of ADC measurements in the assessment of lymph nodes in the staging work-up of patients with NHL was still unknown, because previous studies only investigated whether ADC measurements allow histological differentiation of pathologic lymph nodes rather than assessing whether they can discriminate normal from lymphomatous lymph nodes. Interestingly, ADC measurements may also be used as a noninvasive predictor of malignancy grade. Several studies have shown that ADC measurements may aid in grading brain tumors [23,24,32-36], with high-grade brain tumors having a lower ADC than low-grade brain tumors, probably due to higher cellularity of the former. However, the value of ADC measurements in grading NHLs was still unknown.

In the present study, ADCs (in  $10^{-3}$  mm<sup>2</sup>/s) of lymphomatous lymph nodes in patients with NHL ( $0.70 \pm 0.22$ ) were significantly lower than those of normal lymph nodes in healthy volunteers ( $1.00 \pm 0.15$ ). Furthermore, ROC analysis showed that a sensitivity of 78.1% (95% CI: 60.0-90.7%) and a specificity of 100% (95% CI: 81.5-100%) can be achieved when using an optimal cut-off ADC value of 0.80. This may suggest that a lymph node with an ADC lower than 0.80 in a patient with NHL is very probably lymphomatous. This finding can be explained by the fact that most lymphoma types mostly consist of densely packed cellular tissue with very little extracellular space [8], which considerably impedes the diffusivity of water molecules. On the other hand,

our results indicate that ADC measurements in DWI do not allow discrimination of indolent from aggressive lymphomas, given the nonsignificant difference in ADCs between both groups. A possible explanation for this finding may be that cellular density of indolent lymphomas is not too different from that of aggressive lymphomas. This study had several limitations. First, because of the insensitivity of size criteria to diagnose lymphomatous involvement of normal-sized lymph nodes [7] and the practical and ethical impossibility to obtain additional biopsies in the patients with NHL, only enlarged lymphomatous lymph nodes could be evaluated. In addition, a group of healthy volunteers had to be included to determine the ADC of normal lymph nodes. Although the volunteers were considerably younger than the patients, there is no reason to assume why (ADCs of) lymph nodes in a young population would differ from those in an older population [8]. Furthermore, the same imaging protocol and the same ADC measurement method were applied in both the healthy volunteers and the patients. Second, the site of ADC measurement did not correspond to the site of the initial biopsy in any of the patients. This is because imaging for staging takes place after the diagnosis NHL has been established by means of excisional biopsy. Obtaining additional biopsies of the lymphomatous lymph nodes that were used for ADC analysis would be most desirable, but was simply impossible due to aforementioned reasons. Nevertheless, accepted diagnostic criteria for nodal involvement in NHL [26] were used and pretherapy FDG-PET or follow-up CT studies were reviewed to confirm that the lymph nodes of the patients that were analyzed were indeed lymphomatous. Furthermore, although we cannot exclude the coexistence of aggressive disease in patients with newly diagnosed indolent lymphoma, this probability is very low, because high-grade transformation typically occurs only months to years after initial diagnosis [37-39]. In addition, none of the patients with indolent lymphoma had clinical features (e.g. considerably elevated lactate dehydrogenase or rapid lymphoma growth) that would suggest high-grade transformation. Third, lymph nodes in the healthy volunteers that were selected for ADC measurements did not match to those of the patients with respect to location and size, but this limitation was inherent to the chosen study design. Fourth, the degree of confidence that can be ascribed to measuring ADCs of normal-sized lymph nodes in healthy volunteers is uncertain. Fifth, only two b-values (0 and 1000 s/mm<sup>2</sup>) were used for ADC calculation. It may have been desirable to acquire more b-values in order to obtain more accurate ADCs [9]. However, this would considerably prolong scan time. It should also be mentioned that the use of different MR parameters (in particular the number of b-values) and different methods of ROI analysis (e.g. inclusion of necrotic areas) may have resulted in different ADCs, which limits the general applicability of the ADC threshold that was obtained in the present study. Despite these study limitations, the present results indicate that ADC measurements may be used as an additional tool in the assessment of lymph nodes (e.g. in case of borderline lymph node enlargement at anatomical imaging) in the staging work-up of patients with NHL.

## Conclusion

In conclusion, our results suggest that ADC measurements show promise as a highly specific tool for discrimination of normal lymph nodes from lymphomatous lymph nodes in patients with NHL. However, ADC measurements appear to be of no utility in differentiating indolent from aggressive lymphomas.

## Acknowledgement

This study was supported by ZonMw Program for Health Care Efficiency Research (grant number 80-82310-98-08012).

## References

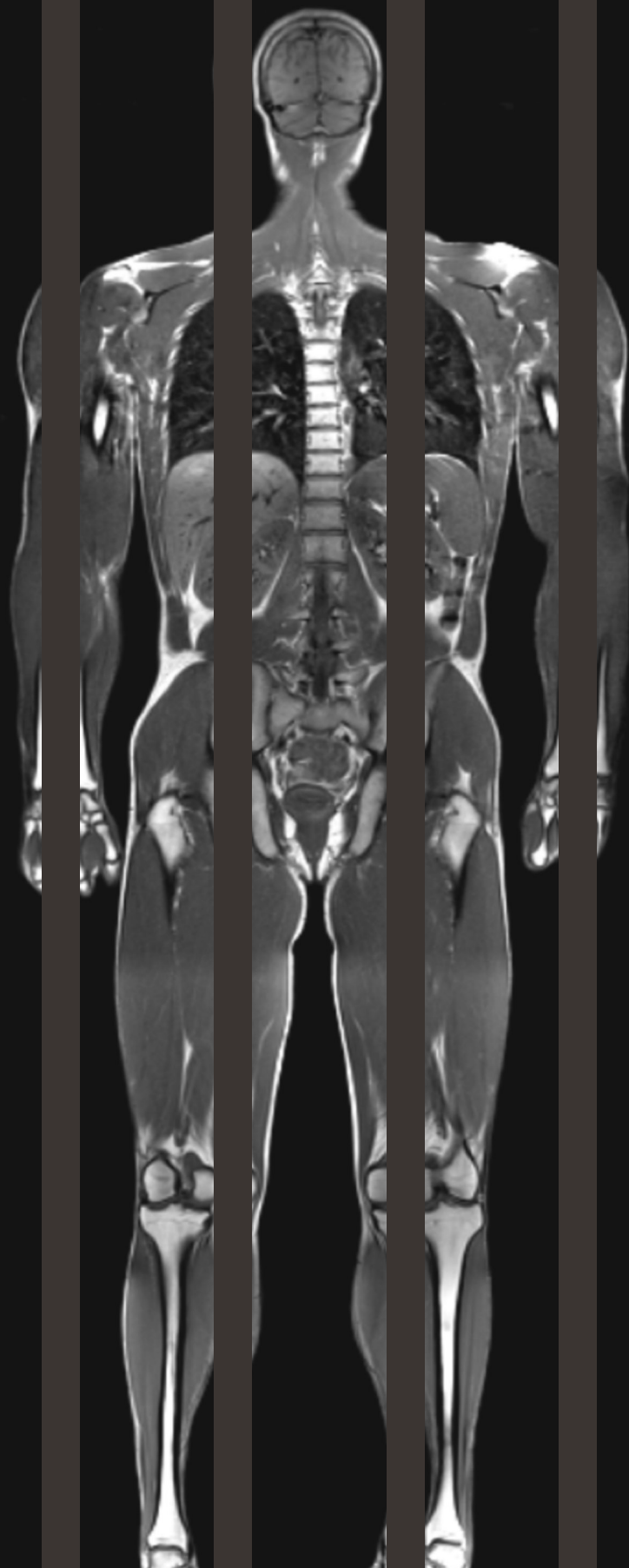
1. Jemal A, Siegel R, Ward E, Hao Y, Xu J, Thun MJ. Cancer Statistics, 2009. *CA Cancer J Clin* 2009;59:225-249
2. Ansell SM, Armitage J. Non-Hodgkin lymphoma: diagnosis and treatment. *Mayo Clin Proc* 2005;80:1087-1097
3. Evans LS, Hancock BW. Non-Hodgkin lymphoma. *Lancet* 2003;362:139-146
4. Kwee TC, van Ufford HM, Beek FJ, et al. Whole-Body MRI, Including Diffusion-Weighted Imaging, for the Initial Staging of Malignant Lymphoma: Comparison to Computed Tomography. *Invest Radiol* 2009;44:683-690
5. Li S, Xue HD, Li J, et al. Application of whole body diffusion weighted MR imaging for diagnosis and staging of malignant lymphoma. *Chin Med Sci J* 2008;23:138-144
6. Lin C, Luciani A, Itti E, et al. Whole-body diffusion-weighted magnetic resonance imaging with apparent diffusion coefficient mapping for staging patients with diffuse large B-cell lymphoma. *Eur Radiol* 2010;20:2027-2038
7. Torabi M, Aquino SL, Harisinghani MG. Current concepts in lymph node imaging. *J Nucl Med* 2004;45:1509-1518
8. Ioachim HL, Medeiros LJ. *Ioachim's Lymph Node Pathology*. Philadelphia, PA: Lippincott Williams and Wilkins, 2008
9. Padhani AR, Liu G, Koh DM, et al. Diffusion-weighted magnetic resonance imaging as a cancer biomarker: consensus and recommendations. *Neoplasia* 2009;11:102-125
10. Sumi M, Van Cauteren M, Nakamura T. MR microimaging of benign and malignant nodes in the neck. *AJR Am J Roentgenol* 2006;186:749-757
11. Sumi M, Nakamura T. Diagnostic importance of focal defects in the apparent diffusion coefficient-based differentiation between lymphoma and squamous cell carcinoma nodes in the neck. *Eur Radiol* 2009;19:975-981
12. Sumi M, Sakihama N, Sumi T, et al. Discrimination of metastatic cervical lymph nodes with diffusion-weighted MR imaging in patients with head and neck cancer. *AJNR Am J Neuroradiol* 2003;24:1627-1634
13. Abdel Razek AA, Soliman NY, Elkhamary S, Alsharaway MK, Tawfik A. Role of diffusion-weighted MR imaging in cervical lymphadenopathy. *Eur Radiol* 2006;16:1468-1477
14. King AD, Ahuja AT, Yeung DK, et al. Malignant cervical lymphadenopathy: diagnostic accuracy of diffusion-weighted MR imaging. *Radiology* 2007;245:806-881
15. Holzapfel K, Duetsch S, Fauser C, Eiber M, Rummeny EJ, Gaa J. Value of diffusion-weighted MR imaging in the differentiation between benign and malignant cervical lymph nodes. *Eur J Radiol* 2009;72:381-387
16. Kim JK, Kim KA, Park BW, Kim N, Cho KS. Feasibility of diffusion-weighted imaging in the differentiation of metastatic from nonmetastatic lymph nodes: early experience. *J Magn Reson Imaging* 2008;28:714-719
17. Vandecaveye V, De Keyzer F, Vander Poorten V, et al. Head and neck squamous cell carcinoma: value of diffusion-weighted MR imaging for nodal staging. *Radiology* 2009;251:134-146
18. Sakurada A, Takahara T, Kwee TC, et al. Diagnostic performance of diffusion-weighted magnetic resonance imaging in esophageal cancer. *Eur Radiol* 2009;19:1461-1469

19. Park SO, Kim JK, Kim KA, et al. Relative apparent diffusion coefficient: determination of reference site and validation of benefit for detecting metastatic lymph nodes in uterine cervical cancer. *J Magn Reson Imaging* 2009;29:383-390
20. Yasui O, Sato M, Kamada A. Diffusion-weighted imaging in the detection of lymph node metastasis in colorectal cancer. *Tohoku J Exp Med* 2009;218:177-183
21. De Bondt RB, Hoeberigs MC, Nelemans PJ, et al. Diagnostic accuracy and additional value of diffusion-weighted imaging for discrimination of malignant cervical lymph nodes in head and neck squamous cell carcinoma. *Neuroradiology* 2009;51:183-192
22. Swerdlow SH, Campo E, Harris NL, et al. WHO Classification of Tumours of Haematopoietic and Lymphoid Tissues (4th ed.). Lyon, France: International Agency for Research on Cancer, 2008
23. Hayashida Y, Hirai T, Morishita S, et al. Diffusion-weighted imaging of metastatic brain tumors: comparison with histologic type and tumor cellularity. *AJNR Am J Neuroradiol* 2006;27:1419-1425
24. Sugahara T, Korogi Y, Kochi M, et al. Usefulness of diffusion-weighted MRI with echo-planar technique in the evaluation of cellularity in gliomas. *J Magn Reson Imaging* 1999;9:53-60
25. Schnapauff D, Zeile M, Niederrhagen MB, et al. Diffusion-weighted echo-planar magnetic resonance imaging for the assessment of tumor cellularity in patients with soft-tissue sarcomas. *J Magn Reson Imaging* 2009;29:1355-1359
26. Tatsumi M, Cohade C, Nakamoto Y, Fishman EK, Wahl RL. Direct comparison of FDG PET and CT findings in patients with lymphoma: initial experience. *Radiology* 2005;237:1038-1045
27. Cheson BD, Pfistner B, Juweid ME, et al; International Harmonization Project on Lymphoma. Revised response criteria for malignant lymphoma. *J Clin Oncol* 2007;25:579-586
28. Sica GT. Bias in research studies. *Radiology* 2006;238:780-789
29. Takahara T, Imai Y, Yamashita T, Yasuda S, Nasu S, Van Cauteren M. Diffusion weighted whole body imaging with background body signal suppression (DWIBS): technical improvement using free breathing, STIR and high resolution 3D display. *Radiat Med* 2004;22:275-282
30. Kwee TC, Takahara T, Ochiai R, Nievelstein RA, Luijten PR. Diffusion-weighted whole-body imaging with background body signal suppression (DWIBS): features and potential applications in oncology. *Eur Radiol* 2008;18:1937-1952
31. Le Bihan D, Breton E, Lallemand D, Aubin ML, Vignaud J, Laval-Jeantet M. Separation of diffusion and perfusion in intravoxel incoherent motion MR imaging. *Radiology* 1988;168:497-505
32. Murakami R, Hirai T, Sugahara T, et al. Grading astrocytic tumors by using apparent diffusion coefficient parameters: superiority of a one- versus two-parameter pilot method. *Radiology* 2009;251:838-845
33. Arvinda HR, Kesavadas C, Sarma PS, et al. Glioma grading: sensitivity, specificity, positive and negative predictive values of diffusion and perfusion imaging. *J Neurooncol* 2009;94:87-96
34. Lee EJ, Lee SK, Agid R, Bae JM, Keller A, Terbrugge K. Preoperative grading of presumptive low-grade astrocytomas on MR imaging: diagnostic value of minimum apparent diffusion coefficient. *AJNR Am J Neuroradiol* 2008;29:1872-1877
35. Higano S, Yun X, Kumabe T, et al. Malignant astrocytic tumors: clinical importance of apparent diffusion coefficient in prediction of grade and prognosis. *Radiology* 2006;241:839-846

36. Bulakbasi N, Guvenc I, Onguru O, Erdogan E, Tayfun C, Ucoz T. The added value of the apparent diffusion coefficient calculation to magnetic resonance imaging in the differentiation and grading of malignant brain tumors. *J Comput Assist Tomogr* 2004;28:735-746
37. Bastion Y, Sebban C, Berger F, et al. Incidence, predictive factors, and outcome of lymphoma transformation in follicular lymphoma patients. *J Clin Oncol* 1997;15:1587-1594
38. O'Brien ME, Easterbrook P, Powell J, et al. The natural history of low grade non-Hodgkin's lymphoma and the impact of a no initial treatment policy on survival. *Q J Med* 1991;80:651-660
39. Horning SJ, Rosenberg SA. The natural history of initially untreated low-grade non-Hodgkin's lymphomas. *N Engl J Med* 1984;311:1471-1475







# Chapter 7<sup>1</sup>

## MRI for the detection of bone marrow involvement in malignant lymphoma

Kwee TC, Kwee RM, Verdonck LF, Bierings MB, Nijelstein RA

Br J Haematol 2008;141:60-68

## Summary

The aim of this study was to systematically review published data on the sensitivity of magnetic resonance imaging (MRI) compared with bone marrow biopsy as reference standard for the detection of bone marrow involvement in patients with malignant lymphoma. A systematic search for relevant studies was performed of the PubMed/MEDLINE and Embase databases. Two reviewers independently assessed the methodological quality of each study. Sensitivity of included studies was calculated. The eleven included studies had moderate methodological quality. Sensitivity of MRI for the detection of bone marrow involvement ranged from 50% to 100%, with a median of 100%. MRI is likely sufficiently sensitive to rule out bone marrow involvement in patients with malignant lymphoma. However, a well-designed study with a large sample size is needed to confirm current results.

## Introduction

The malignant lymphomas, Hodgkin's disease (HD) and non-Hodgkin's lymphoma (NHL), comprise approximately 3.5% of all malignancies worldwide. Annually, an estimated 62,000 new cases of HD and 287,000 new cases of NHL are diagnosed worldwide [1]).

Accurate assessment of the bone marrow is of great importance in staging of malignant lymphoma; bone marrow involvement, which is found in 5-15% of patients with HD and in 20-40% of patients with NHL [2-5], by definition indicates stage IV disease. This may have both therapeutic and prognostic implications [6, 7].

Blind bone marrow biopsy (BMB), usually unilateral, is the standard method to evaluate the bone marrow [8]. However, BMB is an invasive and painful procedure, and has a small but non-negligible risk of complications (mainly hemorrhagic) [9]. In addition, focal bone marrow involvement may be missed by BMB; previous studies showed that in patients with unilaterally proven bone marrow infiltration, contralateral BMB of the iliac crest was negative in 10-60 % [2-5]. It has also been reported that in 33% of paired ipsilateral BMBs of the iliac crest, only one specimen was positive for bone marrow infiltration [4]. Because of the disadvantages of BMB, identification of patients who have minimal risk of bone marrow involvement and in whom BMB may be avoided, would be desirable.

Magnetic resonance imaging (MRI) is a radiation-free, non-invasive imaging modality, which provides visualization of the bone marrow at high spatial resolution [10, 11]. MRI may be used to rule out bone marrow involvement, provided that its sensitivity (i.e. the proportion of patients with bone marrow involvement that MRI is able to detect) is sufficiently high. Furthermore, in patients in whom bone marrow infiltration is suspected on MRI, MRI can be used to guide BMB, thereby reducing the number of sampling errors (**Figure 1**).

The purpose of this study was therefore to systematically review the contemporary literature on the sensitivity of MRI (on a per-patient basis) with BMB as the standard of reference for the detection of bone marrow involvement in patients with malignant lymphoma.

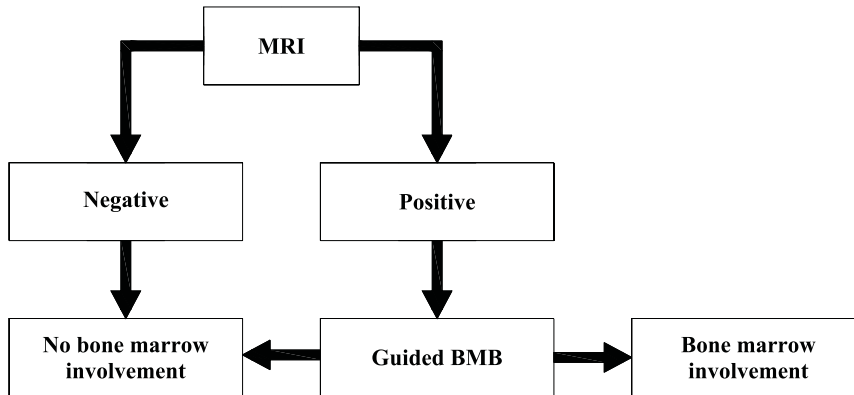


**Figure 1.** Potential role of MRI in the diagnostic work-up of bone marrow assessment in patients with malignant lymphoma, provided that its sensitivity is sufficiently high.

## Methods

### Data sources

A computer-aided search of the PubMed/MEDLINE and Embase databases was conducted to find published articles on the sensitivity of MRI for the detection of bone marrow involvement in patients with malignant lymphoma, in which BMB was used as the standard of reference. The search strategy is presented in **Table 1**. No beginning date limit was used. The search was updated until 13 September 2007. To expand our search, bibliographies of articles which finally remained after the selection process were screened for potentially suitable references.

**Table 1.** Search strategy and results as on 13 September 2007.

#	Search string	PubMed/Medline	Embase
1	Bone marrow	159,628	153,885
2	Magnetic resonance OR MR imaging OR MRI OR Magnetic resonance tomography OR Nuclear magnetic resonance OR NMR	354,270	346,966
3	Hodgkin OR Lymphoma	171,250	115,570
4	#1 AND #2 AND #3	410	446

### Study selection

In the first stage, two researchers (T.C.K., R.M.K.) independently reviewed the titles and abstracts of the retrieved articles. Studies not comparing MRI with BMB as reference standard for the detection of bone marrow involvement in patients with malignant lymphoma, studies performed in animals, review articles, meta-analyses, abstracts, editorials or letters, case reports, studies involving ten or fewer patients, tutorials, and guidelines for management were excluded. Studies using low field MRI scanners (<0.5 T) were also excluded, because image quality is inferior compared with higher field scanners ( $\geq 0.5$  T). No language restriction was applied. Articles were rejected if they were clearly ineligible.

In the second stage, the same researchers (T.C.K., R.M.K.) independently evaluated the full-text version of all articles that were found to be potentially eligible for inclusion, using the same inclusion and exclusion criteria as mentioned above. At all stages, disagreements between the two researchers (T.C.K., R.M.K.) were discussed and resolved by consensus.

### Study analysis

For each study, the methodological quality was assessed by using the Quality Assessment of Studies of Diagnostic Accuracy Included in Systematic Reviews (QUADAS) criteria, which is a 14-item instrument [12, 13]. The item "Was the reference standard independent of the index test (i.e. the index test did not form part of the reference standard)?" did not apply and was thus removed from the standard QUADAS list. Two items were added to the standard QUADAS list: "Was comparator review bias avoided?" and "Was the reproducibility (interobserver variability) of MRI described?" The complete list of quality items is presented in **Table 2**. For each item, two researchers (T.C.K., R.M.K.) independently assessed whether it was fulfilled (yes or no). If it was unclear from the information provided in an article as to whether an item was fulfilled, the item was rated as "unclear". Both "no" and "unclear" responses were interpreted as indicating that the quality criterion was not met. Disagreements were discussed and resolved by consensus. Total quality score was expressed as a percentage of the maximum score of 15.

Sensitivity of MRI for the detection of bone marrow involvement on a per-patient basis, with corresponding 95% CIs, were calculated from the original numbers given in the included studies. The number of indeterminate/intermediate results per study was extracted. A forest plot was constructed to display the results.

**Table 2.** Criteria list used to assess the methodological quality of the studies.

Quality item	Positive score
Was the spectrum of patients representative of the patients who will receive the test in practice?	Patient selection was not based on age, gender, or clinical stage (as derived from method of recruitment or characteristics of those included)
Were selection criteria clearly described?	It was clear how patients were selected for inclusion
Is the reference standard likely to correctly classify the target condition?	BMB (either unilateral or bilateral) applied as standard of reference
Is the time period between reference standard and index test short enough to be reasonably sure that the target condition did not change between the two tests?	Time interval between MRI and BMB $\leq 7$ days
Did the whole sample or a random selection of the sample, receive verification using a reference standard of diagnosis?	All patients, or a random sample of patients who underwent MRI, also underwent BMB
Did patients receive the same reference standard regardless of the index test result?	All patients underwent BMB regardless of MRI findings
Was the execution of the index test described in sufficient detail to permit replication of the test?	1) All of the following MRI parameters described: field strength, coil type, TR, TE, FOV, matrix size, section thickness, slice orientation, imaged region of interest 2) Interpreter of MRI mentioned
Was the execution of the reference standard described in sufficient detail to permit replication?	1) Site(s) of BMB mentioned 2) Interpreter of BMB mentioned
Were the index test results interpreted without knowledge of the results of the reference standard?	MRI was interpreted without knowledge of the BMB findings
Were the reference standard results interpreted without knowledge of the results of the index test?	BMB was interpreted without knowledge of the MRI findings
Were uninterpretable / intermediate test results reported?	All MRI results, including uninterpretable/ indeterminate/intermediate were reported
Were withdrawals from the study explained?	It is clear what happened to all patients who entered the study
Were the same clinical data available when test results were interpreted as would be available when the test is used in practice?	Clinical data were available when MRI was interpreted
Was comparator review bias avoided?	Blinding MRI to the other imaging modality, if another imaging modality (e.g. FDG-PET or FDG-PET/CT) was simultaneously investigated
Was the reproducibility (interobserver) of MRI described?	MRI was assessed independently by two or more observers, and interobserver agreement was calculated

BMB: bone marrow biopsy; CT: computed tomography; FDG-PET:  $^{18}\text{F}$ -fluoro-2-deoxyglucose positron emission tomography; MRI: magnetic resonance imaging; TR: repetition time; TE: echo time; FOV: field of view



## Results

### Literature search

The computer-aided search revealed 410 articles from PubMed/MEDLINE and 446 articles from Embase (**Table 1**). Reviewing titles and abstracts from PubMed/MEDLINE revealed 25 articles potentially eligible for inclusion. Reviewing titles and abstracts from Embase revealed 25 articles potentially eligible for inclusion, of which 23 were already identified by the PubMed/MEDLINE search. Thus, 27 studies [14-40] remained for possible inclusion and were retrieved in full text version. Screening of the references of these 27 articles did not bring up new articles. After reviewing the full article, five studies were excluded because the same data were used in later studies [17, 21-23, 28] Four studies were excluded because they did not supply sufficient information to calculate sensitivity [16, 20, 30, 40]. Four studies were excluded because the imaged region of interest did not correspond to the site of BMB [31, 34, 37, 38]. Two studies were excluded because MRI was performed at <0.5 T [24, 33]. One study was excluded because it used bone marrow aspiration as the standard of reference [36]. Eleven studies were finally included (**Table 3**). The total number of patients in a study ranged from 23 to 107 (median, 34 patients). The reported age ranged from 11 to 86 years, and the proportion of male patients ranged from 43% to 88%.

### Methodological quality assessment

For each of the 11 included studies, 15 methodological quality items were assessed (**Table 4**). The total quality score, expressed as a fraction of the maximum score, ranged from 40% to 73%, with a median of 60%. All studies were assigned a positive score for inclusion of the correct spectrum of patients (quality item 1). Most studies (91%) avoided verification bias (quality items 5 and 6) and the majority of studies (82%) avoided comparator review bias (quality item 14). However, most studies (82%) did not clearly describe how patients were selected for inclusion (quality item 2). In eight studies (73%), the time between MRI and BMB (possibly) exceeded 7 days (quality item 4). The majority of studies did not sufficiently describe how MRI and BMB were performed (55% and 73%, quality items 7 and 8, respectively). Ten studies did not explicitly mention whether BMB was interpreted without knowledge of the MRI findings (quality item 10). None of the studies explicitly mentioned whether clinical data were available when MRI was interpreted (quality item 13), and none of the studies described the interobserver reproducibility of MRI (quality item 15).

Table 3. Characteristics of the 11 included studies.

Study and year	No. of patients	Mean or median age in years (range)	Sex (M/F)	HD / NHL	Initial staging / restaging	Field strength (T)	Coil	Sequence, plane(s)	Imaged region of interest	Interpreter(s) MRI
Ribrag <i>et al.</i> , 2007	47	50 (24-75)	23/24	NHL	Initial staging	1.5	Body	-T1, C -STIR, C	Whole-body	Two radiologists
Brennan <i>et al.</i> , 2005	23	NR (22-75)	13/10	Both	Both	1.5	Body	-STIR, A+C	Whole-body	Two radiologists
Al-Mulhim, 2005	30	NR (18-45)	18/12	NHL	Initial staging	1.5	NR	-T1, C -STIR, C -T2, C	Pelvis and both femurs	NR
Iizuka-Mikami <i>et al.</i> , 2004	34	62.4 (NR)	22/12	NHL	NR	1.5	Body	-T1, C -STIR, C	From head to thigh	Two MRI specialists
Yasumoto <i>et al.</i> , 2002	53	55.6 (11-86)	33/20	Both	NR	1.5	Body phased-array	-T1, A -T2 fs, A -STIR, A -DW fs, A	Iliac crests	Two radiologists
Althoefer <i>et al.</i> , 1997	32	47 (17-79)	17/15	Both	NR	1.0	NR	-T1, C/S -T2, C/S	From the thoracic vertebra to the femoral heads	Two radiologists
Tardivon <i>et al.</i> , 1995	40	32 (15-58)	32/8	Both	Both	1.5	NR	-T1, with or without T2 or T2*, C/S	Dorsolumbar spine, pelvis, and both proximal femurs	Senior radiologist
Kauczor <i>et al.</i> , 1993	30	35.8 (18-67)	13/17	HD	Both	1.5	Body	-T1, C+S	From the third lumbar vertebra to the proximal femur	Three observers
Assoun <i>et al.</i> , 1993	43	43 (18-82)	22/21	Both	Initial staging	0.5	NR	-T1, C/S	Lumbar spine, pelvis, and proximal femurs	Two observers
Knauf <i>et al.</i> , 1991	27	50.3 (23-68)	NR	NHL	NR	1.5	NR	-T1, NR	Lumbar spine, pelvis, and proximal femurs	NR
Linden <i>et al.</i> , 1989	107	49 (13-83)	NR	Both	Both	1.5	NR	-T1, C	Lumbar spine, pelvis, and both femurs	NR

A: axial; C: coronal; S: sagittal; DW: diffusion-weighted; Fs: fat saturation (frequency-selective); HD: Hodgkin's disease; NHL: non-Hodgkin's lymphoma; NR: not reported; STIR: short tau inversion recovery; T1: T1-weighted; T2: T2-weighted; T2\*: T2\*-weighted

Table 4. Quality assessment of the 11 included studies.

Study and year	Quality items											% of maximum score				
	1	2	3	4	5	6	7	8	9	10	11		12	13	14	15
Ribrag <i>et al</i> , 2007	+	+	+	+	+	+	+	-	+	-	+	+	-	+	-	73
Brennan <i>et al</i> , 2005	+	-	+	-	-	-	+	-	-	-	+	+	-	+	-	40
Al-Mulhim, 2005	+	-	+	-	+	+	-	-	-	-	+	+	-	+	-	47
Iizuka-Wikami <i>et al</i> , 2004	+	-	+	+	+	+	+	+	+	-	+	+	-	-	-	67
Yasumoto <i>et al</i> , 2002	+	-	+	+	+	+	+	-	+	-	+	+	-	+	-	67
Althoefer <i>et al</i> , 1997	+	+	+	-	+	+	-	+	+	+	+	+	-	+	-	73
Tardivon <i>et al</i> , 1995	+	-	+	-	+	+	-	+	+	-	+	+	-	+	-	60
Kauczor <i>et al</i> , 1993	+	-	+	-	+	+	+	-	+	-	+	+	-	+	-	60
Assoun <i>et al</i> , 1993	+	-	+	-	+	+	-	-	+	-	+	+	-	+	-	53
Knauf <i>et al</i> , 1991	+	-	+	-	+	+	-	-	-	-	+	+	-	+	-	47
Linden <i>et al</i> , 1989	+	-	+	-	+	+	-	-	-	-	+	+	-	-	-	40

+ Quality item fulfilled; - Quality item not fulfilled or unclear

## Sensitivity of MRI

The results of the 11 included studies are presented in **Figure 2**. Sensitivity of MRI for the detection of bone marrow involvement ranged from 50.0% to 100%, with a median of 100%. None of the studies reported indeterminate/intermediate results.

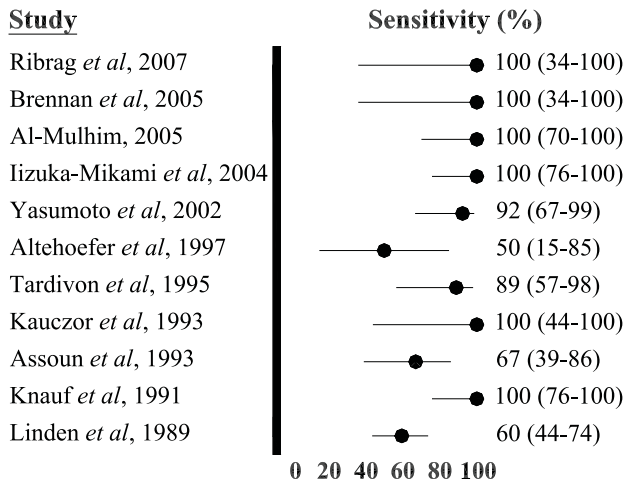


**Figure 2.** Sensitivities of the 11 included studies investigating MRI for the detection of bone marrow involvement in malignant lymphoma.

## Discussion

This systematic review included 11 studies investigating the sensitivity of MRI for the detection of bone marrow involvement in patients with malignant lymphoma. The reported estimates of sensitivity vary among the included studies. Six of the included studies had excellent results, with sensitivities of 100% [14, 19, 25-27, 32]. Two other studies reported high sensitivities of around 90%. The studies of Althoefer *et al.* [15], Assoun *et al.* [18], and Linden *et al.* [29], however, were outliers with sensitivities of 50%, 67%, and 60%, respectively (**Figure 2**). Althoefer *et al.* [15] and Assoun *et al.* [18] performed MRI at 1.0 T and 0.5 T, respectively, which results in poorer signal-to-noise ratio compared to MRI at 1.5 T; this may explain the low sensitivities observed in their studies. Assoun *et al.* [15] and Linden *et al.* [29] limited their imaging protocol to a T1-weighted sequence. Additional MRI sequences (e.g. a fat-saturated T2-weighted sequence and/or a short tau inversion recovery [STIR] sequence) might have increased sensitivity. Furthermore, Linden *et al.* [29] classified the bone marrow into three categories: normal (class 0), suggestive of reactive changes (class I), and suspicious for tumor infiltration (class II). Differentiation between class I and class II changes was unreliable; 14 of 45 (31%) class I changes on MRI proved to be class II changes

after bone marrow biopsy. If class I changes on MRI would have been regarded as suspicious for bone marrow involvement, sensitivity of MRI would have increased to 95.7%, although at the expense of decreased specificity (i.e. the proportion of patients that do not have bone marrow involvement that MRI will call negative). Specificity of MRI, however, was not assessed in this systematic review, because BMB is prone to sampling errors [2-5] and is therefore an imperfect reference standard to exclude bone marrow involvement. For the same reason and because of their dependence on disease prevalence, positive and negative predictive values of MRI (i.e. the probability that a patient with a positive/negative MRI will in fact have/be free of bone marrow involvement) were not assessed.

The included studies had moderate methodological quality. In nine studies (82%), there was poor reporting of the method of cohort assembly. In 73% of the included studies, there was possible disease progression bias. Index test and reference test should be described in sufficient detail, because if tests are executed in different ways then this would be expected to impact on test performance. However, the majority of studies did not give a sufficient description of the execution of MRI and BMB (55% and 73%, respectively). None of the included studies explicitly mentioned whether clinical data were available when MRI was interpreted, whereas these data are available in practice. Furthermore, in all studies it was not clear whether BMB was interpreted blindly of MRI, which might have lead to test review bias. Also, none of the studies described the interobserver reproducibility of MRI. Because of the moderate methodological quality and underlying heterogeneity of the included studies (potential sources of variability included variations in scanning protocols, patient characteristics, and experience of image interpreters), we omitted meta-analyzing the results of individual studies. It should also be noted that the number of patients with bone marrow involvement in the included studies was small, which lead to imprecise estimates of sensitivity (**Figure 2**). To demonstrate an arbitrary sensitivity of 95% with arbitrary 95% confidence intervals of 5%, at least 73 patients with bone marrow involvement should be investigated [41]. Since bone marrow involvement is found in only 5-15% of patients with HD, and in 20-40% of patients with NHL [2-5], a large sample size should be studied to reach more definitive conclusions on the value of MRI for ruling out bone marrow involvement in patients with malignant lymphoma. Future studies should also separately analyze patients undergoing MRI prior to any treatment (i.e. MRI performed as part of initial staging) and patients undergoing MRI after therapy (i.e. MRI performed as part of restaging), since treatment effects may cause local or generalized changes in bone marrow signal intensity on MRI [42], which in turn may affect diagnostic performance. It should also be determined which MRI sequence is optimal for bone marrow assessment in malignant lymphoma. Yasumoto et al. [29] addressed this issue by investigating the diagnostic performance of 4 different MR sequences: T1-weighted, fat-saturated T2-weighted, STIR, and fat-saturated diffusion-weighted (**Table 3**). T1-

weighted imaging had the highest sensitivity (92%), and diffusion-weighted imaging with fat saturation and STIR imaging had the highest specificity (92.5% and 92%, respectively) [29]. A combination of T1-weighted imaging and STIR imaging yielded the highest sensitivity and specificity (85% and 97%, respectively). However, these results are based on only 9 patients with 13 positive BMBs of the iliac crest [29].

Vassilakopoulos et al. [43] identified six independent clinical and laboratory prognostic factors for bone marrow involvement in HD: B symptoms, stage III/IV disease prior to BMB, anaemia, leukocytes  $< 6 \times 10^9/L$ , age 35 years or older, and iliac/inguinal involvement. They concluded that stage IA/IIA HD patients without anaemia and leukopaenia, stage IA/IIA HD patients younger than 35 years with either anaemia or leukopaenia but no inguinal/iliac involvement, and stage IIIA/IVA HD patients without any of these 4 risk factors, do not need BMB [43]. Although useful in HD patients, this clinical prediction rule does not apply to patients with NHL. Furthermore, in contrast to MRI, it does not predict where a possible bone marrow lesion is located. Therefore, it cannot be used to guide BMB and to reduce the number of sampling errors (i.e. false-negatives).

Positron emission tomography (PET) with the radiolabeled glucose analog  $^{18}F$ -fluoro-2-deoxyglucose (FDG) has gained a role in staging and follow-up of malignant lymphomas [44], and can also be used to assess the bone marrow. A recent meta-analysis investigated the diagnostic performance of FDG-PET in evaluating bone marrow involvement in malignant lymphoma, with BMB as reference standard. Pooled sensitivity of FDG-PET, however, was only 51% (95% CI, 38–64%) [45]. Thus, the results of this meta-analysis suggest that FDG-PET cannot reliably rule out bone marrow involvement.

A combination of FDG-PET and computed tomography (i.e. FDG-PET/CT fusion) has the potential to become the gold standard in staging of malignant lymphoma [46]. To our knowledge, only two studies investigated the value of FDG-PET/CT fusion for the detection of bone marrow involvement in malignant lymphoma. Ribrag et al. [32] investigated both MRI and FDG-PET/CT fusion in 43 patients with aggressive NHL. BMB indicated the presence of bone marrow involvement in 2/43 patients, which was confirmed by both MRI and FDG-PET [32]. Schaefer et al.'s study [47] included 22 patients with HD and 28 patients with aggressive NHL in whom FDG-avid bone lesions were detected by FDG-PET/CT fusion. All CT images of FDG-PET/CT fusion scans were analyzed independently regarding morphological osseous changes and compared with FDG-PET results. In the 50 patients, 193 FDG-avid bone lesions were found on FDG-PET/CT fusion. No additional morphological bone infiltration was detected on CT compared with FDG-PET. All direct biopsies ( $n=18$ ) of the FDG-avid bone lesions were positive for bone marrow involvement. In the remaining 32 patients, results from standard blind BMB were available, and eight patients (25%) had positive findings on histology [47]. A major disadvantage of Schaefer et al.'s study [47] is that

no patients without FDG-avid bone lesions were included. Consequently, sensitivity of FDG-PET/CT fusion could not be assessed. Thus, more studies on FDG-PET/CT fusion are needed. Compared to MRI, both FDG-PET and FDG-PET/CT fusion have several disadvantages, among which the requirement for patients to fast prior to scanning, the intravenous administration of a radioisotope, and the relatively long scanning time. In addition, radiation dose is a point of concern in FDG-PET/CT fusion [46].

Bone marrow metastases are most frequently localized in the hematopoietic (red) marrow because of its richer blood supply compared to fatty (yellow) marrow. At birth, visually all marrow is of the red type. Conversion of red to yellow marrow begins in the postnatal period, first in the extremities, progressing from the peripheral towards the axial skeleton and from diaphysis to the metaphysis of individual long bones. By the age of 25 years, marrow conversion is usually complete, and red marrow is predominantly seen in the axial skeleton and in the proximal part of the appendicular skeleton. Consequently, in adults, the most common sites for bone marrow metastases are the vertebrae (69%), pelvis (41%), proximal femoral metaphyses (25%), and skull (14%) [48]; these body regions should at least be included in an MRI protocol for bone marrow assessment. Two of the studies included in this systematic review [19, 32] used whole-body MRI for bone marrow assessment. Whole-body MRI enables detection of bone marrow metastases throughout the entire skeleton and may detect metastases that can be missed with MRI protocols that examine only selected areas. Especially pediatric patients may benefit from a whole-body MRI examination, since bone marrow metastases in the peripheral skeleton are more common in children than in adults [48]. An additional advantage of whole-body MRI is the possibility of complete staging of malignant lymphoma [19, 49] (**Figure 3**).

In conclusion, MRI is likely sufficiently sensitive to rule out bone marrow involvement in patients with malignant lymphoma. However, a well-designed study with a large sample size is needed to confirm current results.

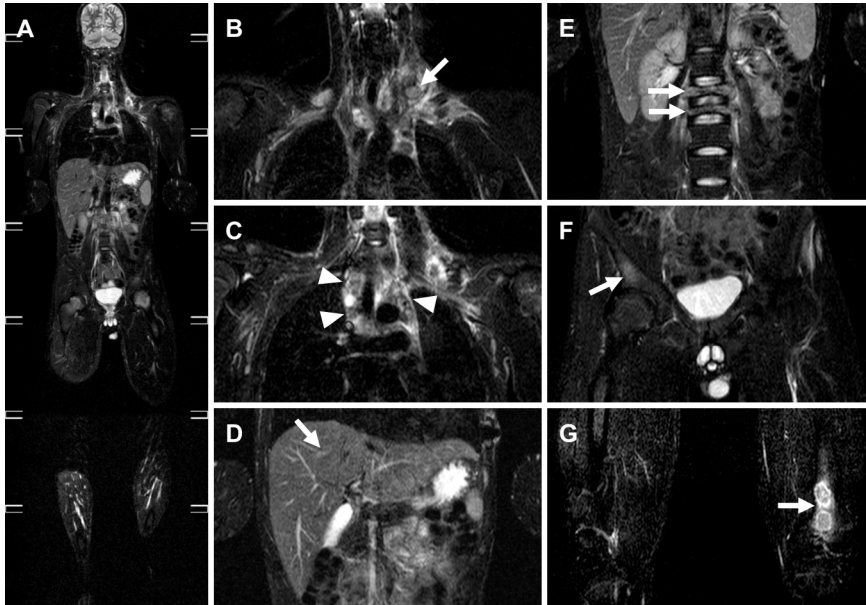


**Figure 3.** Whole-body MRI of a 16-year-old male with stage IV Hodgkin's disease, including multifocal bone marrow involvement. (A) Coronal whole-body STIR overview image. (B-G) Magnified images show (B) left supraclavicular lymph node involvement (arrow), (C) mediastinal lymph node involvement (arrowheads), (D) a metastasis in the right lobe of the liver (arrow), (E) destruction and collapse of the second and third lumbar vertebrae, (F) right iliac wing involvement (arrow), and (G) a lesion in the left distal femoral metaphysis (arrow). Bone marrow involvement was confirmed by guided BMB of the involved lumbar vertebrae.

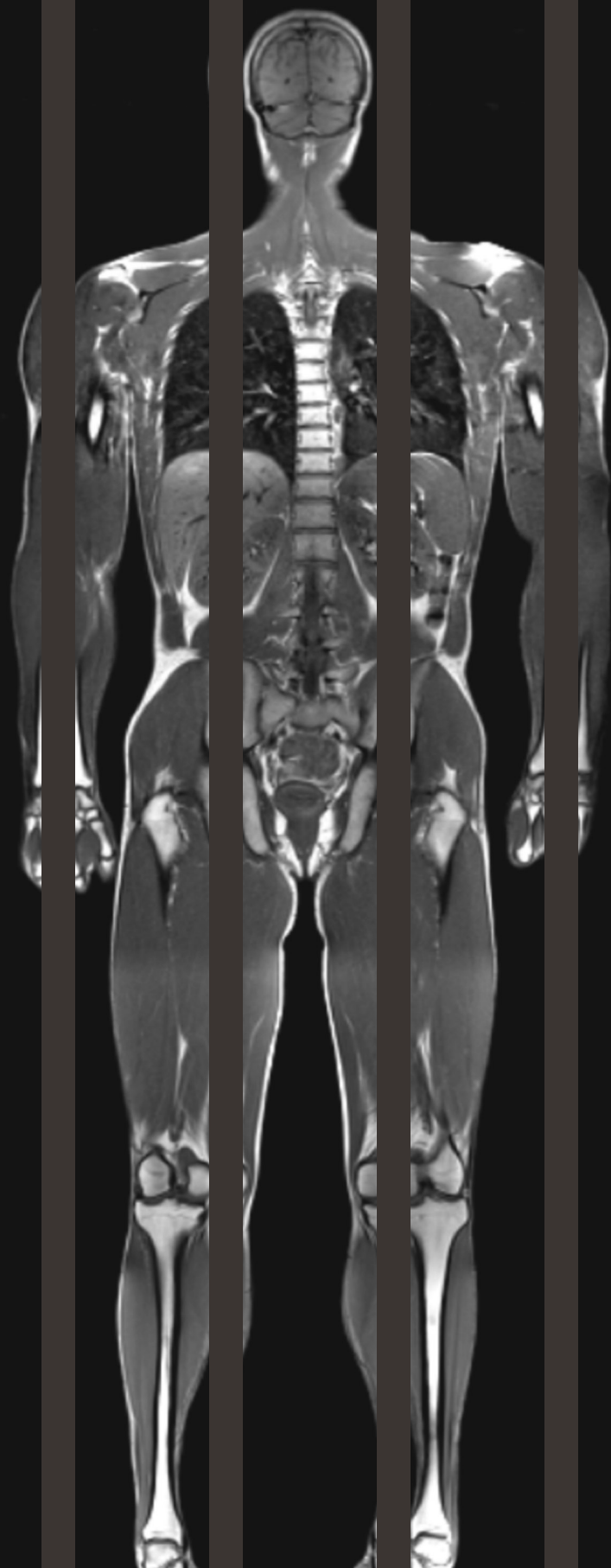


## References

1. Parkin DM, Bray FI, Devesa SS. Cancer burden in the year 2000. The global picture. *Eur J Cancer* 2001;37 Suppl 8:S4-S66
2. Brunning RD, Bloomfield CD, McKenna RW, Peterson LA. Bilateral trephine bone marrow biopsies in lymphoma and other neoplastic diseases. *Ann Intern Med* 1975;82:365-366
3. Collier BS, Chabner BA, Gralnick HR. Frequencies and patterns of bone marrow involvement in non-Hodgkin lymphomas: observations on the value of bilateral biopsies. *Am J Hematol* 1977;3:105-119
4. Haddy TB, Parker RI, Magrath IT. Bone marrow involvement in young patients with non-Hodgkin's lymphoma: the importance of multiple bone marrow samples for accurate staging. *Med Pediatr Oncol* 1989;17:418-423
5. Wang J, Weiss LM, Chang KL, et al. Diagnostic utility of bilateral bone marrow examination: significance of morphologic and ancillary technique study in malignancy. *Cancer* 2002;94:1522-1531
6. Armitage J.O. (2005) Staging non-Hodgkin lymphoma. *CA Cancer J Clin* 2005;55:368-376
7. Connors JM. State-of-the-art therapeutics: Hodgkin's lymphoma. *J Clin Oncol* 2005;23:6400-6408
8. Lister TA, Crowther D, Sutcliffe SB, et al. Report of a committee convened to discuss the evaluation and staging of patients with Hodgkin's disease: Cotswolds meeting. *J Clin Oncol* 1989;7:1630-1636
9. Bain BJ. Morbidity associated with bone marrow aspiration and trephine biopsy - a review of UK data for 2004. *Haematologica* 2006;91:1293-1294
10. Schmidt GP, Reiser MF, Baur-Melnyk A. Whole-body imaging of the musculoskeletal system: the value of MR imaging. *Skeletal Radiology* 2007;36:1109-1119
11. Vande Berg BC, Lecouvet FE, Michaux L, Ferrant A, Maldague B, Malghem J. Magnetic resonance imaging of the bone marrow in hematological malignancies. *Eur Radiol* 1998;8:1335-1344
12. Whiting P, Rutjes AW, Reitsma JB, Bossuyt PM, Kleijnen J. The development of QUADAS: a tool for the quality assessment of studies of diagnostic accuracy included in systematic reviews. *BMC Med Res Methodol* 2003;3:25
13. Whiting PF, Weswood ME, Rutjes AW, Reitsma JB, Bossuyt PN, Kleijnen J. Evaluation of QUADAS, a tool for the quality assessment of diagnostic accuracy studies. *BMC Med Res Methodol* 2006;6:9
14. Al-Mulhim FA. Magnetic resonance imaging of pelvic and femoral bones for detection of bone marrow infiltration in patients with non-Hodgkins lymphoma. *Saudi Med J* 2005;26:31-36
15. Althoefer C, Blum U, Bathmann J, et al. Comparative diagnostic accuracy of magnetic resonance imaging and immunoscintigraphy for detection of bone marrow involvement in patients with malignant lymphoma. *J Clin Oncol* 1997;15:1754-1760
16. Amano Y, Tajika K, Uchiyama N, Takahama K, Dan K, Kumazaki T. Staging of malignant lymphoma with three-station black-blood fast short-inversion time inversion recovery (STIR). *Magn Reson Med Sci* 2003;2:9-15
17. Assoun J, Poey C, Attal M, et al. Magnetic resonance imaging in the bone sites of malignant non-Hodgkin's lymphoma. Apropos of 16 cases. *Ann Radiol* 1991;34:383-386,389-392
18. Assoun J, Poey C, Attal M, et al. Bone marrow involvement in malignant lymphoma: MRI with biopsy correlation. *Rev Image Med* 1993;5:15-21

19. Brennan DD, Gleeson T, Coate LE, Cronin C, Carney D, Eustace SJ. A comparison of whole-body MRI and CT for the staging of lymphoma. *AJR Am J Roentgenol* 2005;185:711-716
20. Daldrup-Link HE, Rummeny EJ, Ihssen B, Kienast J, Link TM. Iron-oxide- enhanced MR imaging of bone marrow in patients with non-Hodgkin's lymphoma: differentiation between tumor infiltration and hypercellular bone marrow. *Eur Radiol* 2002;12:1557-1566
21. Dohner H, Guckel F, Knauf W, et al. Magnetic resonance imaging of bone marrow in lymphoproliferative disorders: correlation with bone marrow biopsy. *Br J Haematol* 1989;73:12-17
22. Guckel F, Dohner H, Knauf W, Ho AD, Semmler W, van Kaick G. MR tomography detection of bone marrow infiltration by malignant lymphomas. *Onkologie* 1989;12 Suppl 1:S34-S37
23. Guckel F, Semmler W, Dohner H, et al. NMR tomographic imaging of bone marrow infiltrates in malignant lymphoma. *RöFo* 1989;150:26-31
24. Hoane BR, Shields AF, Porter BA, Shulman HM. Detection of lymphomatous bone marrow involvement with magnetic resonance imaging. *Blood* 1991;78:728-738
25. Iizuka-Mikami M, Nagai K, Yoshida K, et al. Detection of bone marrow and extramedullary involvement in patients with non-Hodgkin's lymphoma by whole-body MRI: comparison with bone and <sup>67</sup>Ga scintigraphies. *Eur Radiol* 2004;14:1074-1081
26. Kauczor HU, Bentz M, Bischoff H, et al. Bone marrow involvement in Hodgkin's disease: MR tomography and chemical-shift imaging. *RöFo* 1993;159:555-561
27. Knauf WU, Guckel F, Dohner H, Semmler W, Trumper L, Ho AD. Detection of bone marrow infiltration by non-Hodgkin's lymphoma--comparison of histological findings, analysis of gene rearrangements, and examination by magnetic resonance imaging. *Klin Woch* 2002;74:345-350
28. Linden A, Zankovich R, Theissen P, Diehl V, Schicha H. Malignant lymphoma: bone marrow imaging versus biopsy. *Radiology* 1989;173:335-339
29. Linden A, Zankovich R, Theissen P, Schauerer G, Diehl V, Schicha H. Bone marrow scintigraphy and magnetic resonance tomography in malignant lymphomas: comparison with histologic results. *Nuklearmedizin* 1989;28:166-171
30. Olson DO, Shields AF, Scheurich CJ, Porter BA, Moss AA. Magnetic resonance imaging of the bone marrow in patients with leukemia, aplastic anemia, and lymphoma. *Invest Radiol* 1986;21:540-546
31. Ozguroglu M, Esen Ersavasti G, Demir G et al. Magnetic resonance imaging of bone marrow versus bone marrow biopsy in malignant lymphoma. *Path Oncol Res* 1999;5:123-128
32. Ribrag V, Vanel D, Leboulleux S, et al. Prospective study of bone marrow infiltration in aggressive lymphoma by three independent methods: Whole-body MRI, PET/CT and bone marrow biopsy. *Eur J Radiol* 2008;66:325-331
33. Richards MA, Webb JA, Jewell SE, Amess JA, Wrigley PF, Lister TA. Low field strength magnetic resonance imaging of bone marrow in patients with malignant lymphoma. *Br J Cancer* 1988;57:412-415
34. Smith SR, Roberts N, Percy DF, Edwards RH. Detection of bone marrow abnormalities in patients with Hodgkin's disease by T1 mapping of MR images of lumbar vertebral bone marrow. *Br J Cancer* 1992;65:246-251
35. Tardivon AA, Munck JN, Shapeero LG, et al. Can clinical data help to screen patients with lymphoma for MR imaging of bone marrow? *Ann Oncol* 1995;6:795-800

36. Tesoro-Tess JD, Balzarini L, Ceglia E, Petrillo R, Santoro A, Musumeci R. Magnetic resonance imaging in the initial staging of Hodgkin's disease and non-Hodgkin lymphoma. *Eur J Radiol* 1991;12:81-90
37. Tsunoda S, Takagi S, Tanaka O, Miura Y. Clinical and prognostic significance of femoral marrow magnetic resonance imaging in patients with malignant lymphoma. *Blood* 1997;89:286-290
38. Varan A, Cila A, Buyukpamukcu M. Prognostic importance of magnetic resonance imaging in bone marrow involvement of Hodgkin disease. *Med Pediatr Oncol* 1999;32:267-271
39. Yasumoto M, Nonomura Y, Yoshimura R, et al. MR detection of iliac bone marrow involvement by malignant lymphoma with various MR sequences including diffusion-weighted echo-planar imaging. *Skelet Radiol* 2002;31:263-269
40. Zhang L, Mandel C, Yang ZY, et al. Tumor infiltration of bone marrow in patients with hematological malignancies: dynamic contrast-enhanced magnetic resonance imaging. *Chin Med J* 2006;119:1256-1262
41. Jones SR, Carley S, Harrison M. An introduction to power and sample size estimation. *Emerg Med J* 2003;20:453-458
42. Daldrup-Link HE, Henning T, Link TM. MR imaging of therapy-induced changes of bone marrow. *Eur Radiol* 2007;17:743-761
43. Vassilakopoulos TP, Angelopoulou MK, Constantinou N, et al. Development and validation of a clinical prediction rule for bone marrow involvement in patients with Hodgkin lymphoma. *Blood* 2005;105:1875-1880
44. Jhanwar YS, Straus DJ. The role of PET in lymphoma. *J Nucl Med* 2006;47:1326-1334
45. Pakos EE, Fotopoulos AD, Ioannidis JP. 18F-FDG PET for evaluation of bone marrow infiltration in staging of lymphoma: a meta-analysis. *J Nucl Med* 2005;46:958-963
46. Kwee TC, Kwee RM, Nievelstein RA. Imaging in staging of malignant lymphoma: a systematic review. *Blood* 2008;111:504-516
47. Schaefer NG, Strobel K, Taverna C, Hany TF. Bone involvement in patients with lymphoma: the role of FDG-PET/CT. *Eur J Nucl Med Mol Imaging* 2007;34:60-67
48. Padhani A, Husband J. Bone. In: Husband JES, Reznick RH, eds. *Imaging in oncology*;1989:765-786. Isis Medical Media, Oxford.
49. Kellenberger CJ, Miller SF, Khan M, Gilday DL, Weitzman S, Babyn PS. Initial experience with FSE STIR whole-body MR imaging for staging lymphoma in children. *Eur Radiol* 2004;14:1829-1841



# Chapter 7<sup>2</sup>

Whole-body  
magnetic resonance imaging,  
including diffusion-weighted  
imaging, for diagnosing  
bone marrow involvement in  
malignant lymphoma

Kwee TC, Fijnheer R, Ludwig I, Quarles van Ufford HME, Uiterwaal CS,  
Bierings MB, Takahara T, Nievelstein RA

## Abstract

### Purpose

To determine the value of whole-body magnetic resonance imaging (MRI), including diffusion-weighted imaging (DWI), for diagnosing bone marrow involvement in malignant lymphoma using blind bone marrow biopsy (BMB) as the standard of reference.

### Materials and Methods

Forty-eight consecutive patients with newly diagnosed malignant lymphoma prospectively underwent whole-body MRI (T1-weighted and short inversion time inversion recovery [n=48] and DWI [n=44]) and blind BMB of the posterior iliac crest. Whole-body magnetic resonance images were interpreted by a radiologist who was blinded to BMB findings. Patient-based sensitivities of whole-body MRI (without and with DWI) for diagnosing bone marrow involvement were calculated, along with binomial exact 95% confidence intervals (CIs), using BMB as the standard of reference. Sensitivity of whole-body MRI without DWI was compared to that of whole-body MRI with DWI using a McNemar test.

### Results

Whole-body MRI without DWI and whole-body MRI with DWI were positive in only 5 of 12 and 5 of 11 patients with a positive BMB, yielding sensitivities of 41.7% (95% CI: 19.3-68.1%) and 45.5% (95% CI: 21.3-72.0%), respectively. Sensitivity of whole-body MRI without DWI was not significantly different ( $P=1.000$ ) from that of whole-body MRI with DWI.

### Conclusion

The results of this study show that whole-body MRI (without and with DWI) is negative for bone marrow involvement in a considerable proportion of patients with a positive BMB. Therefore, whole-body MRI is not sufficiently reliable yet to replace BMB for bone marrow assessment in malignant lymphoma.

## Introduction

The malignant lymphomas, Hodgkin lymphoma (HL) and non-Hodgkin lymphoma (NHL), comprise approximately 5.0% of all cancers and account for approximately 3.7% of all cancer deaths in the United States [1]. Accurate staging is of crucial importance in malignant lymphoma, because it determines prognosis and treatment planning [2, 3]. Of particular importance is the detection or exclusion of bone marrow involvement, which, if present, by definition indicates the highest stage (stage IV) according to the Ann Arbor staging system [2, 3]. The currently used method for the diagnosis of bone marrow involvement is unilateral or bilateral blind bone marrow biopsy (BMB) of the iliac crest. However, BMB is an invasive and painful procedure, and has a small but non-negligible risk of (hemorrhagic) complications [4, 5]. Therefore, identifying patients who have minimal risk of bone marrow involvement and in whom BMB may be avoided, would be desirable. Recently, whole-body magnetic resonance imaging (MRI) has become available as a potential alternative to computed tomography (CT) for staging of malignant lymphoma [6-8]. An advantage of MRI over CT is that it allows visualizing the bone marrow, at a good spatial resolution [9]. Furthermore, in addition to conventional T1- and T2-weighted MRI sequences, diffusion-weighted MRI (DWI), a sequence that is sensitive to the random (Brownian) extra-, intra-, and transcellular motion of water molecules, is emerging as a powerful technique for the detection of lesions throughout the entire body, including the bone marrow [8, 10, 11]. The advantage of DWI over conventional MRI sequences is expected to lie in its high lesion-to-background contrast, which potentially improves detectability of bone marrow lesions [8, 10, 11]. If MRI is accurate in excluding bone marrow involvement, it may spare patients unnecessary BMBs. Important advantages of whole-body MRI over MRI protocols that examine only selected areas are its ability to detect bone marrow metastases throughout the entire bone marrow while at the same time allowing complete staging of extramedullary disease. The purpose of this study was therefore to determine the value of whole-body MRI, including DWI, in diagnosing bone marrow involvement in malignant lymphoma using BMB as the standard of reference.

## Materials and Methods

### Patients

This prospective multicenter study was approved by the institutional review board of the University Medical Center Utrecht and all patients were enrolled after they had been properly informed and provided written informed consent. Patients aged 8 years and older with newly diagnosed, histologically proven malignant lymphoma were prospectively included. All patients underwent whole-body MRI and blind BMB of the posterior iliac crest (either unilateral or bilateral) in a random order, and before start of treatment. BMBs were interpreted by experienced hematopathologists who

were blinded to whole-body MRI findings, as part of routine clinical care. Patients with general contraindications to MRI, such as implanted pacemaker and claustrophobia, were excluded from enrollment. In total, 48 consecutive patients (32 men and 16 women; mean age: 48.4 years; age range: 13-82 years) with newly diagnosed, histologically proven malignant lymphoma (HL: n=10; NHL: n=38; low-grade NHL: n=13; intermediate-grade NHL: n=4, high-grade NHL: n=21) prospectively underwent whole-body MRI and BMB (**Table 1**). Whole-body MRI, including DWI, was performed in 44 patients. Three of 48 patients (aged 15, 78, and 82 years) did not tolerate the MRI examination for more than 30 minutes, and one patient (aged 25 years) had osteosynthetic material in the spine which may cause considerable artifacts at DWI; these four patients only underwent conventional whole-body MRI (T1-weighted [T1W] and short inversion time inversion recovery [STIR]), without DWI. Unilateral BMB was performed in 40 patients, and bilateral BMB was performed in 8 patients. Time interval between whole-body MRI and BMB ranged from 0 to 37 days, with 41 of 48 BMBs (85.4%) being performed before whole-body MRI.

#### MRI

Whole-body MRI was performed using a 1.5-T system (Achieva, Philips Healthcare, Best, The Netherlands). Four spacers were placed on the original patient table. Subsequently, an additional table platform was mounted on top of these four spacers. In this way, sufficient space was created to freely move the lower part of a surface coil over a distance of approximately 110 cm along the z-axis (necessary for DWI), without the need to reposition the patients who were lying on top of the additional table platform.

First, coronal whole-body T1W and STIR images were acquired, using the built-in body coil for signal reception. Images were acquired under free breathing, except for the stations covering the chest, abdomen, and pelvis, which were acquired using breathholding (T1W) or respiratory triggering (STIR). Applied sequence parameters for T1W were as follows: single-shot turbo spin-echo imaging, repetition time (TR)/echo time (TE) of 537/18 ms, slice thickness/gap of 6/1 mm, number of slices of 30 per station, field of view (FOV) of 530 × 265 mm<sup>2</sup>, acquisition matrix of 208 × 287, number of signal averages (NSA) of 1, acquired voxel size of 1.27 × 1.85 × 6.00 mm<sup>3</sup>, reconstructed voxel size of 1.04 × 1.04 × 6.00 mm<sup>3</sup>, scan time of 47 s per station, 7 stations in total. Applied sequence parameters for STIR were as follows: single-shot turbo spin-echo imaging, TR/TE/inversion time (IR) of 2444/64/165 ms, slice thickness/gap of 6/1 mm, number of slices of 30 per station, FOV of 530 × 265 mm<sup>2</sup>, acquisition matrix of 336 × 120, NSA of 2, acquired voxel size of 1.58 × 2.21 × 6.00 mm<sup>3</sup>, reconstructed voxel size of 1.04 × 1.04 × 6.00 mm<sup>3</sup>, scan time of 44 s per station, 7 stations in total. Total actual scan time of T1W and STIR whole-body MRI was approximately 25-30 minutes.

Second, axial diffusion-weighted images of the head/neck, chest, abdomen, and pelvis were acquired under free breathing, using a 4-element phased array surface coil for



**Table 1.** Patient characteristics

No.	Sex	Age	Lymphoma classification	Type of BMB
1	F	14	HD, nodular sclerosing type	Bilateral
2	F	16	HD, nodular sclerosing type	Bilateral
3	M	16	HD, nodular sclerosing type	Bilateral
4	M	29	Diffuse large B-cell lymphoma	Unilateral
5	M	67	Follicular lymphoma	Unilateral
6	M	15	Anaplastic large cell lymphoma	Bilateral
7	M	53	Mantle cell lymphoma	Unilateral
8	M	17	HD, nodular sclerosing type	Bilateral
9	F	61	Diffuse large B-cell lymphoma	Unilateral
10	F	44	Diffuse large B-cell lymphoma	Unilateral
11	F	59	Diffuse large B-cell lymphoma	Unilateral
12	M	78	Diffuse large B-cell lymphoma	Unilateral
13	F	64	Diffuse large B-cell lymphoma	Unilateral
14	M	58	Diffuse large B-cell lymphoma	Unilateral
15	F	62	Diffuse large B-cell lymphoma	Unilateral
16	F	74	Diffuse large B-cell lymphoma	Unilateral
17	F	63	Mucosa-associated lymphoid tissue lymphoma	Unilateral
18	M	68	Small lymphocytic lymphoma	Unilateral
19	F	13	Diffuse large B-cell lymphoma	Unilateral
20	M	82	Follicular lymphoma	Unilateral
21	M	13	HD, nodular sclerosing type	Bilateral
22	M	62	Diffuse large B-cell lymphoma	Unilateral
23	F	22	HD, nodular sclerosing type	Unilateral
24	M	69	Diffuse large B-cell lymphoma	Unilateral
25	M	56	Small lymphocytic lymphoma	Unilateral
26	M	62	Diffuse large B-cell lymphoma	Unilateral
27	M	22	Anaplastic large cell lymphoma	Unilateral
28	M	25	Diffuse large B-cell lymphoma	Unilateral
29	F	53	HD, lymphocyte predominance type	Unilateral
30	M	59	Diffuse large B-cell lymphoma	Unilateral
31	M	74	Diffuse large B-cell lymphoma	Unilateral
32	M	62	Mantle cell lymphoma	Unilateral
33	M	34	HD, nodular sclerosing type	Unilateral
34	M	47	Diffuse large B-cell lymphoma	Unilateral
35	M	43	Nodal marginal zone lymphoma	Unilateral
36	M	43	Mucosa-associated lymphoid tissue lymphoma	Unilateral
37	M	47	Follicular lymphoma	Unilateral
38	F	17	HD, nodular sclerosing type	Bilateral
39	M	40	Follicular lymphoma	Unilateral
40	F	72	Nodal marginal zone lymphoma	Unilateral
41	M	71	Small lymphocytic lymphoma	Unilateral
42	M	55	Follicular lymphoma	Unilateral
43	F	60	Diffuse large B-cell lymphoma	Unilateral
44	M	45	Diffuse large B-cell lymphoma	Unilateral
45	M	73	Mantle cell lymphoma	Unilateral
46	M	62	Mantle cell lymphoma	Unilateral
47	F	16	HD, nodular sclerosing type	Bilateral
48	M	64	Follicular lymphoma	Unilateral

signal reception. This surface coil was sequentially moved to image the separate stations of the whole-body DWI examination, without patient repositioning. Applied sequence parameters for DWI of the head/neck station were as follows: single-shot spin-echo echo-planar imaging (EPI), TR/TE/IR of 8612/78/180 ms, slice thickness/gap of 4/0 mm, number of slices of 60, FOV of  $450 \times 360 \text{ mm}^2$ , acquisition matrix of  $128 \times 81$ , motion probing gradients in three orthogonal axes, b values of 0 and  $1000 \text{ s/mm}^2$ , NSA of 3, half scan factor of 0.651, parallel acquisition (SENSitivity Encoding) factor of 2, EPI factor of 43, acquired voxel size of  $3.52 \times 4.50 \times 4.00 \text{ mm}^3$ , reconstructed voxel size of  $1.76 \times 1.76 \times 4.00 \text{ mm}^3$ , and scan time of 4 minutes and 4 s. Applied sequence parameters for DWI of the chest, abdominal, and pelvic stations were identical, except for a TR of 6962 s, spectral presaturation inversion recovery fat suppression, and scan time of 3 minutes and 20 s for each of the three stations. Total actual scan time of whole-body DWI was approximately 20-25 minutes.

Seamless coronal whole-body T1W and STIR images were created by merging separately acquired stations using software implemented in the standard operating console. Axial diffusion-weighted images were first coronally reformatted with a slice thickness/gap of both 3.5/0mm and 7.0/0mm, and then merged to create seamless coronal whole-body diffusion-weighted images. Whole-body diffusion-weighted images were displayed using greyscale inversion.

#### Image analysis

All images were transferred to and interpreted by means of a Picture Archiving and Communications System that allows manual window level setting. A board-certified radiologist (RAJN, with 14 years of clinical experience with MRI), blinded to BMB findings, evaluated two separate sets of whole-body magnetic resonance images: whole-body MRI without DWI (i.e. T1W and STIR only) and whole-body MRI with DWI (i.e. T1W, STIR, and DWI). The observer was aware that the patients had malignant lymphoma, but unaware of the type and grade of lymphoma and other imaging findings. Bone marrow involvement was considered present if both T1W demonstrated any focal area with a signal intensity equal or lower than that of surrounding muscle and intervertebral discs and STIR demonstrated that the same area has a signal intensity higher than that of surrounding muscle. Furthermore, bone marrow involvement was considered present if DWI showed any focal area with a signal intensity that exceeded the signal intensity of the surrounding background; in case of equivocal findings, any signal intensity higher than that of the spinal cord was considered positive for bone marrow involvement at DWI. Although the majority of BMBs was performed before whole-body MRI, the observer was aware of this issue. In addition, BMB usually causes a mild signal change at a limited portion of the posterior iliac crest, with a characteristic shape, making differentiation from lymphomatous bone marrow involvement relatively straightforward (**Figure 1**).

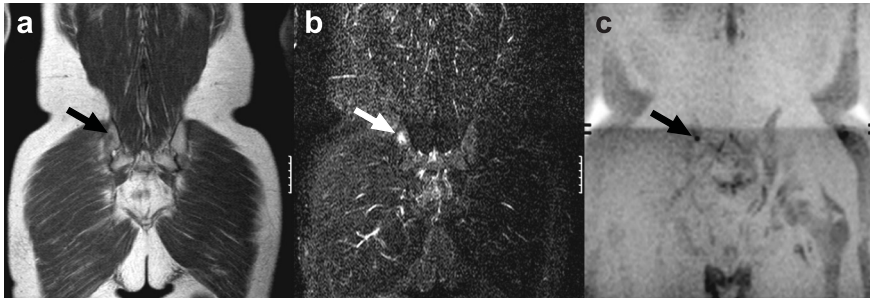


**Figure 1.** Typical MRI findings after BMB of the posterior iliac crest in a 45-year-old male with diffuse-large B-cell lymphoma. Note the mild signal changes at a limited portion of the posterior iliac crest at (coronal) T1W (a), STIR (b), and (gray-scale inverted) diffusion-weighted MRI (c) (arrows). Also note the characteristic small, rounded shape of the signal intensity changes, matching the shape of the needle that was used for BMB.

#### Statistical analysis

It is well known that focal bone marrow involvement can be missed by BMB; previous studies showed that 10-60% patients with unilaterally proven bone marrow involvement had a negative contralateral BMB of the iliac crest [12-15]. It has also been reported that in 33% of paired ipsilateral BMBs of the iliac crest, only one specimen was positive for bone marrow infiltration [14]. Therefore, BMB is not a suitable reference standard to calculate specificity and negative and positive predictive values of whole-body MRI. Therefore, only (patient-based) sensitivities of whole-body MRI (without and with DWI) for diagnosing bone marrow involvement were calculated, along with binomial exact 95% confidence intervals (CIs). Whole-body MRI was considered to be sufficiently sensitive compared to BMB in case its sensitivity was equal to or higher than 95%. Sensitivity of whole-body MRI without DWI was compared to that of whole-body MRI with DWI using a McNemar test. *P* values less than 0.05 were considered to indicate a significant difference. Statistical analyses were executed using Statistical Package for the Social Sciences version 12.0 software (SPSS, Chicago, IL).

#### Results

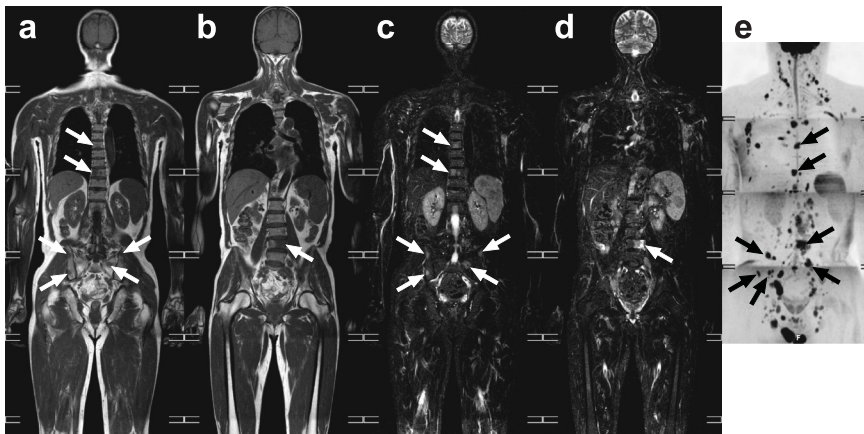
**Tables 2 and 3** show the results of T1W and STIR whole-body MRI, and T1W, STIR, and diffusion-weighted whole-body MRI compared to results of BMB regarding the diagnosis of bone marrow involvement. Whole-body MRI without DWI and whole-body MRI with DWI were positive in only 5 of 12 and 5 of 11 patients with a positive BMB, yielding sensitivities of 41.7% (95% CI: 19.3-68.1%) and 45.5% (95% CI: 21.3-72.0%), respectively. Sensitivity of whole-body MRI without DWI was not significantly different ( $P=1.000$ ) from that of whole-body MRI with DWI. **Figures 2 and 3** show two representative whole-body MRI examples.

**Table 2.** Results of T1W and STIR whole-body MRI compared to those of BMB regarding the diagnosis of bone marrow involvement.

T1W and STIR	BMB	No. of cases
+	+	5
+	-	8
-	+	7
-	-	28

**Table 3.** Results of T1W, STIR and diffusion-weighted whole-body MRI compared to those of BMB regarding the diagnosis of bone marrow involvement.

T1W, STIR, and DWI	BMB	No. of cases
+	+	5
+	-	8
-	+	6
-	-	25

**Figure 2.** True positive whole-body MRI in a 64-year-old male with follicular lymphoma. Unilateral BMB of the right posterior iliac crest revealed bone marrow involvement. Coronal T1W (a, b), STIR (c, d), and (gray-scale inverted) diffusion-weighted whole-body MRI (e) not only show widespread supra- and infradiaphragmatic nodal disease and splenic involvement, but also extensive bone marrow involvement in the thoracic and lumbar vertebrae, sacrum, and pelvic bone (arrows).

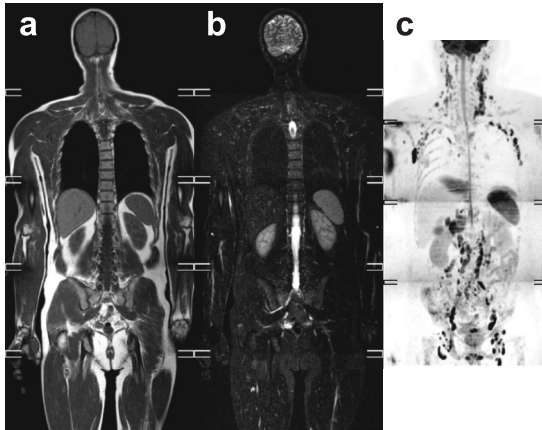


**Figure 3.** False-negative whole-body MRI in a 56-year-old male with small lymphocytic lymphoma. Unilateral BMB of the right posterior iliac crest revealed bone marrow involvement. Coronal T1W (a), STIR (b), and (gray-scale inverted) diffusion-weighted whole-body MRI (c) only show widespread supra- and infradiaphragmatic nodal disease, but no signs of bone marrow involvement.

## Discussion

Bone marrow involvement is found in 5–15% of patients with HL and in 20–40% of patients with NHL [12–15], and has important prognostic and therapeutic implications [2, 3]. BMB is currently considered as the gold standard for diagnosing bone marrow involvement, but is invasive and has a risk of hemorrhagic complications [4, 5]. MRI, which is noninvasive and does not use any ionizing radiation, is generally regarded as a highly sensitive method for the detection of bone marrow abnormalities [9, 16]. Therefore, it may be used to identify patients who do not have any bone marrow involvement, thereby reducing the number of BMBs. Of note, a recent systematic review [9, 16] reported that published sensitivities of MRI for the detection of bone marrow involvement in malignant lymphoma ranged from 50% to 100%, with a median of 100%. However, the majority of previous studies applied MRI protocols that examine only selected body regions (mostly lumbar spine, pelvis and proximal femurs) [16]. Major disadvantage of these MRI protocols are that bone marrow involvement outside the image volume is missed and that they do not allow complete staging of the malignant lymphoma because of the absence of full body coverage. In this respect, whole-body MRI is clearly favored. It should also be noted that MRI protocols of selected body regions are generally not comparable to whole-body MRI, since the latter allows less time to acquire different MRI sequences and imaging planes, and generally employs a greater slice thickness and lower spatial resolution.

The results of the present study that used BMB as the standard of reference indicate that whole-body MRI (both without and with DWI) is not sufficiently sensitive for diagnosing bone marrow involvement in malignant lymphoma given the fact that the 95% CIs for sensitivities did not include 95%. Two previous studies [6, 17] reported the value of whole-body MRI for bone marrow assessment compared to BMB. Brennan

et al. [6] performed axial and coronal STIR whole-body MRI and sagittal T1-weighted MRI of the spine in 23 patients with malignant lymphoma. Seventeen patients were in clinical remission and six were being actively treated for disease. BMB results were available in 18 patients. MRI correctly predicted marrow invasion in two patients, and also correctly predicted normal or noninvaded marrow in 16 patients, yielding a patient-based sensitivity of 100% (95% CI: 34.2-100%) [6]. In another study by Ribrag et al. [17] coronal T1W and STIR whole-body MRI were performed in 43 patients with newly diagnosed malignant lymphoma. In nine patients, whole-body MRI showed focal bone marrow abnormalities, of which two were confirmed by BMB. The other 34 patients had no bone marrow involvement at whole-body MRI or BMB. Their results also correspond to a high patient-based sensitivity of 100% (95% CI: 34.2-100%) [17]. A limitation of the studies by Brennan et al. [6] and Ribrag et al. [17] is that a very low number of patients with histologically proven bone marrow involvement were included (n=2 in both studies); this explains the very wide 95% CIs for sensitivity in their studies. Furthermore, Brennan et al. [6] only included 4 patients with low-grade lymphomas, whereas Ribrag et al. [17] exclusively included patients with high-grade lymphomas. Thus, the results of previous studies on the value of whole-body MRI for diagnosing bone marrow involvement are rather inconclusive and are mainly applicable to patients with high-grade lymphomas. In the present study, number of patients with histologically proven bone marrow involvement was higher (n=12), and both low-grade and high-grade lymphomas were included.

The present study also assessed the additional value of whole-body DWI in assessing the bone marrow in patients with malignant lymphoma. DWI is expected to improve lesion detectability thanks to its high lesion-to-background contrast [8, 10, 11]. However, sensitivity of whole-body MRI with DWI was not significantly higher than that of whole-body MRI without DWI. In a previous study by Yasumoto et al. [18] who assessed the bone marrow in 53 patients with malignant lymphoma using an MRI protocol that covered the iliac crests, sensitivity of T1W, STIR, and DWI (92%, 85%, and 77%, respectively) were not significantly different either. However, it should be noted that Yasumoto et al. [18] applied a relatively long TE of 123 ms and a NSA of only 1 for DWI (most likely due to gradient strength limitations of their system at that time), which yields a low signal-to-noise ratio and likely impairs lesion detectability. On the other hand, in a study by Nakanishi et al. [19] in 30 patients with various (non-lymphomatous) malignancies, region-based sensitivity of the combination of T1W, STIR, and diffusion-weighted whole-body MRI for the detection of bone marrow metastases (96%) was significantly higher than that of the combination of T1W and STIR whole-body MRI (88%). Future studies with larger sample sizes are necessary to prove the assumed advantage of whole-body MRI with DWI over conventional whole-body MRI alone in detecting lymphomatous bone marrow involvement.

Another interesting finding of the present study is that in eight patients, whole-body MRI (both without and with DWI) was positive, while BMB was negative. Whole-body MRI in these eight patients may well be true positive, since it is known that BMB may miss focal bone marrow involvement [12-15]. Thus, sensitivity of whole-body MRI may in fact be higher than was calculated in this study, because of the imperfect sensitivity of BMB (the standard of reference) itself. In addition, it can be argued that the combination of whole-body MRI *with* BMB may well provide the best sensitivity for the detection of bone marrow involvement in patients with malignant lymphoma. On the other hand, MRI is rather nonspecific given the fact that it visualizes a wide variety of both benign and malignant lesions [9, 11]. However, obtaining additional biopsies of the lesions that were only seen at whole-body MRI for verification was not possible due to practical and ethical reasons. Thus, studies comparing lymphoma recurrence between whole-body MRI positive patients with a positive BMB and whole-body MRI positive patients with a negative BMB, or, ideally, follow-up whole-body MRI studies are needed to provide insight into the rate of correct upstaging by whole-body MRI. Although our results indicate that whole-body MRI cannot replace BMB yet as an initial screening tool for bone marrow involvement in patients with malignant lymphoma, whole-body MRI findings may still be used to guide BMB. This, in turn, may reduce the number of sampling errors (i.e. false negatives). Especially when using whole-body MRI instead of CT for staging (CT is currently the mainstay in staging of malignant lymphoma [20], but provides no information on the presence or absence of bone marrow disease [21]), this may be an attractive diagnostic approach. Another imaging modality that is worthwhile to mention is <sup>18</sup>F-fluoro-2-deoxyglucose positron emission tomography (FDG-PET). FDG-PET, either as a stand-alone modality or in combination with CT (i.e. FDG-PET/CT) has gained an important role in the diagnostic management of malignant lymphoma [20, 22] and may also be used to evaluate bone marrow involvement [23]. However, although a recent meta-analysis [24] reported an overall specificity of 91% (95% CI, 85%-95%) for FDG-PET in diagnosing bone marrow involvement, overall sensitivity of FDG-PET was only 51% (95% CI: 38-64%). Thus, FDG-PET cannot reliably rule out bone marrow involvement either. Nevertheless, similar to whole-body MRI, it may be used to guide BMB; these promising roles of whole-body MRI and FDG-PET should be the subject of future studies.

A limitation of the present study is that the majority of BMBs were obtained before whole-body MRI. However, it was not possible to schedule all whole-body MRI examinations before BMB due to logistic reasons at our institutions. Nevertheless, the observer was aware of this issue, and MRI signal changes after BMB are usually mild and have a characteristic shape over a short trajectory, making differentiation from lymphomatous bone marrow involvement relatively straightforward. Furthermore, sensitivities were calculated on a patient level rather than on a region or lesion level. In addition, the likelihood that lymphomatous bone marrow involvement is only present



at the small region where the BMB has been performed is very low. Another drawback is that although T1W and STIR were truly acquired of the entire body, this was not the case for DWI because the upper part of the head, upper extremities, and lower extremities were just outside the FOV when acquiring diffusion-weighted images. Therefore, the applied DWI protocol fails to detect bone marrow involvement in the peripheral skeleton. Nevertheless, bone marrow metastases are most frequently localized in the haematopoietic (red) marrow because of its richer blood supply compared to fatty (yellow) marrow [25]. In addition, most of the red bone marrow of this mainly adult population (by the age of 25 years, the red marrow is predominantly seen in the axial skeleton and in the proximal part of the appendicular skeleton) was imaged at DWI. Another limitation is that only patients with newly diagnosed malignant lymphoma were included. Treatment effects due to irradiation, chemotherapy or other new treatment regimens may cause local or generalized changes in bone marrow signal intensity [26], and it is still unclear how whole-body MRI (without and with DWI) performs in the assessment of the bone marrow after onset or completion of therapy, or in case of disease recurrence.

In conclusion, the results of this study show that whole-body MRI (without and with DWI) is negative for bone marrow involvement in a considerable proportion of patients with a positive BMB. Therefore, whole-body MRI is not sufficiently reliable yet to replace BMB for bone marrow assessment in malignant lymphoma. Against our expectation, sensitivity of whole-body MRI with DWI was not significantly higher than that of whole-body MRI without DWI. BMB remains necessary in the staging work-up of patients with malignant lymphoma until more advanced whole-body MRI protocols (e.g. at higher field strengths, or using a higher spatial resolution) have proved to achieve a higher diagnostic performance.

## Acknowledgements

This study was supported by ZonMw Program for Health Care Efficiency Research (grant number 80-82310-98-08012). T.C.K was supported by a ZonMW AGIKO stipend (grant number 92003497).

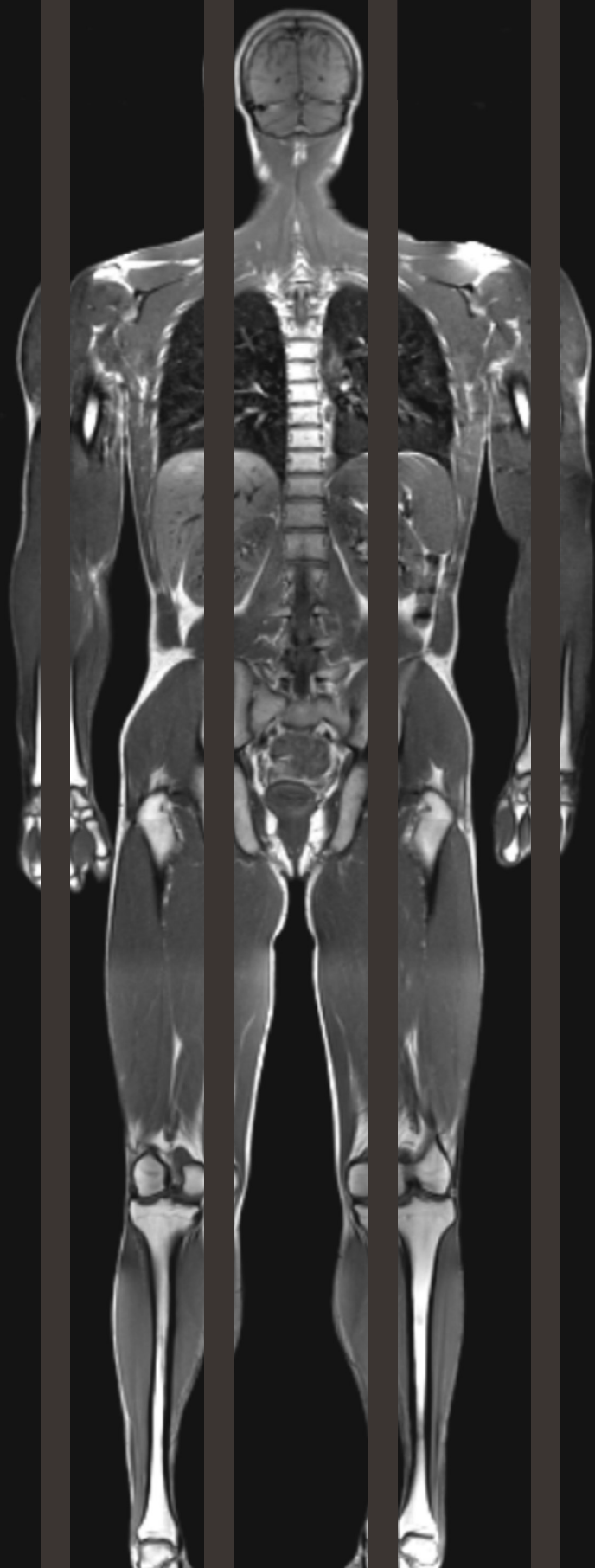


## References

1. Jemal A, Siegel R, Ward E, Hao Y, Xu J, Thun MJ. Cancer statistics, 2009. *CA Cancer J Clin* 2009;59:225-249
2. Armitage JO. Staging non-Hodgkin lymphoma. *CA Cancer J Clin*. 2005;55:368-376
3. Connors JM. State-of-the-art therapeutics: Hodgkin's lymphoma. *J Clin Oncol* 2005;23:6400-6408
4. Bain BJ. Morbidity associated with bone marrow aspiration and trephine biopsy - a review of UK data for 2004. *Haematologica* 2006;91:1293-1294
5. Bairey O, Shpilberg O. Is bone marrow biopsy obligatory in all patients with non-Hodgkin's lymphoma? *Acta Haematol* 2007;118:61-64
6. Brennan DD, Gleeson T, Coate LE, Cronin C, Carney D, Eustace SJ. A comparison of whole-body MRI and CT for the staging of lymphoma. *AJR Am J Roentgenol* 2005;185:711-716
7. Kellenberger CJ, Miller SF, Khan M, Gilday DL, Weitzman S, Babyn PS. Initial experience with FSE STIR whole-body MR imaging for staging lymphoma in children. *Eur Radiol* 2004;14:1829-1841
8. Kwee TC, Quarles van Ufford HM, Beek FJ, et al. Whole-Body MRI, Including Diffusion-Weighted Imaging, for the Initial Staging of Malignant Lymphoma: Comparison to Computed Tomography. *Invest Radiol*. 2009;44:683-690
9. Schmidt GP, Reiser MF, Baur-Melnyk A. Whole-body imaging of bone marrow. *Semin Musculoskelet Radiol* 2009;13:120-133
10. Kwee TC, Takahara T, Ochiai R, Nievelstein RA, Luijten PR. Diffusion-weighted whole-body imaging with background body signal suppression (DWIBS): features and potential applications in oncology. *Eur Radiol* 2008;18:1937-1952
11. Dietrich O, Biffar A, Reiser MF, Baur-Melnyk A. Diffusion-weighted imaging of bone marrow. *Semin Musculoskelet Radiol* 2009;13:134-144
12. Brunning RD, Bloomfield CD, McKenna RW, Peterson LA. Bilateral trephine bone marrow biopsies in lymphoma and other neoplastic diseases. *Annals of Internal Medicine* 1975;82:365-366
13. Coller BS, Chabner BA, Gralnick HR. Frequencies and patterns of bone marrow involvement in non-Hodgkin lymphomas: observations on the value of bilateral biopsies. *American Journal of Hematology* 1977;3:105-119
14. Haddy TB, Parker RI, Magrath IT. Bone marrow involvement in young patients with non-Hodgkin's lymphoma: the importance of multiple bone marrow samples for accurate staging. *Medical and Pediatric Oncology* 1989;17:418-423
15. Wang J, Weiss LM, Chang KL, et al. Diagnostic utility of bilateral bone marrow examination: significance of morphologic and ancillary technique study in malignancy. *Cancer* 2002;94:1522-1531
16. Kwee TC, Kwee RM, Verdonck LF, Bierings MB, Nievelstein RA. Magnetic resonance imaging for the detection of bone marrow involvement in malignant lymphoma. *Br J Haematol* 2008;141:60-68
17. Ribrag V, Vanel D, Leboulloux S, et al. Prospective study of bone marrow infiltration in aggressive lymphoma by three independent methods: whole-body MRI, PET/CT and bone marrow biopsy. *Eur J Radiol* 2008;66:325-331
18. Yasumoto M, Nonomura Y, Yoshimura R, et al. MR detection of iliac bone marrow involvement by malignant lymphoma with various MR sequences including diffusion-weighted echo-planar imaging. *Skeletal Radiol* 2002;31:263-269

19. Nakanishi K, Kobayashi M, Nakaguchi K, et al. Whole-body MRI for detecting metastatic bone tumor: diagnostic value of diffusion-weighted images. *Magn Reson Med Sci* 2007;6:147-155
20. Kwee TC, Kwee RM, Nievelstein RA. Imaging in staging of malignant lymphoma: a systematic review. *Blood* 2008;111:504-516
21. Vinnicombe SJ, Reznik RH. Computerised tomography in the staging of Hodgkin's disease and non-Hodgkin's lymphoma. *Eur J Nucl Med Mol Imaging* 2003;30 Suppl 1:S42-55
22. Juweid ME, Stroobants S, Hoekstra OS, et al; Imaging Subcommittee of International Harmonization Project in Lymphoma. Use of positron emission tomography for response assessment of lymphoma: consensus of the Imaging Subcommittee of International Harmonization Project in Lymphoma. *J Clin Oncol* 2007;25:571-578
23. Basu S, Torigian D, Alavi A. Evolving concept of imaging bone marrow metastasis in the twenty-first century: critical role of FDG-PET. *Eur J Nucl Med Mol Imaging* 2008;35:465-471
24. Pakos EE, Fotopoulos AD, Ioannidis JP. <sup>18</sup>F-FDG PET for evaluation of bone marrow infiltration in staging of lymphoma: a meta-analysis. *J Nucl Med* 2005;46:958-963
25. Padhani A, Husband J. 1998. Bone. In: Husband JES, Reznik RH (Eds.) *Imaging in Oncology*. Oxford: Isis Medical Media Ltd., pp. 765-786
26. Daldrup-Link HE, Henning T, Link TM. MR imaging of therapy-induced changes of bone marrow. *Eur Radiol* 2007;17:743-761





# Chapter 8<sup>1</sup>

Whole-body MRI, including diffusion-weighted imaging, for the initial staging of malignant lymphoma: comparison to computed tomography

Kwee TC, Quarles van Ufford HME, Beek FJ, Takahara T, Uiterwaal CS, Bierings MB, Ludwig I, Fijnheer R, Nivelstein RA

Invest Radiol 2009;44:683-690

## Abstract

### Purpose

To assess the value of whole-body magnetic resonance imaging (MRI), including diffusion-weighted imaging (DWI), for the initial staging of malignant lymphoma, compared with computed tomography (CT).

### Materials and methods

Thirty-one consecutive patients with newly diagnosed malignant lymphoma prospectively underwent whole-body MRI (T1-weighted and short inversion time inversion recovery [n=31], and DWI [n=28]) and CT. Ann Arbor stages were assigned by one radiologist according to whole-body MRI findings, and by another radiologist according to CT findings. Differences in staging between whole-body MRI (without and with DWI) and CT were resolved using other (imaging) studies (including <sup>18</sup>F-fluoro-2-deoxyglucose positron emission tomography and bone marrow biopsy) and follow-up studies as reference standard.

### Results

Staging results of whole-body MRI without DWI were equal to those of CT in 74% (23/31), higher in 26% (8/31), and lower in 0% (0/31) of patients, with correct/incorrect/unresolved overstaging relative to CT in 3, 2, and 2 patients, respectively, and incorrect staging of both modalities in 1 patient. Staging results of whole-body MRI with DWI were equal to those of CT in 75% (21/28), higher in 25% (7/28), and lower in 0% (0/28) of patients, with correct/incorrect overstaging relative to CT in 6 and 1 patient(s), respectively.

### Conclusion

Our results suggest that initial staging of malignant lymphoma using whole-body MRI (without DWI and with DWI) equals staging using CT in the majority of patients, while whole-body MRI never understaged relative to CT. Furthermore, whole-body MRI mostly correctly overstaged relative to CT, with a possible advantage of using DWI.

## Introduction

The malignant lymphomas, Hodgkin's disease (HD) and non-Hodgkin's lymphoma (NHL), comprise approximately 5% to 6% of all malignancies and are the fifth most frequently occurring type of cancer in the United States. Annually, an estimated 9260 new cases of HD and 81 850 new cases of NHL are diagnosed in the United States [1]. Once the diagnosis malignant lymphoma has been established by biopsy of a particular site, determination of disease extent (staging) is important for appropriate treatment planning and determining prognosis. In addition, knowing the sites of involvement at time of diagnosis makes it possible to accurately restage at the end of therapy and document a complete remission. Computed tomography (CT) is still the most commonly used imaging modality for initial staging of patients with malignant lymphoma, although its role is expected to be replaced by combined <sup>18</sup>F-fluoro-2-deoxyglucose positron emission tomography (FDG-PET)/CT [2]. Major disadvantages of CT, however, are the use of ionizing radiation and the application of a iodinated contrast agent, which may cause secondary cancers and induce allergic reactions, respectively [3-7]. Magnetic resonance (MR) imaging (MRI) does not have these disadvantages and may be an attractive alternative to CT. Technological advances, including the development of high-performance magnetic field gradients, parallel imaging, and the sliding table platform, made whole-body MRI clinically feasible [8-15]. Whole-body MRI has in particular shown potential for the staging of a variety of malignancies [8-15]. Furthermore, MRI is able to provide both anatomical and functional information within a single examination. In particular, the development and clinical application of whole-body diffusion-weighted imaging (DWI) is under active investigation. DWI allows visualization and measurement of the random (Brownian) extra-, intra-, and transcellular motion of water molecules, driven by their internal thermal energy (i.e. diffusion). Since many malignant tumors exhibit an impeded diffusion, whole-body DWI is a potentially powerful technique for the staging of malignancies, including malignant lymphomas [10, 16, 17]. In addition, whole-body DWI offers a high lesion-to-background contrast, making it a sensitive technique for the detection of lesions [10, 16, 17]. The purpose of this study was therefore to assess the value of whole-body MRI, including DWI, for the initial staging of malignant lymphoma, compared with CT.

## Materials and Methods

### Protocol, Support, and Funding

This prospective multicenter study was approved by the institutional review board of the University Medical Center Utrecht and was supported by ZonMw Program for Health Care Efficiency Research (grant number 80-82310-98-08012).

## Study participants

All patients were enrolled after they had been properly informed and provided written informed consent. Patients aged 8 years and older with newly diagnosed, histologically proven malignant lymphoma were prospectively included. All patients underwent whole-body MRI and CT within 15 days of diagnosis, in a random order, and before start of treatment. CT was performed as part of the routine clinical care. Patients with general contraindications to MRI, such as implanted pacemaker and claustrophobia, were excluded from enrollment. In total, thirty-one consecutive patients (17 men and 14 women; mean age, 46.5 years; age range, 12-82 years) with newly diagnosed, histologically proven malignant lymphoma (HD: n=7; NHL: n=23; non-specified lymphoproliferative disorder: n=1) prospectively underwent whole-body MRI and CT between May 2006 and December 2008 (**Table 1**). Whole-body MRI, including DWI, was performed in 28 patients. Three of 31 patients (aged 14, 78, and 82 years) did not tolerate the MRI examination for more than 30 minutes and only underwent conventional whole-body MRI (T1-weighted [T1W] and short inversion time [IR] inversion recovery [STIR]), without DWI.

**Table 1.** Baseline characteristics of included patients.

Characteristics	HD	NHL
No. of patients	7	23
Sex (n)		
Men	4	13
Women	3	10
Age (y)		
Mean ± SD	16.0 ± 2.9	57.1 ± 18.2
Range	13 - 22	12 - 81
Pathological subtype (n)		
Nodular sclerosing HD	6	
Lymphocyte-rich HD	1	
Follicular B-cell lymphoma		5
Diffuse large B-cell lymphoma		12
Mantle cell lymphoma		1
Mucosa-associated lymphoid tissue lymphoma		1
Small lymphocytic lymphoma		2
Anaplastic large cell lymphoma		2

## MRI

Whole-body MRI was performed using a 1.5-T system (Achieva, Philips Healthcare, Best, The Netherlands). Four spacers were placed on the original patient table. Subsequently, an additional table platform was mounted on top of these four spacers. In this way, sufficient space was created to freely move the lower part of a surface coil



over a distance of approximately 110 cm along the z-axis (necessary for DWI), without the need to reposition the patients who were lying on top of the additional table platform.

First, coronal T1W and STIR whole-body images were acquired, using the built-in body coil for signal reception. Images were acquired under free breathing, except for the stations covering the chest, abdomen, and pelvis, which were acquired using breathholding (T1W) or respiratory triggering (STIR). Applied sequence parameters for T1W were as follows: single-shot turbo spin-echo imaging, repetition time (TR)/echo time (TE) of 537/18 ms, slice thickness/gap of 6/1 mm, number of slices of 30 per station, field of view of  $530 \times 265 \text{ mm}^2$ , acquisition matrix of  $208 \times 287$ , number of signal averages of 1, acquired voxel size of  $1.27 \times 1.85 \times 6.00 \text{ mm}^3$ , reconstructed voxel size of  $1.04 \times 1.04 \times 6.00 \text{ mm}^3$ , scan time of 47 s per station, 7 stations in total. Applied sequence parameters for STIR were as follows: single-shot turbo spin-echo imaging, TR/TE/inversion time (IR) of 2444/64/165 ms, slice thickness/gap of 6/1 mm, number of slices of 30 per station, field of view of  $530 \times 265 \text{ mm}^2$ , acquisition matrix of  $336 \times 120$ , number of signal averages of 2, acquired voxel size of  $1.58 \times 2.21 \times 6.00 \text{ mm}^3$ , reconstructed voxel size of  $1.04 \times 1.04 \times 6.00 \text{ mm}^3$ , scan time of 44 s per station, 7 stations in total. Total actual scan time of T1W and STIR whole-body MRI was approximately 25-30 minutes.

Second, axial diffusion-weighted images of the head/neck, chest, abdomen, and pelvis were acquired under free breathing, using a 4-element phased-array surface coil for signal reception. This surface coil was sequentially moved to image the separate stations of the whole-body DWI examination, without patient repositioning. Applied sequence parameters for DWI of the head/neck station were as follows: single-shot spin-echo echo-planar imaging (EPI), TR/TE/IR of 8612/78/180 ms, slice thickness/gap of 4/0 mm, number of slices of 60, field of view of  $450 \times 360 \text{ mm}^2$ , acquisition matrix of  $128 \times 81$ , motion probing gradients in three orthogonal axes, b values of 0 and  $1000 \text{ s/mm}^2$ , number of signal averages of 3, half scan factor of 0.651, parallel imaging (SENSitivity Encoding) factor of 2, EPI factor of 43, acquired voxel size of  $3.52 \times 4.50 \times 4.00 \text{ mm}^3$ , reconstructed voxel size of  $1.76 \times 1.76 \times 4.00 \text{ mm}^3$ , and scan time of 4 minutes and 4 s. Applied sequence parameters for DWI of the chest, abdominal, and pelvic stations were identical, except for a TR of 6962 s, spectral presaturation inversion recovery fat suppression, and scan time of 3 minutes and 20 s for each of the three stations. Total actual scan time of whole-body DWI was approximately 20-25 minutes.

Seamless coronal whole-body T1W and STIR images were created by merging separately acquired stations using software implemented in the standard operating console. Axial diffusion-weighted images were first coronally reformatted with a slice thickness/gap of both 3.5/0mm and 7/0mm, and then merged to create seamless coronal whole-body diffusion-weighted images. Whole-body diffusion-weighted images were displayed using greyscale inversion.

## CT

CT scanning of the neck, chest, abdomen, and pelvis was performed using 16-, 40, and 64-slice CT scanners (Philips Brilliance, Philips Healthcare, Best, The Netherlands, and Somatom Sensation, Siemens Medical Systems, Knoxville, TN, USA). All patients ingested an oral contrast agent (Telebrix Gastro, Guerbet, The Netherlands) and received an intravenous non-ionic iodinated contrast agent (Ultravist 300, Schering, Berlin, Germany) before scanning. The administered amount of CT contrast agents was adjusted according to age and weight. All CT images were acquired with a slice thickness/increment of 1-1.5/0.7-0.8 mm, and were reconstructed to contiguous axial 5-mm slices. Tube voltage and tube setting were adjusted according to age, weight, and body region.

### Image analysis

All images were transferred to and interpreted by means of a Picture Archiving and Communications System that allows manual window level setting. A board-certified radiologist (RAJN, with 14 years of clinical experience with MRI), blinded to CT findings, evaluated two separate sets of whole-body MR images: the images from conventional whole-body MRI alone (T1W and STIR) and the combined conventional whole-body MR/whole-body diffusion-weighted images (T1W, STIR, and DWI). The CT images were evaluated by another board-certified radiologist (FJB, with 24 years of clinical experience with CT), who was blinded to MRI findings. The observers were aware that the patients had malignant lymphoma, but unaware of the type and grade of lymphoma and other imaging findings.

Presence and extent of nodal and extranodal pathology was systematically assessed by both the MR observer and the CT observer. Lymph nodes greater than 10 mm in the short-axis diameter were considered positive at all MR sequences and CT. At T1W, STIR, and CT images, extranodal pathology was evaluated as follows: area of abnormal attenuation/signal intensity (relative to the surrounding tissue) in the spleen, bone or bone marrow, and liver; nodule or infiltration in the lung; and mass of soft-tissue attenuation/abnormal signal intensity (relative to the surrounding tissue) in other extranodal sites. At DWI, several normal extranodal structures (including brain, salivary glands, tonsils, spleen, gallbladder, adrenal glands, prostate, testes, penis, endometrium, ovaries, spinal cord, peripheral nerves, and bone marrow) (may) exhibit an impeded diffusion [16, 17]. Any focally increased signal intensity in these structures at DWI was considered positive for tumor involvement. In all other areas, any signal intensity higher than that of the spinal cord was considered positive for tumor involvement. Apparent diffusion coefficient (ADC) measurements were not used for tissue characterization, because there are no ADC criteria yet for differentiating malignant from non-malignant lesions in DWI.

Subsequently, patients were classified according to the Ann Arbor staging system (stage I-IV) [18, 19].

## Data analysis

Agreement and disagreement between whole-body MRI (without and with DWI) and CT regarding staging according to the Ann Arbor staging system were calculated, along with binomial exact 95% confidence intervals (CIs), using Stata version 10 software (StataCorp LP, College Station, TX, USA).

Differences in staging between whole-body MRI (without and with DWI) and CT were resolved using other (imaging) studies (including FDG-PET and bone marrow biopsy) and follow-up studies (including CT) as the standard of reference, if available. The availability of these diagnostic tests depended on the request of the treating hematologist(s), blinded to the whole-body MRI findings. Of note, blind bone marrow biopsy was routinely performed in all patients with malignant lymphoma, independent of CT, FDG-PET or other imaging findings. FDG-PET and bone marrow biopsy are highly specific for the diagnosis of bone marrow involvement in malignant lymphoma, but lack sensitivity [20-24]. Therefore, when FDG-PET or bone marrow biopsy demonstrated bone marrow involvement, bone marrow involvement was confirmed. However, when FDG-PET or bone marrow biopsy did not demonstrate bone marrow involvement, bone marrow involvement could not be excluded. Parenchymal lesions of FDG avid malignant lymphomas (including HD, diffuse large B-cell lymphoma, follicular lymphoma, and mantle cell lymphoma) are well visualized at FDG-PET [25, 26], with high sensitivity and specificity when combined with anatomical imaging, such as CT or MRI [2]. Therefore, parenchymal lesions seen both at FDG-PET and CT or MRI were considered positive for the presence of malignant lymphoma. Furthermore, parenchymal lesions not seen at FDG-PET were considered negative for the presence of malignant lymphoma. Finally, lesions that decreased in size at follow-up imaging were considered positive for the presence of malignant lymphoma.

## Results

Results, including causes and locations of discrepant staging between CT and whole-body MRI (without and with DWI) are summarized in **Tables 2 and 3**, and representative examples are displayed in **Figures 1 to 5**. In 23 of 31 patients (74%; 95% CI: 57-86%), whole-body MRI without DWI and CT were in agreement regarding assigned Ann Arbor stage. In 8 of 31 patients (26 %; 95% CI: 14-43%) staging results of whole-body MRI without DWI were higher than those of CT, while whole-body MRI without DWI never understaged relative to CT. In three patients, whole-body MRI correctly overstaged relative to CT, while in two other patients, whole-body MRI incorrectly overstaged relative to CT (**Figures 3 and 4**). Furthermore, in one patient both whole-body MRI without DWI and CT incorrectly staged, while in another two patients the causes of discrepant staging remained unresolved.

**Table 2.** Comparisons among CT, MRI without DWI, and MRI with DWI with respect to equal staging, overstaging, and understaging relative to each other.

<b>Comparison</b>	<b>Equal staging</b>	<b>Overstaging</b>	<b>Understaging</b>
MRI without DWI relative to CT	74.2% (23/31)	25.8% (8/31)	0.0% (0/31)
MRI with DWI relative to CT	75.0% (21/28)	25.0% (7/28)	0.0% (0/28)
MRI with DWI relative to MRI without DWI	82.1% (23/38)	10.7% (3/28)	7.1% (2/28)

In 21 of 28 patients (75%; 95% CI: 57-87%), whole-body MRI with DWI and CT were in agreement regarding assigned Ann Arbor stage. In 7 of 28 patients (25 %; 95% CI: 13-43%) staging results of whole-body MRI with DWI were higher than those of CT, while whole-body MRI with DWI never understaged relative to CT. Whole-body MRI with DWI correctly overstaged relative to CT in 6 patients, but incorrectly overstaged one patient.

In 23 of 28 patients (82%; 95% CI: 64-92%), whole-body MRI without DWI and whole-body with DWI were in agreement regarding assigned Ann Arbor stage. Disagreement between whole-body MRI without DWI and whole-body with DWI occurred in 5 of 28 patients (18%; 95% CI: 8-36%), of which 4 were correctly staged by whole-body DWI with DWI, while one case remained unresolved.

**Table 3.** Discrepant Ann Arbor stages among CT, MRI without DWI, and MRI with DWI, causes of discrepancy in staging, findings of other (imaging) studies and/or follow-up studies, and final Ann Arbor stage.

Patient	Ann Arbor stage		Causes of discrepancy in staging		Findings of other (imaging) studies and/or follow-up studies	Final Ann Arbor stage
	CT	MRI without DWI	MRI with DWI	MRI without DWI		
1	I	I	II	-Bilateral cervical lymph node involvement only at MRI with DWI	Sizes of bilateral cervical lymph nodes decrease at follow-up imaging	II
15	II	IV	IV	-Sternal lesion only at MRI without DWI -Lung lesion and perianal lesion only at MRI with DWI	No sternal lesion at FDG-PET, but high FDG uptake left hilar lymph node and perianal lesion at FDG-PET	IV
17	III	IV	IV	-Right axillary and splenic lymph node involvement only at CT -Waldayer's ring involvement only at MRI without DWI -Mesenteric lymph node involvement and bone marrow involvement only at MRI without and with DWI	Sizes of axillary lymph nodes and size of spleen decrease, and mesenteric lesion appears to be an accessory spleen at follow-up imaging; positive bone marrow biopsy	IV
18	I	I	II	-Mesenteric lymph node involvement only at MRI with DWI	Size of mesenteric lymph node decreases at follow-up imaging	II
20	I	II	II	-Cervical lymph node and Waldayer's ring involvement only at MRI without and with DWI	Decrease in size of cervical lymph nodes at follow-up imaging	II
21	III	IV	NA	-Rib involvement, gastrointestinal/mesenteric mass, liver and kidney involvement only at MRI without DWI	Negative iliac crest bone marrow biopsy; no osseous, liver, or kidney lesions at FDG-PET	Unresolved

Table 3. Continued

Patient	Ann Arbor stage		Causes of discrepancy in staging	Findings of other (imaging) studies and/or follow-up studies	Final Ann Arbor stage
	CT	MRI with/without DWI			
25	II	III	-Left infraclavicular, paraaortic and left inguinal lymph node involvement only at MRI without DWI	No infradiaphragmatic disease at FDG-PET, in FDG-avid lymphoma	II
27	I	IV	-Acetabular bone marrow involvement only at MRI without DWI	No bone marrow lesions at FDG-PET, iliac crest bone marrow biopsy negative	Unresolved
31	I	II	-Left cervical lymph node involvement only at MRI without and with DWI -Waldeyer's ring involvement only at MRI with DWI	Only left axillary lymph node involvement at FDG-PET	I

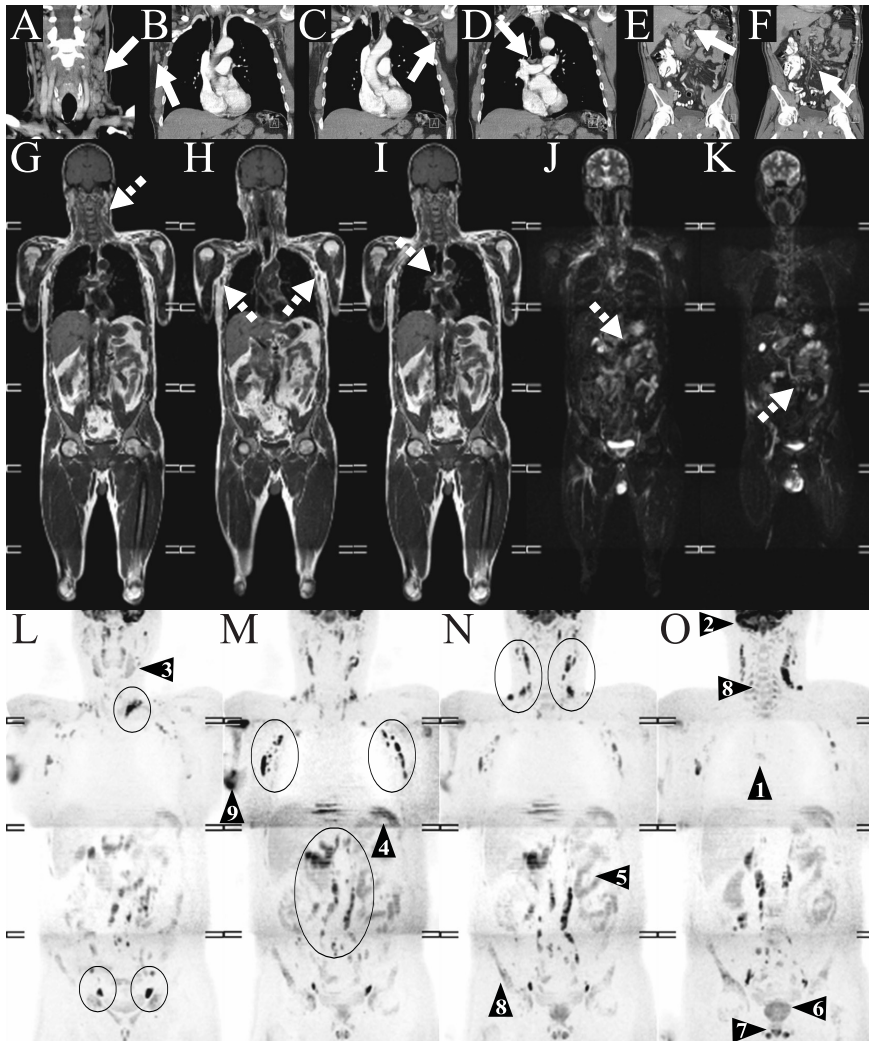


**Figure 1.** A 56-year-old man with stage III small lymphocytic lymphoma, at both CT (upper row, A-F), conventional (T1W and STIR) whole-body MRI (middle row, G-K), and whole-body DWI (lower row, L-O). Coronally reformatted CT images of the neck (A), chest (B-D), and abdomen/pelvis (E-F) (different image magnifications) show cervical, axillary, mediastinal, paraaortal, and mesenteric lymph node involvement (continuous arrows). Identical lesions are detected at T1W whole-body MRI (G-I) and STIR whole-body MRI (J, K) (dashed arrows). Whole-body DWI highlights all pathological lymph nodes (encircled) with superior lesion-to-background contrast compared to CT and conventional whole-body MRI. However, note that the mediastinal lesion exhibited only low signal intensity at whole-body DWI, probably due to (incoherent) cardiac motion (O, arrowhead 1). Also note that several normal structures are highlighted at whole-body DWI, including brain (O, arrowhead 2), salivary glands (L, arrowhead 3), spleen (M, arrowhead 4), small intestines (N, arrowhead 5), prostate (O, arrowhead 6), penis (O, arrowhead 7), and bone marrow (N and O, arrowhead 8). However, these organs do not show any focally increased signal intensity that would suggest lymphomatous involvement. Furthermore, note the poorly suppressed fat in the right upper extremity. However, since the DWI dataset is three-dimensional, and images can be reformatted and evaluated in any plane, residual fat signal can usually easily be discriminated from lymphomatous lesions.



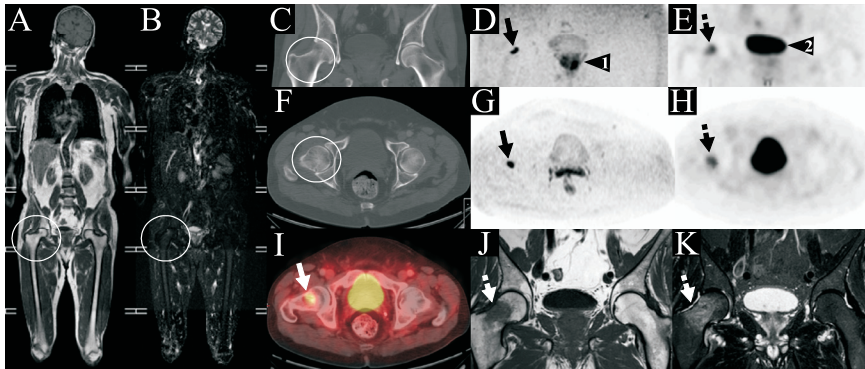


**Figure 2.** A 62-year-old man with diffuse large B-cell lymphoma (patient 24, **Table 3**), in whom bone marrow involvement was only detected at whole-body DWI, and missed at both CT, conventional (T1W and STIR) whole-body MRI, and blind bone marrow biopsy of the iliac crest. T1W whole-body MRI (**A**) and STIR whole-body MRI (**B**) show minimal focal hypointense and hyperintense signal in the right femoral bone marrow (encircled), respectively. However, this lesion was missed when evaluating conventional whole-body MRI only. Coronally reformatted CT (**C**) and axial CT (**F**) of the pelvic region do not show any evident femoral bone lesion either (encircled). However, coronally reformatted DWI (**D**) and axial DWI (**G**) of the pelvic region clearly show a lesion in the right femoral bone marrow (continuous black arrows). The lesion is also depicted at coronally reformatted FDG-PET (**E**) and axial FDG-PET (**H**) of the pelvic region (dashed black arrows), FGG-PET/CT fusion (**I**) (continuous white arrow), and dedicated follow-up T1W (**J**) and STIR MRI (**K**) (dashed white arrows). A second image-guided biopsy confirmed the femoral bone marrow lesion. Note the similarity between DWI (**D**, **G**) and FDG-PET (**E**, **H**), although the lesion is better delineated at DWI, thanks to its higher spatial resolution. Also note the normal appearing prostate at DWI (**D**, arrowhead 1) and normal FDG accumulation in the bladder at FDG-PET (**E**, arrowhead 2).

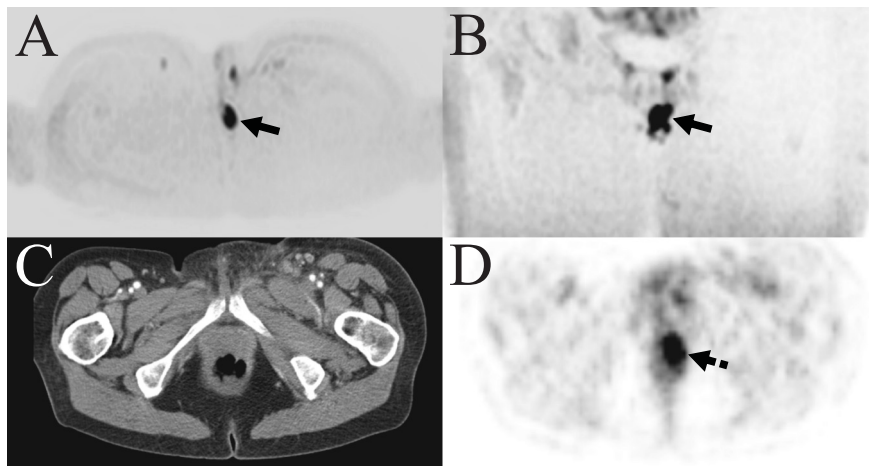


**Figure 3.** A 52-year-old woman with diffuse large B-cell lymphoma (patient 15, **Table 3**), in whom a perianal lesion was detected at whole-body DWI, but remained undiagnosed at CT. Axial (**A**) and coronally reformatted DWI (**B**) of the pelvic region show a perianal lesion exhibiting an impeded diffusion (arrows). The lesion was not depicted at axial CT (**C**). Axial FDG-PET (**D**) confirms the lesion (dashed arrow). Despite the fact that this is an unlikely location for malignant lymphoma, the fact that it was detected is clinically important. Although the true nature of this perianal lesion was uncertain, it was initially classified as a lymphomatous. Of note, the lesion disappeared at follow-up imaging.



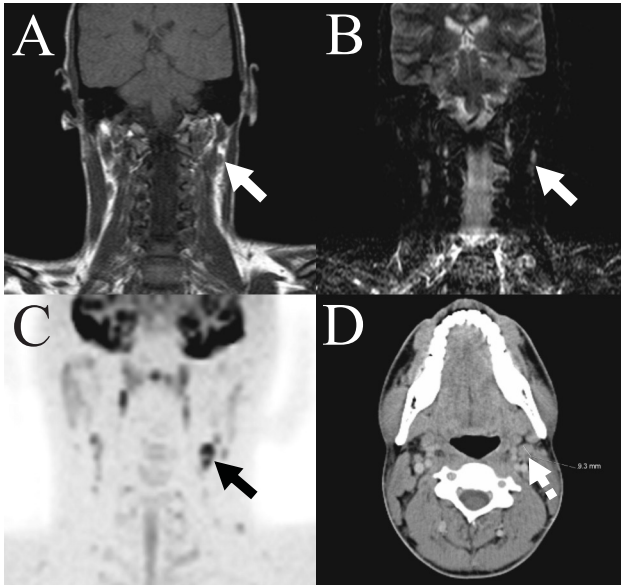


**Figure 4.** A 22-year-old man with anaplastic large cell lymphoma (patient 31, Table 3), in whom whole-body MRI (without and with DWI) incorrectly diagnosed a cervical lymph node as malignant. Coronal T1W (A), STIR (B), and DWI (C) depicted a left cervical lymph node with a short-axis diameter that slightly exceeded the maximum upper limit of 10 mm (arrows). At CT (D), this lymph node had a short-axis diameter just below the upper limit of 10 mm (dashed arrow). This cervical lymph node was negative at FDG-PET (not shown), indicating a false-positive MRI result.

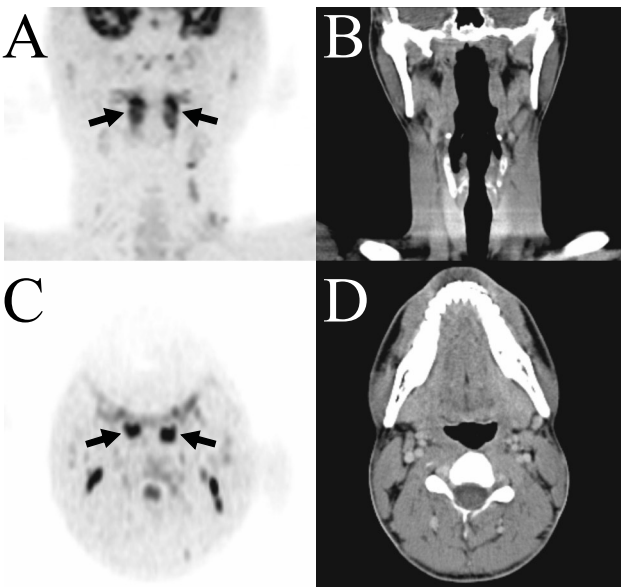


**Figure 5.** A 22-year-old man with anaplastic large cell lymphoma (patient 31 (same patient as in Figure 4), Table 3) in whom Waldeyer's ring involvement was incorrectly diagnosed at DWI. Coronally reformatted DWI (A) and axial DWI (C) show high signal intensity in the area of Waldeyer's ring. This normal finding was mistaken for lymphomatous involvement. Corresponding coronally reformatted CT (B) and axial CT (D) show no lesions. FDG-PET did not show any pathologically increased FDG uptake, confirming that Waldeyer's ring was not involved.

## Discussion

CT is the most commonly used imaging modality for staging malignant lymphoma because of its widespread availability and relatively low cost. Although combined FDG-PET/CT is gradually replacing CT, it has not been proven yet that it is diagnostically superior and more cost-effective than CT in the initial staging of malignant lymphoma. Therefore, CT is still the standard imaging modality for initial staging of malignant lymphoma [2]. A major disadvantage of CT is exposure of the patient to ionizing radiation, which may induce secondary cancers. In the present era, where HD can be cured in at least 80% of patients [27] and similar proceedings have been achieved in the treatment of certain types of NHLs [28, 29], prevention of secondary malignancies due to CT radiation is an important issue. Another disadvantage of CT is the administration of iodinated contrast agents, which may cause adverse reactions, including rarely occurring but life-threatening contrast-induced nephrotoxicity and anaphylactic shock [7]. Whole-body MRI does not have these disadvantages and may therefore be an attractive alternative.

Two previous studies reported the feasibility of whole-body MRI using STIR [30, 31]. Brennan et al. [30] performed a study in 23 adults (both for initial staging and restaging) and reported that whole-body MRI using STIR enables disease staging and that it compared favourably with CT for the detection of lymph nodes larger than 12 mm in short-axis diameter and for the detection of bone marrow involvement. Kellenberger et al. [31] performed a study in 8 children (both for initial staging and restaging) and reported that whole-body MRI using STIR is a sensitive technique for staging malignant lymphoma and that it is superior to blind bone marrow biopsy and conventional imaging (including CT, gallium-67 scintigraphy, and bone scintigraphy) in the detection of bone marrow involvement, at initial diagnosis. However, whole-body MRI using STIR lacked specificity for diagnosing recurrent or residual disease [31].

In the present study, we used conventional whole-body MR sequences (T1W and STIR), along with whole-body DWI, which is a novel approach of assessing tumors and metastases throughout the entire body [10, 16, 17]. Our initial results indicate that in the majority of patients staging using whole-body MRI (without and with DWI) equals staging using CT (**Figure 1**). Whole-body MRI (without and with DWI) never understaged relative to CT, which reflects the inherent higher sensitivity of MRI for the detection of lesions, thanks to its sufficiently high spatial resolution and superior soft tissue contrast. Furthermore, in most cases, whole-body MRI (without and with DWI) correctly overstaged relative to CT.

Of note, whole-body MRI without DWI detected one case of bone marrow involvement which was missed at CT (patient 17, **Table 3**), while whole-body MRI with DWI detected two cases of bone marrow involvement, which were all missed at CT

(patients 17 and 24, **Table 3**). This well reflects one of the weaknesses of CT, in that it is not reliable in the detection of bone marrow disease [32], while MRI has excellent sensitivity for the detection of bone marrow involvement [33], which, if present, by definition indicates stage IV disease [18, 19]. At present, blind bone marrow biopsy, usually unilateral, is the standard method to evaluate the bone marrow [18].

However, bone marrow biopsy is prone to sampling errors and therefore has a limited sensitivity [20-23]. In one patient (patient 24, **Table 3**), a first blind bone marrow biopsy of the iliac crest was negative, but whole-body MRI with DWI suggested the presence of a femoral bone marrow lesion (**Figure 2**). A second image-guided biopsy confirmed the femoral bone marrow lesion. Thus, regardless of the small number of cases in the present study, whole-body MRI-guided bone marrow biopsy has the potential to reduce sampling errors [33]. In addition, this approach may reduce the number of unnecessary bone marrow biopsies, which are invasive, painful, and have a small but non-negligible risk of complications [33, 34]. Causes of the remaining correctly overstaged cases relative to CT are probably related to the inherent higher sensitivity of MRI for the detection of lesions. Interestingly, the number of correctly overstaged patients using whole-body MRI with DWI was higher than using whole-body MRI without DWI. This may be related to the fact that whole-body DWI is able to highlight (subtle) lesions that can be overlooked at conventional whole-body MRI (T1W and STIR) [16]. Thus, although future studies with larger sample sizes are necessary, our initial results support the use of whole-body DWI as a useful adjunct to conventional whole-body MRI for the initial staging of malignant lymphoma.

One patient (patient 25, **Table 3**) was incorrectly overstaged relative to CT at whole-body MRI without DWI, while another patient (patient 31, **Table 3**) was incorrectly overstaged relative to CT at both whole-body MRI without DWI and whole-body MRI with DWI. This was due to the fact that in both patients certain lymph nodes had a short-axis diameter that was slightly larger than 10 mm at whole-body MRI, whereas these lymph nodes were smaller than 10 mm at CT (**Figure 4**). Explanations for this discrepancy are slight variation in the method of measurement between the two observers and the fact that lymph nodes were measured in the coronal plane at T1 and STIR whole-body MRI, whereas they were measured in the axial plane at CT (**Figure 4**). Furthermore, in one of the two patients (patient 31, **Table 3**) Waldeyer's ring involvement was incorrectly diagnosed at whole-body DWI (**Figure 5**). This can be explained by the fact that the normal Waldeyer's ring already has a high signal intensity at DWI [16, 17], which, in this case, was erroneously mistaken to represent lymphomatous involvement (**Figure 5**). Although the number of correctly overstaged patients is considerably higher than the number that was incorrectly overstaged, future studies are required to determine the possible consequences of incorrect overstaging relative to CT. In addition, although this was not done in the present study, perhaps the use of ADC measurements in equivocal lymph nodes may increase

the diagnostic performance of MRI in the initial staging of malignant lymphoma. Of note, a few studies [35-37] reported significantly lower ADCs of malignant lymphoma compared to non-metastatic lymph nodes.

A limitation of the present study is the lack of a true gold standard, because most lesions detected by whole-body MRI (without and with DWI) and CT were not histologically proven. Clarifying all discrepant findings between whole-body MRI (without and with DWI) and CT with biopsy would be most desirable, but was practically and ethically not possible. Instead, a careful use of findings of other (imaging) studies (FDG-PET and bone marrow biopsy) and follow-up studies, if available, was used to resolve discrepancies. Nonetheless, discrepant findings could not be resolved in two patients (patients 21 and 27, **Table 3**). Furthermore, lymph nodes greater than 10 mm in the short-axis diameter were considered positive, although it is well known that size criteria lack the desired accuracy for characterizing lymph nodes [38]. Nevertheless, this is still the best available approach in clinical practice. Although still imperfect, using (combined) FDG-PET/CT as the reference standard may be an alternative approach. However, FDG-PET and/or combined FDG-PET/CT are not yet routinely performed in all patients with newly diagnosed malignant lymphoma in our hospital. Another limitation is that only patients with newly diagnosed malignant lymphoma were included, and it is still unclear how whole-body MRI (without and with DWI) performs in the follow-up and restaging of malignant lymphoma. Future studies should also determine the intra- and interobserver variability of whole-body MRI (without and with DWI). Interestingly, to the best of our knowledge, such a reproducibility study has never been performed for CT either, although CT has been used for staging malignant lymphoma for over two decades [2, 39]. Another unsolved issue is the cost-effectiveness of whole-body MRI. It should be realized that whole-body MRI is a relatively time-consuming examination (in the present study the complete whole body MRI examination, including DWI, took approximately 45-55 minutes). Therefore, patient throughput is relatively low compared to CT and combined PET/CT scanners, which are currently able to perform a whole-body examination in less than 15 s and less than 20 minutes, respectively. On the other hand, the costs for a whole-body MRI examination are approximately two times less than that of a whole-body FDG-PET/CT examination [40]. Furthermore, in contrast to FDG-PET, whole-body MRI does not require any fasting before scanning and does not use any radiotracers. Last but not least, the absence of ionizing radiation (thereby eliminating the risk of secondary malignancies due to CT radiation, which is especially of concern in children) and the absence of iodinated contrast agents (thereby eliminating the risk of CT contrast agent-induced adverse reactions) favor whole-body MRI. In addition, the present study also showed that whole-body MRI can be successfully performed without using gadolinium-based MR contrast agents, which may cause nephrogenic systemic fibrosis (a potentially disabling and life-threatening disease) in patients with renal failure [41].

Thus, a cost-effectiveness analysis is required.

In conclusion, our results suggest that initial staging of malignant lymphoma using whole-body MRI (without DWI and with DWI) equals staging using CT in the majority of patients, while whole-body MRI never understaged relative to CT. Furthermore, whole-body MRI mostly correctly overstaged relative to CT, with a possible advantage of using DWI. Future studies with larger sample sizes are necessary to confirm the assumed advantage of whole-body MRI and DWI over CT.

### Acknowledgement

This study was supported by ZonMw Program for Health Care Efficiency Research (grant number 80-82310-98-08012). Furthermore, the authors would like to thank Willem P.Th.M. Mali, MD, PhD, Professor, University Medical Center Utrecht (Department of Radiology) for his contribution to this study.

## References

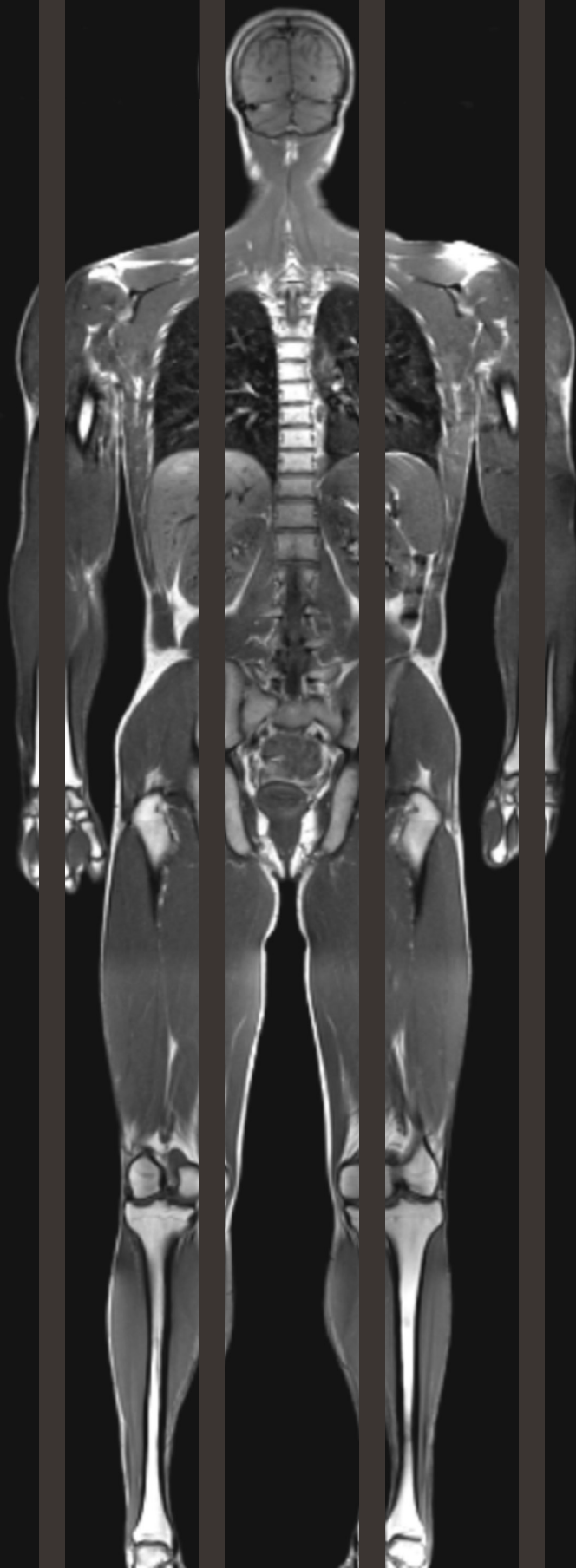
1. Jemal A, Siegel R, Ward E, Murray T, Xu J, Thun MJ. Cancer statistics, 2007. *CA Cancer J Clin* 2007;57:43-66
2. Kwee TC, Kwee RM, Niveststein RA. Imaging in staging of malignant lymphoma: a systematic review. *Blood* 2008;111:504-516
3. Brenner DJ, Hall EJ. Computed tomography--an increasing source of radiation exposure. *N Engl J Med* 2007;357:2277-2284
4. Semelka RC, Armao DM, Elias J Jr, Huda W. Imaging strategies to reduce the risk of radiation in CT studies, including selective substitution with MRI. *J Magn Reson Imaging* 2007;25:900-909
5. Barentsz J, Takahashi S, Oyen W, Mus R, De Mulder P, Reznik R, Oudkerk M, Mali W. Commonly used imaging techniques for diagnosis and staging. *J Clin Oncol* 2006;24:3234-3244
6. Executive Summary Board on Radiation Effects Research—Division on Earth and Life Studies editor Health Risks from Exposure to Low Levels of Ionizing Radiation: BEIR VII—Phase 2. Washington, DC: National Academy Press; 2005
7. Namasivayam S, Kalra MK, Torres WE, Small WC. Adverse reactions to intravenous iodinated contrast media: a primer for radiologists. *Emerg Radiol* 2006;12:210-215
8. Lauenstein TC, Semelka RC. Emerging techniques: whole-body screening and staging with MRI. *J Magn Reson Imaging* 2006;24:489-498
9. Plathow C, Aschoff P, Lichy MP, et al. Positron emission tomography/computed tomography and whole-body magnetic resonance imaging in staging of advanced nonsmall cell lung cancer--initial results. *Invest Radiol* 2008;43:290-297
10. Lichy MP, Aschoff P, Plathow C, et al. Tumor detection by diffusion-weighted MRI and ADC-mapping--initial clinical experiences in comparison to PET-CT. *Invest Radiol* 2007;42:605-613
11. Schmidt GP, Wintersperger B, Graser A, Baur-Melnyk A, Reiser MF, Schoenberg SO. High-resolution whole-body magnetic resonance imaging applications at 1.5 and 3 Tesla: a comparative study. *Invest Radiol* 2007;42:449-459
12. Schmidt GP, Baur-Melnyk A, Herzog P, et al. High-resolution whole-body magnetic resonance image tumor staging with the use of parallel imaging versus dual-modality positron emission tomography-computed tomography: experience on a 32-channel system. *Invest Radiol* 2005;40:743-753
13. Schlemmer HP, Schäfer J, Pfannenbergl C, et al. Fast whole-body assessment of metastatic disease using a novel magnetic resonance imaging system: initial experiences. *Invest Radiol* 2005;40:64-71
14. Lauenstein TC, Goehde SC, Herborn CU, Goyen M, Oberhoff C, Debatin JF, Ruehm SG, Barkhausen J. Whole-body MR imaging: evaluation of patients for metastases. *Radiology* 2004;233:139-148
15. Antoch G, Vogt FM, Freudenbergl LS, Nazaradeh F, Goehde SC, Barkhausen J, Dahmen G, Bockisch A, Debatin JF, Ruehm SG. Whole-body dual-modality PET/CT and whole-body MRI for tumor staging in oncology. *JAMA* 2003;290:3199-3206
16. Kwee TC, Takahara T, Ochiai R, Niveststein RA, Luijten PR. Diffusion-weighted whole-body imaging with background body signal suppression (DWIBS): features and potential applications in oncology. *Eur Radiol* 2008;18:1937-1952

17. Takahara T, Imai Y, Yamashita T, Yasuda S, Nasu S, Van Cauteren M. Diffusion weighted whole body imaging with background body signal suppression (DWIBS): technical improvement using free breathing, STIR and high resolution 3D display. *Radiat Med* 2004;22:275-282
18. Lister TA, Crowther D, Sutcliffe SB, Glatstein E, Canellos GP, Young RC, Rosenberg SA, Coltman CA, Tubiana M. Report of a committee convened to discuss the evaluation and staging of patients with Hodgkin's disease: Cotswolds meeting. *J Clin Oncol* 1989;7:1630-1636
19. Armitage JO. Staging non-Hodgkin lymphoma. *CA Cancer J Clin.* 2005;55:368-376.
20. Brunning RD, Bloomfield CD, McKenna RW, Peterson LA. Bilateral trephine bone marrow biopsies in lymphoma and other neoplastic diseases. *Ann Intern Med* 1975;82:365-366
21. Coller BS, Chabner BA, Gralnick HR. Frequencies and patterns of bone marrow involvement in non-Hodgkin lymphomas: observations on the value of bilateral biopsies. *Am J Hematol* 1977;3:105-119
22. Haddy TB, Parker RI, Magrath IT. Bone marrow involvement in young patients with non-Hodgkin's lymphoma: the importance of multiple bone marrow samples for accurate staging. *Med Pediatr Oncol* 1989;17:418-423
23. Wang J, Weiss LM, Chang KL, Slovak ML, Gaal K, Forman SJ, Arber DA. Diagnostic utility of bilateral bone marrow examination: significance of morphologic and ancillary technique study in malignancy. *Cancer* 2002;94:1522-1531
24. Pakos EE, Fotopoulos AD, Ioannidis JP. 18F-FDG PET for evaluation of bone marrow infiltration in staging of lymphoma: a meta-analysis. *J Nucl Med* 2005;46:958-963
25. Tsukamoto N, Kojima M, Hasegawa M, Oriuchi N, Matsushima T, Yokohama A, Saitoh T, Handa H, Endo K, Murakami H. The usefulness of (18)F-fluorodeoxyglucose positron emission tomography ((18)F-FDG-PET) and a comparison of (18)F-FDG-pet with (67)gallium scintigraphy in the evaluation of lymphoma: relation to histologic subtypes based on the World Health Organization classification. *Cancer* 2007;110:652-659
26. Elstrom R, Guan L, Baker G, Nakhoda K, Vergilio JA, Zhuang H, Pitsilos S, Bagg A, Downs L, Mehrotra A, Kim S, Alavi A, Schuster SJ. Utility of FDG-PET scanning in lymphoma by WHO classification. *Blood* 2003;101:3875-3876
27. Connors JM. State-of-the-art therapeutics: Hodgkin's lymphoma. *J Clin Oncol* 2005;23:6400-6408
28. Ansell SM, Armitage J. Non-Hodgkin lymphoma: diagnosis and treatment. *Mayo Clin Proc.* 2005;80:1087-1097
29. Hennessy BT, Hanrahan EO, Daly PA. Non-Hodgkin lymphoma: an update. *Lancet Oncol* 2004;5:341-353
30. Brennan DD, Gleeson T, Coate LE, Cronin C, Carney D, Eustace SJ. A comparison of whole-body MRI and CT for the staging of lymphoma. *AJR Am J Roentgenol* 2005;185:711-716
31. Kellenberger CJ, Miller SF, Khan M, Gilday DL, Weitzman S, Babyn PS. Initial experience with FSE STIR whole-body MR imaging for staging lymphoma in children. *Eur Radiol* 2004;14:1829-1841
32. Vinnicombe SJ, Reznik RH. Computerised tomography in the staging of Hodgkin's disease and non-Hodgkin's lymphoma. *Eur J Nucl Med Mol Imaging* 2003;30 Suppl 1:S42-S55
33. Kwee TC, Kwee RM, Verdonck LF, Bierings MB, Nievelstein RA. Magnetic resonance imaging for the detection of bone marrow involvement in malignant lymphoma. *Br J Haematol* 2008;141:60-68
34. Bain BJ. Morbidity associated with bone marrow aspiration and trephine biopsy - a review of UK data for 2004. *Haematologica* 2006;91:1293-1294

35. Sumi M, Sakihama N, Sumi T, et al. Discrimination of metastatic cervical lymph nodes with diffusion-weighted MR imaging in patients with head and neck cancer. *AJNR Am J Neuroradiol* 2003;24:1627-1634
36. Sumi M, Van Cauteren M, Nakamura T. MR microimaging of benign and malignant nodes in the neck. *AJR Am J Roentgenol* 2006;186:749-757
37. Abdel Razek AA, Soliman NY, Elkhamary S, Alsharaway MK, Tawfik A. Role of diffusion-weighted MR imaging in cervical lymphadenopathy. *Eur Radiol* 2006;16:1468-1477
38. Torabi M, Aquino SL, Harisinghani MG. Current concepts in lymph node imaging. *J Nucl Med* 2004;45:1509-1518
39. Kreel L. The EMI whole body scanner in the demonstration of lymph node enlargement. *Clin Radiol* 1976;27:421-429
40. Plathow C, Walz M, Lichy MP, Aschoff P, Pfannenbergl C, Bock H, Eschmann SM, Claussen CD, Schlemmer HP. Cost considerations for whole-body MRI and PET/CT as part of oncologic staging. *Radiologe* 2008;48:384-396
41. Thomsen HS. Nephrogenic systemic fibrosis: A serious late adverse reaction to gadodiamide. *Eur Radiol* 2006;16:2619-2621







# Chapter 8<sup>2</sup>

Whole-body MRI, including  
diffusion-weighted imaging,  
for staging newly diagnosed  
lymphoma: comparison to  
computed tomography  
in 101 patients

Kwee TC, Vermoolen MA, Akkerman EA, Kersten MJ, Fijnheer R,  
Ludwig I, Beek FJ, Van Leeuwen MS, Bierings MB, Zsiros J, Quarles van Ufford HME,  
De Klerk JMH, Adam J, Stoker J, Uiterwaal CS, Nievelstein RA

In submission

## Abstract

### Purpose

To compare whole-body magnetic resonance imaging (MRI), including diffusion-weighted imaging (DWI), to computed tomography (CT) for staging newly diagnosed lymphoma.

### Materials and methods

One hundred and one consecutive patients with newly diagnosed lymphoma prospectively underwent whole-body MRI (T1-weighted and T2-weighted short inversion time inversion recovery [n=101], and DWI [n=96]) and CT. Ann Arbor stages were assigned according to whole-body MRI and CT findings. Disagreements in staging between whole-body MRI (without and with DWI) and CT were resolved using bone marrow biopsy, <sup>18</sup>F-fluoro-2-deoxyglucose positron emission tomography (FDG-PET), and follow-up FDG-PET, CT, and whole-body MRI studies as reference standard.

### Results

Staging results of whole-body MRI without DWI were equal to those of CT in 65.4% (66/101), higher in 30.7% (31/101), and lower in 4.0% (4/100) of patients, with correct/incorrect/unresolved overstaging and incorrect/unresolved understaging relative to CT in 13/12/6 and 3/1 patient(s), respectively. Staging results of whole-body MRI with DWI were equal to those of CT in 62.5% (60/96), higher in 32.3% (31/96), and lower in 5.2% (5/96) of patients, with correct/incorrect/unresolved overstaging and incorrect/unresolved understaging relative to CT in 18/10/3 and 4/1 patient(s), respectively.

### Conclusion

Staging of newly diagnosed lymphoma using whole-body MRI (without and with DWI) equals staging using CT in the majority of patients. Disagreements between whole-body MRI and CT are mostly caused by overstaging of the former relative to the latter, with the number of correctly and incorrectly overstaged cases being approximately equal. The potential advantage of DWI is still unproven.

## Introduction

The lymphomas, Hodgkin lymphoma (HL) and non-Hodgkin lymphoma (NHL), comprise approximately 5% to 6% of all malignancies and are the fifth most frequently occurring type of cancer in the Western world [1]. Accurate staging of lymphoma is of major importance, because of its prognostic and therapeutic implications [2-3]. Computed tomography (CT) is still the most commonly used imaging modality for staging newly diagnosed lymphoma [4]. In addition to CT, it is recommended to perform baseline <sup>18</sup>F-fluoro-2-deoxyglucose positron emission tomography (FDG-PET) to facilitate the interpretation of posttreatment FDG-PET [5, 6]. However, the benefit of performing baseline FDG-PET has not been proven yet. An important disadvantage of CT is the use of ionizing radiation, which may cause second cancers in later life [7]. Because the survival rates of patients with HL and NHL have considerably increased over the past few decades, the goal of current therapies is to maximize cure rates while minimizing late toxicity such as infertility, premature menopause, cardiac disease, and, very importantly, risk of second neoplasms [2-4]. In line with the objective of this treatment paradigm, prevention of radiation-induced cancer associated with CT scanning is becoming increasingly important. Whole-body magnetic resonance imaging (MRI) is feasible [9-13] and may be a good radiation-free alternative to CT for staging lymphoma. Furthermore, the implementation of diffusion-weighted imaging (DWI) in a whole-body MRI protocol may be of advantage. DWI is an MRI sequence that is sensitive to the random (Brownian) motion of water molecules. Many malignant tumors, including lymphomas, exhibit an impeded water diffusion and can be highlighted at DWI. Because of its potentially high lesion-to-background contrast, DWI may facilitate image evaluation and improve staging accuracy [14, 15]. Until now, only a few studies with a relatively small number of patients have investigated the utility of whole-body MRI for staging lymphoma [9-13], and only a few feasibility studies have applied DWI in this setting [11, 13]. Larger scale studies are necessary to determine whether whole-body MRI can be a good alternative to CT for staging newly diagnosed lymphoma. The purpose of this prospective study in 101 consecutive patients was therefore to compare whole-body MRI, including DWI, to CT for staging newly diagnosed lymphoma.

## Materials and Methods

### Protocol, Support, and Funding

This prospective multicenter study was approved by the institutional review boards of the University Medical Center Utrecht, the Meander Medical Center Amersfoort, and the Academic Medical Center Amsterdam. The Dutch Organization for Health Research and Development (ZonMw), Health Care Efficiency Research programme, funded the study (ZonMw grant number 80-82310-98-08012). ZonMw approved the

study protocol after consulting national and international independent reviewers. Data collection, data analysis, and interpretation of data, writing of the paper, and decision to submit were left to the authors' discretion and were not influenced by ZonMw.

### *Patients*

All patients were enrolled after they had been properly informed and provided written informed consent. Patients aged 8 years and older with newly diagnosed, histologically proven lymphoma were prospectively included. All patients were consecutively enrolled (May 2006 - October 2010) after they had been properly informed and had provided written informed consent. The parent(s) or guardian(s) of all patients aged below 18 years also provided written informed consent. All patients underwent whole-body MRI and CT from the neck to the groins within 15 days of diagnosis, in a random order, and before start of treatment. CT was performed as part of the routine clinical care. Patients with general contraindications to MRI, such as an implanted pacemaker and claustrophobia, were excluded from enrollment. A total of 124 patients were potentially eligible for inclusion. However, 23 patients had to be excluded because of the following reasons: unwillingness to undergo an additional whole-body MRI examination due to psychological stress, physical complaints, logistic circumstances, and/or other unexplained reasons (n=17), claustrophobia (n=1), psychological stress during the MRI examination (n=2), technical problems of the MRI system (n=1), other disease than lymphoma (n=1), and absence of a diagnostic CT-scan from the neck to the groins (n=1). Thus, a total of 101 consecutive patients (62 men and 39 women; mean age, 49.8 years; age range, 12-82 years) with newly diagnosed, histologically proven lymphoma (HL: n=22; NHL: n=75; unspecified lymphoproliferative disorder: n=4) prospectively underwent whole-body MRI and CT (**Table 1**), of whom 31 were included in a previous analysis [11]. Whole-body MRI, including DWI, was performed in 96 patients. Four patients who could not tolerate the MRI examination for more than 30 minutes, and one patient with a spondylodesis only underwent conventional whole-body MRI (T1-weighted [T1W] and T2-weighted short inversion time [IR] inversion recovery [STIR]), without DWI.

**Table 1.** Characteristics of included patients.

Characteristics	HL	NHL
No. of patients	22	79
Sex (n)		
Men	13	49
Women	9	30
Age (y)		
Mean $\pm$ SD	24.4 $\pm$ 12.3	56.8 $\pm$ 16.7
Range	13 - 55	12 - 82
Pathological subtype (n)		
Nodular sclerosing HL	18	
Lymphocyte-rich HL	2	
Nodular lymphocyte predominant HL	2	
Diffuse large B-cell lymphoma		31
Follicular lymphoma		16
Mantle cell lymphoma		8
Extranodal marginal zone lymphoma		8
Nodal marginal zone lymphoma		3
Small lymphocytic lymphoma		3
Anaplastic large cell lymphoma		2
Waldenström's macroglobulinemia		2
Angioimmunoblastic T-cell lymphoma		1
T-cell NHL not otherwise specified		1
Unspecified lymphoproliferative disorder		4

### Whole-body MRI

Whole-body MRI was performed using a 1.5-T system (Achieva, Philips Healthcare, Best, The Netherlands or Magnetom Avanto, Siemens Medical Solutions, Erlangen, Germany). First, coronal T1-weighted (T1W) turbo spin-echo and half-Fourier multishot T2-weighted STIR (T2W-STIR) turbo spin-echo whole-body images were acquired using either the built-in body coil (Achieva, Philips Healthcare) or whole-body phased-array surface coils (Magnetom Avanto, Siemens Medical Solutions) for signal reception. Images were acquired under free breathing, except for the stations covering the chest, abdomen, and pelvis, which were acquired using breath-holding or respiratory triggering. Sequence parameters for T1W were: repetition time (TR)/echo time (TE) of 537/18 ms, slice thickness/gap 6/1 mm, field of view (FOV) of 500 (Magnetom Avanto) or 530 (Achieva)  $\times$  265 mm<sup>2</sup>, acquisition matrix of 208  $\times$  287, number of excitations of 1, acquired voxel size of 1.27  $\times$  1.85  $\times$  6.00 mm<sup>3</sup>, reconstructed voxel size of 1.04  $\times$  1.04  $\times$  6.00 mm<sup>3</sup>, craniocaudal coverage of 185.5 cm, total effective scan time of 5 min 29 s. Parameters for T2W-STIR were as follows: TR/TE/inversion time (IR) 2444/64/165 ms, slice thickness/gap of 6/1 mm, FOV of 500 (Magnetom Avanto) or 530 (Achieva)  $\times$ , acquisition matrix of 336  $\times$  120, number of excitations

of 2, acquired voxel size of  $1.58 \times 2.21 \times 6.00 \text{ mm}^3$ , reconstructed voxel size of  $1.04 \times 1.04 \times 6.00 \text{ mm}^3$ , craniocaudal coverage of 185.5 cm, total effective scan time 5 min 8 s. Total actual scan time of T1W and T2W-STIR whole-body MRI was approximately 25-30 minutes.

Second, axial diffusion-weighted images of the head/neck, chest, abdomen, and pelvis were acquired under free breathing, using phased-array surface coils for signal reception. Applied sequence parameters for DWI of the head/neck station were as follows: single-shot spin-echo echo-planar imaging (EPI), TR/TE/IR of 8612/78/180 ms, slice thickness/gap of 4/0 mm, number of slices of 60, FOV of  $450 \times 360 \text{ mm}^2$ , acquisition matrix of  $128 \times 81$ , receiver bandwidth of 1874 Hz/pixel, motion probing gradients in three orthogonal axes, b-values of 0 and  $1000 \text{ s/mm}^2$ , number of signal averages of 3, partial Fourier (half scan) factor of 0.651, parallel acquisition (SENSitivity Encoding) factor of 2, echo train length of 43, acquired voxel size of  $3.52 \times 4.50 \times 4.00 \text{ mm}^3$ , reconstructed voxel size of  $1.76 \times 1.76 \times 1.76 \text{ mm}^3$ , and scan time of 4 minutes and 4 s. Applied sequence parameters for DWI of the chest, abdominal, and pelvic stations were identical, except for a TR of 6962 s, spectral fat saturation, and scan time of 3 minutes and 20 s for each of the three stations. Total actual scan time of whole-body DWI was approximately 20-25 minutes.

Seamless coronal whole-body T1W and T2W-STIR images were created by merging separately acquired stations using software implemented in the standard operating console. Axial diffusion-weighted images were first coronally reformatted with a slice thickness/gap of both 7/0mm, and then merged to create seamless coronal whole-body diffusion-weighted images. Furthermore, coronal maximum intensity projections were created using the axial source images. Whole-body diffusion-weighted images were displayed using greyscale inversion.

## CT

CT scanning of the neck, chest, abdomen, and pelvis was performed using 16-, 40, and 64-slice CT scanners (Philips Brilliance, Philips Healthcare, Best, The Netherlands, and Somatom Sensation, Siemens Medical Systems, Knoxville, TN, USA). All patients ingested an oral contrast agent (Telebrix Gastro, Guerbet, The Netherlands) and received an intravenous non-ionic iodinated contrast agent (Ultravist 300, Bayer Schering, Berlin, Germany) before scanning. The administered amount of CT contrast agents was adjusted according to age and weight. All CT images were acquired with a slice thickness/increment of 1-1.5/0.7-0.8 mm, and were reconstructed to contiguous axial 5-mm slices. Tube voltage and tube setting were adjusted according to age, weight, and body region.

## Image analysis

All images were transferred to and interpreted by means of a Picture Archiving and Communications System (Easy Vision, Philips Healthcare, Best, The Netherlands)



that allows manual window level setting. A board-certified radiologist (R.A.J.N., with more than 15 years of clinical experience with MRI) who was blinded to CT findings, evaluated two separate sets of whole-body magnetic resonance images: whole-body MRI without DWI (i.e. T1W and T2W-STIR only) and whole-body MRI with DWI (i.e. T1W, T2W-STIR, and DWI). The CT images were evaluated by another board-certified radiologist (FJB, with 25 years of clinical experience with CT), who was blinded to MRI findings. The observers were aware that the patients had lymphoma, but unaware of the type and grade of lymphoma, findings of other diagnostic tests, and follow-up data. Presence and extent of nodal and extranodal pathology was systematically assessed by both the MR observer and the CT observer. Standardized scoring forms were used to classify nodal and extranodal regions as positive or negative for disease. Nodal regions, as defined at the Rye Symposium in 1965, included left and right cervical (including supraclavicular, occipital, and pre-auricular), left and right axillary, left and right infraclavicular, mediastinal, hilar, para-aortic, mesenteric, left and right pelvic, and left and right inguinal femoral lymph node regions [4]. Extranodal regions included spleen, bone marrow inside the head/neck and trunk, bone marrow outside the head/neck and trunk, lung, liver, bowel (including gastric), and other (including sites such as muscle, subcutaneous tissue, and breast). Lymph nodes greater than 10 mm in the short-axis diameter were considered positive at all MR sequences and CT. Lymph node sizes were measured in the axial plane at CT, and in the coronal plane at T1W and T2W-STIR. Lymph node size measurements on diffusion-weighted images were not made because these are highly dependent on the applied window level and window width. Rather, diffusion-weighted images were only used to visually detect potential nodal abnormalities. At T1W, T2W-STIR, and CT images, extranodal pathology was evaluated as follows: area of abnormal attenuation/signal intensity (relative to the surrounding tissue) in the spleen, bone or bone marrow, and liver; nodule or infiltration in the lung; and mass of soft-tissue attenuation/abnormal signal intensity (relative to the surrounding tissue) in other extranodal sites. At DWI, several normal extranodal structures (including brain, salivary glands, tonsils, spleen, gallbladder, adrenal glands, prostate, testes, penis, endometrium, ovaries, spinal cord, peripheral nerves, and bone marrow) (may) exhibit an impeded diffusion [14, 15]. Any focally increased signal intensity in these structures at DWI was considered positive for tumor involvement. In all other areas, any signal intensity higher than that of the spinal cord was considered positive for tumor involvement. Apparent diffusion coefficient (ADC) measurements were not used for tissue characterization, because there are no prospectively validated ADC criteria yet for differentiating malignant from non-malignant lesions at DWI. Subsequently, patients were classified according to the Ann Arbor staging system (stage I-IV) [4, 16].

## Data analysis

Agreement and disagreement between whole-body MRI (without and with DWI) and CT regarding staging according to the Ann Arbor staging system were calculated, along with binomial exact 95% confidence intervals (CIs), using Stata version 10 software (StataCorp LP, College Station, TX, USA). Disagreements in staging between whole-body MRI (without and with DWI) and CT were resolved using findings of FDG-PET, bone marrow biopsy, and/or follow-up FDG-PET, CT, and whole-body MRI studies as standard of reference, if available. Blind bone marrow biopsy of the posterior iliac crest was routinely performed in all patients, independently of CT, FDG-PET or other imaging findings. The availability of FDG-PET and follow-up FDG-PET and CT studies depended on the request of the treating hematologist who was blinded to whole-body MRI findings. Follow-up whole-body MRI studies were available in a random sample of patients as part of another investigation. Importantly, bone marrow biopsy and FDG-PET are highly specific for the diagnosis of bone marrow involvement in lymphoma, but lack sensitivity [17-21]. Therefore, if FDG-PET or bone marrow biopsy demonstrated bone marrow involvement, bone marrow involvement was confirmed. However, if FDG-PET or bone marrow biopsy did not demonstrate bone marrow involvement, bone marrow involvement could not be excluded. Parenchymal lesions of FDG-avid lymphomas (including HL, diffuse large B-cell lymphoma, follicular lymphoma, and mantle cell lymphoma) are well visualized at FDG-PET [22-24], with high sensitivity and specificity when combined with anatomical imaging, such as CT or MRI [5]. Therefore, parenchymal lesions seen both at FDG-PET and CT or MRI were considered positive for lymphoma. In addition, parenchymal lesions not seen at FDG-PET in patients with FDG-avid lymphomas were considered negative for lymphoma. Finally, lesions that changed in size at follow-up CT or whole-body MRI, and lesions whose FDG uptake changed at follow-up FDG-PET were considered positive for the presence of lymphoma.

## Results

Whole-body MRI without DWI compared to CT

In 66 of 101 patients (65.4%; 95% CI: 55.7-73.9%), whole-body MRI without DWI and CT were in agreement regarding assigned Ann Arbor stage (**Table 2, Figures 1 and 2**). Overstaging of whole-body MRI without DWI relative to CT occurred in 31 of 101 patients (30.7%; 95% CI: 22.5-40.3%) (**Table 2**), and was correct/incorrect/unresolved in 13/12/6 patients, respectively (**Table 3, Figures 3 and 4**). Bone marrow involvement was the main cause of correct overstaging whereas incorrect overstaging mostly occurred in lymph nodes and the liver (**Table 3**). Understaging of whole-body MRI without DWI relative to CT occurred in 4 of 101 patients (4.0%; 95% CI: 1.6-9.7%) (**Table 2**), and was incorrect/unresolved in 3/1 patients, respectively (**Table 3, Figures 6 and 7**). Missed lung/pleural lesions were the main cause of incorrect understaging (**Table 3**).

**Table 2.** Ann Arbor staging results of whole-body MRI without DWI (-DWI) compared to those of CT (CT).

CT \ -DWI	I	II	III	IV
I	14	2		7
II	2	13	3	3
III		1	17	14
IV	1	1	1	22

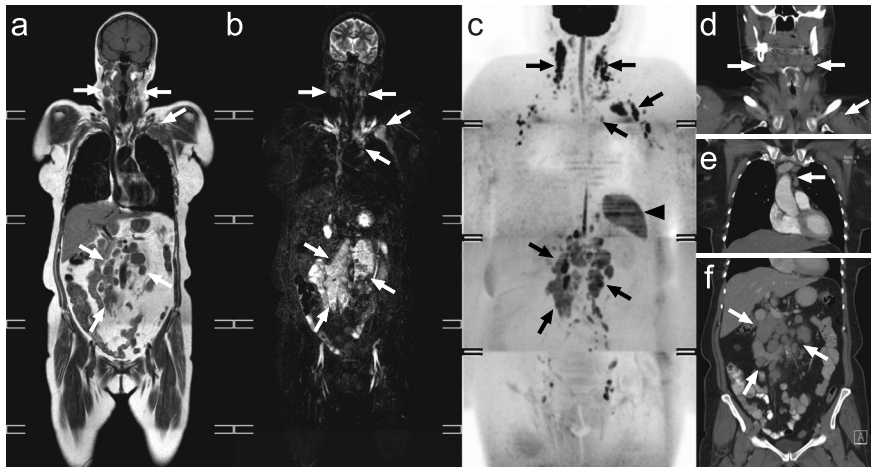


**Figure 1.** Coronal T1W (a), T2W-STIR (b), and maximum intensity projection greyscale inverted diffusion-weighted (c) images, and coronal CT images of the head/neck (d), chest (e), and abdomen/pelvis (f) in a 60-year-old female with diffuse large B-cell lymphoma. Both T1W, T2W-STIR, DWI, and CT show bilateral cervical, left infraclavicular, mediastinal, mesenteric, and para-aortic lymph node involvement (arrows), corresponding to stage III disease. Also note normal high signal intensity of the spleen (arrowhead).

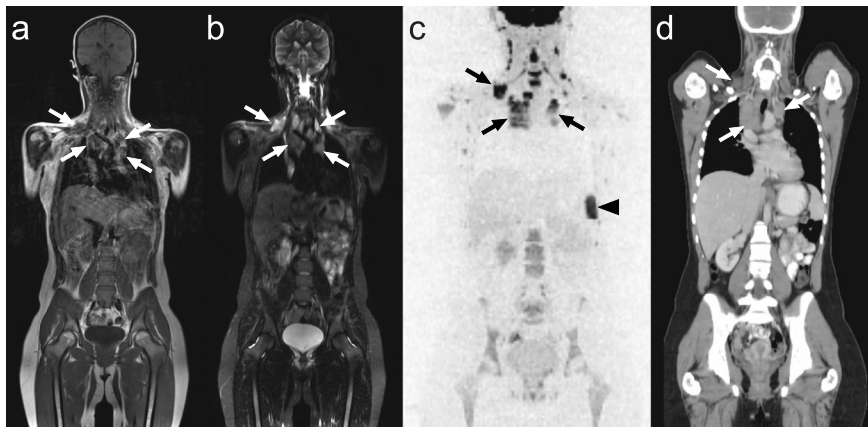


**Figure 2.** Coronal T1W (a), T2W-STIR (b), greyscale inverted diffusion-weighted (c), and coronal CT (d) images in a 17-year-old female with lymphocyte-rich HL. Both T1W, T2W-STIR, DWI, and CT show right cervical, mediastinal, and hilar lymph node involvement (arrows), corresponding to stage II disease. Also note normal high signal intensity of the spleen (arrowhead).

**Table 3.** Numbers and locations of discrepancies in staging between whole-body MRI without DWI and CT, classified according to correct, incorrect, or unresolved overstaging and understaging of the former relative to the latter.

<b>Overstaging whole-body MRI without DWI relative to CT (n=31)</b>	
Correct: n=13	-Bone marrow: n=12 -Left cervical lymph node: n=1 -Liver: n=1
Incorrect: n=12	-Liver: n=2 -Left cervical lymph node: n=1 -Right cervical lymph node: n=1 -Hilar lymph node: n=1 -Left infraclavicular, para-aortic, and left inguinal/femoral lymph nodes: n=1 -Right inguinal/femoral lymph node: n=1 -Lung/pleura: n=1 -Liver and kidney: n=1 -Liver and testis: n=1 -Right cervical and para-aortic lymph nodes, and liver: n=1 -Para-aortic and mesenteric lymph nodes, and liver: n=1
Unresolved: n=6	-Bone marrow: n=5 -Bone marrow, gastrointestinal/mesenteric mass, liver and kidney: n=1
<b>Understaging whole-body MRI without DWI relative to CT (n=4)</b>	
Correct: n=0	NA
Incorrect: n=3	-Lung/pleura: n=2 -Mediastinal lymph node: n=1
Unresolved: n=1	-Pericard: n=1

NA: not applicable

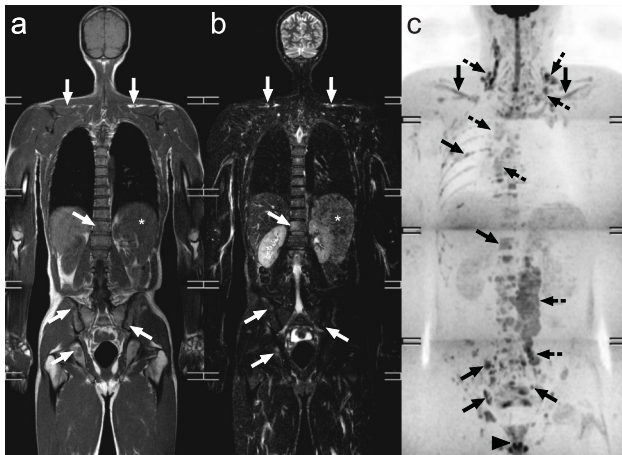


**Figure 3.** Coronal T1W (a), T2W-STIR (b), and maximum intensity projection greyscale inverted diffusion-weighted (c) images in a 45-year-old male with nodular sclerosing HL. CT (not shown) suggested lymph node involvement above and below the diaphragm, without any signs of bone marrow involvement, corresponding to stage III disease. However, extensive (bilateral clavicular, costal, vertebral, and pelvic) bone marrow involvement was seen at T1W, T2W-STIR, and DWI (a-c, continuous arrows), corresponding to stage IV disease. Bone marrow involvement was confirmed at FDG-PET

and by blind bone marrow biopsy of the iliac crest. Also note supra- and infradiaphragmatic lymph node involvement at T1W, T2W-STIR, and DWI (a-c, dashed arrows), and normal high signal intensity of the prostate at DWI (c, arrowhead).

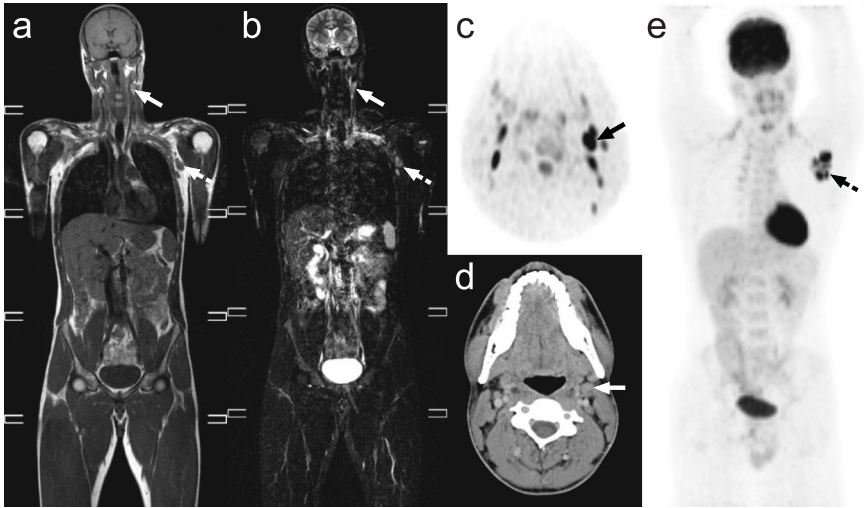


**Figure 4.** Coronal T1W (a) and T2W-STIR (b) images, axial greyscale inverted diffusion-weighted (c) and CT (d) images at the level of the neck, and coronal maximum intensity projection FDG-PET (e) in a 22-year-old male with anaplastic large cell lymphoma. Both whole-body MRI (without and with DWI) (a and b, dashed arrow) and CT (not shown) indicated a left axillary lymph node to be lymphomatous. A left cervical lymph node was also judged to be lymphomatous at whole-body MRI (a-c, continuous arrows), because its short-axis diameter, as measured in the coronal plane at T1W and T2W-STIR, just exceeded 10 mm. Therefore, stage II disease was assigned based on whole-body MRI findings (without and with DWI). However, this left cervical lymph node was judged to be negative at CT (d, continuous arrow), because its short-axis diameter, as measured in the axial plane, did not exceed 10 mm. Consequently, stage I disease was assigned based on CT findings. FDG-PET (e) showed that only the left axillary lymph node was positive (dashed arrow), indicating that whole-body MRI (without and with DWI) provided incorrect overstaging relative to CT in this case.

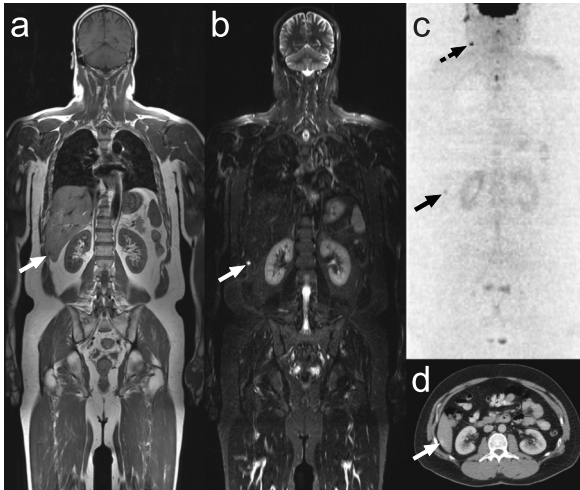


**Figure 5.** Coronal T1W (a), T2W-STIR (b), and greyscale inverted diffusion-weighted (c) images in a 43-year-old male with nodular sclerosing HL. Both whole-body MRI (without and with DWI) and CT showed right cervical lymph node involvement. However, a lesion in the liver was only considered to be lymphomatous at DWI, because of its high signal intensity (c, continuous arrow). Therefore, whole-body MRI findings without DWI and CT suggested stage I disease, whereas whole-body MRI findings with DWI suggested stage IV disease. The liver lesion was negative at FDG-PET and did not change in size at follow-up CT studies after therapy, indicating that the liver was not involved initially and that whole-body MRI with DWI provided incorrect overstaging

relative to CT and whole-body MRI without DWI in this case. Retrospective review show that the liver lesion has low signal intensity at T1W (a, arrow), very high signal intensity at T2W-STIR (b, arrow), and slightly hypervascular at CT (d, arrow). Given its apparent benign nature at FDG-PET and follow-up CT studies, the lesion may have been a hemangioma with a relatively impeded diffusivity. Also note the lymphomatous right cervical lymph node at DWI (c, dashed arrow).



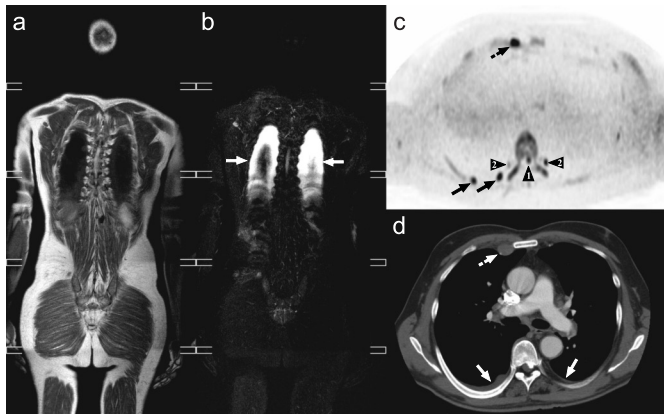


**Figure 6.** Coronal T1W (a) and T2W-STIR (b) images, and axial greyscale inverted diffusion-weighted (c) and CT (d) images at the level of the chest in a 62-year-old male with mantle cell lymphoma. Both whole-body MRI and DWI showed extensive supra- and infradiaphragmatic lymph node involvement (not shown). However, bilateral pleural

involvement was only seen at CT (d, continuous arrows). Therefore, whole-body MRI findings (without and with DWI) suggested stage III disease, whereas CT findings suggested stage IV disease. Follow-up CT studies showed that the pleural thickenings disappeared after therapy, indicating that pleural involvement was present initially and that whole-body MRI (without and with DWI) provided incorrect understaging relative to CT in this case. Retrospective review showed bilateral pleural effusions at T2W-STIR (b, arrows), and pleural nodules at DWI (c, continuous arrows). Also note a pathologically enlarged retrosternal lymph node at DWI and CT (c and d, dashed arrows). At DWI, normal high signal intensity of spinal cord (arrowhead 1) and nerve ganglia (arrowheads 2) can also be noted.

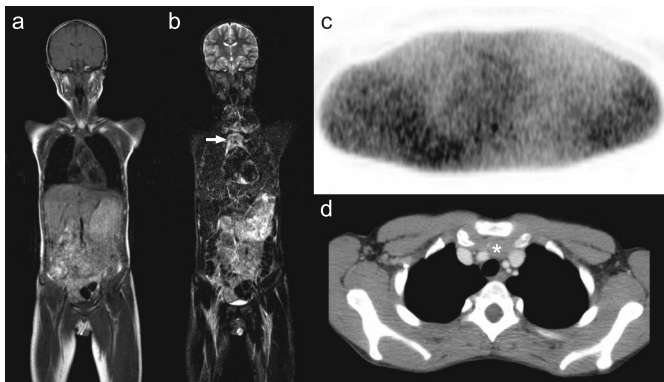


**Figure 7.** Coronal T1W (a) and T2W-STIR (b) images, and axial greyscale inverted diffusion-weighted (c) and CT (d) images at the level of the chest in a 12-year-old male with diffuse large B-cell lymphoma. Both whole-body MRI (without and with DWI) and CT indicated left cervical lymph node involvement (not shown). However, retrosternal lymph node

involvement was only seen at CT (d, asterisk). Therefore, whole-body MRI findings (without and with DWI) suggested stage I disease, whereas CT findings suggested stage II disease. Follow-up CT studies showed that the retrosternal lymphadenopathy disappeared after therapy, indicating that mediastinal lymph node involvement was present initially and that whole-body MRI (without and with DWI) provided incorrect understaging relative to CT in this case. Retrospective review showed that the retrosternal lymph node involvement was also visible at T2W-STIR (b, arrow). This lesion was not visible at DWI, possible because of noisy image quality at the periphery of this station (c).

## Whole-body MRI with DWI compared to CT

In 60 of 96 patients (62.5%; 95% CI: 52.5-71.5%), whole-body MRI with DWI and CT were in agreement regarding assigned Ann Arbor stage (**Table 4, Figures 1 and 2**). Overstaging of whole-body MRI with DWI relative to CT occurred in 31 of 96 patients (32.3%; 95% CI: 23.8-42.2%) (**Table 4**, and was correct/incorrect/unresolved in 18/10/3 patients, respectively (**Table 5, Figures 3, 4, 5, and 8**). Bone marrow involvement was the main cause of correct overstaging, whereas incorrect overstaging mostly occurred in lymph nodes and the liver (**Table 5**). Understaging of whole-body MRI with DWI relative to CT occurred in 5 of 96 patients (5.2%; 95% CI: 2.4-11.6%) (**Table 4**), and was incorrect/unresolved in 4/1 patient(s), respectively (**Table 5, Figures 6 and 7**). Missed lung/pleural lesions and lymphomatous lymph nodes were responsible for incorrect understaging (**Table 5**).

**Table 4.** Ann Arbor staging results of whole-body MRI with DWI (+DWI) compared to those of CT (CT).

CT \ +DWI	I	II	III	IV
I	12	3	1	7
II	2	12	4	4
III			16	12
IV	1		2	20

**Table 5.** Numbers and locations of discrepancies in staging between whole-body MRI with DWI and CT, classified according to correct, incorrect, or unresolved overstaging and understaging of the former relative to the latter.

<b>Overstaging whole-body MRI with DWI relative to CT (n=31)</b>	
Correct: n=18	-Bone marrow: n=12 -Mesenteric lymph node: n=1 -Left and right cervical lymph nodes: n=1 -Lung/pleura: n=1 -Liver: n=1 -Perianal: n=1 -Left cervical lymph node: n=1
Incorrect: n=10	-Liver: n=3 -Right cervical lymph node: n=1 -Right inguinal/femoral lymph node: n=1 -Vagina: n=1 -Liver and testis: n=1 -Left cervical lymph node and Waldeyer's ring: n=1 -Right cervical and para-aortic lymph nodes, and liver: n=1 -Para-aortic and mesenteric lymph nodes, and liver: n=1
Unresolved: n=3	-Bone marrow: n=3
<b>Understaging whole-body MRI with DWI relative to CT (n=5)</b>	
Correct: n=0	NA
Incorrect: n=4	-Lung/pleura: n=2 -Mediastinal lymph node: n=1 -Left axillary lymph node: n=1
Unresolved: n=1	-Pericard: n=1

NA: not applicable

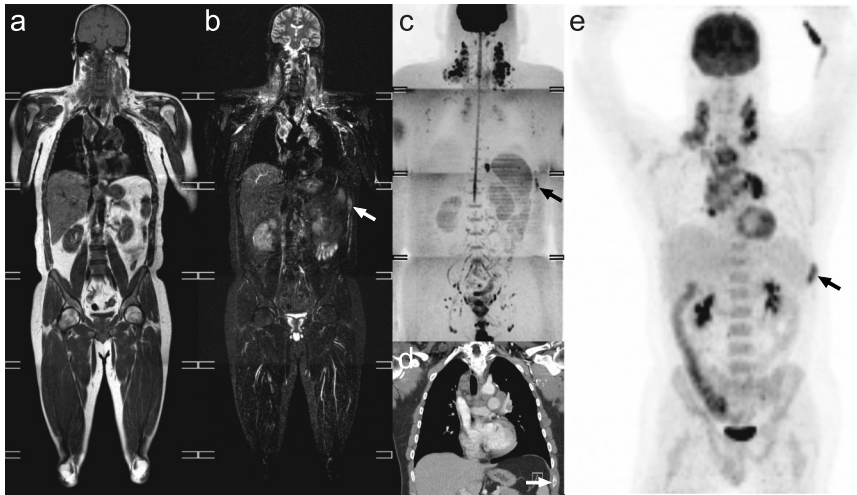


**Figure 8.** Coronal T1W (a), T2W-STIR (b), and maximum intensity projection greyscale inverted diffusion-weighted (c) images, coronal CT (d) image of the chest, and coronal maximum intensity projection FDG-PET (e) in a 34-year-old male with nodular sclerosing HL. Both whole-body MRI (without and with DWI) and CT showed involvement of bilateral cervical, mediastinal, and hilar lymph node stations. However, a lesion of the 9<sup>th</sup> rib was only seen at DWI (c, arrow). Therefore, whole-body MRI findings without DWI and CT suggested stage II disease, whereas whole-body MRI findings with DWI suggested stage IV disease. The rib lesion was positive at FDG-PET, indicating that whole-body MRI provided correct overstaging relative to CT and whole-body MRI without DWI in this case. Retrospective review showed that this rib lesion was also visible at T2W-STIR and CT (b and d, arrows).

#### Whole-body MRI with DWI compared to whole-body MRI without DWI

In 82 of 96 patients (85.4%; 95% CI: 77.0-91.1%), whole-body MRI with DWI and whole-body MRI without DWI were in agreement regarding assigned Ann Arbor stage (Table 6, Figures 1 and 2). Overstaging of whole-body MRI with DWI relative to whole-body MRI without DWI occurred in 8 of 96 patients (8.3%; 95% CI: 4.3-15.6%) (Table 6), and was correct/incorrect/unresolved in 5/4/1 patient(s), respectively (Table 7, Figures 5 and 8). Bone marrow and lymph node involvement were the main causes of correct overstaging, whereas incorrect overstaging mostly occurred in the liver (Table 7). Understaging of whole-body MRI with DWI relative to whole-body MRI without DWI occurred in 6 of 96 patients (6.3%; 95% CI: 2.9-13.0%) (Table 6), and was correct/incorrect/unresolved in 2/1/1 patient(s), respectively (Table 7).



**Table 6.** Ann Arbor staging results of whole-body MRI with DWI (+DWI) compared to those of whole-body MRI without DWI (-DWI).

	+DWI	I	II	III	IV
-DWI					
I		14	2		1
II			11	1	3
III			1	19	1
IV		1	1	3	38

**Table 7.** Numbers and locations of discrepancies in staging between whole-body MRI with DWI and whole-body MRI without DWI, classified according to correct, incorrect, or unresolved overstaging and understaging of the former relative to the latter.

<b>Overstaging whole-body MRI with DWI relative to that without DWI (n=10)</b>	
Correct: n=5	-Bone marrow: n=2 -Mesenteric lymph node: n=1 -Left and right cervical lymph nodes: n=1 -Lung/pleural: n=1
Incorrect: n=4	-Liver: n=2 -Vagina: n=1 -Liver and kidney: n=1
Unresolved: n=1	-Bone marrow: n=1
<b>Understaging whole-body MRI with DWI relative to that without DWI (n=4)</b>	
Correct: n=2	-Left infraclavicular, para-aortic, and left inguinal/femoral lymph nodes: n=1 -Lung/pleura: n=1
Incorrect: n=1	-Lung/pleura: n=1
Unresolved: n=1	-Bone marrow: n=1

## Discussion

The results of this prospective study, which included 101 consecutive patients with newly diagnosed lymphoma, show that staging using whole-body MRI (without and with DWI) equals staging using CT in the majority of cases. However, staging disagreements between whole-body MRI and CT occur in a considerable proportion of patients, with overstaging of the former relative to the latter being far more common than understaging. Interestingly, the number of cases in which whole-body MRI *correctly* provided a different stage than CT (n=16 for whole-body MRI without DWI and n=18 for whole-body MRI with DWI) was approximately equal to the number of cases in which whole-body MRI *incorrectly* provided a different stage than CT (n=14 for whole-body MRI without DWI and n=15 for whole-body MRI with DWI). Thus, whole-body MRI has both strengths and weaknesses compared to CT. The most common site where whole-body MRI (both without and with DWI) provided correct

overstaging relative to CT was the bone marrow. This is thanks to one of the well-known advantages of MRI over CT, in that it has excellent sensitivity for the detection of bone marrow involvement [25] (which, if present, by definition indicates stage IV disease [2-4, 16]), while CT is not very suitable for the evaluation of the bone marrow [26]. Incorrect overstaging of whole-body MRI (both without and with DWI) relative to CT mostly occurred in lymph nodes and the liver. The former can be explained by the fact that lymph nodes were measured in the coronal plane at whole-body MRI, whereas they were measured in the axial plane at CT. This problem may be solved by acquiring T1W and/or T2W-STIR sequences in the axial plane. Note that diffusion-weighted images are less suitable for this purpose, because size measurements on these images are highly dependent on the applied window level and window width. The latter is mainly due to the fact that several cavernous liver hemangiomas were erroneously classified as lymphomatous at whole-body MRI, whereas they were correctly classified at CT. In a real clinical setting, the liver lesions detected at whole-body MRI may have received additional diagnostic work-up, but in this study the observer was forced to classify a lesion as positive or negative. There were no cases in which whole-body MRI (both without and with DWI) provided correct understaging relative to CT. On the other hand, missed lung/pleural lesions and lymphomatous lymph nodes were responsible for incorrect understaging of whole-body MRI (both without and with) relative to CT. The former can be explained by the fact that MRI of the lung may be affected by cardiac and respiratory motion and susceptibility artefacts, which may cause signal loss. This is especially a problem in DWI because of the use of EPI. Another cause may be relative unfamiliarity with the interpretation of whole-body MRI/DWI examinations in the chest. The latter can in part be explained by the fact that lymph nodes were measured in the coronal plane at whole-body MRI, whereas they were measured in the axial plane at CT. It should also be noted that staging disagreements between whole-body MRI and CT could not be resolved in several cases (n=7 for whole-body MRI without DWI and n=4 for whole-body MRI with DWI). The bone marrow was the most common site of unresolved staging disagreements; negative FDG-PET and negative bone marrow biopsy findings could not exclude bone marrow involvement that was seen at whole-body MRI in several patients. In addition, follow-up whole-body MRI examinations were mostly not available in such cases.

In the far majority of patients, staging using whole-body MRI with DWI was equal to that without DWI. In a low number of cases DWI findings resulted in *correct* overstaging (n=5), whereas in an approximately equal number of cases DWI findings led to *incorrect* overstaging. Therefore, the additional value of DWI is still unproven. Causes of correct overstaging were miscellaneous, occurring in the bone marrow, lymph nodes, and lung/pleura. These cases demonstrate that DWI can draw the attention of the reader to pathologic areas of high signal intensity that have remained unnoticed at conventional whole-body MRI sequences. On the other hand, incorrect

overstaging, occurring in the liver, kidney, and vagina, show that high signal intensity lesions at DWI are not specific for cancer. In an even lower number of cases, DWI findings resulted in correct understaging (n=2) and incorrect understaging (n=1). Correct understaging occurred thanks to the fact that DWI excluded lymphomatous disease in several lymph nodes in one case, and lung/pleura involvement in another case. Incorrect understaging occurred because a lung/pleural lesion was missed in one case, most likely due to signal loss at DWI resulting from physiological motion and/or susceptibility artifacts. In two cases, disagreement in staging between whole-body MRI without DWI and whole-body MRI with DWI remained unresolved.

The feasibility of using whole-body MRI for staging lymphoma has been investigated by previous studies [9, 10, 12, 13]. Kellenberger et al. [9] performed a study in 8 children (either with newly diagnosed lymphoma or with previously treated lymphoma) and reported that whole-body MRI using T2W-STIR is a sensitive technique for staging lymphoma and that it is superior to blind bone marrow biopsy and conventional imaging (including CT, gallium-67 scintigraphy, and bone scintigraphy) in the detection of bone marrow involvement, at initial diagnosis. However, whole-body MRI using T2W-STIR lacked specificity for diagnosing recurrent or residual disease [9]. Brennan et al. [10] performed a study in 23 adults (either with newly diagnosed lymphoma or with previously treated lymphoma) and reported that whole-body MRI using T2W-STIR enables disease staging and that it compared favourably with CT for the detection of lymph nodes larger than 12 mm in short-axis diameter and for the detection of bone marrow involvement. Disadvantages of the studies by Kellenberger et al. [9] and Brennan et al. [10] are their small study populations and the inclusion of both newly diagnosed and treated lymphoma. Punwani et al. [12] compared T2W-STIR whole-body MRI to FDG-PET/CT as reference standard for staging 26 pediatric and adolescent patients with newly diagnosed lymphoma. There was very good agreement between MR imaging and the enhanced PET/CT reference standard for nodal and extranodal staging ( $\kappa=0.96$  and  $\kappa=0.86$ , respectively) which improved following elimination of perceptual errors ( $\kappa=0.97$  and  $\kappa=0.91$ , respectively). The sensitivity and specificity of MR imaging (following removal of perceptual error) were 98% and 99%, respectively, for nodal disease and 91% and 99%, respectively, for extranodal disease. The authors of this study concluded that T2W-STIR whole-body MRI can accurately depict nodal and extranodal disease and may provide an alternative nonionizing imaging method for anatomic disease assessment at initial staging [12]. An important difference between Punwani et al.'s study [12] and the present study is that the former included 26 patients with HL and only 3 patients with NHL, whereas the latter included 22 patients with HL and 79 patients with NHL. Bone marrow involvement in HL is less common than in NHL [2-4], as a result of which only a few patients with actual bone marrow involvement may have been included in Punwani et al.'s study [12]. Furthermore, Punwani et al. [12] acquired both coronal

and axial T2W-STIR images, which may have improved the evaluation of lymph nodes compared to our T1W and T2W-STIR sequences that were acquired in the coronal plane only. Of note, bone marrow involvement and lymph nodes were the locations where most staging disagreements between whole-body MRI (without and with DWI) occurred in the present study. Lin et al. [13] compared whole-body DWI to FDG-PET/CT as reference standard for pretreatment staging of diffuse large B-cell lymphoma in 15 patients. Whole-body DWI findings matched PET/CT findings in 277 regions (94%) ( $\kappa=0.85$ ,  $P<0.0001$ ), yielding sensitivity and specificity for DWI lymph node involvement detection of 90% and 94%. Combining non-quantitative (visual) ADC analysis with size measurement increased specificity of whole-body DWI to 100% with 81% sensitivity. For organ involvement, the two techniques agreed in all 20 recorded organs (100%). Ann Arbor stages agreed in 14 (93%) of the 15 patients. The authors of this study concluded that whole-body DWI with visual ADC analysis can potentially be used for lesion detection and staging in patients with diffuse large B-cell lymphoma [13]. However, because of the limited number of patients in Lin et al.'s study [13], no definitive conclusions can be drawn. Moreover, their study did not prove that whole-body MRI with DWI improves staging performance compared to whole-body MRI without DWI.

This study had several limitations. First, a histopathological reference standard was lacking, because it would be practically and ethically impossible to obtain biopsies of lymphomatous lesions seen at imaging. Instead, bone marrow biopsy, FDG-PET, and follow-up FDG-PET, CT and whole-body MRI studies were reviewed to resolve disagreements in staging between CT and whole-body MRI (without and with DWI). Nevertheless, disagreements in staging between the imaging modalities could not be resolved in several patients. Second, lymph nodes greater than 10 mm in the short-axis diameter at either CT or whole-body MRI were considered positive, although size measurements may be inaccurate [27]. Nevertheless, this is still the best available approach in clinical practice. In addition, there are no prospectively validated ADC criteria yet for differentiating lymphomatous from non-lymphomatous lymph nodes at DWI. Third, lymph nodes were measured in the coronal plane at whole-body MRI and in the axial plane at CT, which may explain some of the staging disagreements in the present study. Fourth, only one observer assessed the whole-body MRI datasets. Future inter- and intraobserver studies are required. Fifth, no comparison was made with FDG-PET/CT. However, CT is still the most commonly used imaging modality for staging newly diagnosed lymphoma [5], and the benefit of performing baseline FDG-PET has not been proven yet. For this reason, FDG-PET is not yet routinely performed in all patients with newly diagnosed lymphoma in the participating hospitals. Sixth, this study only focused on staging newly diagnosed lymphoma. Staging performance of both CT and whole-body MRI after therapy may be different and requires further investigation. Another important issue that should be investigated by future studies

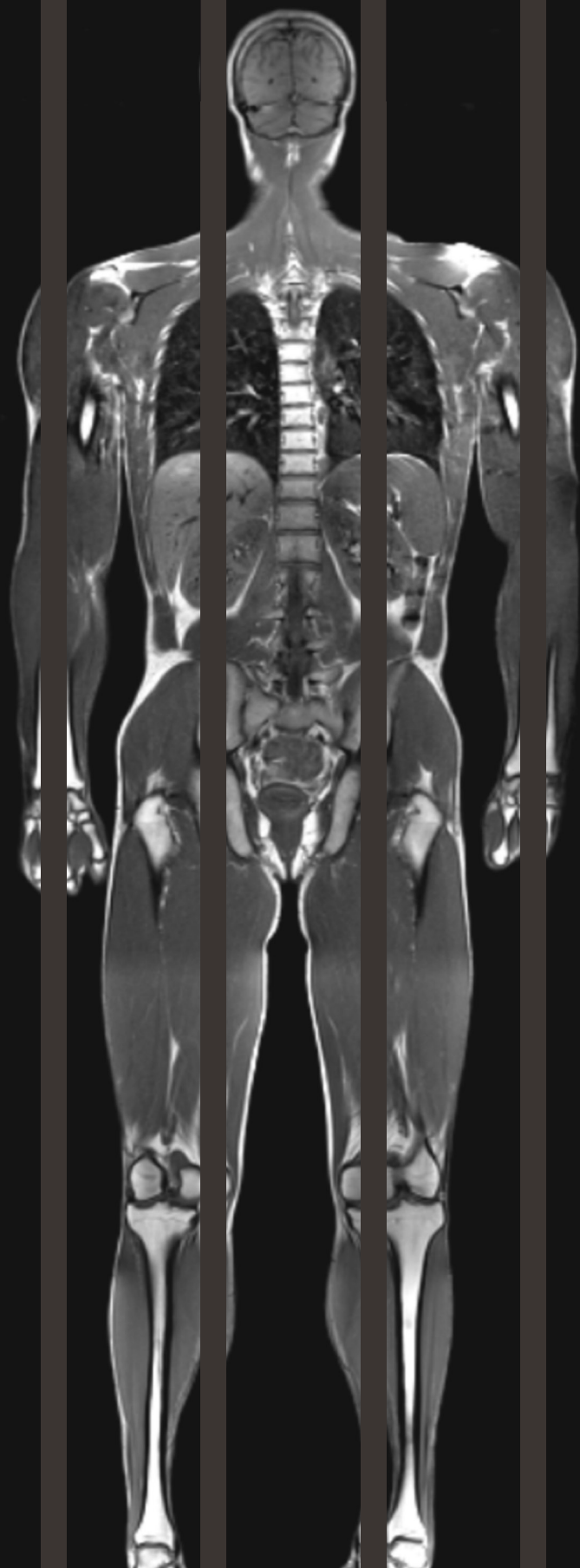
is the cost-effectiveness of whole-body MRI, taking into account different age groups and different whole-body MRI protocols with different acquisition times.

In conclusion, staging of newly diagnosed lymphoma using whole-body MRI (without and with DWI) equals staging using CT in the majority of patients. Disagreements between whole-body MRI and CT are mostly caused by overstaging of the former relative to the latter, with the number of correctly and incorrectly overstaged cases being approximately equal. This underlines the fact that both whole-body MRI and CT are unique imaging modalities, each having its own strengths and weaknesses. The potential advantage of DWI in a whole-body MRI protocol for staging newly diagnosed lymphoma is still unproven.

## References

1. Jemal A, Siegel R, Xu J, Ward E. Cancer statistics, 2010. *CA Cancer J Clin* 2010;60:277-300
2. Connors JM. State-of-the-art therapeutics: Hodgkin's lymphoma. *J Clin Oncol* 2005;23:6400-6408
3. Ansell SM, Armitage J. Non-Hodgkin lymphoma: diagnosis and treatment. *Mayo Clin Proc* 2005;80:1087-1097
4. Armitage JO. Staging non-Hodgkin lymphoma. *CA Cancer J Clin.* 2005;55:368-376
5. Kwee TC, Kwee RM, Nievelstein RA. Imaging in staging of malignant lymphoma: a systematic review. *Blood* 2008;111:504-516
6. Cheson BD, Pfistner B, Juweid ME, et al; International Harmonization Project on Lymphoma. Revised response criteria for malignant lymphoma. *J Clin Oncol* 2007;25:579-586
7. Delbeke D, Stroobants S, de Kerviler E, Gisselbrecht C, Meignan M, Conti PS. Expert opinions on positron emission tomography and computed tomography imaging in lymphoma. *Oncologist* 2009;14 Suppl 2:S30-S40
8. Brenner DJ, Hall EJ. Computed tomography – an increasing source of radiation exposure. *N Engl J Med* 2007;357:2277-2284
9. Kellenberger CJ, Miller SF, Khan M, Gilday DL, Weitzman S, Babyn PS. Initial experience with FSE STIR whole-body MR imaging for staging lymphoma in children. *Eur Radiol* 2004;14:1829-1841
10. Brennan DD, Gleeson T, Coate LE, Cronin C, Carney D, Eustace SJ. A comparison of whole-body MRI and CT for the staging of lymphoma. *AJR Am J Roentgenol* 2005;185:711-716
11. Kwee TC, Quarles van Ufford HM, Beek FJ, et al. Whole-Body MRI, including diffusion-weighted imaging, for the initial staging of malignant lymphoma: comparison to computed tomography. *Invest Radiol* 2009;44:683-690
12. Punwani S, Taylor SA, Bainbridge A, et al. Pediatric and adolescent lymphoma: comparison of whole-body STIR half-Fourier RARE MR imaging with an enhanced PET/CT reference for initial staging. *Radiology* 2010;255:182-190
13. Lin C, Luciani A, Itti E, et al. Whole-body diffusion-weighted magnetic resonance imaging with apparent diffusion coefficient mapping for staging patients with diffuse large B-cell lymphoma. *Eur Radiol* 2010;20:2027-2038
14. Takahara T, Imai Y, Yamashita T, Yasuda S, Nasu S, Van Cauteren M. Diffusion weighted whole body imaging with background body signal suppression (DWIBS): technical improvement using free breathing, STIR and high resolution 3D display. *Radiat Med* 2004;22:275-282
15. Kwee TC, Takahara T, Ochiai R, Nievelstein RA, Luijten PR. Diffusion-weighted whole-body imaging with background body signal suppression (DWIBS): features and potential applications in oncology. *Eur Radiol* 2008;18:1937-1952
16. Lister TA, Crowther D, Sutcliffe SB, et al. Report of a committee convened to discuss the evaluation and staging of patients with Hodgkin's disease: Cotswolds meeting. *J Clin Oncol* 1989;7:1630-1636
17. Brunning RD, Bloomfield CD, McKenna RW, Peterson LA. Bilateral trephine bone marrow biopsies in lymphoma and other neoplastic diseases. *Ann Intern Med* 1975;82:365-366
18. Coller BS, Chabner BA, Gralnick HR. Frequencies and patterns of bone marrow involvement in non-Hodgkin lymphomas: observations on the value of bilateral biopsies. *Am J Hematol* 1977;3:105-119

19. Haddy TB, Parker RI, Magrath IT. Bone marrow involvement in young patients with non-Hodgkin's lymphoma: the importance of multiple bone marrow samples for accurate staging. *Med Pediatr Oncol* 1989;17:418-423
20. Wang J, Weiss LM, Chang KL, Slovak ML, Gaal K, Forman SJ, Arber DA. Diagnostic utility of bilateral bone marrow examination: significance of morphologic and ancillary technique study in malignancy. *Cancer* 2002;94:1522-1531
21. Pakos EE, Fotopoulos AD, Ioannidis JP. 18F-FDG PET for evaluation of bone marrow infiltration in staging of lymphoma: a meta-analysis. *J Nucl Med* 2005;46:958-963
22. Tsukamoto N, Kojima M, Hasegawa M, et al. The usefulness of (18)F-fluorodeoxyglucose positron emission tomography ((18)F-FDG-PET) and a comparison of (18)F-FDG-pet with (67)gallium scintigraphy in the evaluation of lymphoma: relation to histologic subtypes based on the World Health Organization classification. *Cancer* 2007;110:652-659.
23. Elstrom R, Guan L, Baker G, et al. Utility of FDG-PET scanning in lymphoma by WHO classification. *Blood* 2003;101:3875-3876.
24. Weiler-Sagie M, Bushelev O, Epelbaum R, et al. (18)F-FDG avidity in lymphoma readdressed: a study of 766 patients. *J Nucl Med* 2010;51:25-30
25. Kwee TC, Kwee RM, Verdonck LF, Bierings MB, Nievelstein RA. Magnetic resonance imaging for the detection of bone marrow involvement in malignant lymphoma. *Br J Haematol* 2008;141:60-68
26. Vinnicombe SJ, Reznick RH. Computerised tomography in the staging of Hodgkin's disease and non-Hodgkin's lymphoma. *Eur J Nucl Med Mol Imaging* 2003;30 Suppl 1:S42-S55
27. Torabi M, Aquino SL, Harisinghani MG. Current concepts in lymph node imaging. *J Nucl Med* 2004;45:1509-1518





# Chapter 8<sup>3</sup>

Newly diagnosed lymphoma:  
initial results with whole-body  
T1-weighted, STIR, and  
diffusion-weighted MRI  
compared with <sup>18</sup>F-FDG PET-CT

Quarles van Ufford HM, Kwee TC, Beek FJ, Takahara T,  
Fijnheer R, Nievelstein RA, De Klerk JMH

## Abstract

### Objective

To compare whole-body MRI, including diffusion-weighted imaging (DWI), to <sup>18</sup>F-FDG PET-CT for staging newly diagnosed lymphoma.

### Methods

Twenty-two consecutive patients with newly diagnosed lymphoma prospectively underwent whole-body MRI-DWI (T1-weighted and short inversion time inversion recovery [n=22] and DWI [n=21]) and <sup>18</sup>F-FDG PET-CT. Whole-body MRI-DWI was independently evaluated by two blinded observers. Interobserver agreement was assessed and whole-body MRI-DWI was compared to <sup>18</sup>F-FDG PET-CT.

### Results

$\kappa$  values for interobserver agreement at whole-body MRI-DWI for all nodal regions together and for all extranodal regions together were 0.676 and 0.452, respectively.  $\kappa$  values for agreement between whole-body MRI-DWI and <sup>18</sup>F-FDG PET-CT for all nodal regions together and for all extranodal regions together were 0.597 and 0.507, respectively. Ann Arbor stage according to whole-body MRI-DWI was concordant to that of <sup>18</sup>F-FDG PET-CT in 77% (17/22) of patients, whereas understaging and overstaging relative to <sup>18</sup>F-FDG PET-CT occurred in 0% (0/22) and 23% (5/22) of patients, respectively. In 9% (2/22) of patients, whole-body MRI-DWI overstaging relative to <sup>18</sup>F-FDG PET-CT would have had therapeutic consequences.

### Conclusion

Our early results indicate that overall interobserver agreement at whole-body MRI-DWI is moderate to good. Overall agreement between whole-body MRI-DWI and <sup>18</sup>F-FDG PET-CT is moderate. Whole-body MRI-DWI does not understage relative to <sup>18</sup>F-FDG PET-CT in patients with newly diagnosed lymphoma. In a minority of patients, whole-body MRI-DWI leads to clinically important overstaging relative to <sup>18</sup>F-FDG PET-CT. <sup>18</sup>F-FDG PET-CT remains the gold standard for staging lymphoma until future, larger studies have shown that whole-body MRI-DWI provides correct upstaging in such cases.

## Introduction

The lymphomas, Hodgkin's disease (HD) and non-Hodgkin lymphoma (NHL), comprise approximately 5% to 6% of all malignancies and are the fifth most frequently occurring type of cancer in the Western World [1]. Accurate staging of patients with newly diagnosed lymphoma is of crucial importance because it allows appropriate treatment planning and it aids in the determination of prognosis [2, 3]. Previously, CT was the single imaging modality for staging as well as therapy evaluation. However, its role during therapy evaluation is gradually being replaced by combined 2-deoxy-2-[<sup>18</sup>F]fluoro-D-glucose ([<sup>18</sup>F]-FDG) positron emission tomography (PET)-CT [4, 5]. Combined <sup>18</sup>F-FDG PET-CT is currently regarded as the gold standard for staging high-grade lymphoma [6], although it should be noted that additional bone marrow biopsy is still considered mandatory [7]. The unique value of <sup>18</sup>F-FDG PET to CT lies in its high lesion-to-background contrast and its ability to quantify glucose metabolism (usually done by means of semi-quantitative standardised uptake value [SUV] measurements). SUV measurements may be of value as a biomarker for tumor grade [8, 9], for guiding biopsies [10], and for the determination of response to therapy in patients with lymphoma [11-13]. Possible disadvantages of <sup>18</sup>F-FDG PET-CT, however, are exposure of the patient to ionizing radiation and its relatively high costs [14, 15]. MRI does not use any ionizing radiation and may be a good alternative to <sup>18</sup>F-FDG PET-CT for the staging of lymphoma. Technological developments have enabled the routine clinical use of whole-body MRI [16], allowing for complete tumor staging. Commonly applied sequences for whole-body MRI include (contrast-enhanced) T1-weighted (T1W) and (fat-suppressed) T2-weighted (T2W) or short inversion time inversion recovery (STIR) imaging. Previous studies have shown the particular utility of STIR whole-body MRI for staging malignant lymphoma [6]. STIR is a sensitive method for the detection of parenchymal and bone marrow lesions, that are generally highlighted as high signal intensity structures on this sequence [6]. Another exciting development is the introduction of whole-body diffusion-weighted MRI (DWI) [17, 18]. A potential advantage of DWI over conventional MRI sequences in the evaluation of lymphoma is the high lesion-to-background contrast that can be obtained thanks to the relatively low diffusivity of lymphomatous tissue [19-21]. The aim of this study was therefore to compare staging using whole-body MRI-DWI (i.e. T1W, STIR, and DWI) to staging using <sup>18</sup>F-FDG PET-CT in patients with newly diagnosed lymphoma.

## Materials and Methods

### Patients

This prospective study was approved by the local Institutional Review Board, and written informed consent was obtained from all study participants. Inclusion criteria were: age of 8 years and older, and newly diagnosed, histologically proven lymphoma.

Exclusion criteria were: general contraindications to MRI (such as implanted pacemaker and claustrophobia) and a previous malignancy. All patients underwent whole-body MRI-DWI, <sup>18</sup>F-FDG PET-CT, and unilateral blind bone marrow biopsy of the iliac crest within 15 days of diagnosis, in a random order, and before start of treatment. <sup>18</sup>F-FDG PET-CT and bone marrow biopsy were performed as part of routine clinical care. In total, twenty-two consecutive patients (16 men and 6 women; mean age 59.9 ± 14.3 years; range 22-81 years) were included between August 2008 and October 2009. Patient characteristics, divided into HD and NHL patients, are shown in **Table 1**. Whole-body MRI-DWI was successfully performed in 21 patients, while one patient (81 years of age) could not tolerate the MRI examination for more than 25-30 minutes and only underwent conventional (T1W and STIR) whole-body MRI, without DWI. <sup>18</sup>F-FDG PET-CT was performed in all patients.

**Table 1.** Characteristics of included patients.

Characteristics	HD	NHL
No. of patients	2	20
Sex ( <i>n</i> )		
Men	2	13
Women	0	7
Age ( <i>y</i> )		
Mean ± SD	38.5 ± 7.8	61.1 ± 13.0
Range	33-44	22-81
Pathological subtype ( <i>n</i> )		
Nodular sclerosing Hodgkin's disease	2	
Follicular B-cell lymphoma		4
Diffuse large B-cell lymphoma		7
Marginal zone B-cell lymphoma		4
Small-cell lymphocytic lymphoma		3
Mantle cell lymphoma		1
Anaplastic large cell lymphoma		1

#### Whole-body MRI-DWI

Whole-body MRI-DWI was performed using a 1.5-T system (Achieva, Philips Healthcare, Best, The Netherlands). Four spacers were placed on the original patient table. Subsequently, an additional table platform was mounted on top of these four spacers. In this way, sufficient space was created to freely move the lower part of a surface coil over a distance of approximately 110 cm along the z-axis (necessary for DWI), without the need to reposition the patient who is lying on top of the additional table platform [22]. Although this approach resulted in narrowing of the bore diameter by approximately 6.5 cm, all patients could be accommodated within the MRI scanner. First, coronal T1W and STIR images were acquired, using the built-in body coil for signal

reception. Images were acquired under free breathing, except for the stations covering the chest, abdomen, and pelvis, which were acquired using breath holding (T1W) or respiratory triggering (STIR). Applied sequence parameters for T1W were as follows: single-shot turbo spin-echo imaging, repetition time (TR)/echo time (TE) of 537/18 ms, slice thickness/gap of 6/1 mm, number of slices of 30 per station, field of view (FOV) of 530 × 265 mm<sup>2</sup>, acquisition matrix of 208 × 287, number of signal averages of 1, acquired voxel size of 1.27 × 1.85 × 6.00 mm<sup>3</sup>, reconstructed voxel size of 1.04 × 1.04 × 6.00 mm<sup>3</sup>, scan time of 47 s per station, 7 stations in total. Applied sequence parameters for STIR were as follows: single-shot turbo spin-echo imaging, TR/TE/inversion time (IR) of 2444/64/165 ms, slice thickness/gap of 6/1 mm, number of slices of 30 per station, FOV of 530 × 265 mm<sup>2</sup>, acquisition matrix of 336 × 120, number of signal averages of 2, acquired voxel size of 1.58 × 2.21 × 6.00 mm<sup>3</sup>, reconstructed voxel size of 1.04 × 1.04 × 6.00 mm<sup>3</sup>, scan time of 44 s per station, 7 stations in total. Total actual scan time of T1W and STIR whole-body MRI was approximately 25-30 minutes. Second, axial diffusion-weighted images of the head/neck, chest, abdomen, and pelvis were acquired under free breathing, using a 4-element phased array surface coil for signal reception. This surface coil was sequentially moved to image the separate stations of the whole-body DWI examination, without patient repositioning. Applied sequence parameters for DWI of the head/neck station were as follows: single-shot spin-echo echo-planar imaging (EPI), TR/TE/IR of 8612/78/180 ms, slice thickness/gap of 4/0 mm, number of slices of 60, FOV of 450 × 360 mm<sup>2</sup>, acquisition matrix of 128 × 81, receiver bandwidth of 1874 Hz/pixel, motion probing gradients in three orthogonal axes, b-values of 0 and 1000 s/mm<sup>2</sup>, number of signal averages of 3, half scan factor of 0.651, parallel acquisition (SENSitivity Encoding) factor of 2, EPI factor of 43, acquired voxel size of 3.52 × 4.50 × 4.00 mm<sup>3</sup>, reconstructed voxel size of 1.76 × 1.76 × 1.76 mm<sup>3</sup>, and scan time of 4 minutes and 4 s. Applied sequence parameters for DWI of the chest, abdominal, and pelvic stations were identical, except for a TR of 6962 s, spectral presaturation inversion recovery fat suppression, and scan time of 3 minutes and 20 s for each of the three stations. Total actual scan time of whole-body DWI was approximately 20-25 minutes.

Seamless coronal whole-body T1W and STIR images were created by merging separately acquired stations using software implemented in the standard operating console. Axial diffusion-weighted images were first coronal reformatted with a slice thickness/gap of both 3.5/0mm and 7/0mm, and then merged to create seamless coronal whole-body diffusion-weighted images. Whole-body diffusion-weighted images were displayed using greyscale inversion.

#### <sup>18</sup>F-FDG PET-CT

Whole-body PET-CT images were obtained with an integrated 40-slice PET-CT scanner (Biograph 40 TruePoint PET-CT, Siemens Medical Systems, Knoxville, TN, USA). Patients ingested oral contrast material and fasted for 6 hours before receiving 3 MBq/kg body

weight of <sup>18</sup>F-FDG intravenously. Before injection of <sup>18</sup>F-FDG, blood glucose levels were checked to be less than 11 mmol/L (i.e. less than 198 mg/dL). Sixty minutes after <sup>18</sup>F-FDG injection image acquisition was performed. First, low-dose, unenhanced CT images were acquired using the following parameters: 120 kV, 26-30 mAs (automatic dose modulation), 0.8-second tube rotation time, a pitch of 1.2, and 1.5-mm slice width (reconstructed to contiguous axial 5-mm slices to match section thickness of the PET images). Subsequently, PET-scanning from mid femur to the base of the skull was done in 5 to 6 bed positions, with 3 minutes per bed position. Low-dose CT data were used for attenuation correction of the PET images, which were reconstructed using an ordered-subsets expectation maximization algorithm for 14 subsets and four iterations. The image reconstruction matrix was 128 × 128. Finally, all patients received an intravenous non-ionic iodinated contrast agent (Xenetix 300, Guerbet; 3 mL/s with bolus tracking; scan obtained in portal venous phase), and underwent a full-dose CT scan of neck, chest, abdomen, and pelvis, using the following parameters: 120 kV, 60-160 mAs (automatic dose modulation), 0.8-second tube rotation time, a pitch of 1.2, and 1.5-mm slice width.

In this study all patients diagnosed with lymphoma, independent of the histological subtype, underwent a diagnostic <sup>18</sup>F-FDG PET-CT at the request of the treating haematologists in the routine clinical setting.

#### Image interpretation

All observers were aware that the patients had lymphoma, but unaware of the type and grade of lymphoma and other imaging findings. The observers used a standardized form and rated individual nodal groups as negative or positive for disease. Nodal regions, as defined at the Rye Symposium in 1965, included cervical (including supraclavicular, occipital, and preauricular), axillary, infraclavicular, mediastinal, hilar, para-aortic, mesenteric, pelvic, and inguinal femoral lymph node regions [2]. Extranodal regions included spleen, bone marrow, lung, liver, bowel (including gastric), and other (including sites such as muscle, subcutaneous tissue, and breast). Subsequently, extent of disease was evaluated according to the Ann Arbor staging system (stage I-IV) [2, 3].

The whole-body MRI-DWI dataset (i.e. T1W, STIR, and DWI) was transferred to a Picture Archiving and Communications System (PACS) that allows manual window level setting, and systematically evaluated by a board-certified radiologist (observer 1 [R.A.J.N.], with more than 15 years of clinical experience with MRI). The whole-body MRI-DWI dataset was also independently evaluated by another board-certified radiologist (observer 2 [M.S. v. L.], with more than 15 years of clinical experience with MRI). Both observers were blinded to <sup>18</sup>F-FDG PET-CT findings. Results of observers 1 and 2 were used to determine interobserver agreement, whereas only the results of observer 1 were used for comparison with <sup>18</sup>F-FDG PET-CT. At whole-body MRI-

DWI, lymph nodes greater than 10 mm in the short-axis diameter were considered positive. Lymph node sizes were measured in the coronal plane at T1W and STIR. Lymph node size measurements on diffusion-weighted images were not made because these are highly dependent on the applied window level and window width. Rather, diffusion-weighted images were only used to visually detect potential nodal abnormalities. At T1W and STIR, extranodal pathology was evaluated as follows: area of abnormal signal intensity in the spleen, bone or bone marrow, and liver; nodule or infiltration in the lung; and mass of abnormal signal intensity at other extranodal sites. At DWI, several normal extranodal structures (including brain, salivary glands, tonsils, spleen, gallbladder, adrenal glands, prostate, testes, penis, endometrium, ovaries, spinal cord, peripheral nerves, and bone marrow) may exhibit an impeded diffusion [17, 18]. Any focally increased signal intensity in these structures at DWI was considered positive for tumor involvement. In all other areas, any signal intensity higher than that of the spinal cord was considered positive for tumor involvement. An extranodal site was considered positive for lymphomatous involvement if seen either at T1W/STIR or at DWI. Apparent diffusion coefficient (ADC) measurements were not used for tissue characterization, because there are no ADC criteria yet for differentiating malignant from non-malignant lesions at DWI, and reproducibility of ADC measurements in normal-sized lymph nodes may be limited [23]. In addition, signal intensity characteristics of lymph nodes at DWI were not assessed, because there are no validated signal intensity criteria yet that could aid in the discrimination between lymphomatous and normal lymph nodes.

The unenhanced low-dose <sup>18</sup>F-FDG PET-CT images of the <sup>18</sup>F-FDG PET-CT examination were transferred to a dedicated workstation (e-soft, Siemens Medical Systems, Knoxville, TN, USA), and systematically evaluated by a board-certified nuclear medicine physician (J.M.H. de K., with more than 5 years of clinical experience with <sup>18</sup>F-FDG PET-CT), blinded to diagnostic CT and whole-body MRI-DWI findings. A region with <sup>18</sup>F-FDG uptake above background in a location incompatible with normal anatomy or physiology was considered positive for the presence of lymphomatous involvement [12]. The contrast-enhanced full-dose CT images of the <sup>18</sup>F-FDG PET-CT examination were transferred to and interpreted by means of a PACS, and systematically evaluated by another board-certified radiologist (F.J.B., with 24 years of clinical experience with CT) who was blinded to unenhanced low-dose <sup>18</sup>F-FDG PET-CT and whole-body MRI-DWI findings. Lymph nodes greater than 10 mm in the short-axis diameter as measured in the axial plane were considered positive for lymphomatous involvement. Extranodal abnormalities were evaluated according to the standard CT reading criteria as follows: area of abnormal attenuation in the spleen, bone or marrow, and liver; nodule or infiltration in the lung; and mass of soft-tissue attenuation in other extranodal sites. Findings at low-dose <sup>18</sup>F-FDG PET-CT and contrast-enhanced full-dose CT were combined for disease assessment of each

nodal and extranodal region, and to obtain an Ann Arbor stage. For this purpose, in all patients, any nodal or extranodal site was considered positive for lymphomatous involvement if seen at unenhanced low-dose <sup>18</sup>F-FDG PET-CT, regardless of contrast-enhanced full-dose CT findings. In those patients with an <sup>18</sup>F-FDG avid lymphoma, nodal sites that were classified as positive at contrast-enhanced full-dose CT but negative at low-dose <sup>18</sup>F-FDG PET-CT were considered negative for lymphomatous involvement. This is because the size of these lymph nodes (i.e. greater than 10 mm in the short-axis diameter) exceeds the spatial resolution of PET. Consequently, such lymph nodes should be positive at low-dose <sup>18</sup>F-FDG PET-CT if involved by lymphoma. For the same reason, in those patients with an <sup>18</sup>F-FDG avid lymphoma, extranodal sites that were classified as positive at contrast-enhanced full-dose CT but negative at low-dose <sup>18</sup>F-FDG PET-CT were considered negative for lymphomatous involvement, if the size of those extranodal sites were deemed to be well above the spatial resolution of PET (i.e. greater than approximately 10 mm). However, extranodal sites of small size (i.e. smaller than approximately 10 mm) that were classified as positive at contrast-enhanced full-dose CT but negative at low-dose <sup>18</sup>F-FDG PET-CT were considered positive for lymphomatous involvement. This is because low-dose <sup>18</sup>F-FDG PET-CT can miss small extranodal lesions with a size below the spatial resolution of PET (e.g. small lymphomatous lung deposits). Finally, in those patients with a non-<sup>18</sup>F-FDG avid lymphoma, any nodal or extranodal site was considered positive for lymphomatous involvement if seen at contrast-enhanced full-dose CT.

Unilateral bone marrow biopsies of the iliac crest were interpreted by experienced hematopathologists who were blinded to whole-body MRI-DWI and <sup>18</sup>F-FDG PET-CT findings, as part of routine clinical care.

#### Statistical analysis

Interobserver agreement at whole-body MRI-DWI and agreement between whole-body MRI-DWI and <sup>18</sup>F-FDG PET-CT were analyzed using the unweighted  $\kappa$  statistic, defined as poor (<0.2), fair (>0.2 to ≤0.4), moderate (>0.4 to ≤0.6), good (>0.6 to ≤0.8), and very good (>0.8 to ≤1) agreement. These analyses were done for all nodal regions together, for all extranodal regions together, and for all nodal and extranodal regions separately. Percentages of equal staging, understaging, and overstaging of whole-body MRI-DWI relative to <sup>18</sup>F-FDG PET-CT were calculated, along with binomial exact 95% confidence intervals (CIs). Importantly, note that these percentages do not indicate in how many cases whole-body MRI-DWI provided correct or incorrect staging, but that they represent numbers relative to <sup>18</sup>F-FDG PET-CT. Statistical analyses were executed using Stata version 10 software (StataCorp LP, College Station, TX, USA) and SPSS version 15.0 software (SPSS, Chicago, IL, USA).



## Results

### Interobserver agreement

Results regarding interobserver agreement at whole-body MRI-DWI are displayed in **Table 2**. K values for all nodal regions together and for all extranodal regions together were 0.676 and 0.452, respectively, indicating overall moderate to good interobserver agreement. Interobserver agreement in individual nodal and extranodal regions varied between moderate to very good ( $\kappa > 0.4$ ), except for the hilar lymph node region and the bone marrow in which interobserver agreements were poor ( $\kappa = 0.096$ ) and fair ( $\kappa = 0.252$ ), respectively (**Table 2**).

**Table 2.** Interobserver agreement of whole-body MRI-DWI.

Parameter	$\kappa^*$
All nodal regions	0.676 (0.582-0.769)
All extranodal regions	0.453 (0.264-0.641)
Nodal regions	
-Cervical	0.612 (0.331-0.893)
-Axillary	0.944 (0.836-1.000)
-Infralavicular	0.783 (0.551-1.000)
-Mediastinal	0.416 (0.031-0.801)
-Hilar	0.096 (-0.346-0.538)
-Para-aortic	0.636 (0.336-0.937)
-Mesenteric	NA
-Pelvic	0.515 (0.222-0.808)
-Inguinal femoral	0.784 (0.587-0.981)
Extranodal regions	
-Spleen	0.741 (0.403-1.000)
-Bone marrow	0.252 (-0.051-0.556)
-Lung	0.463 (-0.135-1.000)
-Liver	NA
-Bowel	NA

\* 95% confidence interval in parentheses; NA: not applicable (insufficient number of categories to perform statistical analysis)

Comparison between whole-body MRI-DWI and <sup>18</sup>F-FDG PET-CT

Representative examples are displayed in **Figures 1 to 4**. Results regarding the comparison between whole-body MRI-DWI and <sup>18</sup>F-FDG PET-CT on a per-region basis are displayed in **Table 3**.

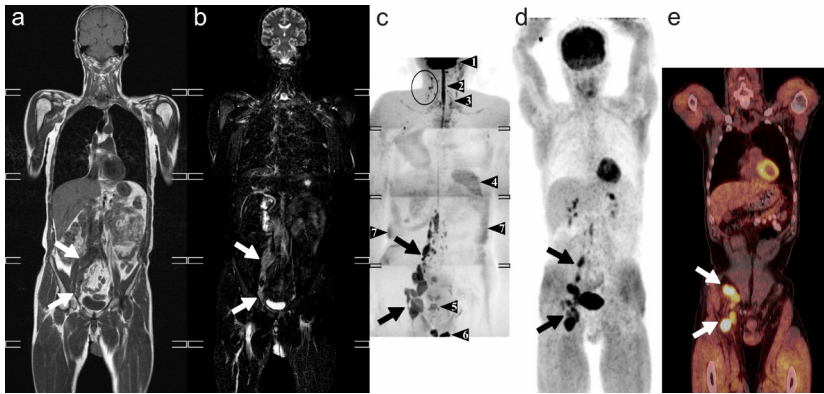


**Figure 1.** A 54-year-old man with stage II follicular B-cell lymphoma (patient 11, **Table 4**) with concordant staging between whole-body MRI-DWI and  $^{18}\text{F}$ -FDG PET-CT. Coronal whole-body T1W (a), STIR (b), maximum intensity projection (MIP) gray-scale inverted diffusion weighted (c), MIP  $^{18}\text{F}$ -FDG PET (d), and combined  $^{18}\text{F}$ -FDG PET-CT (e) show right para-aortic, iliac, and inguinal lymph node involvement (arrows). Note that several normal structures are highlighted at whole-body DWI (c), including brain (arrowhead 1), spinal cord (arrowhead 2), peripheral nerves (arrowhead 3), spleen (arrowhead 4), prostate (arrowhead 5), and testes (arrowhead 6). Also note insufficiently suppressed fat in both flanks (arrowheads 7).

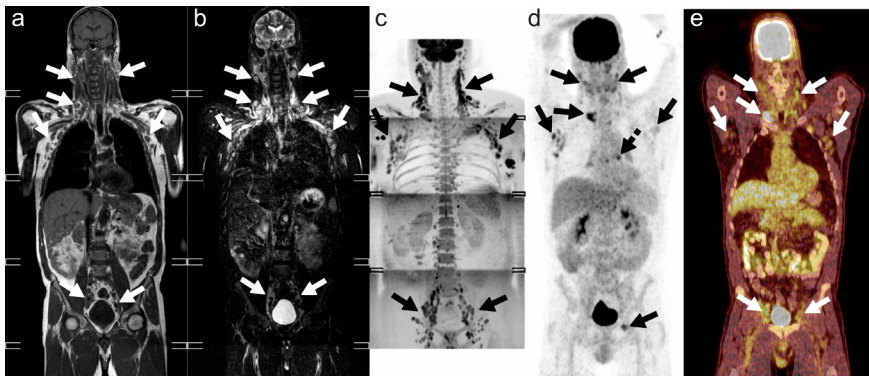


**Figure 2.** A 58-year-old man with stage IV marginal zone B-cell lymphoma (patient 14, **Table 4**) with concordant staging (stage III) of whole-body MRI-DWI and  $^{18}\text{F}$ -FDG PET-CT. Coronal whole-body T1W (a), STIR (b), maximum intensity projection (MIP) gray-scale inverted diffusion weighted (c), MIP  $^{18}\text{F}$ -FDG PET (d), and combined  $^{18}\text{F}$ -FDG PET-CT (e) show extensive lymph node involvement at both sites of the diaphragm (continuous arrows). However, mediastinal lymph node involvement seen at  $^{18}\text{F}$ -FDG PET (d, dashed arrow) was missed at whole-body DWI, probably due to incoherent cardiac motion that induced signal loss. Neither whole-body MRI-DWI nor  $^{18}\text{F}$ -FDG PET-CT detected bone marrow involvement, despite a positive bone marrow biopsy. Note that  $^{18}\text{F}$ -FDG avidity of all lymphomatous lesions in this patient with marginal zone B-cell lymphoma is less than that in the patient with follicular B-cell lymphoma in **Figure 1**. Also note that the bone marrow is well depicted at whole-body DWI (c), which is a normal finding.

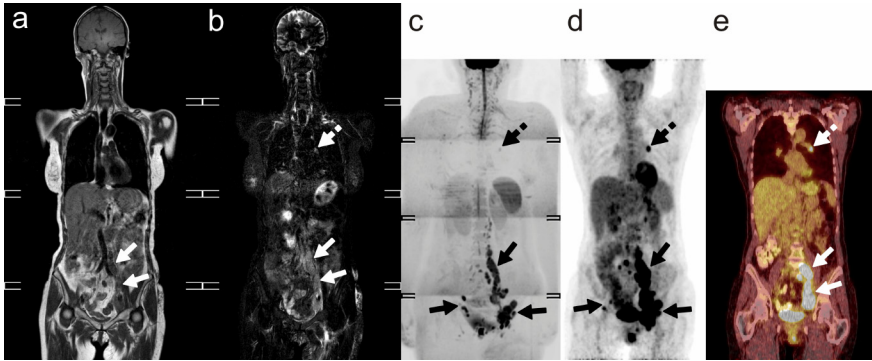


**Figure 3.** A 61-year-old woman with diffuse large B-cell lymphoma (patient 3, Tables 4 and 5) with disagreement in staging between whole-body MRI-DWI and <sup>18</sup>F-FDG PET-CT. Coronal whole-body T1W (a), STIR (b), maximum intensity projection (MIP) gray-scale inverted diffusion weighted (c), MIP <sup>18</sup>F-FDG PET (d), and combined <sup>18</sup>F-FDG PET-CT (e) show para-aortic, iliac, and inguinal lymph node involvement (continuous arrows). At whole-body MRI-DWI, a lung lesion was diagnosed (b, c, dashed arrows), compatible with stage IV disease. The same lesion was depicted at <sup>18</sup>F-FDG PET (d, dashed arrow), but combined <sup>18</sup>F-FDG PET-CT localises the lesion to a hilar lymph node, indicating stage III disease.

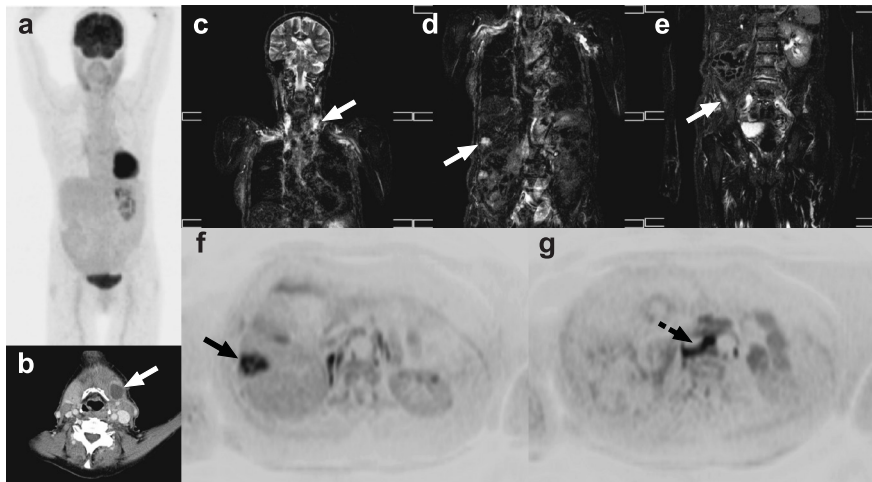


**Figure 4.** A 72-year-old woman with nodal marginal zone lymphoma (patient 15, Tables 4 and 5) with disagreement in staging between whole-body MRI-DWI and <sup>18</sup>F-FDG PET-CT. Coronal maximum intensity projection whole-body <sup>18</sup>F-FDG PET (a) does not show any lymphomatous lesions. However, axial contrast-enhanced CT at the level of the neck (b) shows a left-sided cervical lymph node with a short-axis diameter of 18 mm and necrosis (arrows), which was interpreted as lymphomatous involvement. Therefore, Ann Arbor stage according to <sup>18</sup>F-FDG PET-CT findings was I. Coronal STIR of the head/neck/chest region (c) shows the same left-sided cervical lymph node (arrow), but it was not classified as lymphomatous because it measured 8 mm in short axis. Coronal STIR of the chest/abdominal region (d) shows a lesion in the liver (arrow) which was classified as lymphomatous. This lesion was also seen at CT (not shown), but the CT observer classified this as a hemangioma. Coronal STIR of the abdominal/pelvic region (e) also shows a lesion in the left iliac wing (arrow). Axial gray-scale inverted diffusion-weighted images (f, g) show the same liver lesion that was seen at coronal STIR (arrow) and para-aortic lymph node involvement (dashed arrow). Based on these findings, Ann Arbor stage at whole-body MRI-DWI was IV.

**Table 3.** Agreement between whole-body MRI-DWI and <sup>18</sup>F-FDG PET-CT.

Parameter	$\kappa^*$
All nodal regions	0.597 (0.500-0.694)
All extranodal regions	0.507 (0.323-0.691)
Nodal regions	
-Cervical	0.466 (0.196-0.736)
-Axillary	0.791 (0.597-0.985)
-Infraclavicular	0.482 (0.174-0.791)
-Mediastinal	0.522 (0.158-0.886)
-Hilar	0.371 (0.038-0.705)
-Para-aortic	0.818 (0.582-1.000)
-Mesenteric	0.637 (0.265-1.000)
-Pelvic	0.543 (0.265-0.820)
-Inguinal femoral	0.640 (0.398-0.882)
Extranodal regions	
-Spleen	0.861 (0.597-1.000)
-Bone marrow	0.371 (0.038-0.705)
-Lung	0.776 (0.357-1.000)
-Liver	NA
-Bowel	NA

\* 95% confidence interval in parentheses; NA: not applicable (insufficient number of categories to perform statistical analysis)

$\kappa$  values for all nodal regions together and for all extranodal regions together were 0.597 and 0.507, respectively, indicating overall moderate agreement between the two imaging modalities. Agreement between whole-body MRI-DWI and <sup>18</sup>F-FDG PET-CT in individual nodal and extranodal regions varied between moderate to very good ( $\kappa > 0.4$ ), except for the hilar lymph node region and the bone marrow in which agreements between the two imaging modalities were fair ( $\kappa = 0.371$  for both) (**Table 3**).

Ann Arbor stages according to whole-body MRI-DWI and <sup>18</sup>F-FDG PET-CT, and bone marrow biopsy results of each patient are displayed in **Table 4**. Four patients had non-<sup>18</sup>F-FDG avid lymphomas. In 17 of 22 patients (77.3%; 95% CI: 56.6-89.9%), Ann Arbor stage according to whole-body MRI-DWI was equal to that of <sup>18</sup>F-FDG PET-CT. Whole-body MRI-DWI overstaged relative to <sup>18</sup>F-FDG PET in 5 of 22 patients (22.7%; 95% CI: 10.1-43.4%), but never understaged relative to <sup>18</sup>F-FDG PET (**Table 4**). Causes of discrepant staging are listed in **Table 5**. One cause of overstaging relative to <sup>18</sup>F-FDG PET-CT occurred because whole-body MRI-DWI detected a pulmonary lesion, whereas the same lesion was classified as a positive hilar lymph node at <sup>18</sup>F-FDG PET-CT (**Figure 3**).

**Table 4.** Individual results of included patients: type of lymphoma, <sup>18</sup>F-FDG avidity, Ann Arbor stage according to whole-body MRI-DWI and <sup>18</sup>F-FDG PET-CT and results of bone marrow biopsy. Patients with discrepant scores are displayed in *Italic*. **Table 5** explains the underlying cause of discrepant staging between whole-body MRI-DWI and <sup>18</sup>F-FDG PET-CT.

No.	Lymphoma type	<sup>18</sup> F-FDG avid	Ann Arbor stage		Bone marrow biopsy
			Whole-body MRI-DWI	<sup>18</sup> F-FDG PET-CT	
1	DLBCL	Yes	3	3	Negative
2	DLBCL	Yes	4	4	Negative
3	<i>DLBCL</i>	Yes	4	3	<i>Negative</i>
4	DLBCL	Yes	4	4	Negative
5	DLBCL	Yes	4	4	Negative
6	DLBCL	Yes	4	4	Negative
7	DLBCL	Yes	3	3	Negative
8	<i>FL</i>	Yes	4	3	<i>Negative</i>
9	FL	No	1	1	Negative
10	FL	Yes	1	1	Negative
11	FL	Yes	2	2	Negative
12	MZL, extranodal	Yes	3	3	Positive
13	MZL, extranodal	? No pathology	1	1	Negative
14	MZL, nodal	Yes	3	3	Positive
15	<i>MZL, nodal</i>	<i>No</i>	4	1	<i>Negative</i>
16	SLL	No	3	3	Positive
17	SLL	? No pathology	1	1	Positive
18	SLL	No	1	1	Positive
19	HD, nodular sclerosing	Yes	4	4	Negative
20	HD, nodular sclerosing	Yes	4	4	Positive
21	<i>Anaplastic large cell lymphoma</i>	Yes	2	1	Negative
22	MCL	Yes	4	3	Positive

DLBCL: Diffuse large B-cell lymphoma; FL: Follicular B-cell lymphoma; MZL: Marginal zone lymphoma; SLL: Small-cell lymphocytic lymphoma; HD: Hodgkin's disease, MCL: Mantle cell lymphoma; ? No pathology: unclear whether this lymphoma was <sup>18</sup>F-FDG avid or not, because no pathology was visible at whole-body MRI-DWI and <sup>18</sup>F-FDG PET-CT

Other causes of overstaging relative to <sup>18</sup>F-FDG PET-CT included additional lymph node involvement (n=3), bone marrow, liver, and kidney involvement (n=1), and bone marrow involvement (n=1) that was not identified at <sup>18</sup>F-FDG PET-CT. In 2 of the total number of 22 patients (9.1%; 95% CI: 2.5-27.8%) (patients 15 and 21; **Tables 4 and 5**), whole-body MRI-DWI overstaging relative to <sup>18</sup>F-FDG PET-CT would have had therapeutic consequences (i.e. local therapy would not be an option anymore due to a shift from stage I disease to a higher stage disease).

**Table 5.** Causes of discrepant staging between whole-body MRI-DWI and <sup>18</sup>F-FDG PET-CT.

Patient no.	Ann Arbor stage		Causes of discrepant staging
	Whole-body MRI-DWI	<sup>18</sup> F-FDG PET-CT	
3	IV	III	Lung lesion only at whole-body MRI-DWI, which corresponded to a positive left hilar lymph node at <sup>18</sup> F-FDG PET-CT.
8	IV*	III	Rib, liver, and kidney involvement only at whole-body MRI, not seen at <sup>18</sup> F-FDG PET-CT. Negative bone marrow biopsy.
15	IV	I	Left cervical lymph node involvement at diagnostic CT, in a non- <sup>18</sup> F-FDG avid lymphoma. Para-aortic lymph node, liver involvement, and right iliac crest involvement only at whole-body MRI-DWI. Negative bone marrow biopsy.
21	II	I	Left cervical lymph node involvement only at whole-body MRI-DWI, not seen at <sup>18</sup> F-FDG PET-CT.
22	IV	III	Multiple lymphomatous lymph nodes at both sides of the diaphragm at both whole-body MRI-DWI and <sup>18</sup> F-FDG PET-CT. Midthoracic vertebra and os ilium involvement only at whole-body MRI-DWI. Positive bone marrow biopsy.

\*This patient could not tolerate the MRI examination for more than 30 minutes and only underwent conventional whole-body MRI (T1W and STIR), without DWI.

## Discussion

The clinical application of whole-body MRI-DWI is under active investigation; its comparison to whole-body <sup>18</sup>F-FDG PET-CT is of special interest, since the latter is often regarded as one of the most accurate non-invasive diagnostic tools that is currently available for whole-body oncological imaging [25]. Several advantages of whole-body MRI-DWI over <sup>18</sup>F-FDG PET-CT are that no patient preparation is required, no radiopharmaceuticals have to be administered, and the absence of ionizing radiation. The present study compared whole-body MRI-DWI to <sup>18</sup>F-FDG PET-CT for staging newly diagnosed lymphoma. Overall interobserver agreement at whole-body MRI-DWI was moderate to good, except for the hilar lymph node region and the bone marrow in which interobserver agreements were poor and fair, respectively. The suboptimal interobserver agreement at whole-body MRI may, in part, be explained by the existence of a learning curve for the interpretation of whole-body MRI-DWI datasets. Furthermore, image interpretation was limited by the lack of consensus

quantitative criteria for assessing lymphomatous disease involvement at whole-body MRI-DWI. Interestingly, figures regarding the agreement between whole-body MRI-DWI and <sup>18</sup>F-FDG PET-CT were similar; overall agreement between the two imaging modalities was moderate, except for the hilar lymph node region and the bone marrow in which agreement between the two imaging modalities was fair. Potential difficulties of MRI in the evaluation of the hilar region may be related to the presence of respiratory and cardiac motion artifacts in this area, whereas the bone marrow may show non-specific findings at MRI [26]. Most importantly, our initial results show that staging using whole-body MRI-DWI is equal to that of <sup>18</sup>F-FDG PET-CT in approximately 75% of patients. In the remaining patients, whole-body MRI-DWI overstaged relative to <sup>18</sup>F-FDG PET-CT, but understaging relative to <sup>18</sup>F-FDG PET-CT did not occur. Importantly, whole-body MRI-DWI overstaging relative to <sup>18</sup>F-FDG PET-CT was clinically relevant in 2 of 22 patients. There are several possible explanations why whole-body MRI-DWI overstaged relative to <sup>18</sup>F-FDG PET-CT in some patients. First, the fact that whole-body MRI-DWI located one lesion in the lung in one patient (**Figure 3**), whereas <sup>18</sup>F-FDG PET-CT did not, may be due to the acquisition of T1-weighted and STIR sequences in the coronal plane, which may be less suitable for anatomic localization of pathology than axially acquired images. Second, the additional lymph node involvement detected at whole-body MRI-DWI in some cases can be explained by the fact that lymph nodes were measured in the coronal plane at T1W and STIR, whereas they were measured in the axial plane on the contrast-enhanced full-dose CT component of the <sup>18</sup>F-FDG PET-CT examination. Lymph node size measurements on diffusion-weighted images were not made because these are highly dependent on the applied window level and window width. Third, bone marrow metastases may have been present in some patients for which MRI has been reported to be more sensitive relative to <sup>18</sup>F-FDG-PET-CT [7, 27, 28]. Another important issue is that four patients had non-<sup>18</sup>F-FDG avid lymphomas, which limits the diagnostic reliability of <sup>18</sup>F-FDG PET-CT in these patients.

Interestingly, although this was not the main subject of this study, in 5 of 6 cases with a positive bone marrow biopsy, no bone marrow lesions were visualized at whole-body MRI-DWI and <sup>18</sup>F-FDG PET-CT. In the sixth patient with a positive bone marrow biopsy result, MRI-DWI indicated pathology at two osseous locations while <sup>18</sup>F-FDG PET-CT did not reveal any bone abnormalities. Hence, both modalities appear to have limited sensitivities in detecting lymphomatous bone marrow involvement (**Figure 2**). A plausible explanation for the suboptimal sensitivity of both imaging modalities is that they cannot depict a bone marrow infiltration with only a small percentage of neoplastic cells. Thus, neither whole-body MRI-DWI nor <sup>18</sup>F-FDG PET-CT seem to be sufficiently reliable for the assessment of the bone marrow, and bone marrow biopsy remains a crucial part of the staging work-up of patients with lymphoma.

A limitation of the present study is its relatively small sample size, necessitating the



need for future studies. In our hospital, a baseline <sup>18</sup>F-FDG PET-CT is performed as routine clinical care in all patients diagnosed with lymphoma, independent of the histological (sub)type. In 2007, the imaging subcommittee of the International Harmonization Project, stated that pretherapy <sup>18</sup>F-FDG PET was recommended but not mandatory in patients with HD, diffuse large B-cell lymphoma, follicular lymphoma, and mantle cell lymphoma and mandatory in patients with NHL with variable FDG avidity [13]. However, recently, the expert opinion was adjusted to recommendation of the use of <sup>18</sup>F-FDG PET (<sup>18</sup>F-FDG PET-CT if available) as a baseline for lymphomas that are potentially curable (HD, diffuse large B-cell lymphoma) and to exclude systemic disease in clinically localised lymphoma (HD, diffuse large B-cell lymphoma, follicular lymphoma, mantle cell lymphoma, AIDS-related B-cell lymphoma, nodal and splenic marginal zone lymphoma, peripheral T-cell lymphoma and mucosa-associated lymphoid tumors) [5]. Interestingly, four patients had lymphomas that were not <sup>18</sup>F-FDG avid (**Table 4**), whereas DWI (if performed) always depicted lesions. Thus, DWI may overall be more sensitive than <sup>18</sup>F-FDG PET for the detection of lymphomas [29]. Another limitation of this study is that although bone marrow biopsies of the iliac crest were reviewed in all patients, histopathological correlation at all other locations was lacking. However, obtaining additional biopsies was practically and ethically impossible. Therefore, whole-body MRI-DWI and <sup>18</sup>F-FDG PET-CT staging results were simply compared in the present study without considering either of them as the reference standard. Another limitation is that only patients with newly diagnosed malignant lymphoma were included, and it is still unclear how whole-body MRI (without and with DWI) performs in the follow-up and restaging of malignant lymphoma. Furthermore, it should be acknowledged that the complete whole-body MRI-DWI examination took relatively long (approximately 60 minutes) compared to the <sup>18</sup>F-FDG PET-CT examination (less than 20 minutes). This may be a drawback in very ill patients (e.g. one patient could not complete the examination in the present study), and is a disadvantage with regard to patient throughput in daily clinical practice. Therefore, future studies should assess which (combination of) MRI sequence(s) provide(s) all necessary diagnostic and prognostic information while being time-efficient.

In conclusion, our early results indicate that overall interobserver agreement at whole-body MRI-DWI is moderate to good. Overall agreement between whole-body MRI-DWI and <sup>18</sup>F-FDG PET-CT is moderate. Whole-body MRI-DWI does not understage relative to <sup>18</sup>F-FDG PET-CT in patients with newly diagnosed lymphoma. In a minority of patients, whole-body MRI-DWI leads to clinically important overstaging relative to <sup>18</sup>F-FDG PET-CT. <sup>18</sup>F-FDG PET-CT remains the gold standard for staging lymphoma until future, larger studies have shown that whole-body MRI-DWI provides correct upstaging in such cases.



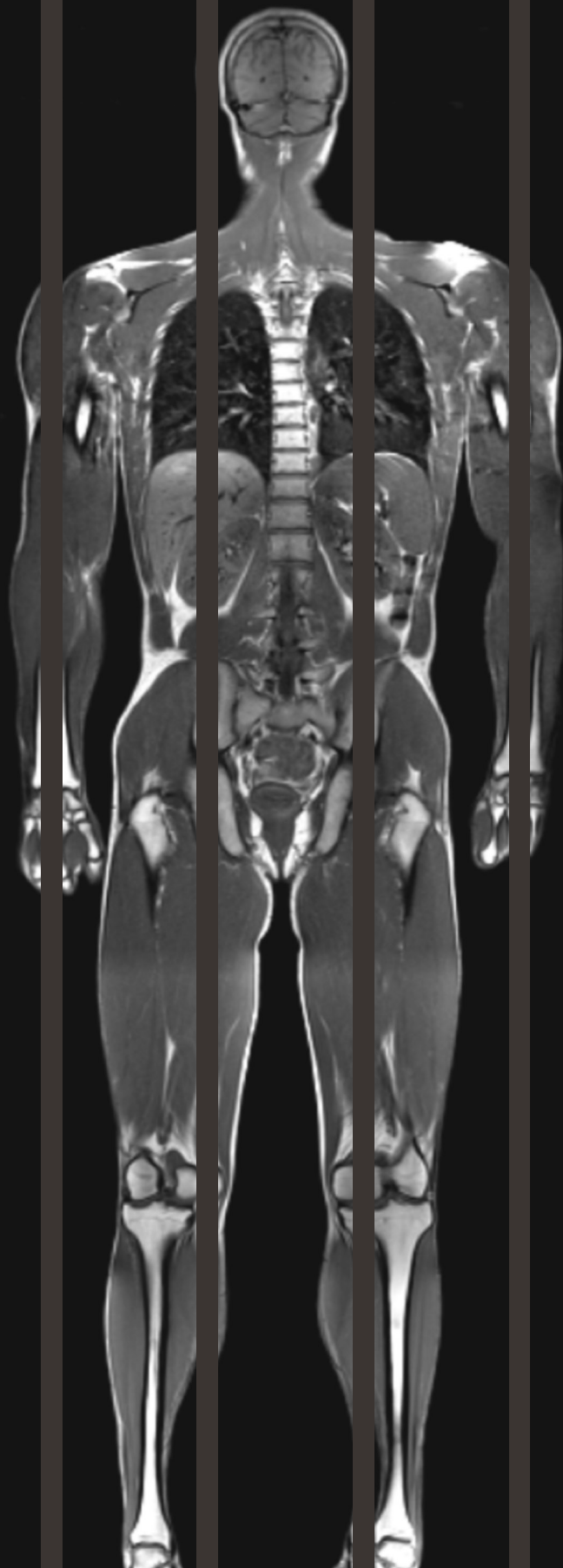
## Acknowledgements

This study was supported by ZonMw Program for Health Care Efficiency Research (grant number 80-82310-98-08012). Furthermore, the authors would like to thank Willem P.Th.M. Mali, MD, PhD, Professor, University Medical Center Utrecht (Department of Radiology) for his contribution to this study.

## References

1. Jemal A, Siegel R, Ward E, Murray T, Xu J, Thun MJ. Cancer statistics, 2007. *CA Cancer J Clin* 2007;57:43-66
2. Armitage JO. Staging non-Hodgkin lymphoma. *CA Cancer J Clin* 2005; 55:368-376
3. Connors JM. State-of-the-art therapeutics: Hodgkin's lymphoma. *J Clin Oncol* 2005;23:6400-6408
4. Seam P, Juweid ME, Cheson BD. The role of FDG-PET scans in patients with lymphoma. *Blood* 2007;110:3507-3516
5. Delbeke D, Stroobants S, de Kerviler, Gisselbrecht C, Meignan M, Conti PS. Expert opinions on positron emission tomography and computed tomography imaging in lymphoma. *Oncologist* 2009;14 Suppl 2:S30-S40
6. Kwee TC, Kwee RM, Nievelstein RA. Imaging in staging of malignant lymphoma: a systematic review. *Blood* 2008;111:504-516
7. Pakos EE, Fotopoulos AD, Ioannidis JP. 18F-FDG PET for evaluation of bone marrow infiltration in staging of lymphoma: a meta-analysis. *J Nucl Med* 2005;46:958-963
8. Rodriguez M, Rehn S, Ahlstrom H, Sundstrom C, Glimelius B. Predicting malignancy grade with PET in non-Hodgkin's lymphoma. *J Nucl Med* 1995;36:1790-1796
9. Schoder H, Noy A, Gonen M, et al. Intensity of 18fluorodeoxyglucose uptake in positron emission tomography distinguishes between indolent and aggressive non-Hodgkin's lymphoma. *J Clin Oncol* 2005;23:4643-4651
10. Boder-Milin C, Kraeber-Bodéré F, Moreau P, Campion L, Dupas B, Le Gouill S. Investigation of FDG-PET-CT imaging to guide biopsies in the detection of histological transformation of indolent lymphoma. *Haematologica* 2008;93:471-472
11. Lin C, Itti E, Haioun C, et al. Early 18F-FDG PET for prediction of prognosis in patients with diffuse large B-cell lymphoma: SUV-based assessment versus visual analysis. *J Nucl Med* 2007;48:1626-1632
12. Juweid ME, Stroobants S, Hoekstra OS, et al. Use of positron emission tomography for response assessment of lymphoma: consensus of the Imaging Subcommittee of International Harmonization Project in Lymphoma. *J Clin Oncol* 2007;25:571-578
13. Cheson BD, Pfistner B, Juweid ME, et al. Revised response criteria for malignant lymphoma. *J Clin Oncol* 2007;25:579-586
14. Huang B, Law MW, Khong PL. Whole-body PET-CT scanning: estimation of radiation dose and cancer risk. *Radiology* 2009;251:166-174
15. Plathow C, Walz M, Lichy MP, et al. Cost considerations for whole-body MRI and PET/CT as part of oncologic staging. *Radiologe* 2008;48:384-396
16. Lauenstein TC, Semelka RC. Whole-body magnetic resonance imaging. *Top Magn Reson Imaging* 2005;16:15-20
17. Takahara T, Imai Y, Yamashita T, Yasuda S, Nasu S, Van Cauteren M. Diffusion weighted whole body imaging with background body signal suppression (DWIBS): technical improvement using free breathing, STIR and high resolution 3D display. *Radiat Med* 2004;22:275-282
18. Kwee TC, Takahara T, Ochiai R, Nievelstein RA, Luijten PR. Diffusion-weighted whole-body imaging with background body signal suppression (DWIBS): features and potential applications in oncology. *Eur Radiol* 2008;18:1937-1952

19. Sumi M, Van CM, Nakamura T. MR microimaging of benign and malignant nodes in the neck. *AJR Am J Roentgenol* 2006;186:749-757
20. King AD, Ahuja AT, Yeung DK, et al. Malignant cervical lymphadenopathy: diagnostic accuracy of diffusion-weighted MR imaging. *Radiology* 2007;245:806-813
21. Holzapfel K, Duetsch S, Fauser C, Eiber M, Rummeny EJ, Gaa J. Value of diffusion-weighted MR imaging in the differentiation between benign and malignant cervical lymph nodes. *Eur J Radiol* 2009;72:381-387
22. Takahara T, Kwee TC, Kifune S, et al. Whole-body MRI using a sliding table and repositioning surface coil approach. *Eur Radiol* 2010;20:1366-1373
23. Kwee TC, Takahara T, Luijten PR, Nievelstein RA. ADC measurements of lymph nodes: Inter- and intra-observer reproducibility study and an overview of the literature. *Eur J Radiol* 2010;75:215-220
24. Basu S, Zaidi H, Alavi A. Clinical and research applications of quantitative PET imaging and positron emission tomography-computed tomography in oncology. *PET Clin* 2007;2:161-172
25. Schmidt GP, Kramer H, Reiser MF, Glaser C. Whole-body magnetic resonance imaging and positron emission tomography-computed tomography in oncology. *Top Magn Reson Imaging* 2007;18:193-202
26. Vande Berg BC, Lecouvet FE, Michaux L, Ferrant A, Maldague B, Malghem J. Magnetic resonance imaging of the bone marrow in hematological malignancies. *Eur Radiol* 1998;8:1335-1344
27. Schmidt GP, Schoenberg SO, Schmid R, et al. Screening for bone metastases: whole-body MRI using a 32-channel system versus dual-modality PET-CT. *Eur Radiol* 2007;17:939-949
28. Kwee TC, Kwee RM, Verdonck LF, Bierings MB, Nievelstein RA. Magnetic resonance imaging for the detection of bone marrow involvement in malignant lymphoma. *Br J Haematol* 2008;141:60-68
29. Elstrom R, Guan L, Baker G, et al. Utility of FDG-PET scanning in lymphoma by WHO classification. *Blood* 2003;101:3875-3876



# Chapter 9

## MRI for staging lymphoma: whole-body or less?

Kwee TC, Akkerman EA, Fijnheer R, Kersten MJ, Zsíros J, Ludwig I, Bierings MB,  
Vermoolen MA, Maarten S. van Leeuwen, Stoker J, Nivelstein RA

## Abstract

### Purpose

To assess whether whole-body magnetic resonance imaging (MRI) detects more clinically relevant lesions (i.e. leading to a change in Ann Arbor stage) than an MRI protocol that only includes the head/neck and trunk (i.e. from cranial vertex to groins, excluding the arms) in patients with lymphoma.

### Materials and methods

One hundred consecutive patients with newly diagnosed lymphoma prospectively underwent T1-weighted and T2-weighted short inversion time inversion recovery whole-body MRI. The number of lymphomatous sites at MRI with a field of view (FOV) limited to the head/neck and trunk, and the additional number of lymphomatous sites at whole-body MRI and their influence on Ann Arbor stage were determined.

### Results

At MRI with a FOV limited to the head/neck and trunk, 507 sites were classified as lymphomatous. At whole-body MRI, 7 additional sites outside the head/neck and trunk in 7 patients (7.0%; 95% confidence interval: 3.4-13.8%) were classified as lymphomatous, but this did never changed Ann Arbor stage.

### Conclusion

Whole-body MRI did not detect any clinically relevant lesions outside the FOV of an MRI protocol that only includes the head/neck and trunk. Therefore, it may be sufficient to only include the head/neck and trunk when using MRI for staging lymphoma.

## Introduction

Hodgkin lymphoma (HL) and non-Hodgkin lymphoma (NHL) comprise approximately 5% to 6% of all malignancies and are the fifth most frequently occurring type of cancer in the Western World [1]. Once the diagnosis of lymphoma has been established by biopsy of a particular site, determination of disease extent (staging) is important for appropriate treatment planning, determining prognosis and monitoring treatment [2-4]. Computed tomography (CT) is the most commonly used imaging modality for the staging of patients with newly diagnosed lymphoma [5]. However, CT is accompanied by a considerable amount of ionizing radiation, which may induce second cancers [6]. Whole-body magnetic resonance imaging (MRI) may be a valuable alternative to CT as there is no associated risk of ionizing radiation exposure [7]. A recent study in 31 patients with lymphoma reported that staging results of whole-body MRI were equal to those of CT in 74% (23/31) and higher in 26% (8/31) of patients, with correct/incorrect/unresolved overstaging relative to CT in 3, 2 and 1 patient(s) respectively [7]. Furthermore, whole-body MRI may be an alternative to <sup>18</sup>F-fluoro-2-deoxy-D-glucose positron emission tomography (FDG-PET)/CT as well [8]. In another study of 31 patients with lymphoma, it was reported that agreement between whole-body MRI and an enhanced FDG-PET/CT reference standard was very good for nodal and extranodal staging ( $k=0.96$  and  $k=0.86$ , respectively) which improved following elimination of perceptual errors ( $k=0.97$  and  $k=0.91$ , respectively). In addition, the sensitivity and specificity of whole-body MRI (following removal of perceptual errors) were reported to be 98% and 99%, respectively, for nodal disease and 91% and 99%, respectively, for extranodal disease [8]. CT is usually performed from the head to the groins (excluding the arms), whereas whole-body MRI refers to MRI of the area from the cranial vertex to the toes (including the arms) (**Figure 1**). However, it is unknown whether a whole-body MRI protocol is necessary, or whether an MRI protocol that only has the usual CT coverage (i.e. from cranial vertex to groins) is comparable while less time-consuming. The aim of this prospective study was therefore to assess whether MRI of the entire body (whole-body MRI) detects more clinically relevant lesions than an MRI protocol that only includes the head/neck and trunk in patients with lymphoma.



**Figure 1.** Coronal T1W whole-body MRI (from cranial vertex to toes, including the arms). The area within the dashed rectangle corresponds to the usual CT coverage for staging lymphoma (i.e. from cranial vertex to groins, excluding the arms).



## Materials and Methods

### Organization and funding

This prospective multicenter study was approved by the institutional review boards of the University Medical Center Utrecht, the Meander Medical Center Amersfoort, and the Academic Medical Center Amsterdam. The Dutch Organization for Health Research and Development (ZonMw), Health Care Efficiency Research programme, funded the study (ZonMw grant number 80-82310-98-08012). ZonMw approved the study protocol after consulting national and international independent reviewers. Data collection, data analysis, and interpretation of data, writing of the paper, and decision to submit were left to the authors' discretion and were not influenced by ZonMw. Of note, the present study does not involve any comparison between whole-body MRI and other diagnostic tests such as CT, FDG-PET(/CT), and bone marrow biopsy regarding tumor staging, because its aim is merely to assess the additional value of a whole-body field of view (FOV) over that of a more limited FOV for the MRI evaluation of lymphoma. Comparative studies (including a larger series of patients) between whole-body MRI and other diagnostic tests will be reported in future, separate manuscripts.

### Study participants

Patients aged 8 years and older with newly diagnosed, histologically proven lymphoma were prospectively included. Children under the age of 8 years were not included, because of the possible need of sedating agents in this patient group. All patients were consecutively enrolled (May 2006 - September 2010) after they had been properly informed and had provided written informed consent. The parent(s) or guardian(s) of all patients aged below 18 years also provided written informed consent. All patients underwent whole-body MRI within 15 days of diagnosis and before start of treatment. Patients with general contraindications to MRI, such as an implanted pacemaker and claustrophobia, were excluded from enrollment.

### MRI protocol

Whole-body MRI was performed using a 1.5-T system (Achieva, Philips Healthcare or Magnetom Avanto, Siemens Medical Solutions). Coronal T1-weighted (T1W) turbo spin-echo and half-Fourier multishot T2-weighted short inversion time inversion recovery (T2W-STIR) turbo spin-echo whole-body images were acquired, using either the built-in body coil (Achieva, Philips Healthcare) or whole-body phased-array surface coils (Magnetom Avanto, Siemens Medical Solutions) for signal reception. Images were acquired under free breathing, except for the stations covering the chest, abdomen, and pelvis, which were acquired using breath-holding or respiratory triggering. Sequence parameters for T1W were: repetition time (TR)/echo time (TE) of 537/18 ms, slice thickness/gap 6/1 mm, FOV of 500 (Magnetom Avanto) or 530

(Achieva)  $\times 265 \text{ mm}^2$ , acquisition matrix of  $208 \times 287$ , number of excitations of 1, acquired voxel size of  $1.27 \times 1.85 \times 6.00 \text{ mm}^3$ , reconstructed voxel size of  $1.04 \times 1.04 \times 6.00 \text{ mm}^3$ , craniocaudal coverage of 185.5 cm, total effective scan time of 5 min 29 s. Parameters for T2W-STIR were as follows: TR/TE/inversion time (IR) 2444/64/165 ms, slice thickness/gap of 6/1 mm, FOV of 500 (Magnetom Avanto) or 530 (Achieva)  $\times$ , acquisition matrix of  $336 \times 120$ , number of excitations of 2, acquired voxel size of  $1.58 \times 2.21 \times 6.00 \text{ mm}^3$ , reconstructed voxel size of  $1.04 \times 1.04 \times 6.00 \text{ mm}^3$ , craniocaudal coverage of 185.5 cm, total effective scan time 5 min 8 s. Total actual scan time of T1W and T2W-STIR whole-body MRI was approximately 25-30 minutes. Seamless coronal whole-body T1W and T2W-STIR images were created by merging separately acquired stations using software implemented in the standard operating console. The applied whole-body MRI protocol yielded a craniocaudal coverage of 185.5 cm, which was deemed to be sufficiently large to image the area from the cranial vertex to toes in the majority of patients. However, if the patient's length exceeded 185.5 cm, the most caudal part of the body (corresponding to the patient's feet/and or distal tibiae) was not included in the image volume. Furthermore, as much as possible of the arms was included in this whole-body MRI protocol that had a (maximum) left-to-right coverage of 50.0 (Magnetom Avanto) or 53.0 cm (Achieva).

#### Evaluation of MRI data

All images were transferred to and interpreted by means of a Picture Archiving and Communications System that allows manual window level setting (Easy Vision, Philips Healthcare, Best, The Netherlands). A board-certified radiologist (R.A.J.N., with 14 years of clinical experience with MRI) evaluated the T1W and T2W-STIR whole-body images. The observer was aware that the patients had lymphoma, but unaware of the type and grade of lymphoma and findings of other imaging modalities. Firstly, image quality of T1W and T2W-STIR whole-body images was graded subjectively based on a general impression and the presence of artefacts. A scale of 1–4 was used (1=very good image quality without artefacts; 2=good image quality with slight, diagnostically irrelevant artefacts; 3=adequate image quality with diagnostically relevant artefacts; 4=inadequate image quality with marked artefacts). Secondly, the observer used a standardized form and rated individual nodal groups as negative or positive for disease. Nodal regions, as defined at the Rye Symposium in 1965, included left and right cervical (including supraclavicular, occipital, and pre-auricular), left and right axillary, left and right infraclavicular, mediastinal, hilar, para-aortic, mesenteric, left and right pelvic, and left and right inguinal femoral lymph node regions [3]. Extranodal regions included spleen, bone marrow inside the head/neck and trunk, bone marrow outside the head/neck and trunk, lung, liver, bowel (including gastric), and other (including sites such as muscle, subcutaneous tissue, and breast). Lymph nodes greater than 10 mm in the short-axis diameter were considered positive for

lymphomatous involvement. Extranodal pathology was evaluated as follows: area of abnormal attenuation/signal intensity (relative to the surrounding tissue) in the spleen, bone or bone marrow, and liver; nodule or infiltration in the lung; and mass of soft-tissue attenuation/abnormal signal intensity (relative to the surrounding tissue) in other extranodal sites. Subsequently, in each patient an Ann Arbor stage (I-IV) [2-4, 9] was assigned according to 1) MRI findings limited to the head/neck and trunk (i.e. from cranial vertex to groins, excluding the arms), and 2) whole-body MRI findings (i.e. from cranial vertex to toes, including the arms).

A research fellow (T.C.K.) determined the total number of lymphomatous nodal and extranodal sites at MRI with a FOV limited to the head/neck and trunk, and the additional number of lymphomatous nodal and extranodal sites at whole-body MRI. In addition, the proportion of patients with lymphomatous lesions outside the head/neck and trunk was calculated, along with binomial exact 95% confidence intervals (CIs), and the number of patients in whom these lesions would change Ann Arbor stage was determined. No comparison was made with other diagnostic tests such as CT, FDG-PET(/CT), or bone marrow biopsy. In addition, no reference standard was used, because the aim of this study was merely to assess whether whole-body MRI detects more clinically relevant lesions than an MRI protocol with the regular anatomical coverage for staging lymphoma, rather than assessing the diagnostic performance of MRI itself. Statistical analyses were executed using Stata version 10 software (StataCorp LP, College Station, TX, USA).

## Results

A total of 121 patients were potentially eligible for inclusion. However, 21 patients had to be excluded because of the following reasons: unwillingness to undergo an additional whole-body MRI examination due to psychological stress, physical complaints, logistic circumstances, and/or other unexplained reasons (n=17), claustrophobia (n=1), psychological stress during the MRI examination (n=1), technical problems of the MRI system (n=1), other disease than lymphoma (n=1). Thus, a total of 100 consecutive patients (63 men and 37 women; mean age, 50.0 years; median age, 55.5 years; age range, 12-82 years) with newly diagnosed, histologically proven lymphoma (HL: n=20; NHL: n=80) prospectively underwent whole-body MRI (**Table 1**).

In 45 of 100 patients, whole-body MRI could be performed from cranial vertex to toes, whereas in the remaining 55 patients, the distal part of the feet (n=22), the whole feet (n=13), or feet and distal tibiae (n=20) were outside the image volume. In 56 of 100 patients, both arms were completely inside the image volume, whereas in the remaining 44 patients, arms were only partially inside the image volume.

T1W image quality was graded as 1 (very good image quality without artefacts) in 5 cases, as 2 (good image quality with slight, diagnostically irrelevant artefacts) in 70 cases, as 3 (adequate image quality with diagnostically relevant artefacts) in 24

**Table 1.** Characteristics of included patients.

Characteristics	HL	NHL
No. of patients	21	79
Sex (n)		
Men	13	50
Women	8	29
Age (y)		
Mean $\pm$ SD	26.4 $\pm$ 15.3	56.2 $\pm$ 17.3
Range	13 - 55	12 - 82
Histological subtype (n)		
Nodular sclerosing Hodgkin lymphoma	17	
Lymphocyte-rich Hodgkin lymphoma	2	
Nodular lymphocyte predominant Hodgkin lymphoma	2	
Diffuse large B-cell lymphoma		32
Follicular lymphoma		19
Extranodal marginal zone lymphoma		8
Mantle cell lymphoma		7
Nodal marginal zone lymphoma		3
Small lymphocytic lymphoma		4
Anaplastic large cell lymphoma		2
Waldenström's macroglobulinemia		2
Angioimmunoblastic T-cell lymphoma		1
Non-specified lymphoproliferative disorder		1

cases, and as 4 (inadequate image quality with marked artefacts) in 1 case; the mean grading was 2.2. T2W-STIR image quality was graded as 1 in 1 case, as 2 in 85 cases, and as 3 in 14 cases; the mean grading was 2.1. Artefacts at both T1W and T2W-STIR were primarily seen in the chest and abdomen and were caused by respiration, heart pulsation or motion.

At MRI with a FOV limited to the head/neck and trunk, a total of 387 nodal sites (left cervical: n=43; right cervical: n=38; left axillary: n= 26; right axillary: n=19; left infraclavicular: n=22; right infraclavicular: n=13; mediastinal: n=47; hilar: n=24; para-aortic: n=42; mesenteric: n=20; left pelvic: n=19; right pelvic: n=19; left inguinal femoral: n=27; right inguinal femoral) and a total of 120 extranodal sites (spleen: n=21; bone marrow inside the head/neck and trunk: n=29; lung: n=11; liver: n=10; bowel: n=6; other: n=43 [Waldeyer's ring: n=14; thymus: n=11; salivary glands: n=4, kidney: n=4; muscle: n=4; orbit: n=1; tongue: n=1; subdiaphragmatic soft tissue: n=1; bladder: n=1; testis: n=1; skin: n=1]) were classified as lymphomatous (**Table 2**). At whole-body MRI, 1 additional nodal site (right popliteal lymph node: n=1) and 6 additional extranodal sites (bone marrow outside the head/neck and trunk: n=6) were classified as lymphomatous. These additional lesions outside the head/neck and trunk were found in 7 of 100 patients (7.0%; 95% CI: 3.4-13.8%). Clinical details of these seven

**Table 2.** Number of nodal and extranodal sites that was classified as lymphomatous at MRI with a FOV limited to the head/neck and trunk.

<b>Nodal sites (n=387)</b>	<b>Extranodal sites (n=120)</b>
Left cervical (n=43)	Spleen (n=21)
Right cervical (n=38)	Bone marrow inside head/neck and trunk (n=29)
Left infraclavicular (n=22)	Lung (n=11)
Right infraclavicular (n=13)	Liver (n=10)
Left axillary (n=26)	Bowel (n=6)
Right axillary (n=19)	Other (n=43)
Mediastinal (n=47)	
Hilar (n=24)	
Para-aortic (n=42)	
Mesenteric (n=20)	
Left pelvic (n=19)	
Right pelvic (n=19)	
Left inguinal/femoral (n=27)	
Right inguinal/femoral (n=28)	

patients are displayed in **Table 3**. The presence of lymphomatous lesions outside the head/neck and trunk led to a higher Ann Arbor stage in none of these 7 patients. Examples of patients with lymphomatous lesions outside the head/neck and trunk are displayed in **Figures 2-5**.

**Table 3.** Clinical details of the 7 patients with lymphomatous lesions outside the head/neck and trunk. Lymphomatous lesions outside the head/neck and trunk are displayed in italic.

<b>No.</b>	<b>Sex (M/F)</b>	<b>Age (y)</b>	<b>Lymphoma type</b>	<b>Locations of lymphomatous lesions</b>	<b>Ann Arbor stage</b>
1	M	16	Nodular sclerosing Hodgkin lymphoma	Left and right cervical, left infraclavicular, mediastinal, and left and right inguinal lymph nodes; thymus; spleen; liver; bone marrow inside the head/neck and trunk (left humeral head, lumbar vertebrae, left and right ilium, left and right femoral heads); <i>bone marrow outside the head/neck and trunk (left distal femoral metaphysis)</i>	IV
2	F	44	Diffuse large B-cell lymphoma	Right cervical and left inguinal lymph nodes; pleura; chest wall; liver; small intestine; left kidney; bone marrow inside the head/neck and trunk (sternum, left ilium, left greater trochanter); <i>bone marrow outside the head/neck and trunk (right distal tibial metaphysis)</i>	IV

Table 3. Continued

No.	Sex (M/F)	Age (y)	Lymphoma type	Locations of lymphomatous lesions	Ann Arbor stage
3	F	71	Waldenström's macroglobulinemia	Mediastinal, hilar, and left and right inguinal lymph nodes; bone marrow inside the head/neck and trunk (sternal manubrium, right acetabulum); <i>bone marrow outside the head/neck and trunk (right humeral mid-diaphysis, left and right femoral mid-diaphyses, left tibial mid-diaphysis)</i>	IV
4	M	55	Follicular lymphoma	Right pelvic, right inguinal, and right popliteal lymph nodes	II
5	M	65	Nodular sclerosing Hodgkin lymphoma	Mediastinal, para-aortic, left and right pelvic, and right inguinal lymph nodes; bone marrow inside the head/neck and trunk (left and right humeral heads, left and right femoral heads, left and right greater trochanters); <i>bone marrow outside the head/neck and trunk (left proximal/mid-diaphysis, right proximal/mid-/distal diaphysis, right distal femoral metaphysis)</i>	IV
6	M	28	Diffuse large B-cell lymphoma	Left and right axillary, right infraclavicular, para-aortic, left and right pelvic, and left and right inguinal lymph nodes; Waldeyer's ring; bone marrow inside the head/neck and trunk (sacrum); <i>bone marrow outside the head/neck and trunk (left tibial distal diaphysis)</i>	IV
7	M	20	Diffuse large B-cell lymphoma	Para-aortic lymph nodes; right orbit; bone marrow inside the head/neck and trunk (skull, left jaw, clavicles, right scapula, sternum, ribs, vertebrae, right sacrum, left and right femoral mid-diaphyses); bone marrow outside the head/neck and trunk ( <i>left humeral mid-diaphysis, left distal epiphysis, right radius</i> )	IV

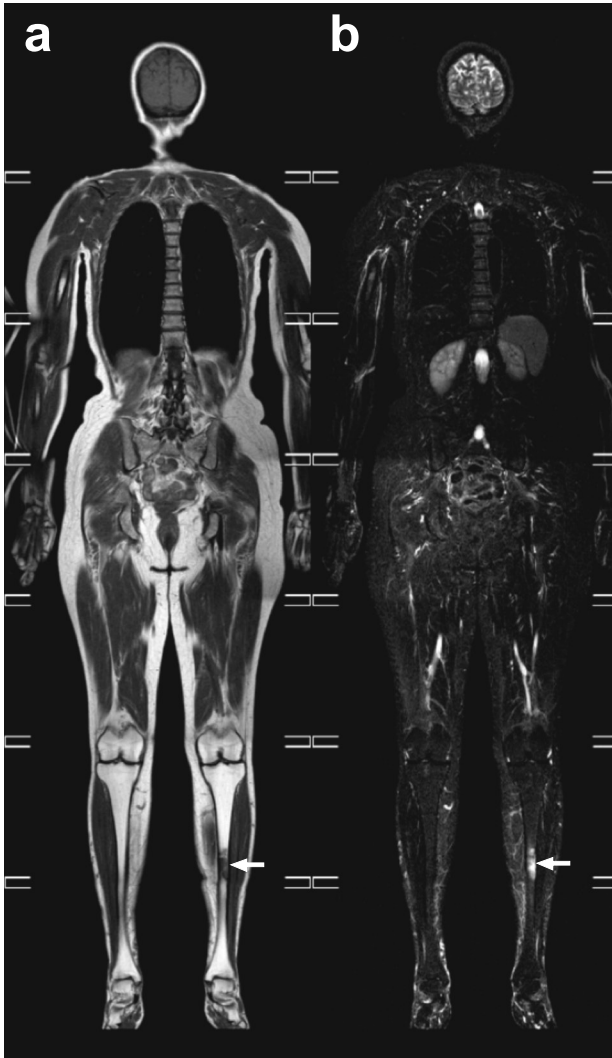


**Figure 2.** Coronal T1W (a) and T2W-STIR (b) whole-body MRI in a 71-year-old female with stage IV Waldenström's macroglobulinemia (Table 3, patient no. 3). A left tibial bone marrow lesion is seen (arrows) that would have remained undetected if only the area from the head to the groins would have been imaged. Nevertheless, the presence of this tibial bone marrow lesion does not change Ann Arbor stage in this patient.



**Figure 3.** Coronal T1W (a) and T2W-STIR (b) whole-body MRI in a 55-year-old male with stage II follicular lymphoma (Table 3, patient no. 4). An enlarged right popliteal lymph node is seen (arrows), suggestive of lymphomatous involvement. This lymph node would have remained undetected if only the area from the head to the groins would have been imaged. Nevertheless, the presence of this enlarged popliteal lymph node does not change Ann Arbor stage in this patient.



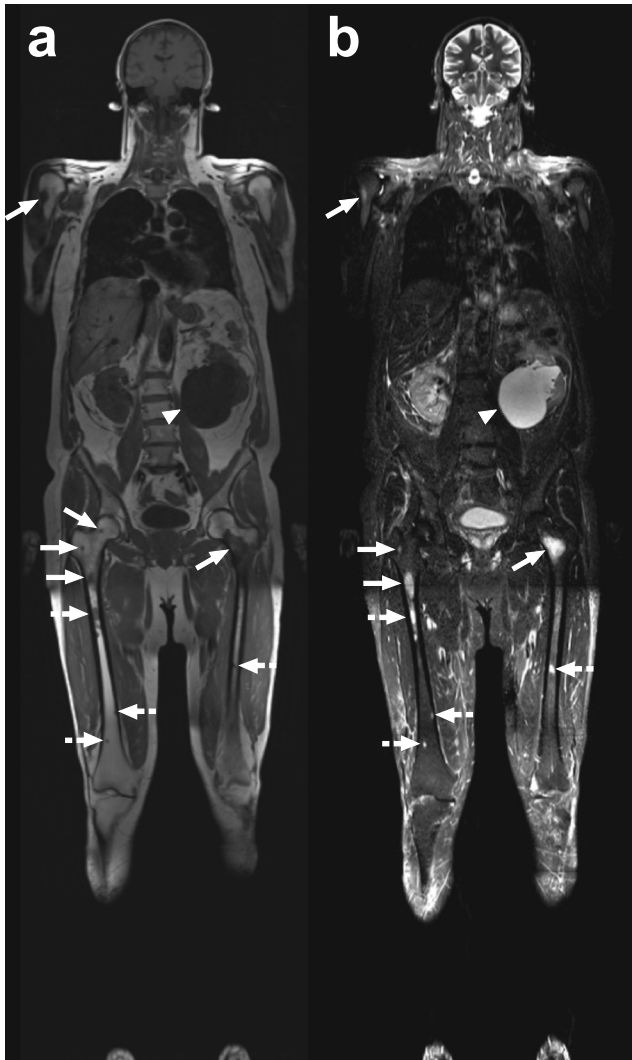


**Figure 4.** Coronal T1W (a) and T2W-STIR (b) whole-body MRI in a 65-year-old male with stage IV nodular sclerosing Hodgkin lymphoma (Table 3, patient no. 5). Bone marrow involvement is shown in the right humeral head and in both femurs (continuous arrows). However, several femoral bone marrow lesions would have been missed if only the area from the head to the groins would have been imaged (dashed arrows). Nevertheless, the presence of these additional femoral bone marrow lesions does not change Ann Arbor stage in this patient. Also note a left-sided hydronephrosis due to ureteropelvic junction stenosis (arrowheads).



**Figure 5.** Coronal T1W (a) and T2W-STIR (b) whole-body MRI in a 65-year-old female with stage IV mantle cell lymphoma. An enlarged right biceps femoris muscle is seen, with increased signal intensity at STIR (arrows), suggestive of lymphomatous involvement. Although a part of this lesion would also have been detected if only the area from the head to the groins would have been imaged, true whole-body MRI allows for the assessment of the extent of the entire lesion. Also note a left-sided pleural effusion (arrowheads).

## Discussion

The results of this prospective study, which included 100 consecutive patients with newly diagnosed lymphoma, show that it is uncommon for these patients to have lesions outside the head/neck and trunk at MRI. Moreover, in the small minority of patients who have lesions outside the head/neck and trunk at MRI, the Ann Arbor stage is not increased as a result of the presence of these lesions. Thus, an MRI protocol that is limited to the head/neck and trunk appears to perform equally well to a true whole-body MRI protocol in terms of Ann Arbor staging.

There are only a few previous studies which investigated the impact of the applied FOV of imaging studies on lesion detection rate in lymphoma. In a study by Nguyen et al. [10] who assessed the prevalence of soft tissue metastases (defined as metastases to skeletal muscle and subcutaneous tissues) outside the standard FOV (i.e. outside the region from the skull-base to upper-thigh) on FDG-PET studies of 88 patients with lymphoma, it was reported that only 1 patient (1.1%) had soft tissue metastases outside the standard FOV. The findings of Nguyen et al. [10] are in line with our study, because none of our patients had soft tissue metastasis outside the head/neck and trunk at MRI. Unfortunately, in that paper the analysis was limited to soft tissue metastases only, and the presence of lymph node and skeletal involvement outside the standard FOV was not assessed. Other case studies have reported that lymphomatous involvement can occur in popliteal lymph nodes [11, 12] and distal skeletal bones [13-16]. Although these case studies only show selective clinical examples, they were also seen in the present, prospective study. That is, of the seven patients with lymphomatous lesions outside the head/neck and trunk at MRI, one patient had an involved popliteal lymph node, and the remaining six patients had distally located bone marrow lesions.

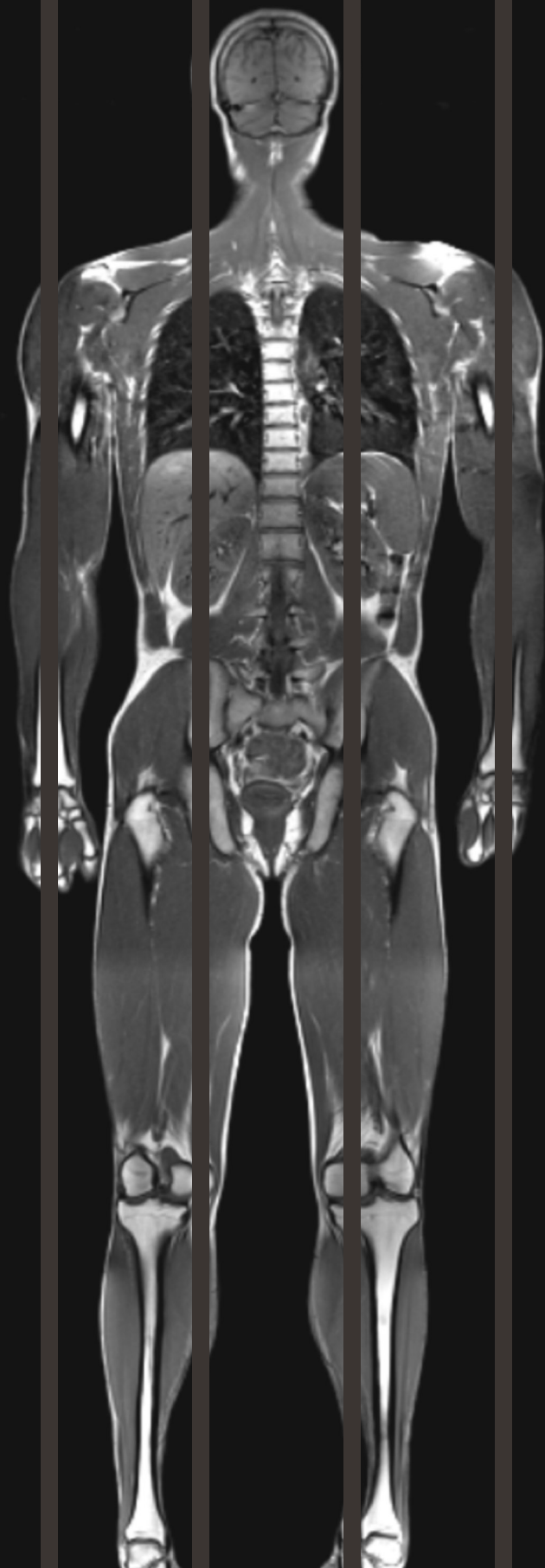
This study has several limitations. Firstly, the complete body could not be imaged in all patients because a fixed FOV was used. Complete craniocaudal coverage was achieved in only 45% of patients, and complete left-to-right coverage was achieved in only 56% of patients. Consequently, the number of lymphomatous lesions outside the head/neck and trunk may have been underestimated. However, it should be noted that the FOV in the left-right direction was already set at a maximum. In addition, although it would be desirable to increase the craniocaudal coverage in tall patients, this was deemed inappropriate because it would exceed the maximum allowable scan time that was set at 30 minutes. Furthermore, as the number of lesions in the lower extremities was very low, it is very unlikely that this limitation in the FOV had substantial effect on the results. Secondly, the results of this study may only be applicable to the MRI sequences that were used in this study. However, T1W and T2W-STIR can be regarded as standard MRI sequences for staging lymphoma [7, 8]. Thirdly, short-axis diameters of lymph nodes could only be measured in the coronal plane, whereas an acquisition

in more than one plane would have allowed for more accurate measurement of lymph node sizes. In addition, according to the revised response criteria for lymphoma, the size of lymph nodes should be measured in the axial plane [17]. Fourthly, only one (experienced) observer assessed the whole-body MRI datasets. Nevertheless, because the present study only compared two different MRI protocols and did not assess the diagnostic performance of MRI, this is less of an issue. Fifthly, the lesions seen at MRI could not be histopathologically confirmed to be lymphomas because of ethical reasons. No comparison was made with other diagnostic tests such as (FDG-PET/CT) and bone marrow biopsy, because this was beyond the scope of the present study. In addition, follow-up MRI examinations were not available for confirmation. Nevertheless, this study aimed to assess whether whole-body MRI detects more clinically relevant lesions than an MRI protocol with the regular anatomical coverage for staging lymphoma, rather than assessing the diagnostic performance of MRI itself. Sixthly, this study only assessed whether whole-body MRI detects more clinically relevant lesions than an MRI protocol that only includes the head/neck and trunk in terms of Ann Arbor staging. However, the detection of lymphomatous lesions outside the head/neck and trunk may have other clinical consequences. For example, bone lesions at risk of fracture may require urgent treatment. Furthermore, the presence of lesions outside the standard FOV for lymphoma staging may have prognostic implications, which should be investigated by future studies. Thus, findings in the extremities could have a significant clinical impact, even though they will not change the Ann Arbor stage.

In conclusion, in our series of patients with newly diagnosed lymphoma, whole-body MRI did not detect any clinically relevant lesions outside the field of view of an MRI protocol that only includes the head/neck and trunk. Therefore, it may be sufficient to only include the head/neck and trunk when using MRI for staging lymphoma.

## References

1. Jemal A, Siegel R, Xu J, Ward E. Cancer statistics, 2010. *CA Cancer J Clin* 2010;60:277-300
2. Connors JM. State-of-the-art therapeutics: Hodgkin's lymphoma. *J Clin Oncol* 2005;23:6400-6408
3. Armitage JO. Staging non-Hodgkin lymphoma. *CA Cancer J Clin* 2005;55:368-376
4. Ansell SM, Armitage J. Non-Hodgkin lymphoma: diagnosis and treatment. *Mayo Clin Proc* 2005;80:1087-1097
5. Kwee TC, Kwee RM, Nieuwstein RA. Imaging in staging of malignant lymphoma: a systematic review. *Blood* 2008;111:504-516
6. Brenner DJ, Hall EJ. Computed tomography – an increasing source of radiation exposure. *N Engl J Med* 2007;357:2277-2284
7. Kwee TC, Quarles van Ufford HM, Beek FJ, et al. Whole-Body MRI, Including Diffusion-Weighted Imaging, for the Initial Staging of Malignant Lymphoma: Comparison to Computed Tomography. *Invest Radiol* 2009;44:683-690
8. Punwani S, Taylor SA, Bainbridge A, et al. Pediatric and adolescent lymphoma: comparison of whole-body STIR half-Fourier RARE MR imaging with an enhanced PET/CT reference for initial staging. *Radiology* 2010;255:182-190
9. Lister TA, Crowther D, Sutcliffe SB, et al. Report of a committee convened to discuss the evaluation and staging of patients with Hodgkin's disease: Cotswolds meeting. *J Clin Oncol* 1989;7:1630-1636
10. Nguyen NC, Chara BT, Osman MM. Prevalence and patterns of soft tissue metastasis: detection with true whole-body F-18 FDG PET/CT. *BMC Med Imaging* 2007;7:8
11. De Beer JD, Bogoch ER, Smythe HA. Lymphoma presenting as a popliteal mass in a patient with rheumatoid arthritis. *J Rheumatol* 1990;17:1242-1243
12. Haase KK, Dürk H, Baumbach A, Saal J, Wehrmann M. Non-Hodgkin's lymphoma presenting as knee monoarthritis with a popliteal cyst. *J Rheumatol* 1990;17:1252-1254
13. Fowles JV, Olweny CL, Katongole-Mbidde E, Lukanga-Ndawula A, Owor R. Burkitt's lymphoma in the appendicular skeleton. *J Bone Joint Surg Br* 1983;65:464-471
14. Allman LM. Metastatic bone involvement of the hallux distal phalanx and cuboid in an elderly patient with non-Hodgkin lymphoma. *Foot Ankle Spec* 2008;1:355-358
15. Jakowski JD, Mayerson J, Wakely PE Jr. Fine-needle aspiration biopsy of the distal extremities: a study of 141 cases. *Am J Clin Pathol* 2010;133:224-231
16. Ruben I, Dighe S, Ajit D, Gujral S, Jambhekar NA, Rekhi B. Pulmonary non-Hodgkin's lymphoma (NHL) of diffuse large B-cell type with simultaneous humeral involvement in a young lady: an uncommon presentation with cytologic implications. *Diagn Cytopathol* 2010;38:217-220
17. Cheson BD, Pfistner B, Juweid ME, et al; International Harmonization Project on Lymphoma. Revised response criteria for malignant lymphoma. *J Clin Oncol* 2007;25:579-586



# Chapter 10

General discussion

Imaging plays a crucial role in the management of patients with newly diagnosed malignant lymphoma, because it provides a non-invasive means to assess disease extent (staging). Accurate staging is important for appropriate treatment planning and determining prognosis [1-3]. The aim of this thesis was to introduce and assess the value of whole-body magnetic resonance (MR) imaging, including diffusion-weighted imaging (DWI), for staging patients with newly diagnosed malignant lymphoma.

Current state of imaging in staging newly diagnosed malignant lymphoma

Computed tomography (CT) is currently the most commonly used means for staging patients with newly diagnosed malignant lymphoma [1-3]. Advantages of CT are its widespread availability and high scan speed, which increases patient throughput. However, a limitation of CT is that it basically only allows for the assessment of gross structural and contrast enhancement changes. Another imaging modality that is playing an increasingly important role in the evaluation of patients with malignant lymphoma is <sup>18</sup>F-fluoro-2-deoxyglucose positron emission tomography (FDG-PET), a method that exploits the increased glycolytic rate of cancer cells [4]. The main advantage of FDG-PET over anatomic-based imaging techniques, such as CT, is its ability to detect metabolic changes in areas involved with malignant lymphoma before structural changes become visible. Furthermore, FDG-PET is known to provide a high lesion-to-background contrast. Meta-analyses have shown that FDG-PET is more accurate than CT in differentiating viable tumor from benign fibrotic tissue in residual masses after therapy [5-7]. However, the value of FDG-PET in the initial staging of malignant lymphoma is less clear. In 2007, the Imaging Subcommittee of International Harmonization Project in Lymphoma stated that pretherapy FDG-PET is not a mandatory requirement for assessment of response after treatment of patients with Hodgkin lymphoma, diffuse large B-cell lymphoma, follicular lymphoma, and mantle cell lymphoma, because these lymphomas are routinely FDG avid. However, pretherapy FDG-PET is strongly encouraged because it facilitates the interpretation of response to therapy [8]. This committee also stated that pretherapy FDG-PET is mandatory for non-Hodgkin lymphomas with variable FDG avidity if PET is used to assess response to treatment [8]. FDG-PET most likely improves initial staging accuracy of CT alone, as was also suggested in the systematic review in **chapter 2**. In addition, it most likely improves and facilitates the interpretation of posttherapy FDG-PET [9]. Many, if not most, institutions already perform pretherapy FDG-PET (most frequently as part of a combined FDG-PET/CT examination), and the number of institutions that use this strategy is only expected to grow [10].

Risks of ionizing radiation associated with CT and FDG-PET(/CT)

A disadvantage of CT and FDG-PET(/CT) is the use of ionizing radiation, which may induce second cancers [11-13]. This issue is of particular interest in children, because rapidly dividing cells are more sensitive to radiation induced effects, and children will



have more years ahead in which cancerous changes might occur [11-13]. **Chapter 3** showed that in pediatric patients with Hodgkin lymphoma, the average fraction of radiation-induced deaths was approximately 0.4% for males and 0.7% for females, while that in adults with non-Hodgkin lymphoma (diffuse large B-cell lymphoma) is approximately 0.07% for males and 0.09% for females. The average radiation-induced life reduction in pediatric patients with Hodgkin lymphoma is approximately 21 days in males and 45 days in females. In adults with non-Hodgkin lymphoma (diffuse large B-cell lymphoma), the average radiation-induced life reduction is approximately 1.5 days in males and 2.0 days in females. Although these numbers may be lower than expected, (FDG-PET/CT) radiation-induced mortality is certainly non-negligible, especially in children. Therefore, the use of radiation-free alternatives, such as magnetic resonance (MR) imaging is advocated [14].

Whole-body MR sequences for staging malignant lymphoma

The concept that MR imaging might become the ultimate whole-body imaging tool was initially proposed by Damadian and Lauterbur in 1980 [15, 16]. However, so far, only a few studies have applied this technique for staging malignant lymphoma [17-19]. Furthermore, these studies only applied a short inversion time inversion recovery (STIR) sequence for whole-body MR imaging [17-19]. STIR is a sensitive method for the detection of parenchymal and bone marrow lesions, which are generally highlighted as high signal intensity structures on this sequence [17-19]. However, additional sequences may improve staging accuracy. For example, T1-weighted imaging may aid in the detection of lymph nodes, may improve evaluation of the mediastinal area (it requires a shorter scan time than STIR imaging and is less prone to motion artifacts), and it may aid in the characterization of bone marrow lesions. Recently, great interest has also emerged in applying diffusion-weighted imaging (DWI) for the detection and evaluation of cancer in the body [20, 21]. The rationale for using DWI for oncological imaging is based on the fact that many malignant tumors exhibit an impeded water mobility, which can be visualized and quantified using DWI [22]. A unique approach of acquiring DWI in the body is the concept of DWIBS [20], which has been described in **chapters 4.1, 4.2, and 4.3**. Image acquisition during free breathing, multiple signal averaging, and background body signal suppression by means of a fat suppression prepulse and strong diffusion weighting, are the main features of DWIBS. Because of its efficient scan time, DWIBS allows performing whole-body DWI. Moreover, its excellent lesion-to-background contrast may facilitate the detection of lymphomatous lesions. **Chapters 8.1, 8.2 and 8.3** show that the addition of DWI to a whole-body MR imaging protocol may detect lesions that have remained unnoticed at T1-weighted and STIR whole-body MR imaging, and that this may lead to upstaging. However, it is important to realize that performing whole-body DWI takes approximately 20-30 additional minutes. This, in turn, decreases patient throughput and increases costs. Moreover, upstaging does not necessarily result in a change in treatment planning. Larger studies

that investigate the effect of DWI findings on treatment planning and outcome are required. Until then, it remains unclear whether the addition of DWI to a whole-body MR imaging protocol for malignant lymphoma staging is cost-effective. More generally speaking, it is still unclear which combination of whole-body MR sequences is most cost-effective in staging malignant lymphoma.

Whole-body MR imaging using a non-integrated surface coil

The use of a whole-body surface coil design is preferred above an integrated transmit-receive body coil for whole-body MR imaging, because the former yields superior signal-to-noise ratio (SNR) and spatial resolution compared to the latter, and allows for parallel imaging [23, 24]. However, most MR systems in routine clinical practice may not yet be equipped with an integrated whole-body surface coil design. Moreover, for a large number of these systems, an easily available upgrade towards fully integrated whole-body surface coil technology may not be available (yet). On the other hand, non-integrated surface coils (some of which are capable of parallel imaging) are widely available. These surface coils, however, have only a limited anatomical coverage. Nevertheless, as shown in **chapter 5**, it is still possible to perform a time-efficient and high-quality whole-body MR examination using a non-integrated surface coil. A large proportion of the whole-body MR studies in this thesis were acquired using this so-called sliding table and repositioning surface coil approach. However, a relative drawback of this approach is narrowing of the bore diameter in the vertical direction because of the use of spacers and an additional table platform. Especially in the Western world, where the prevalence of obesity and the number of large-sized patients is increasing, this may be an issue [25]. Furthermore, narrowing of the bore diameter may increase the risk of claustrophobic events. Finally, this approach requires careful coil (re)positioning, in order to have the center of the coil at or near the center of the magnetic bore. It is therefore necessary for the industry to develop more advanced systems for whole-body MR imaging.

Assessment of lymph nodes at DWI: value of apparent diffusion coefficient measurements

Anatomic-based imaging modalities such as CT and conventional ([contrast-enhanced] T1-weighted and T2-weighted) MR imaging rely on size criteria, which lack the desired accuracy to characterize lymph nodes [26]. In order to improve evaluation of lymph nodes, there is a need for imaging modalities that go beyond anatomical lymph node assessment and that allow for visualization and quantification of physiological and biochemical processes at the cellular level. DWI allows visualization and quantification of the diffusivity of water molecules [22]. Lymph nodes have a relatively impeded diffusivity. Consequently, when using strong diffusion-weighting (i.e. applying high b-values), lymph nodes (both normal and lymphomatous) can be highlighted while surrounding normal tissues are suppressed [20]. Quantification of diffusivity in lymph

nodes by means of apparent diffusion coefficient (ADC) measurements may aid in the histological characterization of lymph nodes, because pathologic processes may lead to differences in diffusivity due to differences in cellularity, intracellular architecture, necrosis, and perfusion. However, the exact value of ADC measurements in the characterization of lymph nodes is still unclear. Although the ADC of metastatic lymph nodes has been reported to be significantly different from those of non-metastatic lymph nodes in numerous studies [27-34], the (considerable) overlap in ADCs between both groups may be an issue. Furthermore, other studies even reported the difference in ADCs between both groups to be non-significant [35-37]. Importantly, inter- and intra-observer reproducibilities of ADC measurements of lymph nodes are still unknown. Serial measurements must be accurate and reproducible, or clinical utility will inevitably be limited [38]. **Chapter 6.1** showed that ranges of mean ADC difference  $\pm$  limits of agreement (in  $10^{-3}$  mm<sup>2</sup>/s) for inter-observer agreement were  $-0.03$  to  $0.02 \pm 0.15$  to  $0.31$ . Ranges of mean ADC difference  $\pm$  limits of agreement (in  $10^{-3}$  mm<sup>2</sup>/s) for intra-observer agreement were  $0.00$  to  $0.04 \pm 0.13$  to  $0.32$ . Thus, reproducibility of ADC measurements is relatively poor. Nevertheless, **chapter 6.2** showed that mean ADC of lymphomatous lymph nodes in patients with non-Hodgkin lymphoma ( $0.70 \times 10^{-3}$  mm<sup>2</sup>/s) was significantly lower ( $P < 0.0001$ ) than that of normal lymph nodes in healthy volunteers ( $1.00 \times 10^{-3}$  mm<sup>2</sup>/s). Thus, ADC measurements show promise for discriminating normal lymph nodes from lymphomatous lymph nodes. On the other hand, **chapter 6.2** also showed that mean ADC of indolent lymphomas ( $0.67 \times 10^{-3}$  mm<sup>2</sup>/s) was not significantly different ( $P = 0.2997$ ) from that of aggressive lymphomas ( $0.74 \times 10^{-3}$  mm<sup>2</sup>/s). Therefore, ADC measurements appear to be of no utility in differentiating indolent from aggressive lymphomas. Based on the poor reproducibility of ADC measurements and the fact that our own study on the value of ADC measurements suffered from several shortcomings, including the absence of direct histopathological correlation, the use of ADC measurements in the assessment of lymph nodes in patients with malignant lymphoma can not (yet) be recommended. Thus, the evaluation of lymph nodes at DWI still relies on size criteria. In spite of this, (high b-value) DWI remains a potentially useful method for lymph node detection [20].

Whole-body MR imaging for detecting bone marrow involvement in malignant lymphoma

Assessment of the bone marrow is of particular importance in malignant lymphoma, because bone marrow involvement represents the highest stage (stage IV) according to the Ann Arbor staging system and has associated therapeutic and prognostic implications [1-3]. Because of its high soft-tissue contrast and good spatial resolution, MR imaging is a potentially useful method for the evaluation of the bone marrow. Therefore, it has the potential to (partially) replace bone marrow biopsy (BMB), which

is currently regarded as the method of choice for the assessment of the bone marrow in malignant lymphoma. The results of the systematic review in **chapter 7.1** indeed suggested that MR imaging is probably sufficiently sensitive to rule out bone marrow involvement in patients with malignant lymphoma. Important advantages of whole-body MR imaging over MR protocols that examine only selected body regions are its ability to detect bone marrow metastases throughout the entire bone marrow while at the same time allowing complete staging of extramedullary disease. However, in our own series of patients that was reported in **chapter 7.2**, sensitivity of whole-body MR imaging without DWI and that of whole-body MR imaging with DWI were (rather unexpectedly) only 41.7% and 45.5%, respectively, when using BMB as the standard of reference. Therefore, whole-body MR imaging is not sufficiently reliable yet to replace BMB for bone marrow assessment in malignant lymphoma. A possible explanation for the discrepancy between the results of the systematic review in **chapter 7.1** and our own results in **chapter 7.2** is the fact that the majority of studies in the systematic review applied MR imaging protocols of only selected body regions (mostly lumbar spine, pelvis and proximal femurs). Such protocols are not comparable to whole-body MR imaging protocols, since the latter allows less time to acquire different MR sequences and imaging planes, and generally employs a greater slice thickness and lower spatial resolution. BMB remains necessary in the staging work-up of patients with malignant lymphoma until more advanced whole-body MR imaging protocols (e.g. at higher field strengths, or using a higher spatial resolution) have proved to achieve a higher diagnostic performance.

Whole-body MR imaging, including diffusion-weighted imaging, compared to CT

Whole-body MR imaging is a potential radiation-free alternative to CT for staging patients with newly diagnosed malignant lymphoma. Therefore, it is important to show that whole-body MR imaging is at least equal to CT. **Chapter 8.1** described our initial results on using whole-body MR imaging, including DWI, compared to CT for the staging of 31 patients with newly diagnosed malignant lymphoma. In this first analysis, staging results of whole-body MR imaging without DWI were equal to those of CT in 74% (23/31), higher in 26% (8/31), and lower in 0% (0/31) of patients, with correct/incorrect/unresolved overstaging relative to CT in 3, 2, and 2 patients, respectively, and incorrect staging of both modalities in 1 patient. Staging results of whole-body MR imaging with DWI were equal to those of CT in 75% (21/28), higher in 25% (7/28), and lower in 0% (0/28) of patients, with correct/incorrect overstaging relative to CT in 6 and 1 patient(s), respectively. In this first analysis, whole-body MR imaging (without and with DWI) never understaged relative to CT, which reflects the high sensitivity of MR imaging for the detection of lesions, thanks to its high soft-tissue contrast and good spatial resolution. Correct whole-body MR imaging overstaging was mainly thanks to the detection of bone marrow involvement that was not seen

at CT. This well reflects one of the weaknesses of CT, in that it is not reliable in the detection of bone marrow disease [39]. Importantly, in this first analysis, the number of correctly overstaged patients using whole-body MR imaging with DWI was higher than using whole-body MR imaging without DWI. This may be related to the fact that whole-body DWI is able to highlight (subtle) lesions that can be overlooked at conventional (T1-weighted and STIR) whole-body MR imaging [20]. Thus, our initial results supported the use of whole-body DWI as a useful adjunct to conventional (T1-weighted and STIR) whole-body MR imaging for the initial staging of malignant lymphoma. Incorrect whole-body MR imaging overstaging occurred due to the fact that a cervical lymph node in one patient had a short-axis diameter that was slightly larger than 10 mm at whole-body MR imaging, whereas these lymph nodes were smaller than 10 mm at CT. Explanations for this discrepancy are slight variation in the method of measurement between the CT reader and the whole-body MR reader and the fact that lymph nodes were measured in the coronal plane at T1-weighted and STIR whole-body MR imaging, whereas they were measured in the axial plane at CT. In another patient, Waldeyer's ring was false positive at whole-body MR imaging with DWI. This can be explained by the fact that the normal Waldeyer's ring already has a high signal intensity that may mimic lymphomatous involvement. The cases in which whole-body MR imaging provided incorrect overstaging can be considered as part of a learning curve. In a few cases, staging discrepancies between whole-body MR imaging and CT could not be resolved. This is related to fact that the lymphomatous lesions detected at whole-body MR imaging and CT could not be confirmed histopathologically, because of practical and ethical concerns. Instead, FDG-PET, BMB, and follow-up imaging (CT) studies served as the standard of reference. Unfortunately, this reference standard is sometimes inadequate. For example, bone marrow lesions that are only seen at whole-body MR imaging can neither be confirmed nor excluded when FDG-PET, BMB, and follow-up CT studies are negative for bone marrow involvement. Although our initial results suggested that initial staging of malignant lymphoma using whole-body MR imaging (without DWI and with DWI) equals staging using CT in the majority of patients, that whole-body MR imaging never understaged relative to CT, and that whole-body MR imaging mostly correctly overstaged relative to CT (with a possible advantage of using DWI), no definitive conclusions could be drawn yet because of the small number of patients.

The number of patients in whom whole-body MR imaging, including DWI, was compared to CT, was increased to 101 in **chapter 8.2**. In this larger sample size, staging results of whole-body MR imaging without DWI were equal to those of CT in 65.4% (66/101), higher in 30.7% (31/101), and lower in 4.0% (4/100) of patients, with correct/incorrect/unresolved overstaging and incorrect/unresolved understaging relative to CT in 13/12/6 and 3/1 patient(s), respectively. Staging results of whole-body MR imaging with DWI were equal to those of CT in 62.5% (60/96), higher in 32.3% (31/96),

and lower in 5.2% (5/96) of patients, with correct/incorrect/unresolved overstaging and incorrect/unresolved understaging relative to CT in 18/10/3 and 4/1 patient(s), respectively. Interestingly, the number of cases in which whole-body MR imaging *correctly* provided a different stage than CT (n=16 for whole-body MR imaging without DWI and n=18 for whole-body MR imaging with DWI) was approximately equal to the number of cases in which whole-body MRI *incorrectly* provided a different stage than CT (n=14 for whole-body MR imaging without DWI and n=15 for whole-body MR imaging with DWI). Similar to our initial study in 31 patients, correct whole-body MR imaging overstaging was mainly thanks to the detection of bone marrow involvement that was not seen at CT. Incorrect overstaging of whole-body MR imaging (both without and with DWI) relative to CT mostly occurred in lymph nodes and the liver. The former can be explained by the fact that lymph nodes were measured in the coronal plane at whole-body MR imaging, whereas they were measured in the axial plane at CT. This problem may be solved by acquiring anatomic sequences in the axial plane. Note that diffusion-weighted images are less suitable for this purpose, because size measurements on these images are highly dependent on the applied window level and window width. The latter is mainly due to the fact that several cavernous liver hemangiomas were erroneously classified as lymphomatous at whole-body MRI, whereas they were correctly classified at CT. In a real clinical setting, the liver lesions detected at whole-body MRI may have received additional diagnostic work-up, but in this study the observer was forced to classify a lesion as positive or negative. On the other hand, missed lung/pleural lesions and lymphomatous lymph nodes were responsible for incorrect understaging of whole-body MR imaging (both without and with) relative to CT. The former can be explained by the fact that MR imaging of the lung may be affected by cardiac and respiratory motion and susceptibility artefacts, which may cause signal loss. This is especially a problem in DWI because of the use of echo-planar imaging. Another cause may be relative unfamiliarity with the interpretation of whole-body MRI/DWI examinations in the chest. The latter can in part be explained by the fact that lymph nodes were measured in the coronal plane at whole-body MR imaging, whereas they were measured in the axial plane at CT. It should also be noted that staging disagreements between whole-body MR imaging and CT could not be resolved in several cases (n=7 for whole-body MR imaging without DWI and n=4 for whole-body MR imaging with DWI). The bone marrow was the most common site of unresolved staging disagreements; negative FDG-PET and negative bone marrow biopsy findings could not exclude bone marrow involvement that was seen at whole-body MRI in several patients. In addition, follow-up whole-body MR imaging examinations were mostly not available in such cases. In the far majority of patients, staging using whole-body MR imaging with DWI was equal to that without DWI. In a low number of cases DWI findings resulted in *correct* overstaging (n=5), whereas in an approximately equal number of cases DWI findings

led to *incorrect* overstaging. Therefore, the additional value of DWI is still unproven. Causes of correct overstaging were miscellaneous, occurring in the bone marrow, lymph nodes, and lung/pleura. These cases demonstrate that DWI can draw the attention of the reader to pathologic areas of high signal intensity that have remained unnoticed at conventional whole-body MR sequences. On the other hand, incorrect overstaging, occurring in the liver, kidney, and vagina, show that high signal intensity lesions at DWI are not specific for cancer. In an even lower number of cases, DWI findings resulted in correct understaging (n=2) and incorrect understaging (n=1). Correct understaging occurred thanks to the fact that DWI excluded lymphomatous disease in several lymph nodes in one case, and lung/pleura involvement in another case. Incorrect understaging occurred because a lung/pleural lesion was missed in one case, most likely due to signal loss at DWI resulting from physiological motion and/or susceptibility artifacts. In two cases, disagreement in staging between whole-body MR imaging without DWI and whole-body MR imaging with DWI remained unresolved. Based on these results, it can be concluded that staging of newly diagnosed malignant lymphoma using whole-body MR imaging (without and with DWI) equals staging using CT in the majority of patients. Disagreements between whole-body MR imaging and CT are mostly caused by overstaging of the former relative to the latter, with the number of correctly and incorrectly overstaged cases being approximately equal. Finally, the potential advantage of DWI is still unproven.

It is difficult to answer the question whether whole-body MR imaging can replace CT for staging newly diagnosed lymphoma. Both whole-body MR imaging and CT have their unique strengths and weaknesses, as shown in our series of patients. Nevertheless, there are three keys that may lead to the successful implementation of whole-body MR imaging in clinical practice. First, further technical developments are required to decrease total examination time, to reduce physiologic motion artifacts (especially in the lung and mediastinum), to ensure consistently high image quality in each patient, and to make the entire examination more patient-friendly and easier to execute. Second, if it is demonstrated that functional whole-body MR techniques (particularly DWI) have an additional advantage over CT (e.g. for early assessment of response to therapy), this may accelerate its implementation in clinical practice. Third, whole-body MR imaging should be integrated with PET. FDG-PET is crucial for posttherapy assessment, and is likely to play another major role in the early assessment of response to therapy in the near future [8, 10]. At present, FDG-PET is most frequently performed as part of a combined FDG-PET/CT examination using integrated PET/CT systems. An FDG-PET/CT examination can be completed within 20 minutes using the same scanner. However, this is currently not the case for whole-body MR imaging. First, a whole-body MR examination takes much longer, and an FDG-PET examination should be done using another (PET/CT) scanner, in another room. This poses a significant burden on the patient, and on logistic and financial



resources. If whole-body MR imaging is ever going to replace CT for staging malignant lymphoma, this problem should be solved. The first solution is to perform sequential imaging by MR and PET systems which are linked by a patient “shuttle”; the patient does not have to get off the examination table of one device to get onto the table of the second device as the transfer is accomplished by the “shuttle”. Nevertheless, the CT component of the PET/CT system is still necessary for transmission scanning with such a method. The second solution is by means of fully integrated systems with technically simultaneous data acquisition; neither patient nor table motion is required when imaging single fields of view [40]. True simultaneous scanning minimizes the geometrical mismatch between PET and MRI data set, and it can eliminate the need for CT transmission scanning. However, several technological difficulties have to be solved for designing a fully integrated whole-body PET/MRI system, including the issues of electromagnetic interference between the two systems and MRI-based attenuation correction [40]. Until these requirements have been met, it is conceivable that CT will be preferred above whole-body MR imaging for staging most patients with malignant lymphoma. Nevertheless, whole-body MR imaging can be regarded as a reasonable alternative to CT, and may replace CT in patients in whom CT radiation is a major issue (e.g. in pregnant patients or young children) or in patients with severe allergy to CT contrast agents.

Whole-body MR imaging, including diffusion-weighted imaging, compared to FDG-PET/CT

FDG-PET/CT is gradually replacing CT alone for staging patients with newly diagnosed malignant lymphoma [10]. However, because of the use of ionizing radiation and the fact that certain lymphoma types cannot be visualized at FDG-PET because of low or no FDG uptake, whole-body MR imaging with DWI may be a good alternative. Therefore, it is of interest to compare staging according to whole-body MR imaging (including DWI) to that of FDG-PET/CT in patients with newly diagnosed malignant lymphoma. **Chapter 8.3** showed that, in a first series of 22 patients with newly diagnosed malignant lymphoma, overall interobserver agreement at whole-body MR imaging (including DWI) is moderate to good. Overall agreement between whole-body MR imaging and FDG-PET/CT is moderate. Interestingly, agreements were poorer in the assessment of the hilar lymph node region and bone marrow. This may be explained by the fact that MR imaging may have potential difficulties in the evaluation of the hilar region due to the presence of respiratory and cardiac motion artifacts in this area, whereas the bone marrow may show non-specific findings at MR imaging. Motion artifacts may be overcome by future technical developments. However, the specificity of MR imaging in the bone marrow may only be improved by using bone marrow-specific contrast agents. These should be the subject of future studies. Another interesting finding was that in 5 of 6 cases with a positive bone marrow biopsy, no bone marrow lesions were visualized at whole-body MR imaging and FDG-PET/CT. In the sixth patient



with a positive bone marrow biopsy result, MR imaging indicated pathology at two osseous locations while FDG-PET/CT did not reveal any bone abnormalities. Hence, both modalities appear to have limited sensitivities in detecting lymphomatous bone marrow involvement. Thus, neither whole-body MR imaging nor FDG-PET/CT seem to be sufficiently reliable for the assessment of the bone marrow, and bone marrow biopsy remains a crucial part of the staging work-up of patients with malignant lymphoma. Importantly, whole-body MR imaging did not understage relative to FDG-PET/CT in our series of patients with newly diagnosed lymphoma. In a minority of patients, whole-body MR imaging led to clinically important overstaging relative to FDG-PET/CT. Nevertheless, more studies including larger sample sizes are needed. In addition, because of the lack of histopathological confirmation, follow-up (imaging) studies are required to determine whether whole-body MR imaging with DWI leads to correct upstaging in certain cases.

MR imaging for staging malignant lymphoma: whole-body or less?

CT is usually performed from the head/neck to the groins (excluding the arms), whereas whole-body MR imaging refers to MR imaging of the area from the cranial vertex to the toes (including the arms). However, it is unknown whether a whole-body MR protocol is necessary, or whether an MR protocol that only has the usual CT coverage (i.e. from cranial vertex to groins) is comparable while less time-consuming. **Chapter 9** showed that, in a series of 100 patients, whole-body MR imaging did not detect any clinically relevant lesions (i.e. lesions that change Ann Arbor stage) outside the field of view (FOV) of an MR imaging protocol that only includes the head/neck and trunk. Thus, valuable scan time can be saved without influencing the final Ann Arbor stage when only the head/neck and trunk are included in an MR imaging protocol for staging malignant lymphoma. Nevertheless, it should be realized that the detection of lymphomatous lesions outside the head/neck and trunk may have other clinical consequences. For example, bone lesions at risk of fracture may require urgent treatment. Furthermore, the presence of lesions outside the standard FOV for malignant lymphoma staging may have prognostic implications. Future studies are necessary to investigate these issues.

Future research directions

The work described in this thesis is only the first step towards implementing whole-body MR imaging in the evaluation of patients with malignant lymphoma. There are several possibilities to improve whole-body MR image quality and staging accuracy. First, given the increasing use of 3.0T-systems that can provide a higher SNR than 1.5T-systems [41], future studies should investigate the feasibility and potential benefit of performing whole-body MR imaging for staging malignant lymphoma at 3.0T. Second, the discrimination between normal-sized non-malignant lymph nodes and normal-sized lymphomatous lymph nodes is still an unsolved issue [26]. Ultrasmall

superparamagnetic iron oxide (USPIO)-enhanced MRI allows for the identification of malignant nodal infiltration independent of lymph node size [42]. Combining USPIO contrast agents with DWI can theoretically highlight lymphomatous lymph nodes while suppressing normal lymph nodes [43]. Furthermore, USPIO contrast agents can suppress normal or hyperplastic red bone marrow [44], as a result of which the evaluation of the bone marrow can be improved. Although USPIO contrast agents are still being developed and not yet widely available, its application in patients with malignant lymphoma may be of interest. On the other hand, it is questionable whether the potentially increased staging accuracy and its effect on treatment planning and outcome will outweigh the costs and patient discomfort associated with using USPIO contrast agents. Third, image blurring of peridiaphragmatic organs at DWI under free breathing may be improved by implementing sophisticated navigator echo techniques that allow for motion correction without prolonging scan time [45, 46]. Fourth, DWI suffers from cardiac-motion induced signal loss in the mediastinal area. Combining DWI with cardiac triggering may solve this problem, although it will prolong scan time. Fifth, whole-body PET/MR systems are currently being developed [40]. The information provided by whole-body MR imaging (including DWI) and FDG-PET can be regarded as complementary. Therefore, staging accuracy of a combined whole-body MR/FDG-PET examination may outperform that of either of the modalities alone. Future studies should investigate whether the previously mentioned technical improvements are feasible and cost-effective.

Staging of newly diagnosed malignant lymphoma using whole-body MR imaging equals that of CT in the majority of cases. Furthermore, the use of whole-body MR imaging instead of CT may prevent radiation-related cancer mortality. However, costs of a whole-body MR examination are currently higher than that of CT, which is, in part, related to the longer scan time of the former. Therefore, a cost-effectiveness analysis is necessary to determine whether whole-body MR imaging compares favourable to CT in the staging of malignant lymphoma, in terms of costs and life years gained.

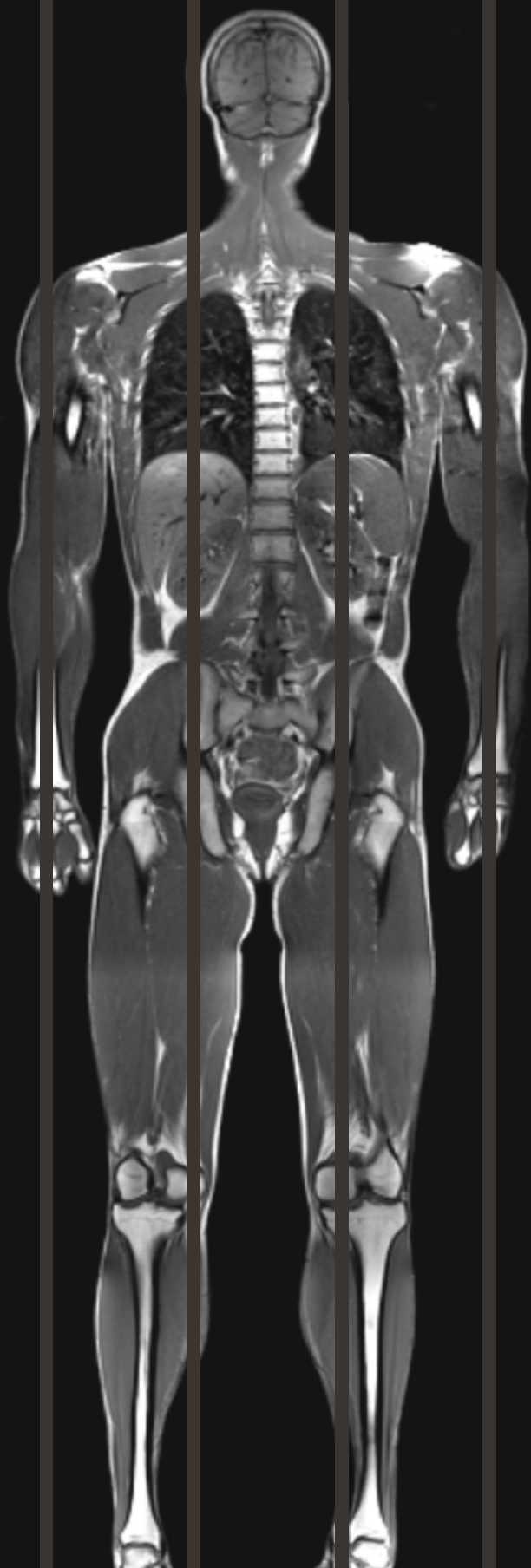
The work in this thesis mainly focused on the comparison between whole-body MR imaging and CT. However, CT is increasingly being replaced by FDG-PET/CT, because the latter is generally regarded as more accurate for staging malignant lymphoma [10]. Future studies with larger sample sizes are necessary to compare whole-body MR imaging, including DWI, to FDG-PET/CT. Future studies should also include long-term patient follow-up to resolve and provide more insight into the effect on clinical outcome of staging discrepancies between the imaging modalities. Finally, it is also very important for future studies to compare whole-body MR imaging, including DWI, to FDG-PET/CT early during treatment to predict treatment success/failure and after treatment to assess complete remission/residual disease.

## References

1. Connors JM. State-of-the-art therapeutics: Hodgkin's lymphoma. *J Clin Oncol* 2005;23:6400-6408.
2. Armitage JO. Staging non-Hodgkin lymphoma. *CA Cancer J Clin* 2005;55:368-376
3. Ansell SM, Armitage J. Non-Hodgkin lymphoma: diagnosis and treatment. *Mayo Clin Proc* 2005;80:1087-1097
4. Rohren EM, Turkington TG, Coleman RE. Clinical applications of PET in oncology. *Radiology* 2004;231:305-332
5. Isasi CR, Lu P, Blaufox MD. A metaanalysis of 18F-2-deoxy-2-fluoro-D-glucose positron emission tomography in the staging and restaging of patients with lymphoma. *Cancer* 2005;104:1066-1074
6. Zijlstra JM, Lindauer-van der Werf G, Hoekstra OS, Hooft L, Riphagen II, Huijgens PC. 18F-fluoro-deoxyglucose positron emission tomography for post-treatment evaluation of malignant lymphoma: a systematic review. *Haematologica* 2006;91:522-529
7. Terasawa T, Nihashi T, Hotta T, Nagai H. 18F-FDG PET for posttherapy assessment of Hodgkin's disease and aggressive Non-Hodgkin's lymphoma: a systematic review. *J Nucl Med* 2008;49:13-21
8. Juweid ME, Stroobants S, Hoekstra OS, et al.; Imaging Subcommittee of International Harmonization Project in Lymphoma. Use of positron emission tomography for response assessment of lymphoma: consensus of the Imaging Subcommittee of International Harmonization Project in Lymphoma. *J Clin Oncol* 2007;25:571-578
9. Quarles van Ufford H, Hoekstra O, de Haas M, et al. On the added value of baseline FDG-PET in malignant lymphoma. *Mol Imaging Biol* 2010;12:225-232
10. Delbeke D, Stroobants S, de Kerviler E, Gisselbrecht C, Meignan M, Conti PS. Expert opinions on positron emission tomography and computed tomography imaging in lymphoma. *Oncologist* 2009;14 Suppl 2:30-40
11. Barentsz J, Takahashi S, Oyen W, et al. Commonly used imaging techniques for diagnosis and staging. *J Clin Oncol* 2006;24:3234-3244
12. Brenner DJ, Hall EJ. Computed tomography--an increasing source of radiation exposure. *N Engl J Med* 2007;357:2277-2284
13. Huang B, Law MW, Khong PL. Whole-body PET/CT scanning: estimation of radiation dose and cancer risk. *Radiology* 2009;251:166-174
14. Semelka RC, Armao DM, Elias J Jr, Huda W. Imaging strategies to reduce the risk of radiation in CT studies, including selective substitution with MRI. *J Magn Reson Imaging* 2007;25:900-909
15. Damadian R. Field focusing n.m.r. (FONAR) and the formation of chemical images in man. *Philos Trans R Soc Lond B Biol Sci* 1980;289:489-500
16. Lauterbur PC. Progress in n.m.r. zeugmatography imaging. *Philos Trans R Soc Lond B Biol Sci* 1980;289:483-487
17. Amano Y, Tajika K, Uchiyama N, Takahama K, Dan K, Kumazaki T. Staging of malignant lymphoma with three-station black-blood fast short-inversion time inversion recovery (STIR). *Magn Reson Med* 2003;2:9-15
18. Kellenberger CJ, Miller SF, Khan M, Gilday DL, Weitzman S, Babyn PS. Initial experience with FSE STIR whole-body MR imaging for staging lymphoma in children. *Eur Radiol* 2004;14:1829-1841

19. Brennan DD, Gleeson T, Coate LE, Cronin C, Carney D, Eustace SJ. A comparison of whole-body MRI and CT for the staging of lymphoma. *AJR Am J Roentgenol* 2005;185:711-716
20. Takahara T, Imai Y, Yamashita T, Yasuda S, Nasu S, Van Cauteren M. Diffusion weighted whole body imaging with background body signal suppression (DWIBS): technical improvement using free breathing, STIR and high resolution 3D display. *Radiat Med* 2004;22:275-282
21. Koh DM, Collins DJ. Diffusion-weighted MRI in the body: applications and challenges in oncology. *AJR Am J Roentgenol* 2007;188:1622-1635
22. Padhani AR, Liu G, Koh DM, et al. Diffusion-weighted magnetic resonance imaging as a cancer biomarker: consensus and recommendations. *Neoplasia* 2009;11:102-125
23. Hargaden G, O'Connell M, Kavanagh E, Powell T, Ward R, Eustace S. Current concepts in whole-body imaging using turbo short tau inversion recovery MR imaging. *AJR Am J Roentgenol* 2003;180:247-252
24. Lauenstein TC, Semelka RC. Emerging techniques: whole-body screening and staging with MRI. *J Magn Reson Imaging* 2006;24:489-498
25. Uppot RN, Sahani DV, Hahn PF, Gervais D, Mueller PR. Impact of obesity on medical imaging and image-guided intervention. *AJR Am J Roentgenol* 2007;188:433-440
26. Torabi M, Aquino SL, Harisinghani MG. Current concepts in lymph node imaging. *J Nucl Med* 2004;45:1509-1518
27. De Bondt RB, Hoebregts MC, Nelemans PJ, et al. Diagnostic accuracy and additional value of diffusion-weighted imaging for discrimination of malignant cervical lymph nodes in head and neck squamous cell carcinoma. *Neuroradiology* 2009;51:183-192
28. Vandecaveye V, De Keyzer F, Vander Poorten V, et al. Head and neck squamous cell carcinoma: value of diffusion-weighted MR imaging for nodal staging. *Radiology* 2009;251:134-146
29. Nakayama J, Miyasaka K, Omatsu T, et al. Metastases in mediastinal and hilar lymph nodes in patients with non-small cell lung cancer: quantitative assessment with diffusion-weighted magnetic resonance imaging and apparent diffusion coefficient. *J Comput Assist Tomogr* 2010;34:1-8
30. Sakurada A, Takahara T, Kwee TC, et al. Diagnostic performance of diffusion-weighted magnetic resonance imaging in esophageal cancer. *Eur Radiol* 2009;19:1461-1469
31. Yasui O, Sato M, Kamada A. Diffusion-weighted imaging in the detection of lymph node metastasis in colorectal cancer. *Tohoku J Exp Med* 2009;218:177-183
32. Kim JK, Kim KA, Park BW, Kim N, Cho KS. Feasibility of diffusion-weighted imaging in the differentiation of metastatic from non-metastatic lymph nodes: early experience. *J Magn Reson Imaging* 2008;28:714-719
33. Park SO, Kim JK, Kim KA, et al. Relative apparent diffusion coefficient: determination of reference site and validation of benefit for detecting metastatic lymph nodes in uterine cervical cancer. *J Magn Reson Imaging* 2009;29:383-390
34. Eiber M, Beer AJ, Holzapfel K, et al. Preliminary results for characterization of pelvic lymph nodes in patients with prostate cancer by diffusion-weighted MR-imaging. *Invest Radiol* 2010;45:15-23
35. Nakai C, Matsuki M, Inada Y, et al. Detection and evaluation of pelvic lymph nodes in patients with gynecologic malignancies using body diffusion-weighted magnetic resonance imaging. *J Comput Assist Tomogr* 2008;32:764-768
36. Lin G, Ho KC, Wang JJ, et al. Detection of lymph node metastasis in cervical and uterine cancers by diffusion-weighted magnetic resonance imaging at 3T. *J Magn Reson Imaging* 2008;28:128-135

37. Roy C, Bierry G, Matau A, Bazille G, Pasquali R. Value of diffusion-weighted imaging to detect small malignant pelvic lymph nodes at 3 T. *Eur Radiol* 2010;20:1803-1811
38. Bland JM, Altman DG. Statistical methods for assessing agreement between two methods of clinical measurement. *Lancet* 1986;1:307-310
39. Vinnicombe SJ, Reznick RH. Computerised tomography in the staging of Hodgkin's disease and non-Hodgkin's lymphoma. *Eur J Nucl Med Mol Imaging* 2003;30 Suppl 1:S42-55
40. Von Schulthess GK, Schlemmer HP. A look ahead: PET/MR versus PET/CT. *Eur J Nucl Med Mol Imaging* 2009;36 Suppl 1:S3-9
41. Schick F. Whole-body MRI at high field: technical limits and clinical potential. *Eur Radiol* 2005;15:946-959
42. Will O, Purkayastha S, Chan C, et al. Diagnostic precision of nanoparticle-enhanced MRI for lymph-node metastases: a meta-analysis. *Lancet Oncol* 2006;7:52-60
43. Thoeny HC, Triantafyllou M, Birkhaeuser FD, et al. Combined Ultrasmall Superparamagnetic Particles of Iron Oxide-Enhanced and Diffusion-Weighted Magnetic Resonance Imaging Reliably Detect Pelvic Lymph Node Metastases in Normal-Sized Nodes of Bladder and Prostate Cancer Patients. *Eur Urol* 2009;55:761-769
44. Senéterre E, Weissleder R, Jaramillo D, et al. Bone marrow: ultrasmall superparamagnetic iron oxide for MR imaging. *Radiology* 1991;179:529-533
45. Takahara T, Kwee TC, Van Leeuwen MS, et al. Diffusion-weighted magnetic resonance imaging of the liver using tracking only navigator echo: feasibility study. *Invest Radiol* 2010;45:57-63
46. Ivancevic MK, Kwee TC, Takahara T, et al. Diffusion-weighted MR imaging of the liver at 3.0 Tesla using TRacking Only Navigator echo (TRON): a feasibility study. *J Magn Reson Imaging* 2009;30:1027-1033



# Chapter 11

Summary

Nederlandse samenvatting

The aim of this thesis was to introduce and assess the value of whole-body magnetic resonance (MR) imaging, including diffusion-weighted imaging (DWI), for the staging of patients with newly diagnosed malignant lymphoma.

Computed tomography (CT) is currently the standard imaging modality for the initial staging of malignant lymphoma, while  $^{18}\text{F}$ -fluoro-2-deoxyglucose positron emission tomography (FDG-PET) has an essential role in restaging after treatment. Early results suggest that FDG-PET/CT outperforms both CT alone and FDG-PET alone. Data on the diagnostic performance of whole-body MR imaging are still lacking. **Chapter 2.**

In children with Hodgkin lymphoma and adults with non-Hodgkin lymphoma (diffuse large B-cell lymphoma), the average fractions of radiation-induced deaths are approximately 0.4% and 0.07% for males, and 0.7 and 0.09% for females, respectively. The average radiation-induced life reduction in pediatric patients with Hodgkin lymphoma is approximately 21 days in males and 45 days in females. In adults with non-Hodgkin (diffuse large B-cell) lymphoma, the average radiation-induced life reduction is approximately 1.5 days in males and 2.0 days in females. **Chapter 3.**

The recently introduced concept of “Diffusion-weighted Whole-body Imaging with Background body signal Suppression” (DWIBS) allows acquisition of volumetric diffusion-weighted images of the entire body. Image acquisition during free breathing, multiple signal averaging, and background body signal suppression by means of a fat suppression pre-pulse and strong diffusion weighting, are the main features of DWIBS. DWIBS highlights areas with an impeded diffusivity, such as occurs in many malignant primary and metastatic tumors, and provides an outstanding visualization of lymph nodes. Although the exact value of DWIBS still has to be established, it has potential use in tumor staging, monitoring response to cancer therapy, and in the detection of tumor persistence or recurrence. Combined with conventional (T1-weighted and short inversion time inversion recovery [STIR]) whole-body MR sequences, DWIBS has the potential to be a good radiation-free alternative to CT for staging malignant lymphoma. **Chapters 4.1, 4.2, and 4.3.**

A time-efficient and high-quality whole-body MR examination can easily be performed by using a non-integrated sliding surface coil approach. **Chapter 5.**

In healthy volunteers, it is shown that apparent diffusion coefficient (ADC) measurements may not be sufficiently reproducible to discriminate malignant from non-malignant lymph nodes. However, future studies which directly compare the ADCs of different nodal pathologies are required to further investigate the inter- and intraobserver reproducibilities of ADC measurements of lymph nodes. Furthermore,



ADC measurements show promise as a highly specific tool for discriminating normal lymph nodes from lymphomatous lymph nodes, but appear to be of no utility in differentiating indolent from aggressive lymphomas. **Chapters 6.1 and 6.2.**

Previous studies show that MR imaging is likely sufficiently sensitive to rule out bone marrow involvement in patients with malignant lymphoma. However, in our own series of patients it is shown that whole-body MR imaging (both without and with DWI) is negative for bone marrow involvement in a considerable proportion of patients with a positive bone marrow biopsy. Therefore, whole-body MR imaging is not sufficiently reliable yet to replace bone marrow biopsy for bone marrow assessment in malignant lymphoma. **Chapters 7.1 and 7.2.**

A first analysis in 31 patients with newly diagnosed malignant lymphoma shows that initial staging of malignant lymphoma using whole-body MR imaging (without DWI and with DWI) equals staging using CT in the majority of patients, while whole-body MR imaging never understaged relative to CT. Furthermore, whole-body MR imaging mostly correctly overstaged relative to CT, with a possible advantage of using DWI. **Chapter 8.1.**

A subsequent analysis in 101 patients with newly diagnosed malignant lymphoma confirms that staging using whole-body MR imaging (without and with DWI) equals staging using CT in the majority of patients. Nevertheless, both whole-body MR overstaging and understaging relative to CT occur, with the former being more common than the latter. The number of cases in which whole-body MR imaging correctly assigns a different stage than CT is approximately equal to the number of cases in which whole-body MR imaging incorrectly assigns a different stage than CT. The potential advantage of DWI is still unproven. **Chapter 8.2.**

In a first series of 22 patients with newly diagnosed malignant lymphoma, it was shown that overall interobserver agreement at whole-body MR imaging (including DWI) is moderate to good. Overall agreement between whole-body MR imaging and FDG PET/CT is moderate. Whole-body MR imaging does not understage relative to FDG-PET/CT in patients with newly diagnosed lymphoma. In a minority of patients, whole-body MR imaging leads to clinically important overstaging relative to FDG-PET/CT. FDG-PET/CT remains the gold standard for staging malignant lymphoma until future, larger studies have shown that whole-body MRI-DWI provides correct upstaging in such cases. **Chapter 8.3.**

Interestingly, in our series of 100 patients, whole-body MR imaging did not detect any clinically relevant lesions (i.e. lesions that change Ann Arbor stage) outside the field of view of an MR imaging protocol that only includes the head/neck and trunk. Therefore, it may be sufficient for future studies to only include the head/neck and trunk when using MR imaging for staging malignant lymphoma. **Chapter 9.**

### **Conclusion**

Whole-body MR imaging, including DWI, is a feasible technique for staging newly diagnosed malignant lymphoma. Both whole-body MR imaging and CT have their unique strengths and weaknesses. Technical developments are required to improve whole-body MR imaging in terms of image quality and workflow, and to integrate whole-body MR imaging with PET. Future research should also focus on the potential advantages of whole-body DWI over CT, especially with regard to the integration of anatomical and functional tissue information that can improve tumor characterization and follow-up. Until then, it is conceivable that CT will be preferred above whole-body MR imaging for staging most patients with malignant lymphoma. Nevertheless, whole-body MR imaging can be regarded as a reasonable alternative to CT, and may replace CT in those populations in which CT radiation is a major issue and in patients at risk for (severe) adverse reactions to CT contrast agents.





# Chapter 11

Summary

Nederlandse samenvatting

Het doel van dit proefschrift is om de waarde van whole-body magnetic resonance (MR) imaging, inclusief diffusie-gewogen MR imaging (DWI), te onderzoeken voor het stageren van patiënten met een nieuw gediagnosticeerd maligne lymfoom.

Computed tomography (CT) is op dit moment de standaard methode voor de initiële stagering van maligne lymfomen, terwijl <sup>18</sup>F-fluoro-2-deoxyglucose positron emission tomography (FDG-PET) een belangrijke rol heeft bij het restageren na therapie. De eerste studies suggereren dat FDG-PET/CT diagnostisch superieur is aan zowel CT alleen en FDG-PET alleen. Data betreffende de diagnostische accuratesse van whole-body MR imaging ontbreken nog. **Hoofdstuk 2.**

De gemiddelde fracties van het aantal (FDG-PET/CT) stralings-geïnduceerde doden bij kinderen met een Hodgkin lymfoom en bij volwassenen met een non-Hodgkin lymfoom (diffuus grootcellig B-cel lymfoom) zijn respectievelijk ongeveer 0,4% en 0,07% bij de mannelijke populatie en ongeveer 0,7 en 0,09% bij de vrouwelijke populatie. De gemiddelde (FDG-PET/CT) stralings-geïnduceerde levensreductie bij pediatrische patiënten met een Hodgkin lymfoom is ongeveer 21 dagen bij jongens en 45 dagen bij meisjes. Bij volwassenen met een non-Hodgkin lymfoom (diffuus grootcellig B-cel lymfoom) is de (FDG-PET/CT) stralings-geïnduceerde levensreductie ongeveer 1,5 dagen bij mannen en ongeveer 2,0 dagen bij vrouwen. **Hoofdstuk 3.**

Middels het recent ontwikkelde concept van “Diffusion-weighted Whole-body Imaging with Background body signal Suppression” (DWIBS) kunnen volumetrische diffusie-gewogen MR beelden van het hele lichaam verkregen worden. Beeldacquisitie onder vrije ademhaling, “multiple signal averaging”, en achtergrondsignaal suppressie door middel van een vetsuppressie “pre-pulse” en sterke diffusie weging zijn de belangrijkste karakteristieken van DWIBS. DWIBS licht alle structuren met een verminderde diffusie op, zoals plaatsvindt in vele primaire en metastatische tumoren, en geeft een uitstekende visualisatie van lymfeklieren. Hoewel de exacte waarde van DWIBS nog onderzocht en vastgesteld moet worden, is het een potentieel waardevolle techniek voor tumor stagering, voor het bepalen van therapierespons en voor de detectie van tumorrecidieven. In combinatie met conventionele (T1-gewogen en “short inversion time inversion recovery” [STIR]) whole-body MR sequenties, kan DWIBS een goed stralingsvrij alternatief zijn voor CT voor het stageren van maligne lymfomen. **Hoofdstukken 4.1, 4.2, and 4.3.**

Een tijdsefficiënte en hoog kwalitatieve whole-body MR scan kan makkelijk worden verkregen door het gebruiken van een “non-integrated sliding surface coil approach”. **Hoofdstuk 5.**

Data bij gezonde vrijwilligers laten zien dat “apparent diffusion coefficient” (ADC) metingen mogelijk niet voldoende reproduceerbaar zijn om een onderscheid te maken tussen maligne en niet-maligne lymfeklieren. Desondanks zijn er toekomstige studies nodig die een directe vergelijking maken tussen de ADCs van verschillende nodale pathologieën om meer inzicht te krijgen in de intra- en interobserver reproduceerbaarheid van ADC metingen van lymfeklieren. Verder is aangetoond dat een ADC meting een potentieel specifieke methode is om normale lymfeklieren van lymfeklieren geïnfiltriseerd met maligne lymfoom te onderscheiden. Aan de andere kant zijn ADC metingen niet bruikbaar om indolente van agressieve lymfomen te differentiëren. **Hoofdstukken 6.1 and 6.2.**

Voorgaande studies hebben laten zien dat MR imaging waarschijnlijk voldoende sensitief is om beenmergpathologie uit te sluiten bij patiënten met een maligne lymfoom. Echter, uit onze eigen studiepopulatie blijkt dat whole-body MR imaging (zowel zonder als met DWI) negatief is bij een aanzienlijke proportie van de patiënten met een positief beenmergbiopsie. Om deze reden is whole-body MR imaging nog niet voldoende betrouwbaar om beenmergbiopsie te vervangen voor het beoordelen van het beenmerg bij maligne lymfomen. **Hoofdstukken 7.1 and 7.2.**

Een eerste analyse bij 31 patiënten met een nieuw gediagnosticeerd maligne lymfoom laat zien dat de initiële stagering van maligne lymfomen middels whole-body MR imaging (zonder en met DWI) gelijk is aan het stageren middels CT bij de meerderheid van de patiënten en dat whole-body MR imaging nooit onderstageert ten opzichte van CT. Bovendien is de overstagering van whole-body MR imaging ten opzichte van CT meestal correct en levert het gebruik van DWI mogelijk een voordeel op. **Hoofdstuk 8.1.**

Een daaropvolgende analyse bij 101 patiënten met een nieuw gediagnosticeerd maligne lymfoom bevestigt dat stagering met whole-body MR imaging (zonder en met DWI) gelijk is aan stageren met CT bij de meerderheid van de patiënten. Echter, zowel overstagering als onderstagering van whole-body MR imaging ten opzichte van CT kunnen optreden, waarbij eerstgenoemde meer voorkomt dan laatstgenoemde. Het aantal gevallen waarin whole-body MR imaging terecht een ander stadium toekent dan CT, is ongeveer gelijk aan het aantal gevallen waarin whole-body MR imaging onterecht een ander stadium toekent dan CT. Het potentiële voordeel van DWI is nog niet bewezen. **Hoofdstuk 8.2.**

Een eerste analyse bij 22 patiënten met een nieuw gediagnosticeerd maligne lymfoom laat zien dat de interobserverovereenkomst van whole-body MR imaging (inclusief DWI) matig tot goed is. Overall is de overeenkomst tussen whole-body MR imaging

en FDG-PET/CT matig. Whole-body MR imaging stageert niet lager dan FDG-PET/CT bij patiënten met een nieuw maligne lymfoom. In de minderheid van de patiënten leidt whole-body MR imaging tot klinisch relevante overstagering ten opzichte van FDG-PET/CT. FDG-PET/CT blijft de gouden standaard voor het stageren van maligne lymfomen totdat toekomstige, grotere studies hebben aangetoond dat whole-body MR imaging correct overstageert in dergelijke gevallen. **Hoofdstuk 8.3.**

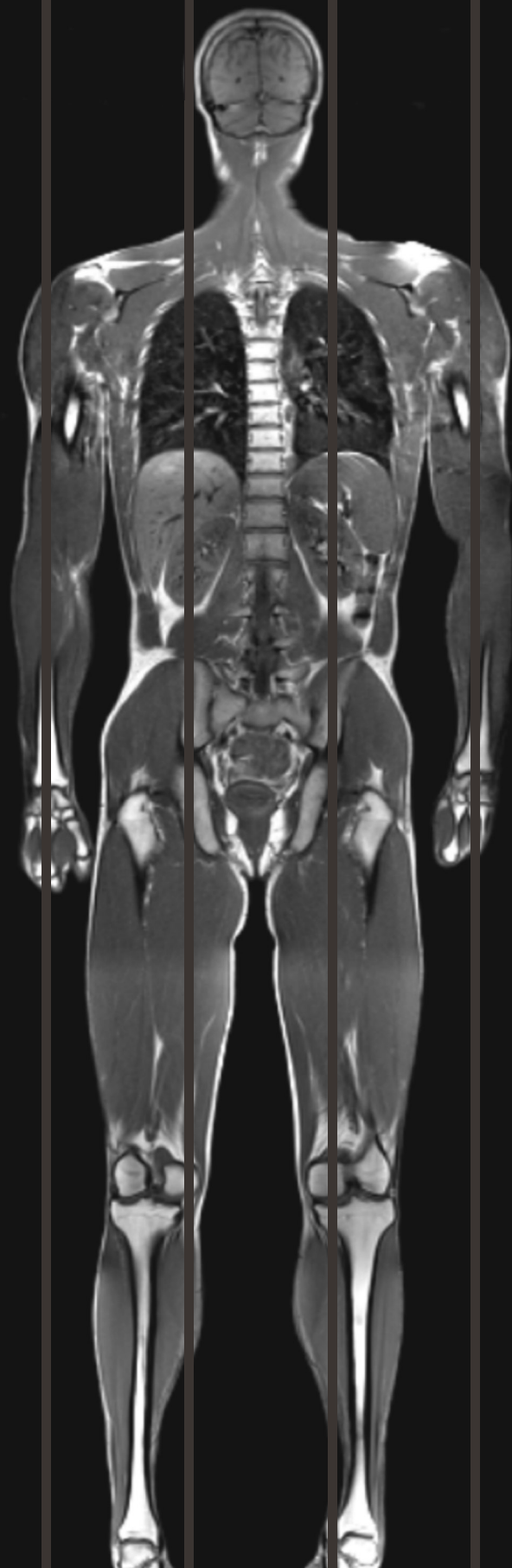
Een interessante constatering was dat in onze serie van 100 patiënten whole-body MR imaging geen klinisch relevante laesies (d.w.z. laesies die het Ann Arbor stadium veranderen) detecteert buiten het beeldbereik van een MR imaging protocol dat alleen maar het gebied van hoofd/nek tot en met romp afbeeldt. Derhalve is het waarschijnlijk voldoende voor toekomstige studies om alleen maar het gebied van hoofd/nek tot en met romp af te beelden wanneer MR imaging gebruikt wordt voor het stageren van maligne lymfomen **Hoofdstuk 9.**

### **Conclusie**

Whole-body MR imaging, inclusief DWI, is een uitvoerbare techniek voor het stageren van nieuw gediagnosticeerde maligne lymfomen. Whole-body MR imaging heeft unieke voordelen en beperkingen ten opzichte van CT. Technische ontwikkelingen zijn nodig om whole-body MR imaging te verbeteren op het gebied van beeldkwaliteit en workflow, en om whole-body MR imaging te integreren met PET. Toekomstig onderzoek moet zich ook richten op de potentiële voordelen van whole-body DWI ten opzichte van CT, met name wat betreft de integratie van anatomische en functionele beeldvorming dat de karakterisering en follow-up van tumoren kan verbeteren. Tot die tijd is het aannemelijk dat CT de voorkeur heeft boven whole-body MR imaging voor het stageren van de meeste patiënten met een maligne lymfoom. Desalniettemin kan whole-body MR imaging worden beschouwd als een redelijk alternatief voor CT, met name in patiëntengroepen waarin CT straling een groter probleem is en bij patiënten met een verhoogd risico op (ernstige) bijwerkingen voor CT contrastmiddelen.







# Chapter 12

Dankwoord

Curriculum vitae

List of publications

Bij mijn onderzoek zijn velen betrokken geweest. Bedankt voor jullie inspanningen en het vertrouwen dat jullie in mij hadden! Bovenal wil ik alle patiënten die aan het onderzoek hebben deelgenomen van harte bedanken. Op het moment dat de diagnose “maligne lymfoom” wordt gesteld, breekt er een periode aan waarin diverse onderzoeken moeten worden verricht en er vaak een intensieve behandeling voor de boeg ligt. Dat deze patiënten ondanks de vaak stressvolle en onzekere tijd waarin ze verkeren toch nog bereid zijn geweest om, geheel belangeloos en puur voor een betere zorg in de toekomst, voor een extra scan naar het ziekenhuis te komen, dwingt veel respect af. Zonder iemand te kort te willen doen, zou ik hier nog een aantal betrokkenen in het bijzonder willen bedanken.

Prof. dr. W.P.Th.M. Mali, promotor; beste professor Mali, u bent onmisbaar geweest voor het opstarten en goed laten verlopen van dit project. Bedankt voor uw goede adviezen waar ik veel van geleerd heb, uw vertrouwen in mij en de vele mogelijkheden die u mij heeft geboden. Ik ben er trots op dat u mijn promotor bent.

Dr. R.A.J. Nievelstein, co-promotor; beste dr. Nievelstein, in 2003 zocht ik naar mogelijkheden om een wetenschappelijke stage te doen. Ik ben zeer blij dat ik destijds bij u aan de slag kon. Blijkbaar was u tevreden over mij, gezien u twee jaar later met het voorstel kwam voor dit project en mij er zeer graag als promovendus bij wilde hebben. Het is mooi om te zien hoe we alles vanaf het begin aan de praat hebben gekregen en het tot een redelijk groot project hebben weten uit te bouwen. Het is zeer prettig om met u samen te werken; we houden beide van precisie en productiviteit. Ik beschouw dit proefschrift zeker niet als een wetenschappelijk eindstation, maar als een momentopname. Ons onderzoek gaat in alle aspecten door en ik hoop dat wij nog lang kunnen blijven samenwerken.

Dr. F.J.A. Beek; beste dr. Beek, bedankt voor uw betrokkenheid bij de studie, het buitengewoon snelle scores van de vele CT's en uw kennis en scherpe opmerkingen die onze manuscripten verbeterd hebben.

Dr. M.S. van Leeuwen; beste Maarten, we zijn heel blij dat je als tweede “MRI reader” wilde optreden, een niet te onderschatten karwei. Jouw enthousiasme en betrokkenheid zijn van grote waarde.

Dr. C.S.P.M. Uiterwaal; beste Cuno, je bent als geen ander in staat om een moeilijk probleem te vereenvoudigen en een ogenschijnlijk eenvoudig probleem op een complexe manier te evalueren. Hoe dan ook, discussies met jou zijn altijd zeer verhelderend en leerzaam. Bedankt voor al je adviezen.

Prof. dr. P.R. Luijten; beste Peter, ik wil je niet alleen bedanken voor je hulp bij het whole-body MRI project, maar ook vanwege het feit dat je me bij diverse andere projecten hebt betrokken en de vele mogelijkheden die je me hebt geboden. Ik ben je zeer dankbaar.

Prof. dr. T. Takahara; dear Taro, thank you for sharing your MRI knowledge, energy, and creativity with me. Your stay in the Netherlands was more than enjoyable and helpful to many of us, including me. It is a pity that you had to go back to Japan. You are a great person and you have a wonderful family. I am looking forward very much to continuing working with you!

Dr. H.M.E. Quarles van Ufford; beste Jet, gezien jij vanuit de PET/CT-zijde al geïnteresseerd was in maligne lymfomen, was het niet verwonderlijk en eigenlijk niet meer dan vanzelfsprekend dat je op den duur bij het project betrokken zou raken. Je bent een heel fijne collega en ik vind het heel plezierig met jou samen te werken. Ik wens je veel succes toe met je toekomstige carrière en hoop dat onze wegen elkaar weer kruisen.

Drs. M.A. Vermoolen; beste Malou, super dat je ook bij het project bent gekomen. Ik vind het erg prettig met je samen te werken! Ik hoop dat het lukt om de kinderstudie succesvol naar Europees multicenter niveau te brengen. Dat zou een unicum binnen de Europese kinderradiologie zijn!

Het trialbureau en de afdeling digitale beeldbewerking in het UMC Utrecht: Anneke Hamersma, Cees Haaring, Adel Kandil, Roy Sanders, Eugène Tymstra, Karin van Rijnbach; bedankt voor jullie onmisbare en zeer belangrijke (logistieke) ondersteuning bij deze studie. Beste Roy, tevens veel dank voor het organiseren van de lay-out van mijn proefschrift!

Alle MRI laboranten in het UMC Utrecht wil ik van harte bedanken. Niels, dankzij jouw kennis en bereidheid buiten kantoor tijd nog door te gaan, hebben we een mooi whole-body MRI protocol voorhanden. Ik wil jou, Greet, Brendan, Ron en Gerrit ook bedanken voor het scannen van een aantal patiënten voor onze studie.

Ik ben de collega's van de Hematologie van het UMC Utrecht, Meander MC Amersfoort en AMC Amsterdam dankbaar voor het includeren van patiënten voor deze studie. Speciale dank aan drs. I. Ludwig, dr. N.W.C.J. van de Donk, dr. E. van der Spek, dr. H.M. van der Straaten, dr. E. Kneppers, dr. L.F. Verdonck, dr. H.K. Nieuwenhuis, Monique Knies, dr. M.B. Bierings, dr. A.B. Versluys, dr. M. Bruin, dr. R. Fijnheer, dr. S. Wittebol, Willemien Bronkhorst, Cock van Roest, dr. M.J. Kersten, dr. J. Zsíros, prof. dr.

H.N. Caron, Bernadette Odijk, Nelia Langeveld en alle andere stafleden, fellows en arts-assistenten hematologie die ik niet bij naam genoemd heb. Zonder jullie bereidheid patiënten te includeren zou het onderzoek onmogelijk zijn geweest.

De afdelingen Radiologie en Nucleaire geneeskunde van het AMC Amsterdam; prof. dr. J. Stoker, dr. E.M. Akkerman, Anneke Heutinck, dr. S. Bipat en dr. J.A. Adam, bedankt voor jullie bereidheid deel te nemen aan deze multicenter studie en al jullie inspanningen.

De afdelingen Nucleaire Geneeskunde en Radiologie van het Meander MC Amersfoort; dr. J.M. de Klerk, dr. L.G. Quekel en dr. B.G.F. Heggelman, ook jullie wil ik bedanken voor deelname aan de studie en de diverse keren dat we in het Meander op bezoek konden komen om de tussentijdse resultaten te bespreken. Dr. A.M. van Raamt; beste Fleur, bedankt voor de diverse keren dat je me hebt geholpen patiëntendata uit het Meander op te zoeken, in de periode dat je daar werkzaam was.

De afdeling Radiologie van het Leiden UMC; dr. J Geleijns en dr. P.W. de Bruin, veel dank voor jullie deskundige hulp bij het berekenen van de geschatte gezondheidsrisico's door het (repetitief) gebruik van (FDG-PET)/CT bij patiënten met een maligne lymfoom.

Philips Healthcare: Gwen Herigault, Fredy Visser, Gabriella Beck, Arianne van Muiswinkel, Arjan Simonetti, Vincent Denolin, Marc van Cauteren, Tetsuo Ogino, Mark Stoesz, Ruud de Boer, thank you for your continuing (technical) support.

Prof. dr. Thomas L. Chenevert and dr. Marko K. Ivancevic from the University of Michigan (Ann Arbor, US); dear Tom and Marko, thank you for your great hospitality in Ann Arbor and good cooperation. I learned a lot from you and I sincerely hope we can do more work together in the future. I would also like to thank Frank Londy, dr. Hero K. Hussain, Peter S. Liu, dr. Craig J. Galbán, prof. dr. Charles R. Meyer, prof. dr. Pia C. Sundgren, and prof. dr. Brian D. Ross.

Prof. dr. Abass Alavi, dr. Drew Torigian, and dr. Sandip Basu from the University of Pennsylvania (Philadelphia, US); it is a great honour working with you. Professor Alavi, you are a living legend and your contributions to medicine are exceptional. Thank you for visiting the UMC Utrecht and the inspiring discussions. I am curious what the PET/MRI future will bring us!

Dr. Dow-Mu Koh and dr. David Collins from the Royal Marsden Hospital (Sutton, UK); you are two gentlemen with tremendous knowledge of MRI and diffusion in particular. It is a great pleasure knowing you and working with you.

Dr. Tetsu Niwa, dr. Tomohiro Yamashita, dr. Takeshi Yoshizako, dr. Yuki Toyoguchi, dr. Reiji Ochiai, dr. Kazuhiro Katahira, dr. Katsuyuki Nakanishi, dr. Yoshiharu Ohno, and prof. dr. Yutaka Imai from Japan: thank you for collaborating in several research projects and thank you for your hospitality when I was in Japan.

Dr. M.A.A.J. van den Bosch, dr. J. Hendrikse en dr. W.B. Veldhuis; beste Maurice, Jeroen en Wouter, bedankt voor jullie prettige samenwerking bij diverse andere projecten.

Dr. M.G. Lam en dr. B. de Keizer; beste Marnix en Bart, bedankt voor jullie adviezen op het gebied van de nucleaire geneeskunde en de goede samenwerking.

Prof. P.D. Siersema en drs. A.M. Leufkens; dank voor de fijne samenwerking bij onze gastroenterologische diffusie MRI studie.

Collega MD/PhD-studenten, bedankt voor de leerzame bijeenkomsten en veel succes met jullie verdere carrières.

Ook dank aan alle andere onderzoekers van de radiologie: Alexander, Anja, Anne, Annemarie, Bartjan, Beatrijs, Bertine, Cécile, Charlotte, Ewout, Hamza, Jan Willem, Jesse, Joost, Mandy, Marianne, Maarten, Martijn, Mies, Nolan, Onno, Reinoud, Rianne, Stan, Stephanie, Tim, Tom, Wilco en alle overige onderzoekers (in het bijzonder degenen die betrokken zijn bij het 7.0T-project) die ik hier nog niet genoemd heb.

Alle radiologen en arts-assistenten radiologie in het UMC Utrecht: ik vind het heel fijn dat ik nu de dagelijkse klinische praktijk met jullie kan meemaken en hoop veel van jullie te leren.

Tenslotte nog dank aan de instanties die dit onderzoek financieel mogelijk hebben gemaakt: ZonMW (ZonMw Program for Health Care Efficiency Research [grant number 80-82310-98-08012] en ZonMW AGIKO stipendium [grant number 92003497]) en het UMC Utrecht (MD/PhD stipend).





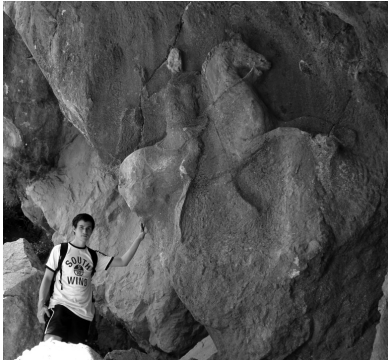
# Chapter 12

Dankwoord

Curriculum vitae

List of publications





The author was born in Nijmegen, The Netherlands, on March 23, 1981. He graduated from high school (Bisschoppelijk College Schöndeln, Roermond, The Netherlands) in 1999. In 2000, he obtained his propaedeutics degree in civil engineering from The Delft University of Technology. In the same year, he started studying medicine at Utrecht University. After obtaining his medical degree in November 2006, he started the research presented in this thesis, under the supervision of prof. dr. W.P.Th.M. Mali and dr. R.A.J. Nivelstein, at the Department of Radiology of the University Medical Center Utrecht. During his PhD, he was a visiting scientist at the Department of Radiology of the University of Michigan, collaborating with prof. dr. T.L. Chenevert on applications of diffusion MRI in cancer. As of January 2011, he started his training in Radiology at the University Medical Center Utrecht under supervision of prof. dr. J.P.J. van Schaik.



# Chapter 12

Dankwoord

Curriculum vitae

List of publications

## Journal articles

1. **Kwee TC**, Basu S, Saboury B, Alavi A, Torigian DA. Functional imaging of cancer Front Biosci; in press
2. Haradome H, Grazioli L, Tinti R, Morone M, Motosugi U, Sano K, Ichikawa T, **Kwee TC**, Colagrande S. Additional value of gadoxetic acid-DTPA-enhanced hepatobiliary phase MR imaging in the diagnosis of early-stage hepatocellular carcinoma: comparison with dynamic triple-phase multidetector CT imaging. J Magn Reson Imaging; in press
3. **Kwee TC**, Basu S, Alavi A. Evolving importance of diffusion-weighted MRI in lymphoma. PET Clinics; in press
4. Basu S, **Kwee TC**, Gatenby R, Saboury B, Torigian DA, Alavi A. Evolving role of molecular imaging with PET in detecting and characterizing heterogeneity of cancer tissue at the primary and metastatic sites, a plausible explanation for failed attempts to cure malignant disorders. Eur J Nucl Med Mol Imaging; in press
5. Basu S, **Kwee TC**, Torigian DA, Saboury B, Alavi A. Suboptimal and inadequate quantification: an alarming crisis in medical applications of PET. Eur J Nucl Med Mol Imaging; in press
6. Takahara T, **Kwee TC**, Sadahiro S, Yamashita T, Toyoguchi Y, Yoshizako T, Horie T, Luijten PR, Imai Y. Low b-value diffusion-weighted imaging for diagnosing strangulated small bowel obstruction: a feasibility study. J Magn Reson Imaging; in press
7. Donswijk ML, Broekhuizen-de Gast HS, Torigian DA, Alavi A, **Kwee TC**, Lam MGEH. PET Assessment of brown fat. PET Clinics; in press
8. **Kwee TC**, Takahara T, Niwa T, Yamashita T, Van Cauteren M, Nievelstein RA, Luijten PR. Technical note: improving background suppression in diffusion-weighted imaging of the abdomen and pelvis using STIR with single-axis diffusion encoding. Magn Reson Imaging; in press
9. **Kwee TC**, Akkerman EM, Fijnheer R, Kersten MJ, Zsíros J, Ludwig I, Bierings MB, Van Leeuwen MS, Stoker J, Nievelstein RA. MRI for staging lymphoma: whole-body or less? J Magn Reson Imaging; in press
10. Chenevert TL, Galban CJ, Ivancevic MK, Rohrer SE, Londy FJ, **Kwee TC**, Meyer CR, Johnson TD, Rehemtulla A, Ross BD. Diffusion coefficient measurement using a temperature controlled fluid for quality control in multi-center studies. J Magn Reson Imaging; in press
11. Quarles van Ufford HM, **Kwee TC**, Beek FJ, Takahara T, Fijnheer R, Nievelstein RA, De Klerk JMH. Whole-body MRI, including diffusion-weighted imaging, compared to 18F-FDG PET-CT in newly diagnosed lymphoma: initial results. AJR Am J Roentgenol 2011;196:662-669

12. **Kwee TC**, De Klerk JMH, Nievelstein RA. Imaging of bone marrow involvement in lymphoma: state of the art and future directions. *ScientificWorldJournal* 2011;11:391-402
13. **Kwee TC**, Basu S, Alavi A. PET and PET/CT for Unknown Primary Tumors. *Methods Mol Biol* 2011;727:317-333
14. **Kwee TC**, Basu S, Saboury B, Torigian DA, Naji A, Alavi A. Beta-cell imaging: limitations and opportunities. *J Nucl Med* 2011;52:493
15. Yamashita T, Takahara T, **Kwee TC**, Kawada S, Horie T, Inomoto C, Hashida K, Yamamuro H, Myojin K, Luijten PR, Imai Y. Diffusion MRI with gadofosveset trisodium as a negative contrast agent for lymph node metastases assessment. *Jpn J Radiol* 2011;29:25-32
16. Takahara T, **Kwee TC**, Haradome H, Aoki K, Matsuoka H, Nakamura A, Honya K, Takahashi M, Yamashita T, Luijten PR, Imai Y. Peristalsis gap sign at cine MR imaging for diagnosing strangulated small bowel obstruction: feasibility study *Jpn J Radiol* 2011;29:11-18
17. **Kwee TC**, Nievelstein RA. Is MRI less accurate than FDG-PET/CT in diagnosing bone marrow involvement in lymphoma? *Eur J Radiol*; in press
18. **Kwee TC**, Basu S, Saboury B, Ambrosini V, Torigian DA, Alavi A. A new dimension of FDG-PET interpretation: assessment of tumor biology. *Eur J Nucl Med Mol Imaging*; in press
19. **Kwee TC**, Basu S, Torigian DA, Saboury B, Alavi A. Defining the role of modern imaging techniques in assessing lymph nodes for metastasis in cancer: evolving contribution of PET in this setting. *Eur J Nucl Med Mol Imaging*; in press
20. **Kwee TC**, Takahara T, Muro I, Van Cauteren M, Imai Y, Nievelstein RA, Mali WP, Luijten PR. Apparent diffusion coefficient measurement in a moving phantom simulating linear respiratory motion. *Jpn J Radiol*;2010;28:578-583
21. **Kwee TC**, Ludwig I, Uiterwaal CS, Quarles van Ufford HME, Vermoolen MA, Fijnheer R, Bierings MB, Nievelstein RA. ADC measurements in the evaluation of patients with non-Hodgkin lymphoma: feasibility study. *MAGMA* 2011;24:1-8
22. Hoff BA, Chenevert TL, Bhojani MS, **Kwee TC**, Rehemtulla A, Le Bihan D, Ross BD, Galbán CJ. Assessment of Multi-Exponential Diffusion Features as MRI Cancer Therapy Response Metrics. *Magn Reson Med* 2010;64:1499-1509
23. **Kwee TC**, Takahara T, Ochiai R, Koh DM, Ohno Y, Nakanishi K, Niwa T, Chenevert T, Luijten PR, Alavi A. Complementary roles of whole-body diffusion-weighted MRI and FDG-PET: state-of-the-art and potential applications. *J Nucl Med* 2010;51:1549-1558
24. **Kwee TC**, Takahara T. Diffusion-weighted MRI for detecting liver metastases: importance of the b-value. *Eur Radiol* 2011;21:150
25. Basu S, **Kwee TC**, Alavi A. PET and PET-CT assessment of gynecological malignancies: beyond FDG. *PET Clin* 2010;5:477-482

26. **Kwee TC**, Takahara T, Katahira K, Nakanishi K. Whole-body MRI for detecting bone marrow metastases. *PET Clin* 2010;5:297-309
27. **Kwee TC**, Takahara T, Vermoolen MA, Bierings MB, Mali WP, Nievelstein RA. Whole-body diffusion-weighted imaging for staging malignant lymphoma in children. *Pediatr Radiol* 2010;40:1592-1602
28. Katahira K, Takahara T, **Kwee TC**, Oda S, Suzuki Y, Morishita S, Kitani K, Hamada Y, Kitaoka M, Yamashita Y. Value of ultra-high-b-value diffusion-weighted MR imaging for the detection of prostate cancer: evaluation in 201 cases with histopathological correlation. *Eur Radiol* 2011;21:188-196
29. **Kwee TC**, Niwa T, Takahara T. Diffusion-weighted Whole-body Imaging with Background body signal Suppression (DWIBS) facilitates detection and evaluation of an anterior rib contusion. *Clin Imaging* 2010;34:298-301
30. **Kwee TC**, Takahara T, Klomp DW, Luijten PR. Imaging of cancer: novel concepts in clinical magnetic resonance imaging. *J Intern Med* 2010;268:120-132
31. Takahara T, **Kwee TC**, Hendrikse J, Van Caueren M, Koh DM, Niwa T, Mali WP, Luijten PR. Subtraction of unidirectionally encoded images for suppression of heavily isotropic objects (SUSHI) for selective visualization of peripheral nerves. *Neuroradiology* 2011;53:109-116
32. Niwa T, Aida N, Takahara T, **Kwee TC**, Fujita K, Shishikura A, Miyata D, Inoue T. Imaging and clinical characteristics of children with multiple foci of micro-susceptibility changes in the brain on susceptibility-weighted magnetic resonance imaging. *Pediatr Radiol* 2010;40:1657-1662
33. Vermoolen MA, **Kwee TC**, Nievelstein RA. Whole-body MRI for staging Hodgkin lymphoma in a pregnant patient. *Am J Hematol* 2010;85:443
34. **Kwee TC**, Galban CJ, Tsien C, Junck L, Sundgren PC, Ivancevic M, Johnson TD, Meyer CR, Rehemtulla A, Ross BD, Chenevert TL. Comparison of apparent diffusion coefficients and distributed diffusion coefficients in high-grade gliomas. *J Magn Reson Imaging* 2010;31:531-537
35. **Kwee TC**, Fijnheer R, Ludwig I, Quarles van Ufford HME, Uiterwaal CS, Bierings MB, Takahara T, Nievelstein RA. Whole-body magnetic resonance imaging, including diffusion-weighted imaging, for diagnosing bone marrow involvement in malignant lymphoma. *Br J Haematol* 2010;149:628-630
36. Willems SM, Koekkoek PS, **Kwee TC**, van den Bosch MA. Diffusion-weighted MRI of the liver for early tumor response assessment: promising technique but evidence is still lacking *Acta Oncol* 2010;49:252-255
37. Takahara T, **Kwee TC**, Van Leeuwen MS, Ogino T, Van Caueren M, Herigault G, Luijten PR, Mali WP. Diffusion-weighted MR imaging of the liver using TRacking Only Navigator echo (TRON): feasibility study. *Invest Radiol* 2010;45 :57-63
38. Takahara T, **Kwee TC**, Kifune S, Ochiai R, Sakamoto T, Niwa T, Van Caueren M, Luijten PR. Whole-body MRI using a sliding table and repositioning surface coil approach. *Eur Radiol* 2010;20:1366-1373



39. Niwa T, Ueno M, Shinya N, Gotoh T, **Kwee TC**, Takahara T, Yoshida T, Ohkawa S, Doiuchi T, Inoue T. Dynamic contrast-enhanced susceptibility-weighted perfusion MRI in advanced pancreatic cancer: semi-automated analysis to predict response to chemotherapy. *NMR Biomed* 2010;23:347-352
40. Takahara T, Hendrikse J, **Kwee TC**, Yamashita T, Van Cauteren M, Polders D, Boer V, Imai Y, Mali WP, Luijten PR. Diffusion-weighted MR neurography of the sacral plexus with unidirectional motion probing gradients. *Eur Radiol* 2010;20:1221-1226
41. **Kwee TC**, Basu S, Cheng G, Alavi A. FDG-PET/CT in carcinoma of unknown primary. *Eur J Nucl Med Mol Imaging* 2010;37:635-644
42. Ivancevic MK, **Kwee TC**, Takahara T, Ogino T, Hussain HK, Liu PS, Chenevert TL. Diffusion-weighted MR imaging of the liver at 3.0T using TRacking Only Navigator echo (TRON): feasibility study. *J Magn Reson Imaging* 2009;30:1027-1033
43. **Kwee TC**, Galban CJ, Tsien C, Junck L, Sundgren PC, Ivancevic M, Johnson TD, Meyer CR, Rehemtulla A, Ross BD, Chenevert TL. Intravoxel water diffusion heterogeneity imaging of human high-grade gliomas. *NMR Biomed* 2010;23:179-187
44. **Kwee TC**, Takahara T, Niwa T, Ivancevic MK, Herigault G, Van Cauteren M, Luijten PR. Influence of cardiac motion on diffusion-weighted magnetic resonance imaging of the liver. *MAGMA* 2009;22:319-325
45. **Kwee TC**, Quarles van Ufford HME, Beek FJ, Takahara T, Uiterwaal CS, Bierings MB, Ludwig I, Fijnheer R, Nievelstein RA. Whole-body MRI, including diffusion-weighted imaging, for the initial staging of malignant lymphoma: comparison to computed tomography. *Invest Radiol* 2009;44:683-690
46. Yamashita T, **Kwee TC**, Takahara T. Whole-body magnetic resonance neurography. *N Engl J Med* 2009;361:538-539
47. **Kwee TC**, Takahara T, Ochiai R, Katahira K, Van Cauteren M, Imai Y, Nievelstein RA, Luijten PR. Whole-body diffusion-weighted magnetic resonance imaging. *Eur J Radiol* 2009;70:409-417
48. Kwee RM, **Kwee TC**. Imaging in assessing lymph node status in gastric cancer. *Gastric Cancer* 2009;12:6-22
49. **Kwee TC**, Takahara T, Luijten PR, Nievelstein RA. ADC measurements of lymph nodes: inter- and intraobserver reproducibility study and an overview of the literature. *Eur J Radiol* 2010;75:215-220
50. Sakurada A, Takahara T, **Kwee TC**, Yamashita T, Nasu S, Horie T, Van Cauteren M, Imai Y. Diagnostic performance of diffusion-weighted magnetic resonance imaging in esophageal cancer. *Eur Radiol* 2009;19:1461-1469
51. **Kwee TC**, Takahara T, Koh DM, Nievelstein RA, Luijten PR. Comparison and reproducibility of ADC measurements in breathhold, respiratory triggered, and free breathing diffusion-weighted MR imaging of the liver. *J Magn Reson Imaging* 2008;28:1141-1148

52. **Kwee TC**, Kwee RM. Combined FDG-PET/CT for the detection of unknown primary tumours: systematic review and meta-analysis. *Eur Radiol* 2009;19:731-744
53. Kwee RM, **Kwee TC**. Predicting lymph node status in early gastric cancer: a systematic review and metaanalysis. *Gastric Cancer* 2008;11:134-148
54. Takahara T, Hendrikse J, Yamashita T, Luijten PR, **Kwee TC**, Imai Y, Mali WP. Diffusion-weighted MR neurography of the brachial plexus: feasibility study. *Radiology* 2008;249:653-660
55. **Kwee TC**, Kwee RM, Alavi A. FDG-PET for diagnosing prosthetic joint infection: systematic review and metaanalysis. *Eur J Nucl Med Mol Imaging* 2008;35:2122-2132
56. Kwee RM, **Kwee TC**. The accuracy of endoscopic ultrasonography in differentiating mucosal from deeper gastric cancer. *Am J Gastroenterol* 2008;103:1801-1809
57. **Kwee TC**, Takahara T, Ochiai R, Nievelstein RA, Luijten PR. Diffusion-weighted whole-body imaging with background body signal suppression (DWIBS): potential applications in oncology. *Eur Radiol* 2008;18:1937-1952
58. **Kwee TC**, Kwee RM, Verdonck LF, Bierings MB, Nievelstein RA. MRI for the detection of bone marrow involvement in malignant lymphoma. *Br J Haematol* 2008;141:60-68
59. **Kwee TC**, Kwee RM, Nievelstein RA. Imaging in staging of malignant lymphoma: a systematic review. *Blood* 2008;111:504-516
60. **Kwee TC**, Kwee RM. Abdominal adiposity and risk of pancreatic cancer. *Pancreas* 2007;35:285-286
61. **Kwee TC**, Kwee RM. MR angiography in the follow-up of intracranial aneurysms treated with Guglielmi detachable coils: systematic review and meta-analysis. *Neuroradiology* 2007;49:703-713
62. Kwee RM, **Kwee TC**. Virchow-Robin spaces at MR imaging. *Radiographics* 2007;27:1071-1086
63. Kwee RM, **Kwee TC**. Imaging in local staging of gastric cancer – a systematic review. *J Clin Oncol* 2007;25:2107-2116
64. **Kwee TC**, Beemer FA, Beek FJ, Nievelstein RA. Knee radiography in the diagnosis of skeletal dysplasias. *Pediatr Radiol* 2006;36:8-15

## Book chapters

1. **Kwee TC**, Basu S, Alavi A. PET and PET/CT for Unknown Primary Tumors” in “Positron Emission Tomography (PET): A Textbook for Clinicians and Imaging Physicians” (editors: M.E. Juweid and O.S. Hoekstra). Humana Press, Totowa, NJ, USA
2. Takahara T, **Kwee TC**. MR Neurography: Imaging of the Peripheral Nerves in “Diffusion-weighted MR Imaging; Applications in the Body” (editors: D.M. Koh and H. Thoeny). Springer, New York, NY, USA
3. Takahara T, **Kwee TC**. Diffusion-weighted Whole-body Imaging with Background body signal Suppression (DWIBS) in “Diffusion-weighted MR Imaging; Applications in the Body” (editors: D.M. Koh and H. Thoeny). Springer, New York, NY, USA
4. Takahara T, **Kwee TC**. Diffusion-weighted imaging of lymph nodes in “Extra-Cranial Application of Diffusion Weighted MRI” (editor: B. Taouli). Cambridge University Press, New York, NY, USA
5. **Kwee TC**, Basu S, Prasad V, Baum RP, Alavi A. PET for measuring therapy response after radionuclide therapy in “Therapeutic Nuclear Medicine” (editor: R.P. Baum). Springer, New York, NY, USA
6. Niwa T, Aida N, **Kwee TC**, Takahara T. Spinal teratoid/rhabdoid tumor: use of diffusion-weighted imaging for diagnosis in “Tumors of the central nervous system” (editor: M.A. Hayat). Springer, New York, NY, USA

